UNIVERSITÀ DEGLI STUDI DI MILANO

TRANSLATIONAL MEDICINE

Dipartimento di Scienze biomediche per la salute

TESI DI DOTTORATO DI RICERCA

hiPSc and mESc as a cellular model to study the mechanisms behind arrhythmias.

BIO/09

Federica Giannetti
R12385

Tutor: prof. Andrea Barbuti

PhD Coordinator: prof. Chiarella Sforza

A.A. 2020-2021

SUMMARY

Mouse embryonic stem cells (mESc) and human induced pluripotent stem cells (hiPSc) are commonly exploited in research for their ability to potentially differentiate into any cell subtype. Regarding cardiac differentiation, today's existing protocols are well advanced in recapitulating and promoting cardiomyocytes (CMs) differentiation, making CMs derived from mESc and hiPSc a good *in vitro* model for analyzing heart pathologies.

In this thesis, these models have been used to characterize and better comprehend the functional output caused by genetic alterations. In the first part, mESc-derived cardiomyocytes help to elucidate the electrical dysregulation produced by the knock-out of Striatin (STRN), a scaffold protein with a role in organizing subcellular multiprotein complexes. STRN loss has been found in patients with dilated cardiomyopathy (DCM) and its mutation linked to DCM and ARVC in dogs. However, STRN physiological role in the cardiac context is not yet clear, for this reason the electrical characterization, by patch-clamp analysis, of mouse embryonic stem cells mESc-derived cardiomyocytes (mCMs) knock out for the STRN gene (STRN-KO) may help elucidating STRN role and its pathological implications. In this context, action potential (AP) analysis showed a higher rate and upstroke velocity of STRN-KO mCMs compared to its isogenic WT control. Accordingly, a significantly larger I_{Na} current density, responsible of the phase 0, was found in STRN-KO than in WT mCMs, while the other currents analyzed (I_f, I_{CaL} and I_{Kr}) were similar. Literature data show that downregulation of STRN destabilize microtubules, and their disassembling increases sodium current in neonatal cardiomyocytes. Here is shown that treating STRN-KO mCMs with the microtubule stabilizer Taxol (10 μM) reverted I_{Na} density to values similar to WT cells. These data lead to the conclusion that STRN loss affects the electrical properties of mCMs likely acting on cytoskeleton stability

and consequently on sodium channels trafficking and/or activity, creating a substrate more prone to develop arrhythmias.

In the second part of the thesis, hiPSc-derived cardiomyocytes, obtained from a patient with atrial fibrillation (AF)carrying a heterozygous GOF point mutation in the PITX2 gene, are used to distinguish if this genetic condition predispose or AF. In GWAS studies, PITX2 is the genetic locus most associated with AF, it is often dysregulated in AF patients and its presence or absence correlates with electrical alterations. Moreover, PITX2 loss of function in zebrafish has been linked to perturbations of metabolic pathways forerunning AF-like phenotypes. APs recorded from small hiPSc-derived CMs (hpCMs) clusters reveals that PITX2-hpCMs are bradycardic, with a larger action potential amplitude and a shorter action potential duration than to three unrelated controls. Moreover, preliminary data obtained from atrial hiPSc-derived CMs, used to further elucidate the consequence of this mutation in the atrial background, showed no differences in I_{CaL} and I_f densities; however, activation curve of I_f is negatively shifted with a higher inverse slope factor in PITX2 atrial hiPSc-derived CMs, implying a minor contribution of this current during the slow diastolic depolarization. Seahorse metabolic analysis indicates that PITX2-haCMs generates more ATP compared to isogenic control, and this difference is due to increased oxidative phosphorylation in mitochondria.

In conclusion, although a more detailed characterization will be required, the PITX2 GOF mutation seems to enhance oxidative phosphorylation and a slower beating rate, altering not only the electrical activity but also the metabolism of cardiomyocytes.

Overall, these *in vitro* models of cardiomyocytes were ideal to identify the functional outcome of genetic alteration, either to investigate the electrical mechanism behind arrhythmias or to characterize the role of a specific protein in the specific cardiac context.

GENERAL INTRODUCTION

Models to study heart diseases

Cardiac contraction is generated by an electrical wave of excitation that spreads throughout the heart; the basis of this stimulus is a balance of electrical currents, which depolarize and repolarize the membrane potential, thus shaping the action potentials (APs). Whenever there is a dysregulation in the generation or propagation of these stimuli an arrhythmic event may kick in.

Molecular mechanisms behind cardiac channelopathies (e.g. cardiac pathologies linked to ion channels alterations) have been successfully analyzed *in vitro* by comparing the properties of wild type and mutated channels overexpressed in heterologous cellular models, transfection of human wild-type channels provided information about their specific properties and how, within the same family, some specific characteristics can be altered[1]. This model has also been used successfully to assess whether a specific mutation modified current properties and thus specifically identifying genetic mechanism as predisposing for arrhythmias[2]. Nevertheless, all these useful information refers to single channels without taking into account the cellular context in which they are expressed, which could alter their behavior[3,4]. The specific context of the expression is fundamental to correctly understand the function and pathological role of ion channels, this is even more true if the genetic mutations concern structural proteins that do not have a fast read-out as ionic channels.

Therefore, animal models are a good compromise when it comes to modeling heart diseases more reliably than the heterologous model. In fact, from animal models that recapitulated the phenotypic effect of human diseases, much information was obtained on the excitability of the heart, the normal function of ion channels, the identification and development of antiarrhythmic drugs and therapies, also studying their safety. However, these models

neither always recapitulate all the molecular mechanism of human alteration, nor their response to therapies and the related off-target. Furthermore, beyond the fact that animal models involve a high-cost effort to generate transgenic mice with specific point mutations and to maintain them.

When a cell is subjected to an arrhythmic pattern of activation, a phenomenon known as maladaptive remodeling kicks in, this remodeling significantly changes the expression of many proteins, and when cardiomyocytes (CMs) are isolated, it results difficult to discriminate between causes and effects of the arrhythmia.

It is important to note that some studies were performed directly on human cardiac samples being theoretically the most reliable study context. This has resulted in a different kind of difficulty, such as the limited availability of healthy samples to use for comparison, the limited number of cardiomyocytes obtainable and the severe remodeling.

Pluripotent stem cell-derived CMs overcome several of these problems, becoming a very common in vitro model being easy to generate, maintain, engineer usable and manageable for basic research. Both mouse Embryonic Stem cells (mESc) and human induced Pluripotent Stem cells (hiPSc) can be successfully differentiated into functional cardiomyocytes.

mESc and cardiac differentiation

Mouse Embryonic stem cells (mESc) were isolated from a mouse blastocyst's inner cell mass (ICM) and they are undifferentiated and pluripotent cells capable of differentiating into any cell type based on the chemoceptive stimulus received. As they have "long term self-renewal", it is possible to keep these cells in culture for a long time through the use of LIF (Leukemia Inhibitory Factor)[5], allowing in-vitro investigation of the early stage of mammalian development and reducing the need of animal models. The use of mESc in vitro is very

common, as they allow the generation of a tissue model that is easily usable and manageable for basic research. They are thus a great tool in gene targeting and in vitro developmental studies to develop stem cells–based therapies and functional drug assays[6,7]. mESc differentiation through the Hanging Drops technique recapitulates in vitro what happens in the normal embryo development, forming cellular aggregates, called Embryoid Bodies (EBs), whose cells differentiate into derivatives of the ectoderm, endoderm, and mesoderm. Cardiomyocytes are among the first cell lineages that is formed, evident from the appearance of spontaneous contractions. mESc-derived cardiomyocytes have a mixed cardiac phenotype including pacemaker, atrial and ventricular CMs[8]. The spontaneous differentiation efficiency, mediated only by the serum in the culture medium, can be improved by the addition of Ascorbic Acid, the synthetic counterpart of vitamin C, enhancing the cardiac commitment[9].

This methodology of differentiation is cost-effective and do not need complex or expensive equipment and create a good study model being something between the two-dimensional (2D) monolayer cell culture and animal models.

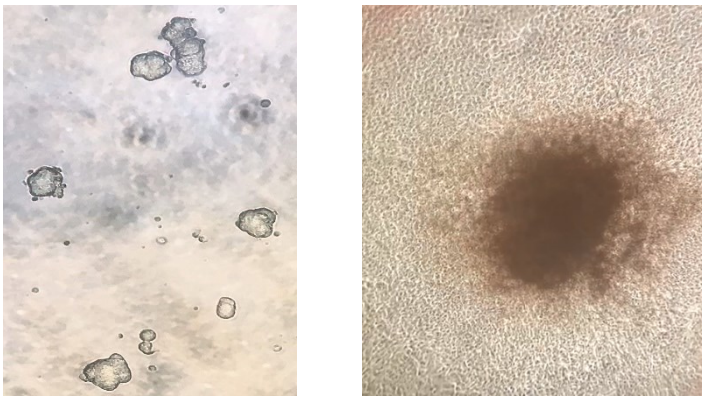

Figure 1: picture of a mESc line colonies (a) and of Embryoid bodies obtained with hanging drop technique (b).

Many groups have tried to isolate cardiomyocytes from EBs, through generating mESc lines expressing reporter genes, such as Atrial Natriuretic Peptide, Heavy Chain of α-Myosin and GATA6[10–12] or using eGFP reporter gene under cardiac development promoter Nkx2.5[13], always obtaining a mixed population of cardiomyocytes. In the past years, our laboratory developed a reliable protocol to produce and select specifically sinoatrial node precursors,

with a selection based on the membrane marker CD166, that continue to mature into fully functional sinoatrial node cardiomyocytes[14]. This allows us to analyze in details regulatory pathways affecting cardiac pacemaking[15].

hIPSc and cardiac differentiation

Human Induced pluripotent stem cells (hiPSc) are an innovative cellular model that put the basis not only of personalized therapy but also of new frontiers for basic research.

In 2006, Yamanaka and colleagues identified some genes specifically expressed by embryonic stem cells, now known as the "Yamanaka factors" (OCT3-4, SOX2, c-MYC and KLF-4)[16]; these factors were then successfully used to reprogram somatic human cells (fibroblasts) into human induced pluripotent stem cells (hiPSc), considered equivalent to human embryonic stem cells but avoiding the ethical issues, and thus capable to differentiate into three germs layer[17]. There are several differentiation protocols to obtain cardiomyocytes from hiPSc based on molecular mechanisms that occur in the embryo during cardiac development. The mostly commonly used differentiation methods are:

1- Spontaneous differentiation through the formation of three-dimensional aggregates called “embryoid bodies” (embryoid bodies or EBs) which follow the initial *in vivo* stages of embryonic development.
2- The differentiation in monolayer, using small molecules, specifically push through the cardiac fate, obtaining a mixed population of CMs.

Spontaneous three-dimensional differentiation through EBs has the advantage of favoring a natural differentiation of all three embryonic layers without the use of chemical inducers and the affordability of the reagent but have a low cardiomyocyte yield (5-10%)[18]. Therefore, most of the protocols use a 2D differentiation in which cells are grown as monolayers and the differentiation efficiency increases, based on supplementing the medium with inductive

factors at specific timing, including bone morphogenic proteins (BMP4), Activin A hormone, fibroblast growth factor (FGF2) and vascular endothelial growth factor (VEGF), in combination with a β-catenin inhibitor (WNT) or low insulin concentrations[19].

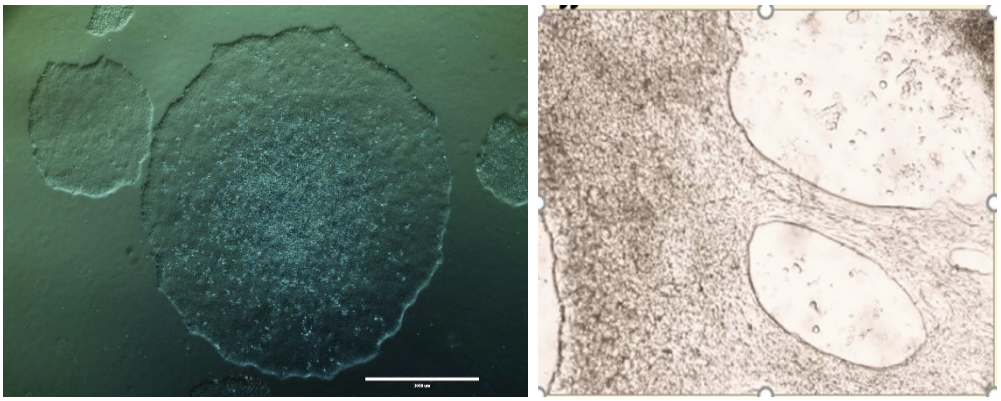

Figure 2: picture of a hiPSc line colony (a) and of hiPSc-derived cardiomyocytes obtained with monolayer differentiation (b).

Both methods have some limitations in the efficiency of generating mature enough cardiomyocytes that resemble the human condition. It is demonstrated by ultrastructural studies that hiPSc-derived cardiomyocytes continue to mature until 1 year in culture[20]. Indeed, the most common critic to this model is the immaturity in their molecular profile and functional activity. Given the difficulties mentioned above in studying arrhythmic diseases of the heart, the idea of having a human experimental model, an unlimited source of specialized cells and with the ability to maintain the patient's genetic context has stimulated efforts to find and improve differentiation methods in different types of somatic cells. Thanks to new technologies, new support scaffolds, new molecular combinations and co-cultures improve the maturity of the obtained CMs or the direction towards a specific cardiac subtype. Concerning this, several groups defined different protocols in order to specifically select or increase the yield of the atrial cardiomyocytes, using prevalently retinoic acid enriched differentiation medium; this molecule has been administrated at different concentrations and incubation times: from 48s to 72 hours[21],[22] up to 96 hours[23]. Furthermore, Lee and colleagues recently demonstrated that it is possible to isolate populations of atrial, ventricular and sinoatrial precursors by flow cytometer selection[24]. In response to the

obvious need to standardize a protocol for atrial differentiation, also exist a commercial kit for atrial differentiation, the STEMdiff Atrial Cardiomyocyte Differentiation Kit.

Conduction system and working myocardium system

As previous mentioned, myocardium is composed by many different types of CMs and consequently two different systems: one to generate and propagate the excitation stimulus that induced the contraction, and the other to actually contract creating the pressure needed for the blood flowing.

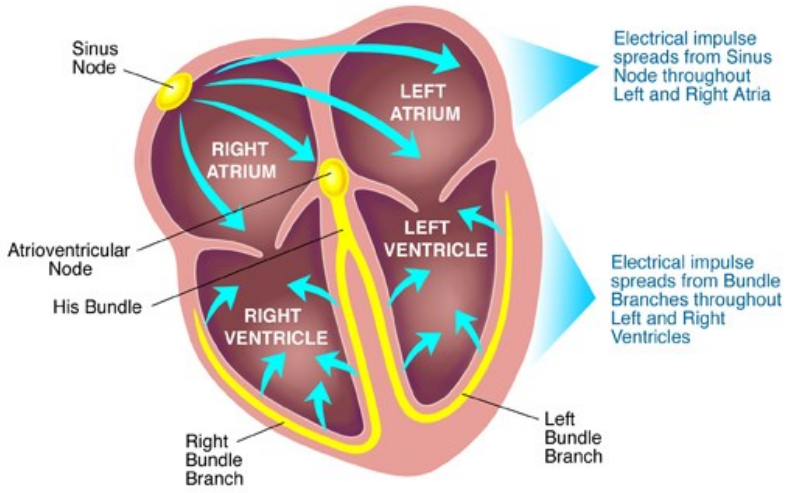

Figure 3: representative scheme of the conduction system. From: https://www.uptodate.com/

The electrical stimulus underlying the contraction is called Action Potential (AP), it is a peculiarity of excitable cells, and it is defined as a fast change in potential due to ions flux through the membrane. AP can be spontaneously generated by all conductions system's CMs, but for a phenomenon called *overdrive suppression*, it physiologically generates from the Sinoatrial Node (SAN), a small tissue located in the upper part of the right atria. Starting from here, AP spreads all over the working CMs composing the atria causing their contraction, while the internodal pathways bring the stimulus to the atrioventricular node (AVN). AVN is fundamental to slow down the AP propagation, allowing sequential and non-simultaneous contraction of atria and ventricles. From here, the stimulus is transmitted to the ventricular working CMs through the His bundle and the Purkinje fibers, allowing the ventricular contraction.

As previously mentioned, AP generates from a rapid flow of different charges through the cellular membrane. This inflow and outflow of positive/negative ions is mediated by ionic channels. Different regions of the heart display AP with different shapes. The various AP shapes are determined by the difference in the type and number of ion channels expressed on the plasma membrane. In general, AP can be defined as slow, peculiar of nodal cells (SAN and AVN), or rapid, typical of atria, ventricular conduction system and working myocardium.

- Rapid action potentials

The rapid AP consists in five phases, that can vary according to the specific type of CM:

- *Phase 0* is the fast depolarization generated from a huge and fast inflow of Na+ ions mediated by the opening of voltage-gated sodium channels. This brings the membrane potential from ~-70 mV, the threshold potential for the Na^+ channels opening, to ~+40 mV where the sodium channels inactivate generating a fast transient depolarizing current. The voltage-dependent inactivation determines the absolute refractory period, i.e. the time in which the cells cannot be re-excited, independently of the magnitude of the stimulus.
- *Phase 1* is a partial repolarization phase, due to the Transient Outward Potassium current (I_{to}), that brings the membrane potential close to 0 mV.
- phase 2 or Plateau phase is characterized by a stable membrane potential around 0 mV, due to a balance between the inflow of calcium and outflow of potassium. During this phase, the calcium entrance through the L-type channels starts the excitation-contraction coupling (ECC - see Excitation contraction coupling paragraph below) and thus allowing transduction of the AP into force generation. phase 2 finish when the potassium currents become preponderant starting phase 3.

- Phase 3 or repolarization phases, where various outgoing potassium currents bring back the membrane voltage to the resting potential (-90 mV); these conductances are the ultra-rapid delayed rectifier (I_{Kur}, only in the atrium), the slow delayed rectifier (I_{Ks}) and the rapid delayed rectifier (I_{Kr}).
- phase 4, the membrane potential is kept to a voltage defined as “resting”, by the Inward Rectifier potassium current (I_{K1}) that act as a “voltage buffer” preventing at weak oscillations of membrane voltage to give rise to an AP.

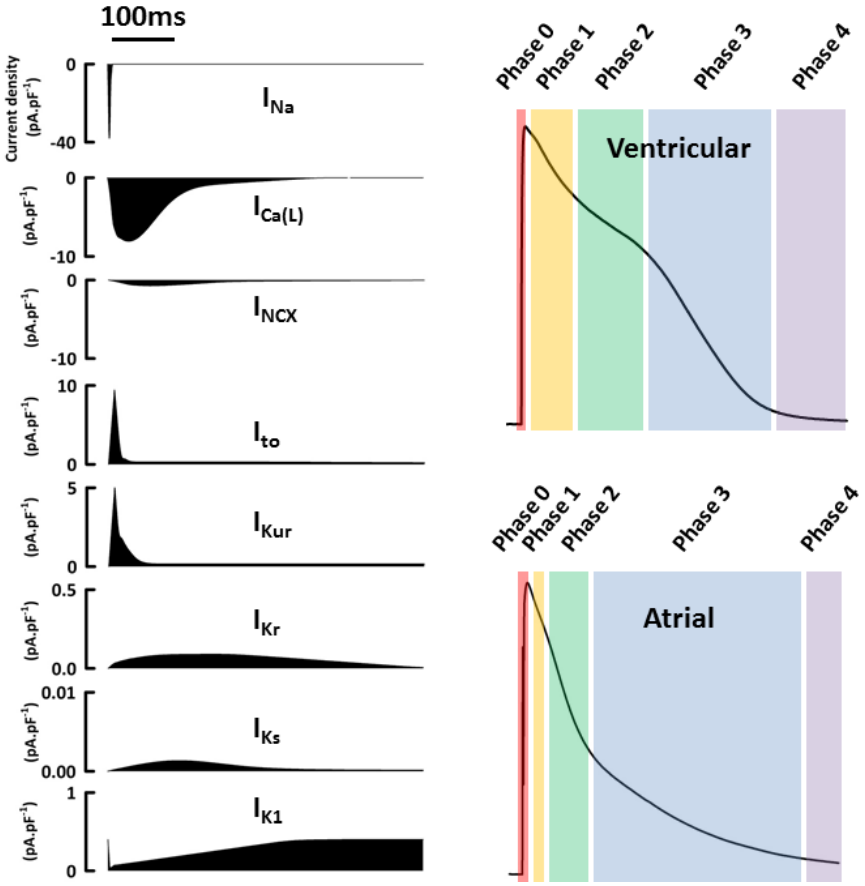

Figure 4: Currents responsible for atrial and ventricular action potential. From: PeaBrainC, CC BY-SA 4.0 <https://creativecommons.org/licenses/by-sa/4.0>, via Wikimedia Commons.

- *Slow action potentials*

These kind of action potentials differs under various aspect from the fast ones: first, the phase 0 is mostly mediated by the L-type calcium channel, that lead a slower depolarization compared to that due to sodium channels, and thus conferring the name of “slow” to these APs. Depending on the species, there could also be a contribution of sodium channels to this phase (e.g in the mouse), but it is not the predominant one. Second, there is no phase 1 and not a proper phase 2, since there is no I_{to} and all the calcium channels, that opened towards the end of phase 4 and during phase 0, are inactivating. Third, nodal cells do not have a resting membrane potential and during phase 4 display a slow depolarization (called slow diastolic depolarization, DD or pacemaker depolarization) where the potential is slowly brought to the threshold of firing. This happens thanks to the lack of I_{K1} and to activation of different conductances: the first half of the DD is determined by the activation of the *funny* (I_f) current[25]; the second half of the DD is due to the activation of T-type calcium channels[26], RYR2 channels, Na^+/Ca^{2+} exchangers (NCX)[27] and L-type channels.

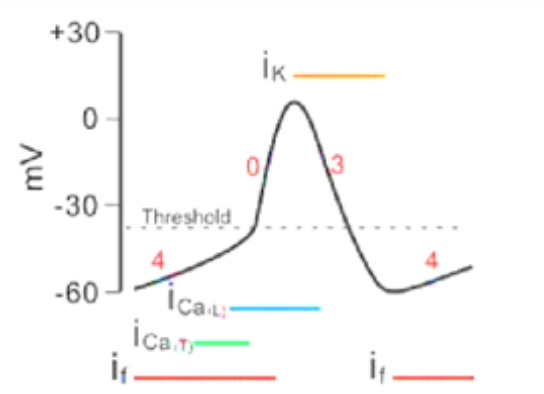

Figure 5: schematic sinoatrial node action potential and conductances underling it.

Ion currents/channels responsible of the APs

As previously mentioned, AP shape is the mirror of the underling conductances. Thus, in cases of mutation/alteration that can alter the cardiac functionality, analysis of APs can broadly guide and help to discriminate what to base the research on. For this reason, among all the ion currents and channels mentioned above, this thesis attention has been directed on certain conductances. The molecular and functional properties of the currents analyzed here are reported below.

Funny current (I_f)

It has been discovered more than 40 years ago, specifically linked to the pacemaker mechanism of autorhythmic cells and was defined funny because of its peculiar properties. Although the role of this current has been mainly studied in brain and heart, it is now well demonstrated that it is variously expressed all over the body[15]. The funny current (I_f) is the main conductance acting during the slow diastolic depolarization, guaranteeing the autorhythmic properties to SAN cells and in general to all the CMs of the conduction system. For this reason, it is also called pacemaker current. I_f molecular mediators are the HCN channels (Hyperpolarization activated Cyclic Nucleotide-gated channels), a family of protein made up four members (HCN1-4) In the heart HCN1, 2 and 4 are differentially expressed in various parts[28], while HCN3 expression has been so far only shown during development[29] is almost absent. These channels conduct a mixed Na^+/K^+ current with a permeability ratio 1:3, respectively. The HCN2 and 4 isoforms are slightly permeable also to calcium[30]. Their role is to activate at hyperpolarized voltages (<-50 mV), that is at the end of the AP repolarization) and bring the membrane potential to the take off potential triggering the AP initiation.

In the heart, the HCN4 isoform is the main subunit; its functional alteration such as, loss-of-functions and gain of function mutations have been variously associated to pathology regarding cardiac arrhythmias as sinus node dysfunction[31], familial sinus bradycardia[32], familial Inappropriate Sinus[33], bradycardia[34] and atrioventricular block[35]. Moreover, I_f has been found altered also in familial atrial fibrillation context[36].

Sodium current (I_{Na})

Voltage-gated sodium channels (NaV) play a critical role in generation of action potential in excitable cells. In mammals, NaV channels belong to a family composed by nine members (Nav1.1–Nav1.9) encoded by same number of genes (SCN1A–SCN11A)[37]. The main role of NaV channels is to induce a fast depolarization of the membrane. They are widely expressed in the nervous systems with the exception of the isoforms Nav1.5 and Nav1.4, which are the cardiac and skeletal muscle isoforms, respectively [38]. Nav1.5 is composed by an α –subunit of approximately 220 kDa that forms the pore, associated with two regulatory β-subunits (β1-β4) of 30 kDa each[39,40]. These channels mediate a fast activation/inactivating inward sodium current (Na^+) that start cardiac AP (Phase 0), as previously described. Their inactivation does not allow the channel to open again at depolarized voltages, determining the refractory period, i.e., the time during which a cell cannot be induced to fire an AP, independently of the magnitude of the stimulus. The recovery from inactivation occurs during the repolarization of the membrane, establishing a protection mechanism.

Mutations in this channel have been linked to several syndromes, leading to sudden cardiac death such as Brugada and long QT syndromes[41].

L-type calcium current (I_{CaL})

The L-type Calcium channels belongs to a voltage-dependent calcium channels family, they are structurally formed by an α1 subunit constituting the pore always associated with

auxiliary subunits (β, α2δ and γ) and calmodulin to assemble the fully functional channel. Depending on the different α1 subunits, these channels have four isoforms (CaV1.1, CaV1.2, CaV1.3 or CaV1.4) that differ for the affinity to dihydropyridines. These channels mediate a calcium influx that start CICR (calcium-induced calcium release) that mediate the excitation contraction coupling (ECC). These channels activate fast (but slower than sodium current) and present a calcium-calmodulin dependent inactivation whose modulation determine the magnitude of the calcium current into the cell, and in the current name “L” stands for “long lasting” referring to their relatively long duration of activation.

These channels are variously expressed all over the body; CaV1.2 and CaV1.3 isoforms are expressed in the heart level, but they are found also in the brain and endocrine cells[42]. CaV1.2 is the isoform responsible for the EC coupling in the working myocardium, while CaV1.3 is also found in SAN and atria[43]. These channels contribute also to the phase 0, specifically in the center of rabbit SAN and not in its periphery[44].

Mutations in these channels are associated with several cardiac arrhythmias, such as long QT syndrome 8, Brugada syndrome, Idiopathic ventricular fibrillation and early repolarization syndrome (for a review see [45]).

Rapid Voltage-Gated Delayed Rectifier Potassium current (I_{Kr})

Rapid Voltage-Gated Delayed Rectifier Potassium channel belongs to Voltage-Gated Delayed Rectifier Potassium channel family, as molecular counterpart of the rapid potassium current I_{Kr}. The channel is composed by an α –subunit called hERG (KCNH2) that co-assembles with a β-subunit called MiRP1 (KCNE2). I_{Kr} is a voltage-dependent current activated in depolarization around -20 mV. Its role occurs during the late repolarization phase 3, having a crucial role in avoiding arrhythmias; indeed, mutation in these channels

subunit, mainly a loss of function, are variously linked to arrhythmias, as congenital long-QT syndrome types, LQT2[46] and LQT6[47] or SQT syndrome[48].

Ultra-Rapid Voltage-Gated Delayed Rectifier Potassium current (I_{Kur})

Another component of the Voltage-Gated Delayed Rectifier Potassium channels are the Ultra-rapid potassium channels also known as Kv1.5, encoded by KCNA5 gene. These channels activate very fast while inactivate slowly, mediating an outward potassium current that contribute to the initial repolarization during phase 3. I_{Kur} is specifically expressed in the atria CMs in humans and dogs, while it is expressed also in the ventricle in mice. The channel is usually associates with ancillary Kvβ subunit (Kvβ1.2, 1.3, 2.1 and 3) that can change the activation and inactivation properties as well as sensitivity to redox state. *KCNA5* loss-of-function mutations are linked to familial atrial fibrillation[49,50].

GENERAL MATERIALS AND METHODS

Maintenance and cardiac differentiation of mESc lines

Mouse embryonic stem cells (mESc) lines, kindly provide by Dr Alessandra Rossini (EURAC research center, Bolzano), were maintained in suspension in the presence of 10^3 U/mL of Leukemia Inhibitory Factor (LIF) in the medium (see table 1), to maintain pluripotency. Cells were dissociated into single cells twice a week using both Tryple Express (Thermo Fisher Scientific), and a mechanical gentle resuspension, then either plated at a density of 5000 cells/cm^2 in mouse ES medium or differentiated (see below).

Cardiac differentiation was induced with the hanging drop technique as previously described[8,51], plating 25.000 cells per mL of differentiation medium (table 2) in drops of 20 µL in the bottom of a 100 mm plate and then kept upside-down to allow the embryoid bodies (EBs) formation. After 7 days (day 7) the EBs were plated on gelatin coated TC dish (Sarstedt). EBs start then to show spontaneously beating portions around day 9. At day 12/13 beating areas of EBs were mechanically dissected and dissociated into single cardiomyocytes (mCMs) with a physiological solution containing 500 U/mL of collagenase IIB (sigma). After 30' of incubation single cells were plated on 35 mm dish (cellstar) coated with gelatin in differentiation medium and refreshed after 24h.

mESc medium		
	Initial Conc/MW	**Final Conc**
KO-DMEM	up to the volume	
β-mercaptoethanol	10 mM	100 µM
NEA	100X	1X
Pen/Strep	100X	1X
KO-SR	15%	
L-glutamine	200 mM	2 mM
LIF	Lot specific	10^3 U/mL

Differentiation medium		
	Initial Conc/MW	**Final Conc.**
DMEM	up to the volume	
β-mercaptoethanol	10 mM	100 µM
NEA	100X	1X
NaPyr	100 mM	1 mM
Pen/Strep	100X	1X
FBS	20%	
L-AA	50 mg/mL	20 µg/mL
L-glutamine	200 mM	4 mM

Tables 1 and 2: mediums compositions.

Drugs treatment for microtubule rearrangement

Before patch-clamp analysis, dissociated mCMs were incubated for 4 hours[52] with either Taxol 10 μM dissolved in DMSO or Colchicine 10 μM dissolved in ETOH. As control conditions, mCMs were incubated for the same time with the appropriate solvent.

Maintenance of hiPSc lines and cardiac differentiation.

Human iPSc lines, kindly provided by Professor Patrizia Dell'Era at Università degli studi di Brescia, have been previously generated both from healthy donors[36,53] and from PBMC obtained from a 24 years-old patient with atrial fibrillation and a PITX2 gain-of-function heterozygous point mutation (A→G; rs138163892), which cause the replacement of a methionine with a valine[54,55]. An isogenic control line, in which the mutation has been reverted to WT, has been also generated. hIPScs were maintained on Matrigel-coated plates in mTeSR-E8 medium (Stem Cell Technologies), and cells were passaged by single cells dissociation using tryple Express (Thermo Fisher ScientIfic) every 5 days and seeded at the density of 20.000 cells/cm^2.

To obtain pacemaker-like cardiomyocytes (hpCMs), we used the standard cardiac differentiation using the PSC Cardiomyocyte Differentiation Kit (Thermo Fisher Scientific) on hiPSc monolayers, following manufacturer's instructions. For obtaining atrial-like cardiomyocytes (haCMs) we used the STEMdiff Atrial Cardiomyocyte Differentiation Kit (Voden). CMs were maintained in culture for 20 days for Seahorse experiments and 30 days for molecular and electrophysiological analysis.

hpCMs clusters were dissociated with Trypsin-EDTA (Sigma) at 37° for 5 minutes, and gently resuspended; single haCMs were dissociated after incubation for 10 minutes in Trypsin-EDTA, and a gentle resuspension. Trypsin was inhibited with medium containing

FBS (10%), and then clusters/cells were plated on 35 mm dish (cellstar) coated with 1 µg/cm^2 Fibronectin (Corning).

Electrophysiology on mCMs, hpCMs and haCMs

	Solution A (mM)	Solution B (mM)	Solution C (mM)	Solution D (mM) Tyrode spencer
NaCl	140	110		137
KCl	5.4	30		5
CaCl2	1.8	1.8	2	2
MgCl2	1	0.5	1	1
Hepes	5	5	25	10
glucose	5.5			10
NMDG			130	
4-AP			10	
pH	7.4 with NaOH	7.4 with NaOH	7.4 with NaOH	7.4 with NaOH

Table 3: extracellular solution

Patch-clamp analysis in whole cell configuration were performed after 24-48 hours after isolation, using different extracellular solution (see table 3) depending on the needs and the cellular type, while patch pipettes were filled with the following intracellular-like solutions:

- for mCMs: 130 KAsp, 10 NaCl, 10 K-HEPES, 2 NaATP, 5 EGTA-KOH, 2 MgCl2, 2 $CaCl_2$, 5 CP, 0.1 GTP (mM) with pH 7.2.
- for hpCMs and haCMs: 120 KCl, 20 Na-HEPES, 10 MgATP, 0.1 EGTA-KOH, 2 $MgCl_2$ (mM) with pH 7.1.

Action potentials (APs) were recorded from spontaneously beating single mCMs, haCMs or hpCMs using patch pipettes of 4-7 MΩ, and evaluated for parameter as:

- BPM: the number of action potentials per minutes.
- Maximal diastolic potential (MDP, mV): most hyperpolarized voltage reached at the endo of autorhythmic APs.

- Action potential amplitude (APA - mV): defined as the difference between the AP peak and MDP.
- Upstroke velocity (V/s): calculated as dV/dt max, indicate the steepness of the phase 0.
- Action potential duration (APD) at different repolarization times (APD - ms): time taken by action potential to repolarize to 30, 50 or 90 percent of the resting values (APD30, 50, 90).
- Action potential duration corrected on frequency (APDc, ms): APD normalized to the rate using Bazett equation

$$APD90c = APD90/\sqrt{IBI}$$

IBI is the inter-beat-interval, the average time that occurs between two potentials.

To evaluate the action potential rate under adrenergic stimulation, hpCMs clusters were superfused with Isoproterenol 100 nM dissolved in solution A.

The "Funny" current (I_f) was recorded adding $BaCl_2$ (1 mM) and $MnCl_2$ (2 mM) to the solution A for mCMs or to solution D for haCMs (table 3) to minimize interference from K^+ and Ca^{2+}, currents using patch pipettes of 4-7 MΩ. Starting from a holding potential (hp) of -30 mV, I_f was activated applying 10 mV hyperpolarizing voltage steps to the range -35/-125 mV long enough to reach steady-state activation, followed by a fully activating step at -125 mV. Steady-state current density-voltage relation was calculated as the ratio between current amplitude and cell capacitance at all voltages. Activation curves were obtained from normalized tail currents and fitted to the Boltzmann equation as described below where $V_{1/2}$ is the half-activation voltage and s the inverse slope factor (ISF):

$$y = 1/\left(1 + exp\left(\left(V - V_{1/2}\right)/s\right)\right)$$

Activation time constants (τ) were calculated by fitting traces to a single exponential curve in the range -75/-125 mV, after an initial delay.

The rapid potassium current (I_{Kr}) is evaluated as E4031-sensitive current (1 mM - a specific blocker of I_{Kr}) in extracellular solution B (table 3), using patch pipettes of 4-7 MΩ. From a hp of -60 mV, a voltage step to +20 mV is given to activate and inactivate the channels (inactivation rate Is faster than activation and thus no current is developed). Voltage steps to the range +30/-110 mV are then applied; since the rate of recovery from inactivation is faster than the rate of deactivation, this part of the protocol allows I_{Kr} channel to recover and the current recorded. A third step to -60 mV is then delivered in order to obtain the activation curve, as described above.

Ultra-rapid potassium current (I_{Kur}) is measured as 4-AP (50 μM) -sensitive current using patch pipettes of 4-7 MΩ. Starting from hp of -55 mV, a pre-step to -45 mV is provided to inactivate the Na channels. Then hyperpolarizing steps spanning in the range of -40/+50 mV are applied to record the I_{Kur} I-V relationship.

The L-type calcium current is recorded as the Nifedipine-sensitive component (10 μM nifedipine– a specific L-type Ca channel blocker) in the extracellular solution C (for mCMs), or solution D (for haCMs) (table 3) TTX 10 μM was also added to exclude/minimize the contribution of the sodium current. Starting from a hp of -70, I_{CaL} was elicited by applying depolarizing steps from -60 to +50 mV, followed by a single step to 0 mV. The tail current at 0 mV was used to obtain the inactivation curve.

Sodium current is measured in extracellular solution A for mCMs of Solution D for haCMs, as described in table 3 in the presence of Nifedipine (10 μM) to block L-type calcium current. Sodium current is evaluated as the TTX 30 μM-sensitive component patch pipettes were in the range of 2-3 MΩ. From an hp of -90 mV the current was activated with depolarizing steps

in the range of -80/+30. The inactivation curve is then obtained from tails current elicited by a subsequent step at -20 mV Both activation and inactivation curves were fitted, as with the other channels, to the Boltzmann equation.

Seahorse analysis

haCMs at day 19 of differentiation have been dissociated to single cells as previously described and seeded in a XF24 cell culture plate at the density of 30000 cells/well, following manufactures instructions. The following day, after the cartridge calibration, cells are wash in XF Real-Time ATP Rate Assay Media (final volume 500 µL) and subject to the experiment. Seahorse calculate the mitochondrial and glycolytic ATP production rate using the oxygen consumption rate (OCR) and the extracellular acidification rate (ECAR) parameter variation in presence of metabolic modulators:

- Oligomycin (1,5 µM): an inhibitor of mitochondrial ATP synthesis.
- Rotenone + antimycin A (0,5 µM): for inducing a complete inhibition of mitochondrial respiration.

Basal OCR and ECAR were first measured, mitoATP production rate were measured after OCR-lowering oligomycin injection while the glycoATP production rate was calculated combining basal ECAR, the buffer factor of the assay medium and mitochondrial-associated acidification after the addition of Rotenone + antimycin A.

qPCR gene expression analysis

RNA samples were extracted from day 28-30 hpCMs/haCMs through Direct-zol RNA Miniprep kit following manufactures instruction; 1 µg of RNA was retrotranscribed to cDNA with Maxima First Strand cDNA Synthesis for RT-qPCR Kit and samples subjected to temperature cycles as follows: 25°C for 10’; 50°C for 15’; 85°C for 5’. To quantify the gene expression q-PCR were performed with SYBR Green PCR Master Mix kit as followed:

- SYBR® Green (2X): 10 µL
- Primer Forward+Reverse (10 µM): 1 µL
- MilliQ water: up to the volume
- cDNA samples: 10 ng

For each gene, whose primers are reported in table 4, every sample was analyzed in triplicate and in addition a negative control where the cDNA was substitute with milliQ water. They were subjected to the following temperature cycles:

1. Activation of HotStarTaq DNA Polymerase: 95°C for 5'.
2. Denaturation phase: 95°C for 15''.
3. Annealing and extension phases: 60°C for 30''.
4. Melting stages: 95° for 15", then 60° for 15" followed by 95° per 15".

Steps 2 and 3 were repeated for 45 times. Results had been analysed using the formula: $2^{-\Delta CT} \times 100$, were ΔCt was the average Ct of the tree samples divided by the housekeeping gene (actin beta). To normalize for variability in cardiomyocytes yield among the various samples, the genes of interest expression was further normalised to cardiac troponin expression (cTNT).

Gene	Primer Forward	Primer Reverse
PITX2A	5'-GCGTGTGTGCAATTAGAGAAAGA	5'-CCGACGATTCTTGAACCAAA
PITX2B	5'-CCAGCAGCAAGTTCTTCCC	5'-CCGACGATTCTTGAACCAAA
PITX2C	5'-CCGCAGAGAAAGATAAAAGCCA	5'-GATTTCTTCGCGTGTGGACA
MYL2	5'-CTGCAGAGAGCTGGGCGGAG	5'-CACTCGCCCAAGGGCAGCAA
MYL7	5'-GGAGTTCAAAGAAGCCTTCAGC	5'-AAAGAGCGTGAGGAAGACGG
MYH6	5'-CTGCGGCCCAGATTCTTCAGGAT	5'-AGTGCGAATGTCAAAGGGCCGG
MYH7	5'-CTTGAGTAGCCCAGGCAGGCACAGCC	5'- CCTGGTCTGCGCTTCTAGCCG
cTNT	5'-AAGCCCAGGTCGTTCATGCCC	5'-CTCCATGCGCTTCCGGTGGA
ACTB	5'-CACTCTTCCAGCCTTCCTTC	5'-AGTGATCTCCTTCTGCATCCT
NR2F2	5'-CCGGGTGGTCGCCTTTATG	5'-GCTTTCCACATGGGCTAGATC
KCNA5	5'-TTCTACCACCGGGAAACGGA	5'-TTCGGGCACTGTCTGGATTC
SLN	5'-CTCTTCAGGTGAGGAGA	5'-AAACAGCTCCCGGGTGTTTA
HK2	5'-ATCCAGAGGAGAGGGGACTT	5'-TCATGGTCCCAACTGTGTCA
CPT1A	5'-GCCCTGAGACGGGGATTAT	5'-GGTGATGTCCATGGTCTCCT
HADHB	5'-GCTGTCCAGACCAAAACGAA	5'-CAAACCCGAAGTGCCAGAC
PGC1A	5'-TGCTCTGTGTCACTGTGGAT	5'-CAGCACACTCGATGTCACTC
CPT1B	5'-AGTGAACCCGAGCTGTGC	5'-CCAGGAGTTGATCCCAGACA
RPL13A	5'-TAGCTGCCCCACAAAACC	5'-TGCCGTCAAACACCCTTGAG

Tables 4: primers sequences forward and reverse.

Statistics

Data were analyzed with Clampfit 10 (Molecular Devices) and Origin Pro 9 (OriginLab). Groups were compared with student t-test. $P < 0.05$ defines statistical significance. Data are presented as mean ± SEM.

STRIATIN KNOCK-OUT INCREASES SODIUM CURRENT IN mESc-DERIVED CMs THROUGH MICROTUBULE DESTABILIZATION.

INTRODUCTION

Striatin protein structure

Striatin (STRN) is a 780 amino acid protein, belonging to a scaffold protein family whose role is to mediate protein-protein interactions. The family is composed by three members, with high homology and very similar structure and intracellular localization: striatin (STRN), S/G2 nuclear autoantigen (STRN3), and zinedin, (STRN4). STRN present 4 functional domains: a caveolin-binding domain, a coiled-coil domain, a Ca^{2+}-calmodulin (CaM)-binding domain, and a Tryptophan- Aspartate repeat domain[56] (figure 6).

The *caveolin-binding domain* motif is located at N-terminal of the protein, where three consensus (φXXXXφXXφ) is highly conserved in STRN homologs from many species. It particularly interacts with Caveolins, a family of protein whose role is structural constituting membrane microdomain named Caveolae. Caveolae functions, among others, is to group together proteins that has to interact in order to facilitate the functional interactions[57]. STRN is well known to interact with caveolin-1[56], the isoform expressed almost ubiquitously in the body, but Nader and colleagues also demonstrated its association with the muscle specific Caveolin-3[58].

The α-helical coiled-coils domain is the oligomerization site of STRN, where a dimer/trimer parallel disposition is more likely to happen, but it is not to be excluded the dimer anti-parallel conformation. This domain seems to be necessary for the binding of STRN-associated proteins such as PP2A (Protein phosphatase 2) and CTTNBP2 (cortactin binding protein 2), and moreover seems to be essential for the right targeting of STRN at synapsis level[59].

STRN binds to calmodulin in a Calcium dependent manner thanks to the *Ca^{2+}-calmodulin (CaM)-binding domain*, even though its role in the calcium signaling is not clear yet, it is likely to function as intracellular calcium sensor. It seems that Ca^{2+}-CaM binding reduces interaction with Cav-1 thus altering STRN subcellular localization[56]. The negative binding regulation of Ca^{2+}-CaM domain affects also on others STRN-binding partners such as Mst3 and Mst4[60]. Tryptophan-Aspartate (WD) domain is a highly conserved motif repeat domain at level of c-terminal, whose role is supposed to help creating a stable structure for striatin-associated proteins docking[61].

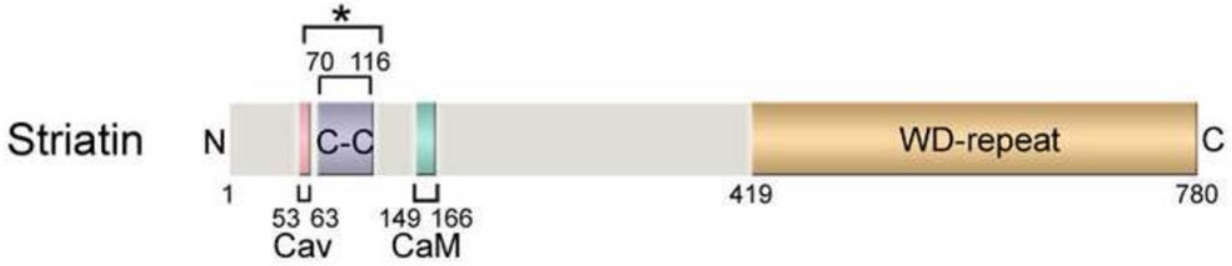

Figure 6: STRN protein structure from Hwang et al., 2014

STRN expression and functionality

It has been firstly found to be abundantly expressed in the rat brain at striatum level (from here its name)[62]; It is well expressed in various tissue such as brain, lung, liver, kidney, testes, B and T lymphocytes, fibroblasts, skeletal muscle and heart[56,63]. In mammals, STRN is the core of large protein complexes, that depending on the interacting partners were called STRIPAK or STRIPAK-like (STRN interacting phosphatase and kinase complexes). The classic STRIPAK complexes core contains PP2A, a kinase belonging to GCKIII subfamily Mst (Mst3, Mst4, Ysk), cerebral cavernous malformation 3 (Ccm3) protein, and striatin interacting proteins 1 and 2 (STRIP1/STRIP2). Additionally, proteins such as cortactin-binding protein 2 family member (CTTNBP2 and CTTNBP2NL), sarcolemmal membrane-associated protein (SLMAP) and a suppressor of IKKε (SIKE) family member are present in

the complexes in a mutually exclusive member, forming thus different STRIPAK complexes (Figure 7). If PP2A and a kinase lack, the complex is called STRIPAK-like.

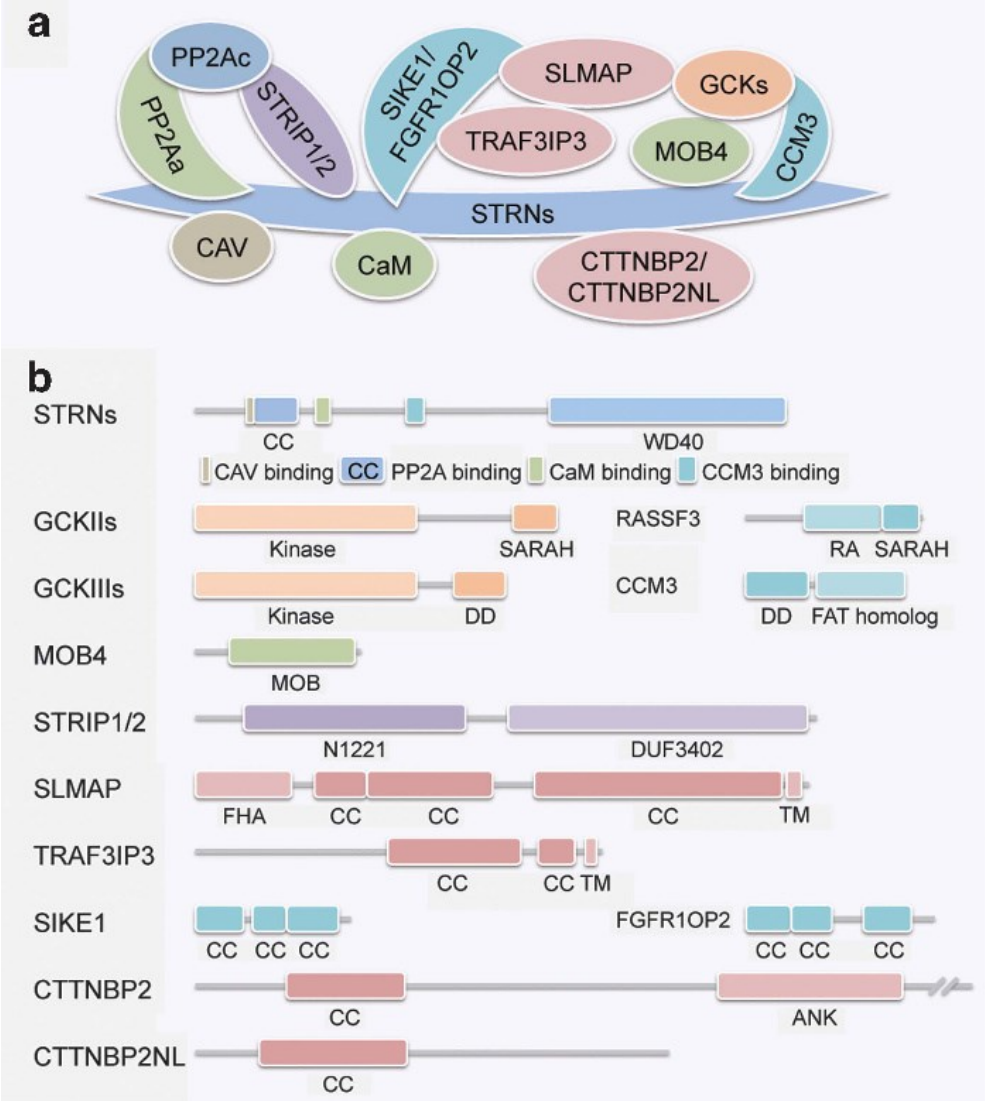

Figure7: STRIPAK complexes from Shi et al., 2016

Thanks to these multiprotein aggregates, Striatin has been involved in many subcellular pathways such as signaling, cell cycle control, apoptosis, vesicular trafficking, Golgi assembly, cell polarity, cell adhesion, cell migration, and mechanical stability[56,63], however its physiological role highly depends on the cellular context and its associated proteins.

The role of STRN in the heart is not completely understood and in the CMs it is often associated with the SLMAP protein at level of intercalated discs (ICDs), desmosomes, T-tubules, caveolae and sarcoplasmic reticulum[63], all key structures for CMs proper

functionality. Indeed, GWAS study found significant association between genetic locus of STRN with QRS interval[64]. It is known that SLMAP in mouse heart have a structural role binding myofibrils and having a regulatory function on excitation-contraction coupling at sarcoplasmatic reticulum ant t-tubules levels: its overexpression leads to an irregular ECG due to an impairment of left ventricle functionality[65,66]. Since STRN colocalize with SLMAP exactly at sarcoplasmatic reticulum ant t-tubules levels, it is not hard to imagine a plausible role of STRN in those pathways, maybe mediated by SLMAP (figure 8).

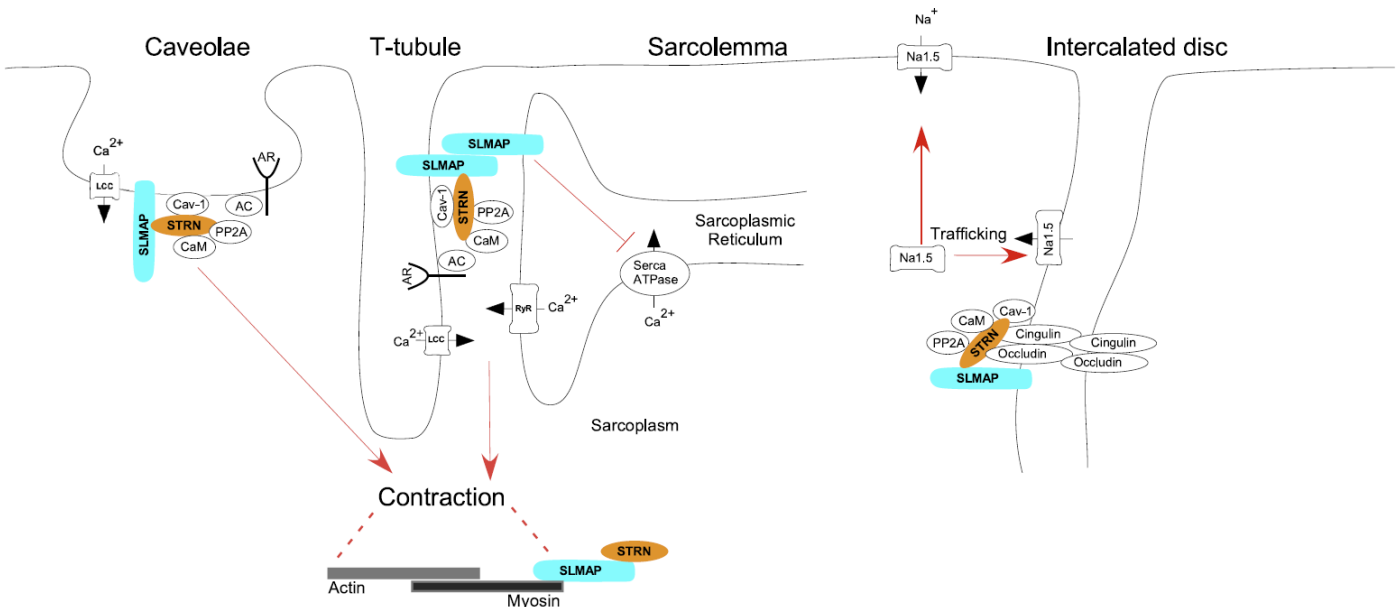

Figure 8: representative scheme of STRN localization in CMs. From Nader et al., 2019

Anyhow, STRN contribution is more easily appreciated in pathological conditions: silencing STRN gene leads to a reduction of tight junction proteins expressions in heterologous cellular model (ZO-1, E-cadherin, and occluding) and its mutation/deletion was associated with arrhythmogenic right ventricular cardiomyopathy (ARVC) and dilated cardiomyopathy (DCM) in a canine model [67–70]. Moreover, STRN presence at ICDs and tight junction level suggest a role in the transmission of action potential. It also seems that STRN alters the rate of contraction, indeed altered level of STRN changed the contraction rate of neonatal rat ventricular cardiomyocytes through modulating the stability of Cav-3/CaM complex in a calcium sensitive manner[58]. In support of this, many important bindings partner of STRN

such as Caveolin-1and -3, Calmodulin, and PP2A are involved in the electrical and mechanical regulation of cardiomyocytes.

STRN and microtubules

Microtubules are polarized polymers composed by heterodimer of α and β-tubulin subunits, whose peculiarity resides in its structural dynamism alternating state of shrink to growth (rescue) and growth to shrink (catastrophe)[71]. These two states result from the assembly (polymerization) and disassembly (depolymerization) of tubulin heterodimer at plus and minus ends respectively.

They play essential roles in many cellular processes, including cell division and migration, maintenance of cell shape, positioning of cellular compartments, and transportation of membranous organelles and vesicles[72]. Microtubules, as a main element of the cardiomyocyte cytoskeleton, interact with proteins such as GTP-binding proteins (e.g. Gi and Gs proteins), microtubule-associated proteins (MAPs), molecular motors like kinesin[73].

MAPs regulate assembly, dynamism, and stability of microtubules, according to their phosphorylation state: dephosphorylated MAPs associate with microtubules and increasing their assembly and stability while phosphorylated MAPs has the opposite effect[74]. One of the phosphatases that regulate MAPs phosphorylation state is the Protein phosphatase 2 (PP2A), one of the known STRN interacting proteins. Of particular interest is that downregulation of STRN in heterologous cell model (HEK) leads to hyperphosphorylation of MAP2 and to a consequent depolymerization of microtubules[75]. Moreover, another STRIPAK component is related to microtubules dynamism: CTTNBP2 colocalizes with microtubules increasing their stability at rat hippocampal neurons level, stimulating microtubules bundle formation. On the contrary, its loss reduces dendritic arborization through an impaired microtubules acetylation[76].

It is known that cytoskeleton is involved in the trafficking, targeting and expression of cardiac ion channels[77,78]. This is clearly demonstrated by the application of drugs that modulate the microtubules state: nocodazole, a microtubules destabilizer, doubled the amplitude of the ultra-rapid potassium current in rat atrial myocytes, the transient outward potassium current and the rapid potassium current in ventricular myocytes. Instead, it reduced the inward rectifier potassium currents[78]. The chemotherapy drug Taxol, which promote tubulin polymerization and thus microtubules stabilization, has been found to reduce sarcolemmal sodium channel expression and thus sodium current density [79] and to alter channels' kinetic properties[80]. Colchicine, a microtubule depolymerizing agent, increased I_{Na} (in a GTP dependent manner)[52], while it seemed not to affect the activation properties of the current[80].

Because of the role of microtubules in the channel trafficking and taking account that STRN indirectly modulate microtubules state and has a scaffolding role in focal points for CMs functionality, it is plausible to imagine STRN as a structural portion of the modulatory machinery of the electrical activity in the cardiomyocytes.

AIM

STRN is a scaffolding protein crucial in many intracellular processes, in cardiomyocytes it seems to localize at sarcolemma, intercalated discs, caveolae and t-tubules, and its loss has been associated with heart dysfunctions indicating an involvement in cardiomyocytes patho-physiology. How STRN loss impair cardiomyocytes functionality associated with arrhythmias is not fully understood, hence we propose a complete electrophysiological characterization of mESc-derived cardiomyocytes (mCMs) in which STRN has been knocked out. We further analysed the link between STRN loss, microtubules polymerization state and sodium current, to explore a possible pathological mechanism and thus identify a plausible therapeutic target.

RESULTS

Spontaneous action potentials

Figure 9a shows representative traces of spontaneous action potential recorded from WT (n=12) and STRN-KO (n=9) mCMs. On these traces we conducted the analysis of various parameters of the APs, depicted in the dot plots of panels b, c, d and e. Rate analysis revealed that STRN-KO mCMs had an higher beating rate compared to the WT ones (5.52±0.63 Hz vs. 3.91±0.34 Hz; p=0.026); another parameter that significantly differed in STRN-KO mCMs is the phase zero's slope that was higher than in WT mCMs (dV/dt max: 12.84±1.59 V/s vs. 7.52±1.00 V/s), suggesting an alteration in the conductances participating to this phase of the AP. The MDP and APA were not altered from the absence

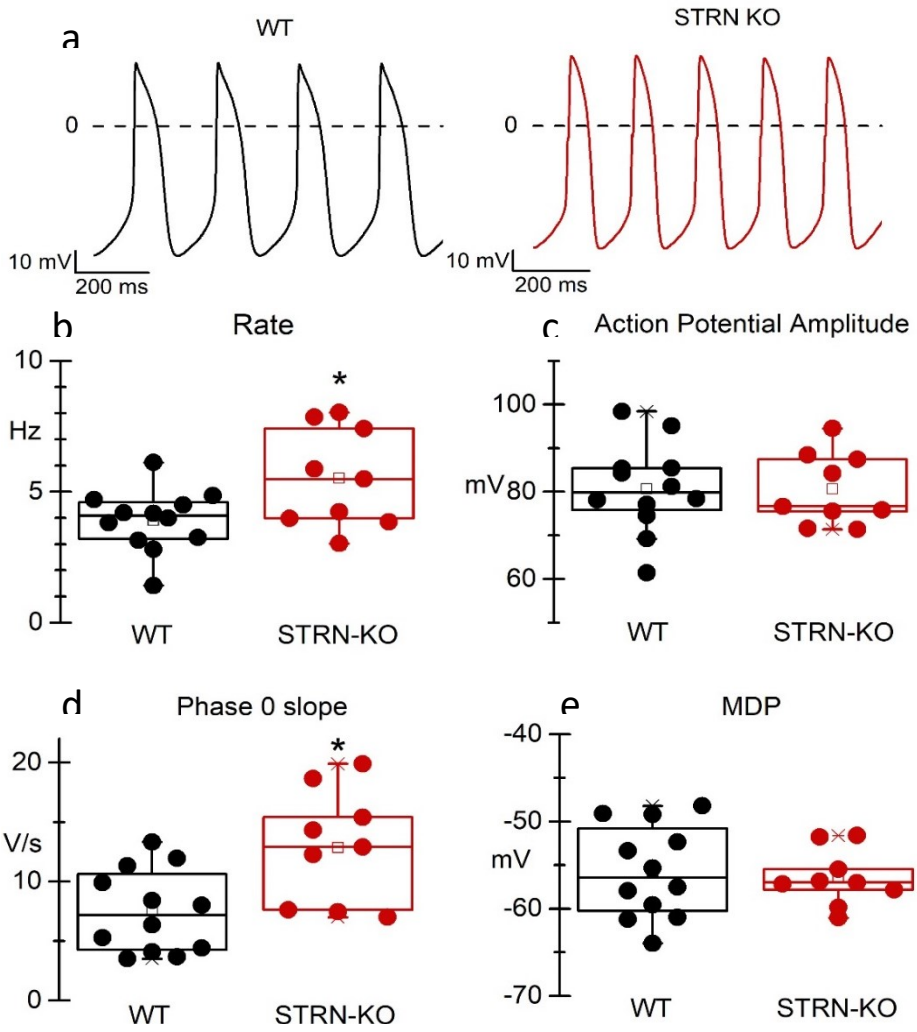

Figure 9: representative traces of WT (Black) and STRN-KO (Red) CMs(a); Boxes plot of rate (b), APA (c), Phase 0 slope (d)

of STRN (MDP: -56.51±1.06 mV vs -55.73±1.53 mV. APA: 80.62±2.75 mV vs. 80.70±2.95 mV. STRN-KO and WT, respectively).

Characterization of ionic currents underline action potential in mCMs

The Funny current

The funny current I_f is the main conductance that drives the slow diastolic depolarization and thus concurs to spontaneously and repetitively generate APs thus setting the beating rate[69]. Both the representative traces and the IV plot (figure 10a and b) show that I_f of STRN-KO mCMs did not differ from that of WT mCMs (maximal conductance: 0.155 ± 0.035 nS n=12 vs. 0.153 ± 0.037 nS n=11 respectively). Kinetic properties also did not change as

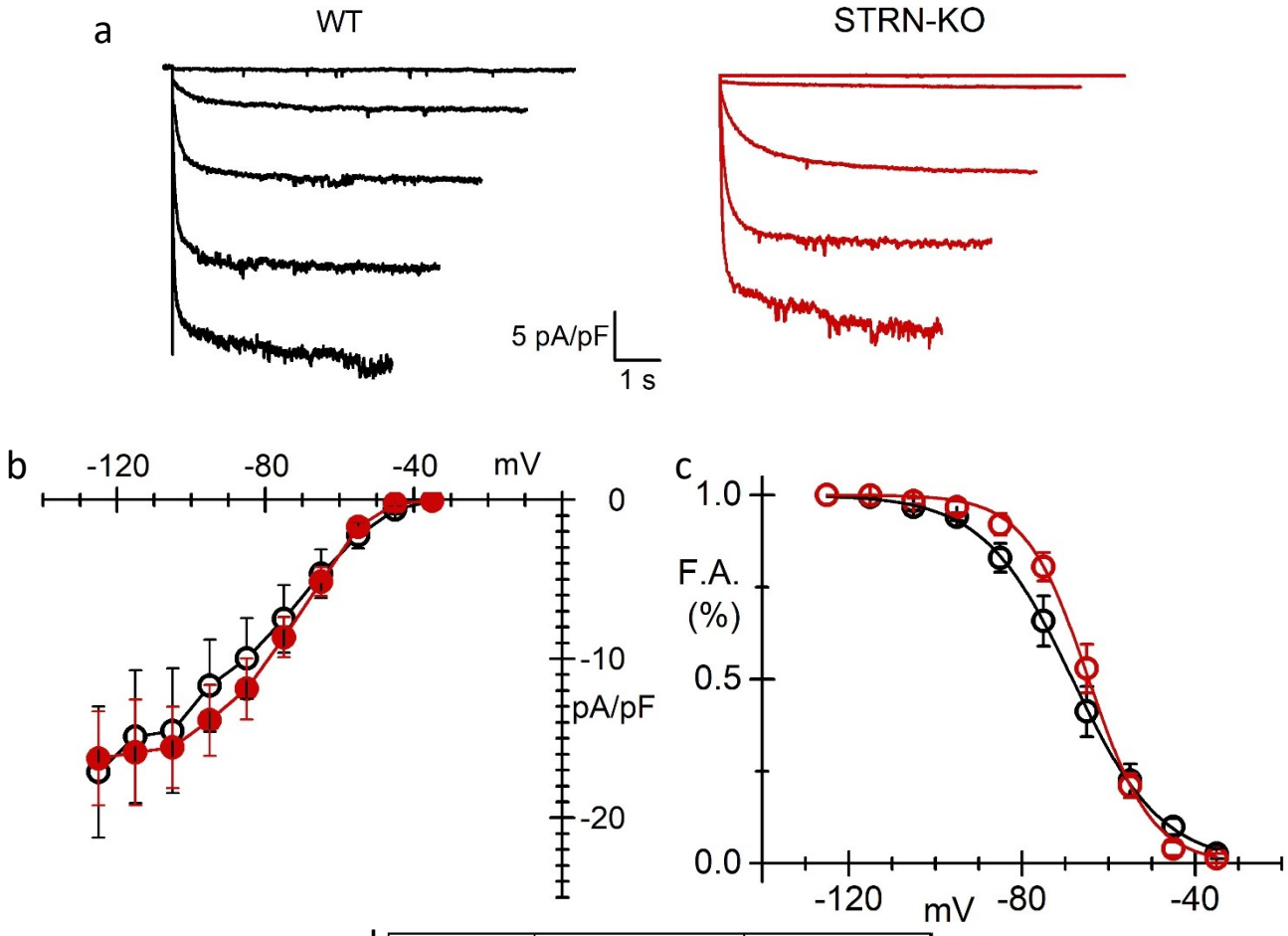

d

	V_{half} (mV)	ISF
STRN-KO	-64.01 ± 1.85	6.67 ± 0.57
WT	-68.52 ± 2.25	8.22 ±0.69

Figure 10: I-V relationship of If current density (a); Activation curves (b); AC parameter table (c).

evident by similar values of both the V_{half} and inverse slope factor obtained from the activation curves (figure 10c and d).

L-type calcium current

Another conductance that can contribute both to the slow diastolic depolarization, (specifically in the pacemaker cells, and to the phase two of the action potential, in the myocardial cardiomyocytes, is the L-type calcium current. Figure 11a shows representative traces recorded from WT and STRN-KO mCMs. I-V curves indicate that the current density did not vary significantly in the KO condition compared to WT (figure 11b); the current densities at +10 mV were: -7.46± 0.76 pA/pF (n=10), -9.58 ± 1.19 pA/pF (n=12) in STRN-

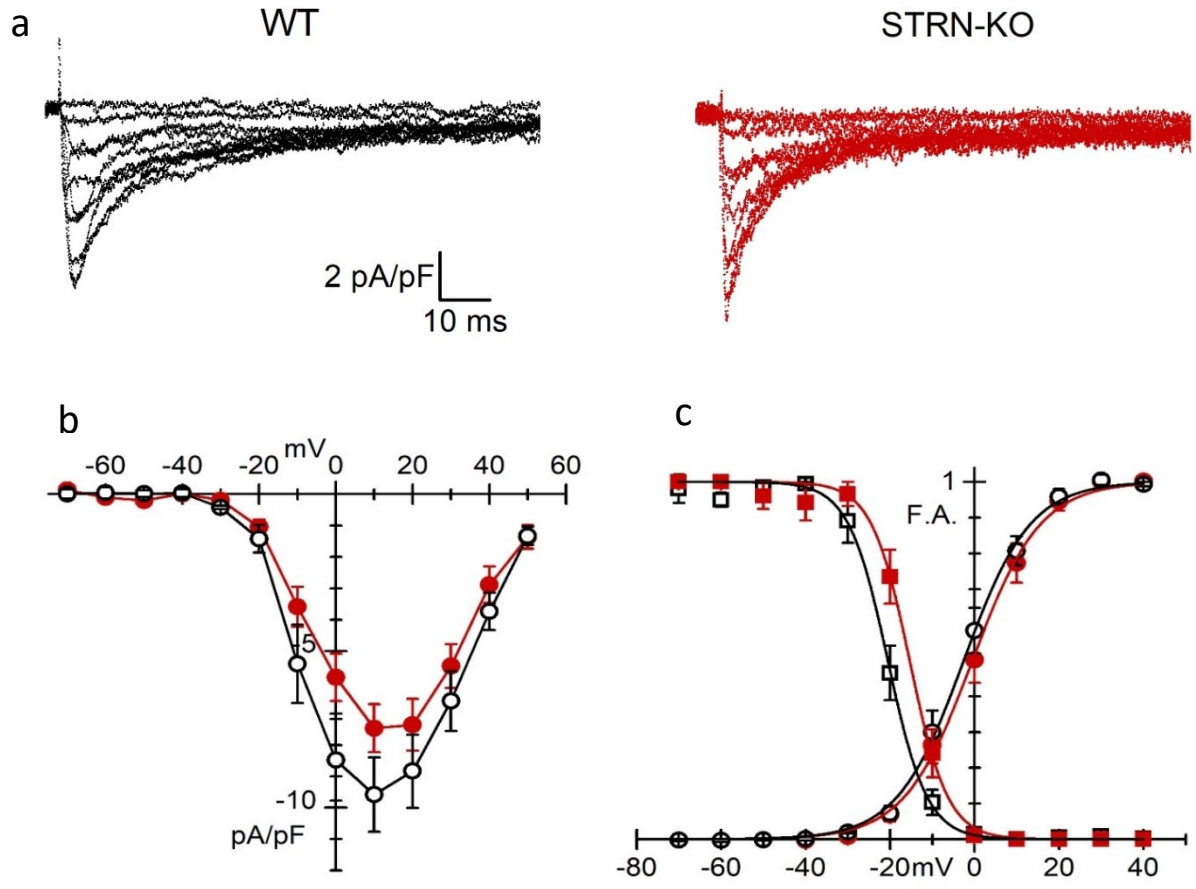

d

	Vhalf AC (mV)	ISF AC	Vhalf IC (mV)	ISF IC
STRN-KO	0.17±2.20	6.93±0.48	-15.79±1.67	4.26±0.16
WT	-2.19±2.14	6.76±0.33	-20.23±1.43	4.27±0.86

Figure 11: representative traces of I_{CaL} WT (Black) and STRN-KO (Red) CMs (a); I-V relationship of I_{CaL} current density (b); Activation curves (circles) and Inactivation curves (squares) (c); table of AC and IC parameter table (d).

KO CMs and WT CMs, respectively. The activation and inactivation properties did not change either, as shown in figure 11b and from the V_{half} and the inverse slope factor (s) in the insert table (figure 11c and d).

Rapid potassium current

Rapid potassium current is one of the most important conductances in the repolarization, the phase 3 of AP. As can be seen from both representative traces, I-V relationship, and activation curves (figure 12a, b and c) there is no differences between I_{Kr} in the STRN-KO

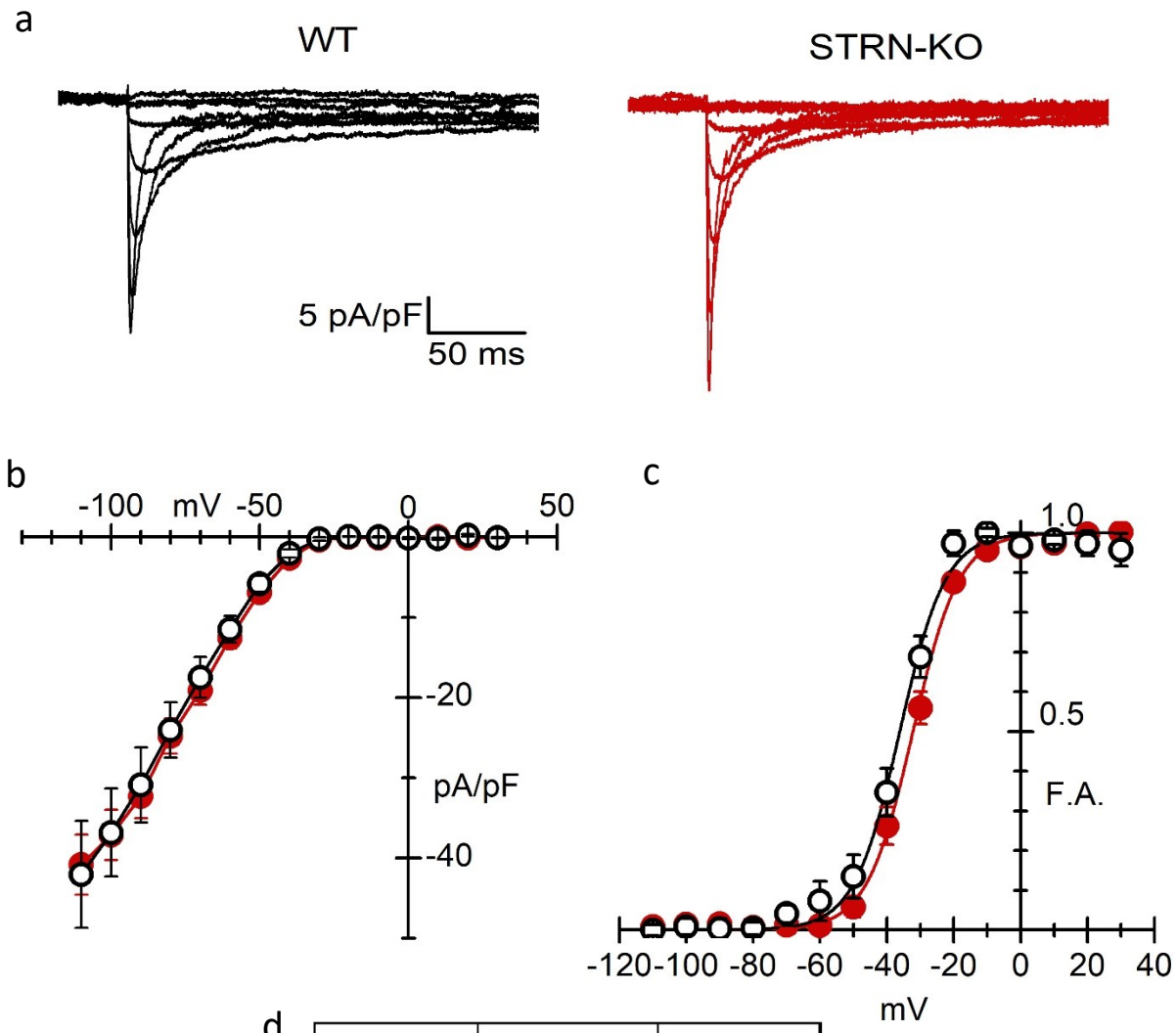

d

	V_{half} (mV)	ISF
STRN-KO	32.81±1.28	5.69±0.41
WT	35.25±1.30	5.39±0.28

Figure128: representative traces of I_{Kr} WT (Black) and STRN-KO (Red) CMs (a). I-V relationship (b); Activation curves (c) and table with AC parameter (d)

mCMs and WT mCMs. The current densities at -110 mV were -40.83 ± 3.74 pA/pF n=16 for STRN-KO mCMs and -42.03±6.69 pA/pF n=23 for WT mCMs, while activation curve parameters are plotted in the table (figure 12d).

Sodium current

Sodium current has been analyzed given its importance in determining phase 0 of Action Potentials and, as can be appreciate both from representative traces and I-V relationship (figure 13a and b), current density in STRN-KO mCMs was almost twice that in WT mCMs (at -20 mV: - 189.24± 38.58 pA/pF n=14 vs. -96.18 ± 21.66 pA/pF n=13, respectively). Kinetic

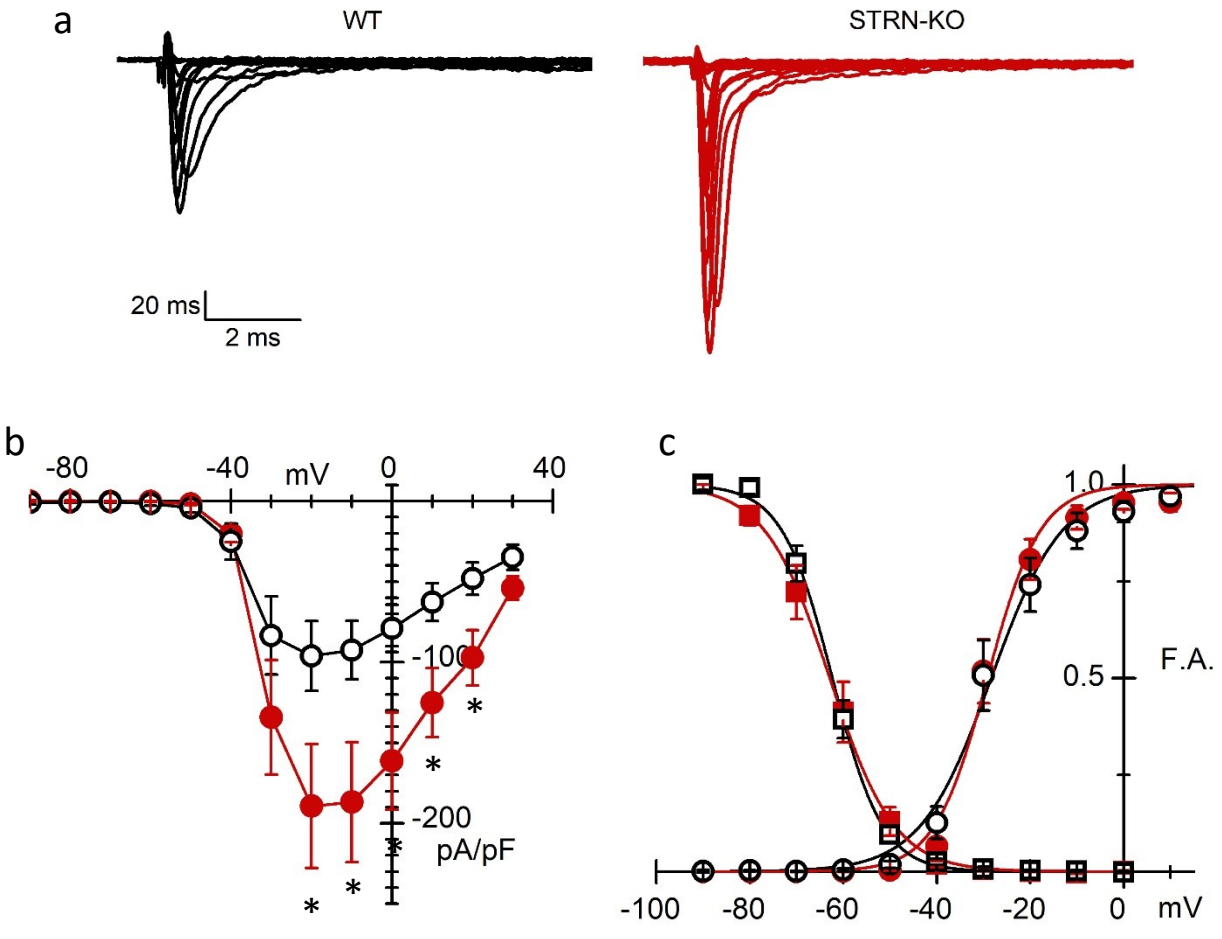

d

	Vhalf AC (mV)	ISF AC	Vhalf IC (mV)	ISF IC
STRN-KO	-28.00±1.63	4.65±0.75	-63.00±2.12	5.14±0.27
WT	-28.06±2.80	5.26±0.84	-62.71±1.31	4.83±0.29

Figure 13: representative traces of I_{Na} WT (Black) and STRN-KO (Red) CMs (a). I-V relationship of I_{Na} current density (b); Activation curves (circles) and Inactivation curves (squares) (c); table of AC and IC parameter (d).

properties, plotted in figure 13c, did not change as evident from the activation and inactivation curves whose parameter are reported in the table (figure 13d).

Microtubule dysregulation effect on sodium current

Considering the role of microtubules in sodium channel trafficking and the STRN role in microtubules regulation, we hypothesized that microtubules may represent the "missing link" between lack of STRN and sodium channels gain of function. We evaluated the sodium current in WT and STRN-KO mCMs after incubating cells with either Taxol that stabilize microtubules or Colchicine, which instead destabilize microtubules.

Although the high variability of these preliminary data, they show that sodium current is not significantly altered in WT CMs neither after Taxol treatment (at -20 mV -113.22 ± 32.27 pA/pF n=5 vs. -70.87 ± 28.67 pA/pF n=6 taxol vs DMSO), nor after colchicine treatment (at -20 -250.35 ± 108.41 pA/pF n=5 vs. -230.39 ± 77.29 n=5 pA/pF Colchicine vs EtOH) as represented in figure 14a and B.

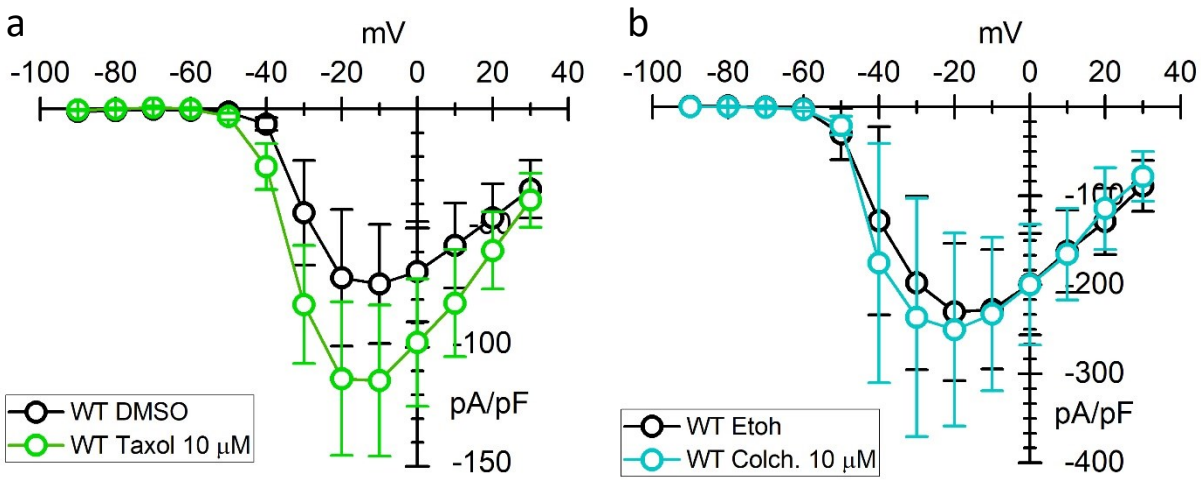

Figure 14: I-V relationship of WT I_{Na} current density after Taxol (green) or DMSO (Black) treatment (a) and after Colchicine (light blue) or ethanol (Black) treatment (b).

On the other hand, Taxol significantly decreased sodium current density in STR-KO mCMs (at -20 -56.99 ± 10.14 mV n=7 vs. -134.05 ± 38.25 n=7 mV Taxol vs DMSO), while colchicine has no significant effect (at -20 -184.88 ± 71.13 mV n=8 vs. -105.42 ± 36.20 n=4 mV Colchicine vs EtOH) as can be seen in figure 15.

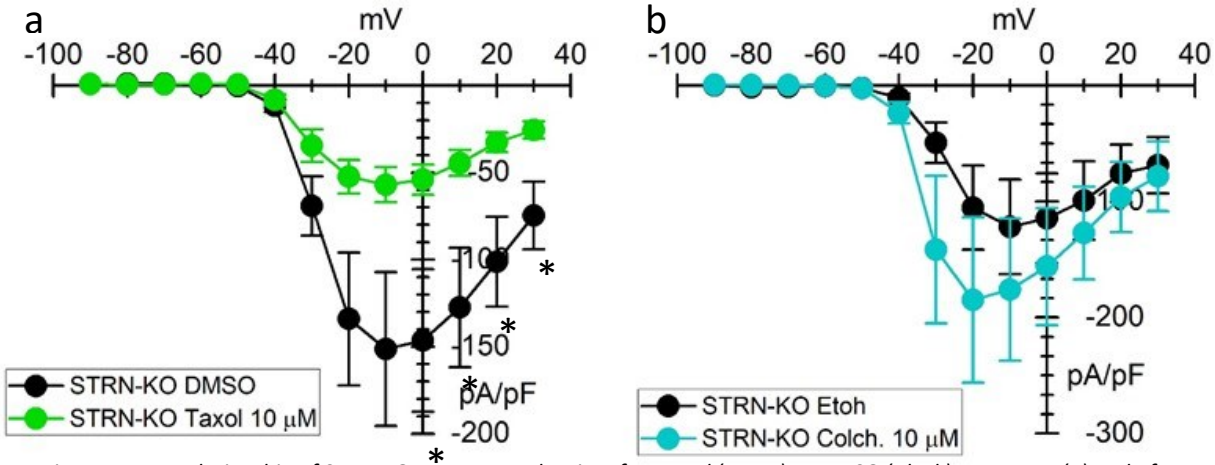

Figure 15: I-V relationship of STRN-KO I_{Na} current density after Taxol (green) or DMSO (Black) treatment (a) and after Colchicine (light blue) or ethanol (Black) treatment (b).

DISCUSSION

In the heart Striatin plays an important role in forming multiprotein complexes, which take part in AP generation, contraction, and cell-cell junctions. Even though striatin absence or downregulation associates with cardiac diseases, the specific mechanisms are still not clear. Data showed above demonstrated that the lack of STRN gene can lead to significant alterations of cardiomyocytes electrophysiological activity predisposing cardiomyocytes to arrhythmias. Here I used mESc as a convenient model to produce cardiomyocytes to study the functional electrical alteration induced by lack of striatin. Spontaneous action potentials generated from single STRN-KO mCMs had a significantly higher rate compared to WT mCMs. This evidence seems to disagree with literature data, in which overexpression of STRN in neonatal rat ventricular cardiomyocytes led to an increased spontaneous contractility while sh-RNA mediated striatin knockdown reduced it[46]. Usually, a higher contraction rate is associated with a higher AP frequency. This discrepancy can be explained by previous data obtained by our collaborators at EURAC research center using a video contraction detection analysis, that showed that the STRN-KO cardiomyocytes had an enhanced probability to develop abortive contractile events compared to WT mCMs (data not shown), and thus coherent with the reduction of a contraction rate reported in literature. This can suggest a dysregulation in the Excitation Contraction Coupling (ECC) mechanism.

In order to explain the increased rate in STRN-KO cardiomyocytes we evaluated the Funny current due to the important role of this conductance in driving the slow diastolic depolarization and the bradycardic and tachycardic phenotypes associated with loss of function and gain of function mutations of HCN4, respectively[20,21]. However, no differences neither in current density nor in the kinetic properties were observed, concluding that the higher rate it is not due to an increased I_f current. Another conductance known to participate at setting the rate of pacemaker cells is the L-type calcium channel[70]. Also, in this case we

did not find differences in neither current density nor in activation curve, concluding that STRN lack did not affect this conductance contribution. The third depolarizing current analyzed was the fast-activating sodium current; This current also has been shown to contribute to spontaneous rate[71]. Moreover, it is important to recall that in STRN-KO mCMs the slope (dV/dt) of the fast depolarization phase 0, a parameter known to be determined by the sodium current, was significantly larger. Interestingly, the significant increase found in sodium current density in the STRN-KO mCMs, without changes neither in its activation nor inactivation curves could be at the basis of both increased rate and increased dV/dt. An increased current density is often associated with a higher number of channels to the membrane or a much less common increase in pore conductance; considering the association of STRN with caveolin proteins, the role of caveolin/caveolae in ion channel trafficking, and the fact that sodium channels have been reported in caveolae, it is likely that the increase is due to alterations of sodium channel trafficking to and/or from the plasma membrane. In literature, there is no evidence of a direct association between STRN and sodium channels; indirect pieces of evidence suggest however that both localize at sarcolemma and intercalated discs (ID). Interestingly both have been found to interact with microtubules that, beside their structural role, are known to be involved in the trafficking of the newly synthesized ion channels toward the cell surface, their anchoring, their endocytosis and backward trafficking/recycling[66]. Moreover, microtubule stabilization or destabilization directly alter sodium current density: Taxol decreased[67] while Colchicine increased it[40]. Noteworthy, depolymerization of microtubules is also caused by lack of STRN, through hyperphosphorylation of MAP2[63]. Thus, experiment using the above-mentioned drugs aimed to identify whether the STRN-KO effect are mediated by microtubules. Preliminary data on WT mCMs treated with Taxol, a microtubule stabilizer, showed a tendency but not statistic reduction of the sodium current. Interestingly, in STRN-KO mCMs, Taxol significantly reduced the currents bringing the density values close to the

treated WT, suggesting that stabilization of microtubules in the STRN-KO context reverts the sodium channels gain of function. Microtubule destabilization by Colchicine on the contrary did not increase the sodium current density either in WT or STRN-KO mCMs. Although more data are needed to confirm this evidence, the lack of Colchicine effect may also be attributed to a technical problem since the drugs is diluted in ethanol that it has been shown to alter by itself the microtubules state[72]. An alternative strategy for investigating the effect of microtubule destabilization would be to use a different drug, such as nocodazole dissolved in DMSO.

In conclusion, my data show that the lack of STRN alters microtubules stability, this causes a significant increase in sodium current that alters the electrical profile of mCMs, inducing a higher beating rate, a faster upstroke velocity. All those conditions contribute to create an ideal arrhythmogenic substrate.

HIPSc-CMS FOR STUDYING A SPECIFIC MUTATION IN PITX2 GENE AND ITS ROLE IN ATRIAL FIBRILLATION ONSET.

INTRODUCTION

Structure and functions

PITX2 (Paired-like homeodomain transcription factor 2) gene encodes for a family of transcription factors, composed by four different isoforms: PITX2A, PITX2B, PITX2C and PITX2D, generated by the alternative splicing of 6 exons of the *PITX2* gene, located on chromosome 4q25[81]. Exons 1, 2, 5 and 6 encode for PITX2A, a 271 aa. protein, while the B isoform derives from alternative splicing of exons 1, 2, 3, 5 and 6, obtaining a longer protein of 317 aa; PITX2C is a protein of 324 aa, encoded by exons 4, 5, and 6, while the D isoform, a 205 aa protein, is derived from the alternative splicing of exon 5 and 6 (figure 16).

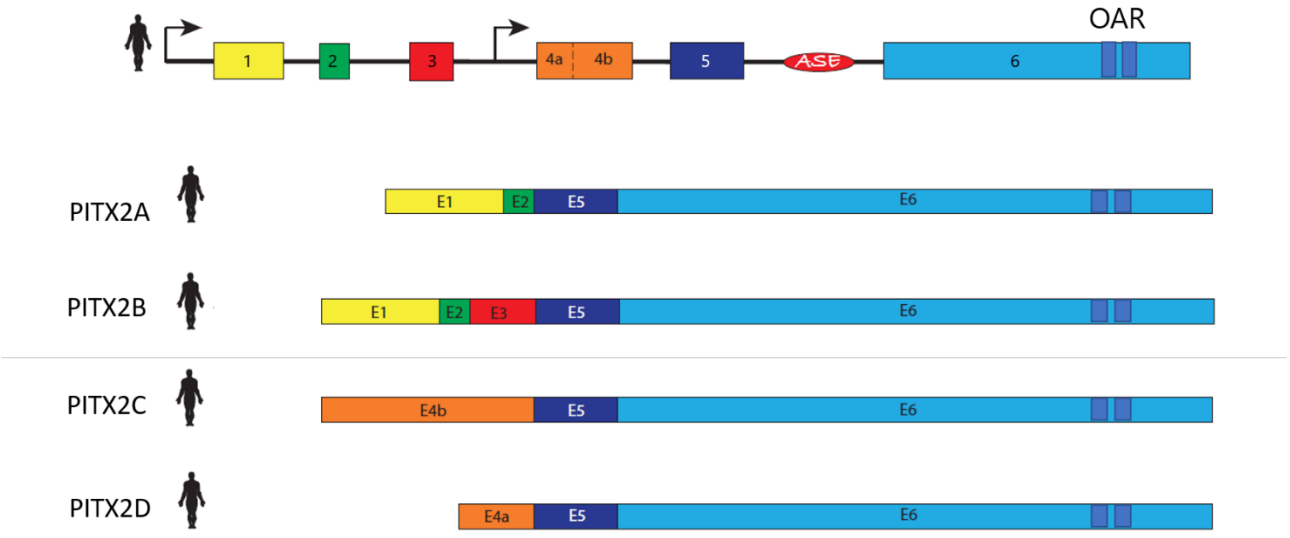

Figure 16: Schematic representation of the gene structure of the 4 human isoforms of the PITX2 gene; Above is the full structure of PITX2; Below is represented the gene structure of the isoforms, with the N-terminal domain, the DNA binding domain, the C-terminal domain and the OAR domain; (modified from Franco et al., 2017).

Structurally, the N-terminal domain differs in all the isoforms while there is a common and pivotal homeodomain (HD) sequence used for DNA binding, fully conserved in the isoform A, B and C. PITX2D, present only in humans, has an incomplete HD which appears to act

more likely as a dominant negative of isoforms A and C than as an appropriate transcription factor. All isoforms share a common C-terminal region, whose presence is fundamental for the transcriptional factor role, since contains a transcriptional activation site. In the same position there is also a highly conserved OAR domain, the function of which is uncertain but appears to be involved in the protein-protein interaction[81].

PITX2 family, plays a fundamental role during the embryonic development, regulating the asymmetry of some organs and the embryonic looping. Indeed, PITX2 is downstream to the Shh/Nodal expression, transducing the left-right asymmetry signal[82–84]. Nodal activates PITX2C expression during the formation of the left mesodermal lateral plate, remaining expressed in the organs that derive from it, like the intestine and the heart[83]. During heart development, PITX2C is expressed in the left portion of the primitive heart tube, remaining later confined to the left atrium[85]. PITX2C inhibit the genetic pathway downstream to Short Stature Homeobox 2 (SHOX2), which through a cascade activation of transcription factor/channels led to sinoatrial node formation, while simultaneously inhibiting the cardiac chamber formation[86] (Figure 17).

The functional importance of this transcription factor has been investigated in a murine model. The total deletion of PITX2 is lethal for the developing embryo, having several morphogenic defects[87]. The heart of PITX2-/- mice is devoided of the atrial septum and is perfectly symmetrical[87,88], effect that is more likely due to PITX2C lack, as specific PITX2C-/- mice have a similar phenotype, suggesting its importance in heart development[89]. Interestingly, the loss of PITX2C results in the lack of inhibition of SAN gene program thus allowing the formation of an ectopic pacemaker tissue also in the left atrium, making the left atrium identical to the right one[86,90]. Moreover, another phenotype of PITX2 lack, is the absence of the pumonary myocardium[90].

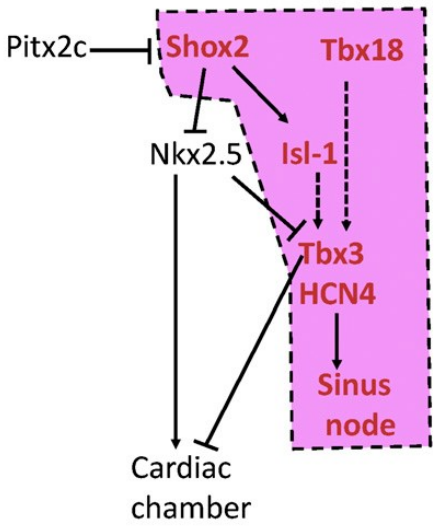

Figure 17: Schematic representation of the mechanisms underlying the formation of the NSA and of the heart chambers (modified from Barbuti et al., 2015).

PITX2 remains expressed also in both the adult mice and human heart, with a trend to decrease with age. Because of the pivotal role of this transcription factor in limiting the SAN gene programming and its association with the formation of the pulmonary myocardium, its involvement in the onset of cardiac pathologies linked to these areas, such as atrial fibrillation, is a likely scenario.

PITX2 and atrial fibrillation

Atrial fibrillation (AF) is the most common heart rhythm disorder whose incidence ranges from 1-2%, in the general population, to 10-12%, in the elderly (>80 years)[91]. In most cases, AF is a multifactorial disease, involving various risk factors such as aging, concomitant diseases, and lifestyle[92]. An Increasing wealth of data is pointing to the importance of a genetic predisposition/background for AF onset. Genomic analysis indicates that some genetic variations (SNP) increase of 22% the risk to develop an inheritable form ofAF[93]. Furthermore, having a first degree relative with paroxysmal AF increase by 40%the probability to develop the pathology[94]. GWAS (Genome-wide association sequencing) studies have identified variants located close to the PITX2 genetic locus as the most associated with early onset AF[95].

In humans, it has been observed that SNPs in PITX2 gene are associated with increased or decreased PITX2 expression levels[96,97]. PITX2C levels have been found either under- or overexpressed in atrial biopsies obtained from AF patients[98–100].

The reduced expression of this transcription factor hadùs been quite extensively studied in relation to its cardiac effects. In mouse Indeed, an atrial-specific deletion both in homozygosis and heterozygosis of PITX2 led to a higher susceptibility to arrhythmic events. Atria, of transgenic animals show a more depolarized resting membrane potential and a shorter action potential amplitude due to alteration in sodium and inward rectifier potassium channels properties[98,99].

Another group identified, in a condition of partial deletion of PITX2 in mouse, a shortening of the action potential duration (APD) a known arrhythmogenic substrate. This shortening has been linked to altered expression of several sarcoplasmatic ion channel and gap/tight junction proteins [101]. APD can be also modulated by L-type Calcium channels, and indeed, in PITX2 mutate mice L-type calcium current has been found decreased[102]. In atria of mice with a postnatal deletion of PITX2 a structural remodelling and damage of the intercalated discs has been noticed[103]. Indeed, One study linked a diminished PITX2 expression to a sarcoplasmatic reticulum CA2+ overload due to increased expression of calsequestrin and phospholamban proteins in spite of a decrease of L-type calcium channels[102]. Moreover, zebrafish with a complete loss-of-function of PITXC has impaired cardiac properties associated with an increased fibrotic and necrotic areas, developping arrhytmyas already at larvae stadium[104].

As previously mentioned, not only a decreased PITX2 expression, but also its increase is associated with the pathology: patient with chronic AF retain higher protein level compared to healthy controls. This induces a larger slow delayed rectifier potassium current (I_{Ks}) and

a diminished L-type calcium current. This relation has been confirmed by heterologous PITX2c overexpression in a murine cardiac cell line (HL-1)[100].

PITX2 gain-of-function confers reparative skills to adult mouse cardiomyocytes after myocardial injury, thanks to its capability of activating oxidative stress genes as NRF2, a regulator of antioxidant response[105]. A high REDOX stress and metabolic abnormalities are conditions causally correlated to AF pathogenesis[106,107]. According to this, Collins and colleagues found that in zebrafish, both gain and loss-of function of PITX2 modify the expression of oxidative phosphorylation and redox genen of atrial CMs, a change occured at early development stages, forerunning the arrhythmias onset[104].

AIM

Atrial fibrillation onset is usually seen as an interplay of various factors including comorbidities and lifestyle, despite this, genetic predisposition is gaining attention: PITX2 gene is highly correlated with AF occurrence; its expression is dysregulated in AF patients and it has been linked to molecular and electrical alterations likely able boost arrhythmias. In collaboration with Prof Dell'Era at University of Brescia and prof Olesen at Cohopenaghen hospital, we obtained an hiPSc line generated from a 24 y-o AF patient with a GOF mutation in PITX2. We used (and are using) this model to generate hiPSc-derived cardiomyocytes that will help to unravel the mechanism by which PITX2 gene mutation may trigger atrial fibrillation. Moreover, this will help to identify a plausible therapeutic target and thus pave the way to precision preventive medicine. In this preliminary phase of the molecular and functional characteriztion, we have compared:

- hiPSc-derived pacemaker cardiomyocytes, hpCMs (because the know inhibitory effect of PITX2C on sinoatrial genetic program) from the PITX2 line and from two unrelated healthy donors.
- hiPSc-derived atrial-like cardiomyocytes (haCMs) from the PITX2 line and from the reverted WT (REV) line that has been avilable only later.

RESULTS

PITX2 mutated hpCMs molecular characterization

After 30-35 days of differentiation, mRNA profile of hpCMs derived both from PITX2 and unrelated CTRLs has been analysed, starting from expression of PITX2A, PITX2B and PITX2C isoforms. As can be appreciated from figure 13 there is no difference between lines, indicating that the gain-of-function is not induced by an increased mRNA transcription. We have then evaluated the specific expression of cardiac troponin (cTNT) being equally express in the two hpCMs populations, indicating that GOF PITX2 mutation did not alter the differentiation efficiency (figure 18a).

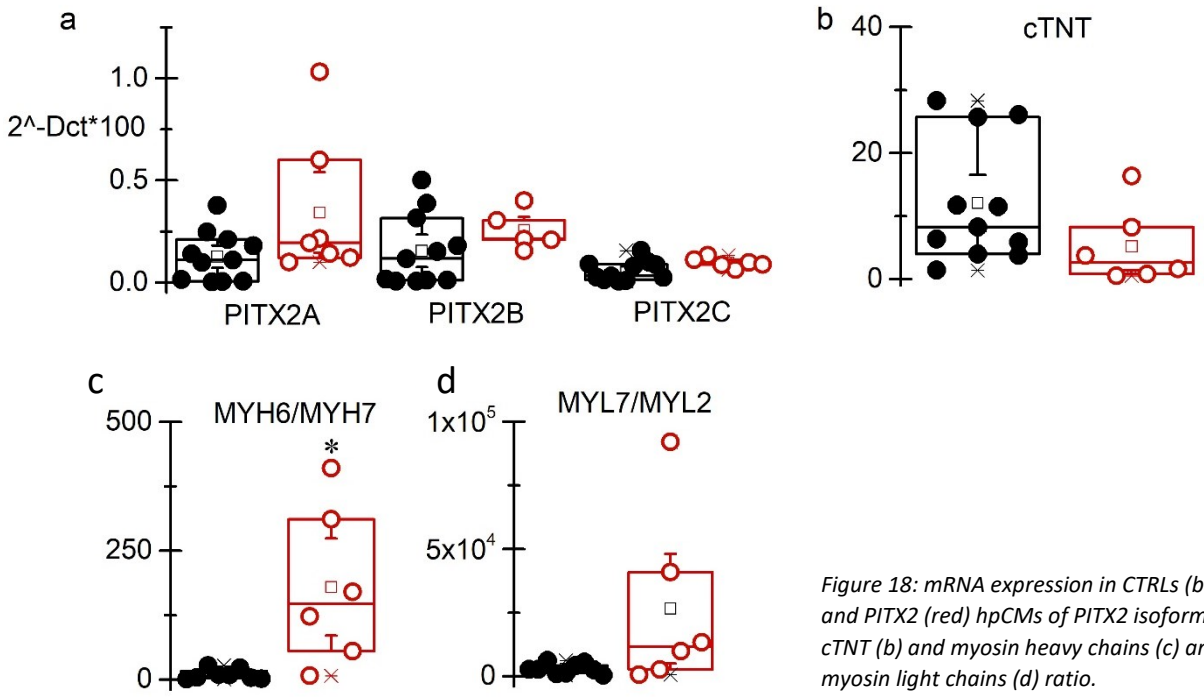

Figure 18: mRNA expression in CTRLs (black) and PITX2 (red) hpCMs of PITX2 isoforms (a) cTNT (b) and myosin heavy chains (c) and myosin light chains (d) ratio.

The expression of both atrial/ventricular myosin heavy chains (MYH6/MYH7) and myosin light chains (MYL7/MYL2) indicates a higher ratio, suggesting of a more immature/atrial phenotype of the PITX2-hpCMs, compared to the CTRLs (Figure 18 c d and e).

Electrophysiological analysis of pacemaker clusters

Action potentials have been recorded from n=62 CTRLs and n=45 PITX2-hpCMs small clusters; as can be seen from both representative traces and box plots (Figure 19 a and b), PITX2-hpCMs were bradycardic compared to CTRLs-hpCMs. Curiously AP duration at 50% and 90% corrected for the difference in rate (ADPc see material and methods), is shorter in

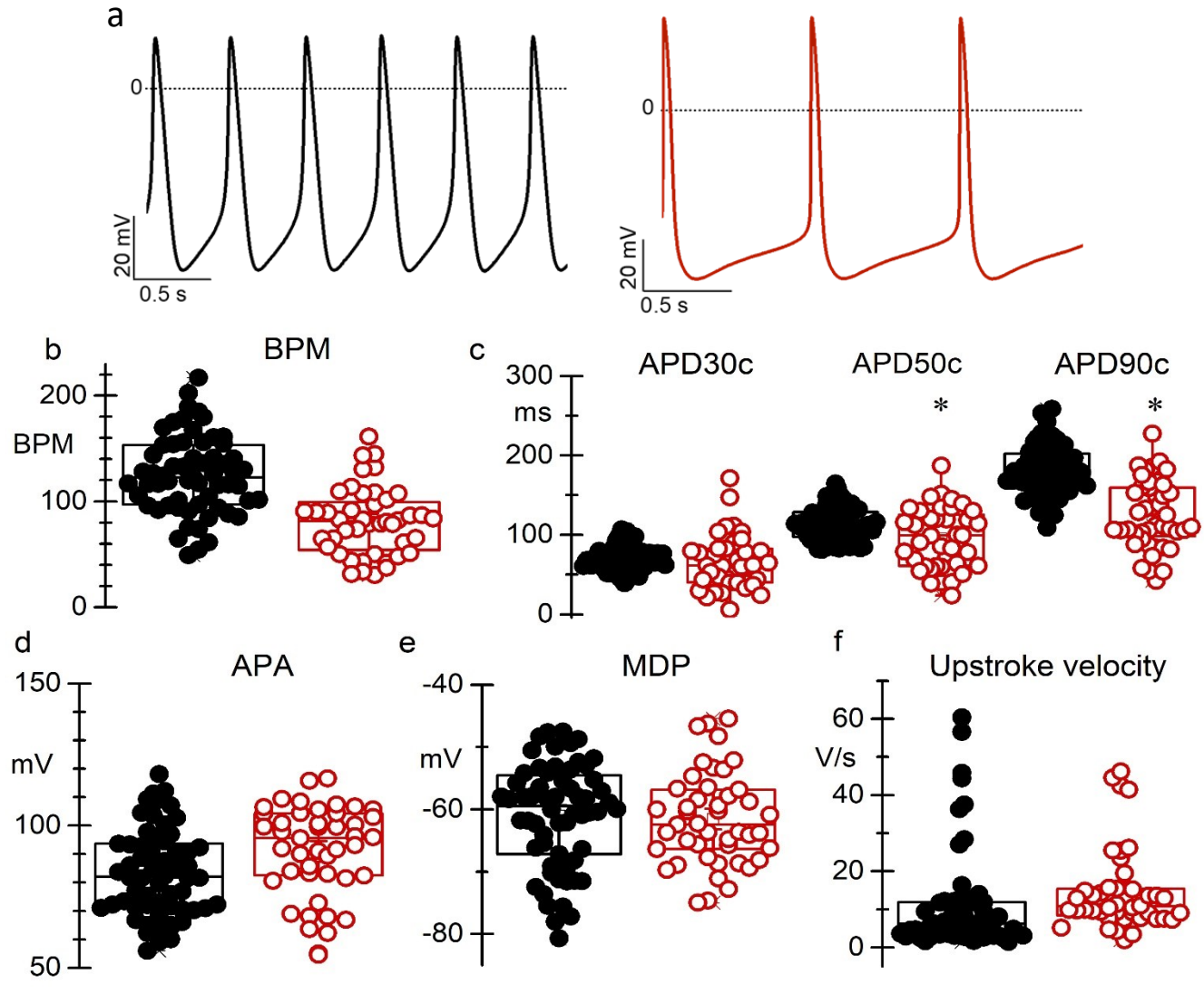

g

	BPM	APD30c (ms)	APD50c (ms)	APD90c (ms)	APA (mV)	MDP (mV)	dV/dt max
PITX2	80.91±4.81	65.32±5.52	95.58±6.02	124.79±6.46	90.92±2.41	-61.57±1.10	14.58±1.63
CTRLs	124.76±4.70	69.90±2.03	113.40±2.66	181.04±3.98	83.31±1.91	-60.97±1.06	11.05±1.70

Figure 19: representative traces of APs recorded CTRLs (Black) and PITX2 (red) hpCMs (a). Box plot of beats per minutes (b), action potential duration (c), action potential amplitude (d), maximum diastolic potential (e), upstroke velocity (f). Table with mean of parameters (g).

PITX2-hpCMs compared to CTRLs-hpCMs (Table 19g), while APD at 30 did not differed in any condition (Table 19g and figure 19c). On average, AP amplitude was larger in PITX2-hpCMs compared the CTRLs, while MDP and upstroke velocity were similar (Table 19g and figure 19d, e and f).

Atrial differentiation evaluation

In order to better characterize the impact of the PITX2 muttaions on the atria, we generated atrial-like cardiomyocytes (haCMs) from both PITX2 and REV lines. The use of REV line is important for addressing molecular and functional alteration within an identical genetic background differing solely for the PITX2 mutation. First of all I have evaluated the ability of the commercial kit use to generate haCMs by comparing expression levels of specific atrial genes in the two lines. Figure 20a shows that mRNA level of the atrial specific markers NR2F2, PITX2C, KCN5A and Sarcolipin is similar; also no significant differences in cardiac troponin expression has been found indicating a similar cardiac differentiation efficiency (figure 20b).

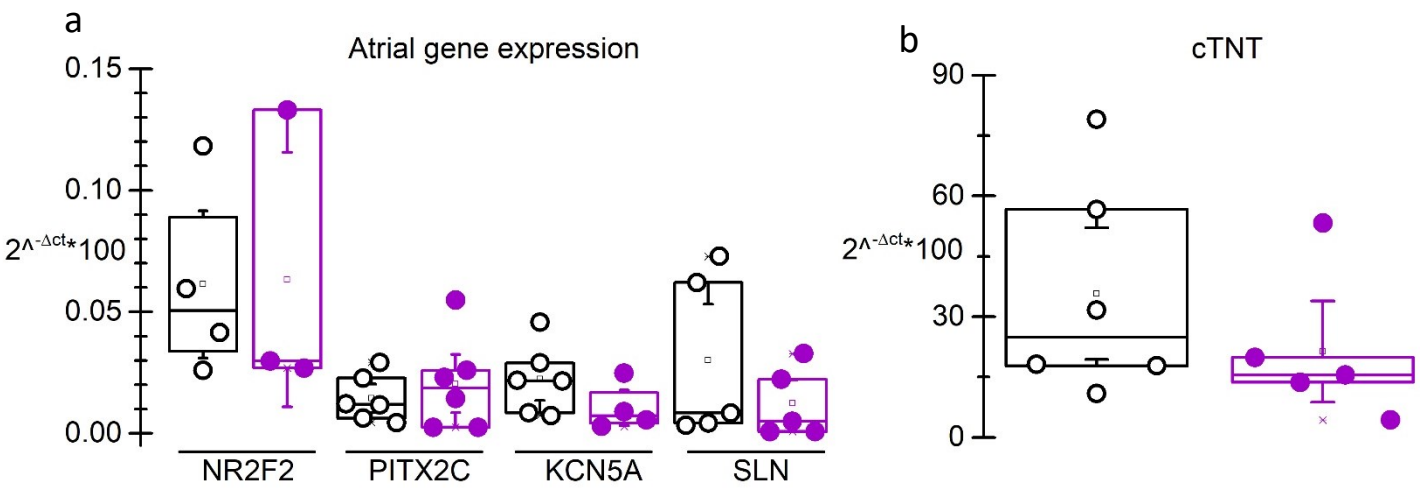

Figure 20: mRNA expression in REV (Black) and PITX2 (Pink) haCMs of NR2F2, PITX2c, KCN5A and SLN (a) and cTNT (b).

From the functional point of view, an important indication of the atrial commitmet is given by the presence of the current mediated from Kv1.5 (KCN5A) channels, the ultra-rapid potassium current that is tipycal of atrial cells. Importantly, as can be seen both from representative traces (figure 21a) and IV curves PITX2 haCMs expressed an apparently smaller I_{Kur} than REV-haCMs, however, differences in conductances were not significant. Importantly, both haCMs displayed a current density significantly higher that that of CTRL-hpCMs (dashed line), confirming the atrial commitment (figure 21b Table 21c).

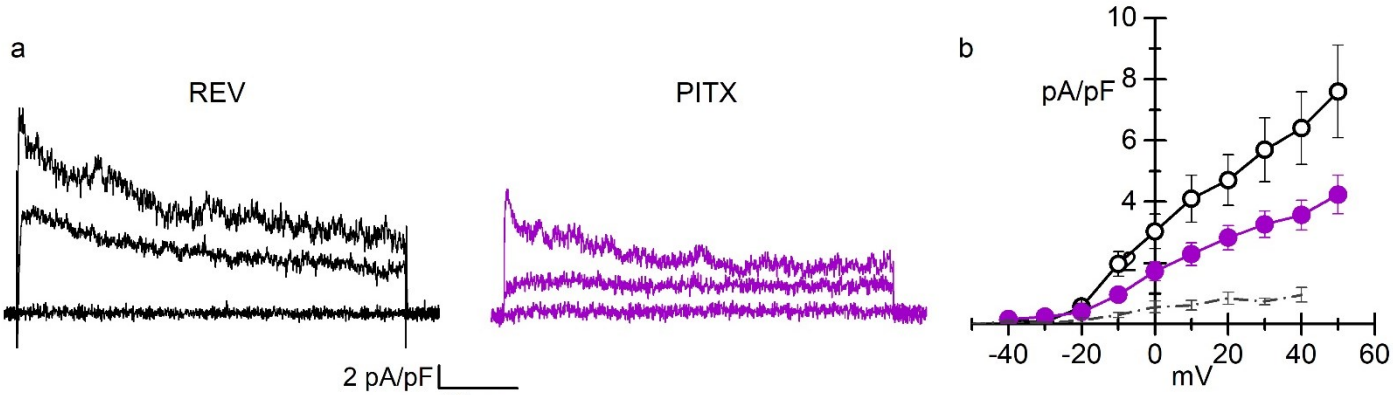

C

	G (pS/pF)
PITX2	54 ± 7.16
REV	132.64 ± 46.7

Figure 21: I_{Kur} in REV (Black) and PITX2 (Pink)-haCMs representative traces (a) and I-V relationship (b).

Spontaneous action potential of Atrial CMs

Preliminary data on spontaneous APs recorded in CTRLs (n=7) and PITX2-haCMs (n=13) can be seen from representative traces and box plots. conversely to what observed in hpCMs, the spontaneous beating frequency did not change among haCMs lines (figure 22 a, b and table g). Also action potential duration at different repolarization percentages (30, 50 and 90) and MDP did not changes, however PITX2-haCMs had a larger action potential amplitude and a faster upstroke velocity compared to REV-haCMs (see figure 22 c d e f and table 22g).

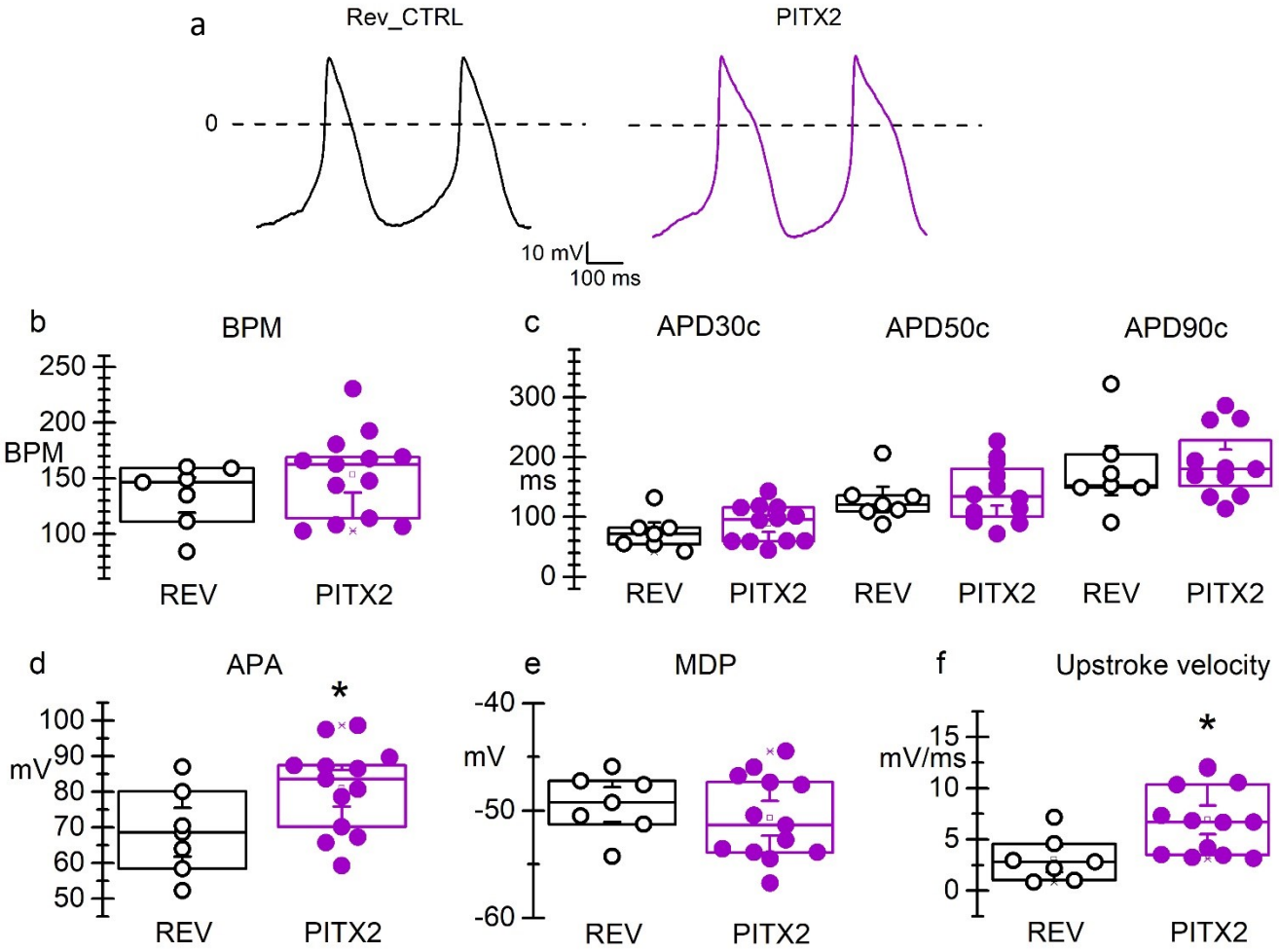

g

	BPM	APD30c (ms)	APD50c (ms)	APD90c (ms)	APA (mV)	MDP (mV)	dV/dt max
PITX2	153.11±10.55	88.96±9.13	140.05±14.07	188.94±15.88	80.94±3.38	-60.71±1.08	6.91±0.93
REV	135.17±10.55	74.08±11.16	129.33±14.22	177.29±27.35	68.66±4.53	-49.43±1.08	3.06±0.83

Figure 22: representative traces of APs recorded in REV (Black) and PITX2 (Pink)-haCMs (a) Box plot of beats per minutes (b), action potential duration (c), action potential amplitude (d), maximum diastolic potential (e), upstroke velocity (f). Table with mean of parameters (g).

Characterization of ionic currents underlyinge action potential in haCMs

Funny current

The funny current is the main conductance involved in the slow diastolic depolarization phase, and thus peculiar of pacemaker cells. Despite the atrial commitment, haCMs are know to be immature and thus they cells displayed spontaneous beating activity[100], and thus the pacemaker funny current. Analysis of I-V relationship revealed that both PITX2 (n=14) and REV-haCMs (n=17) display I_f that, as expected from the similar rate, did not differ among lines (Figure 23a and b). Activation curves analysis instead revealed a small but significant shift to negative potentials of PITX2 I_f (figure 23), better appreciable from the V_{half} parameter in table 23e. Other I_f kinetic features such as Inverse slope factors (ISF) and tau did not change (figure 23 c and d and table 23e).

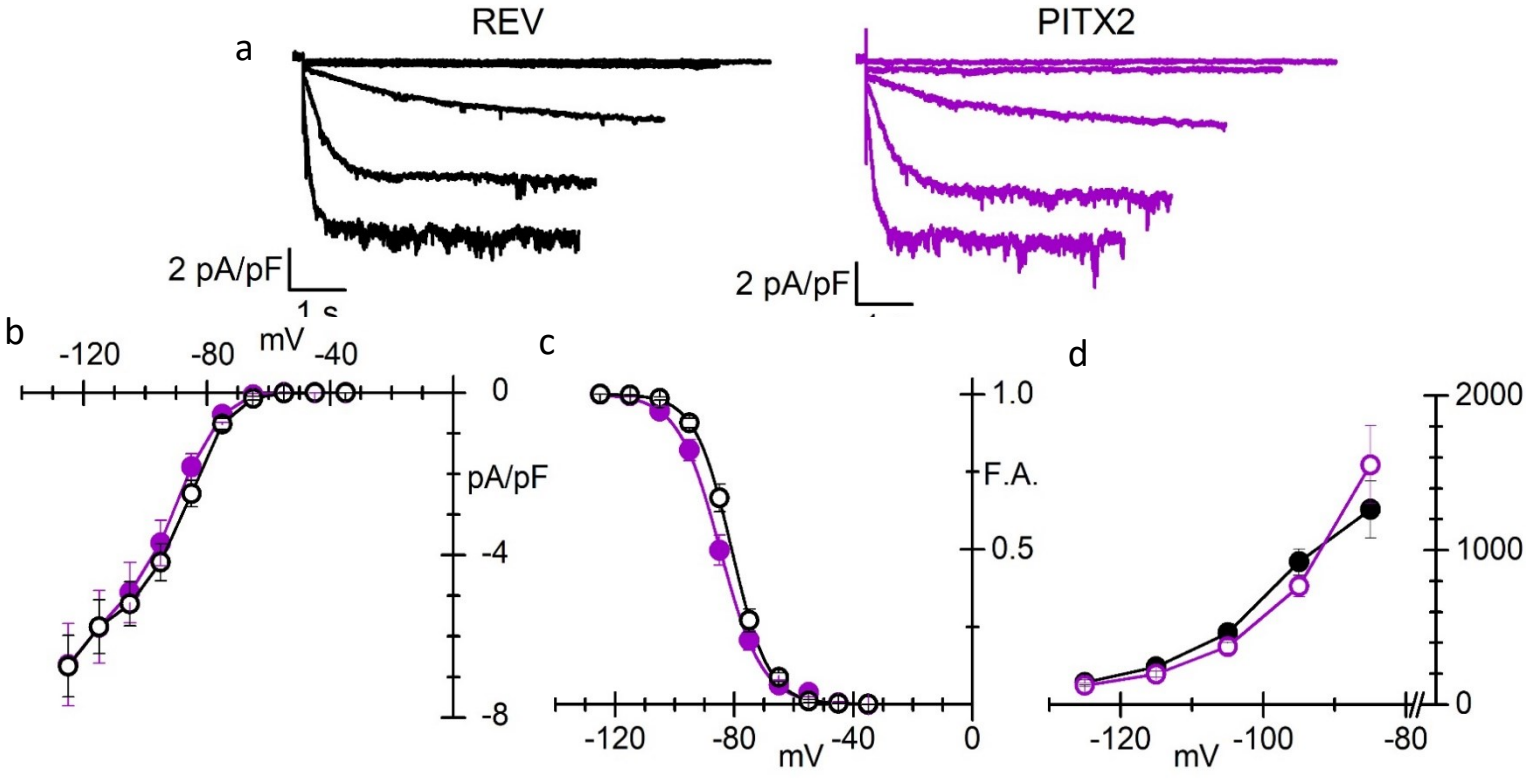

e

	V_{half} (mV)	ISF	Tau -85 mV (ms)
PITX2	-84.78 ± 1.29	6.39 ± 0.37	1262.86 ± 184.88
REV	-80.78 ± 1.29	5.37 ± 0.23	1552.18 ± 251.64

Figure 23: representative traces of I_f recorded in REV (Black) and PITX2 (Pink)-haCMs (a); I-V relationship (b), Activation Curves (c), Tau (d), AC and tau parameters (e).

L-type calcium current

L-type calcium current I-V relationship and activation curves properties did not change among haCMs derived from both lines, as shown in figure 24a and b. The current densities at 0 mV were -8.63 ± 0.61 pA/pF (n=6) in REV-haCMs and -9.71 ± 0.97 pA/pF (n=13) in PITX2-haCMs; activation curves are plotted in figure 24c while the V_{half} and ISF parameters are reported in table 24d.

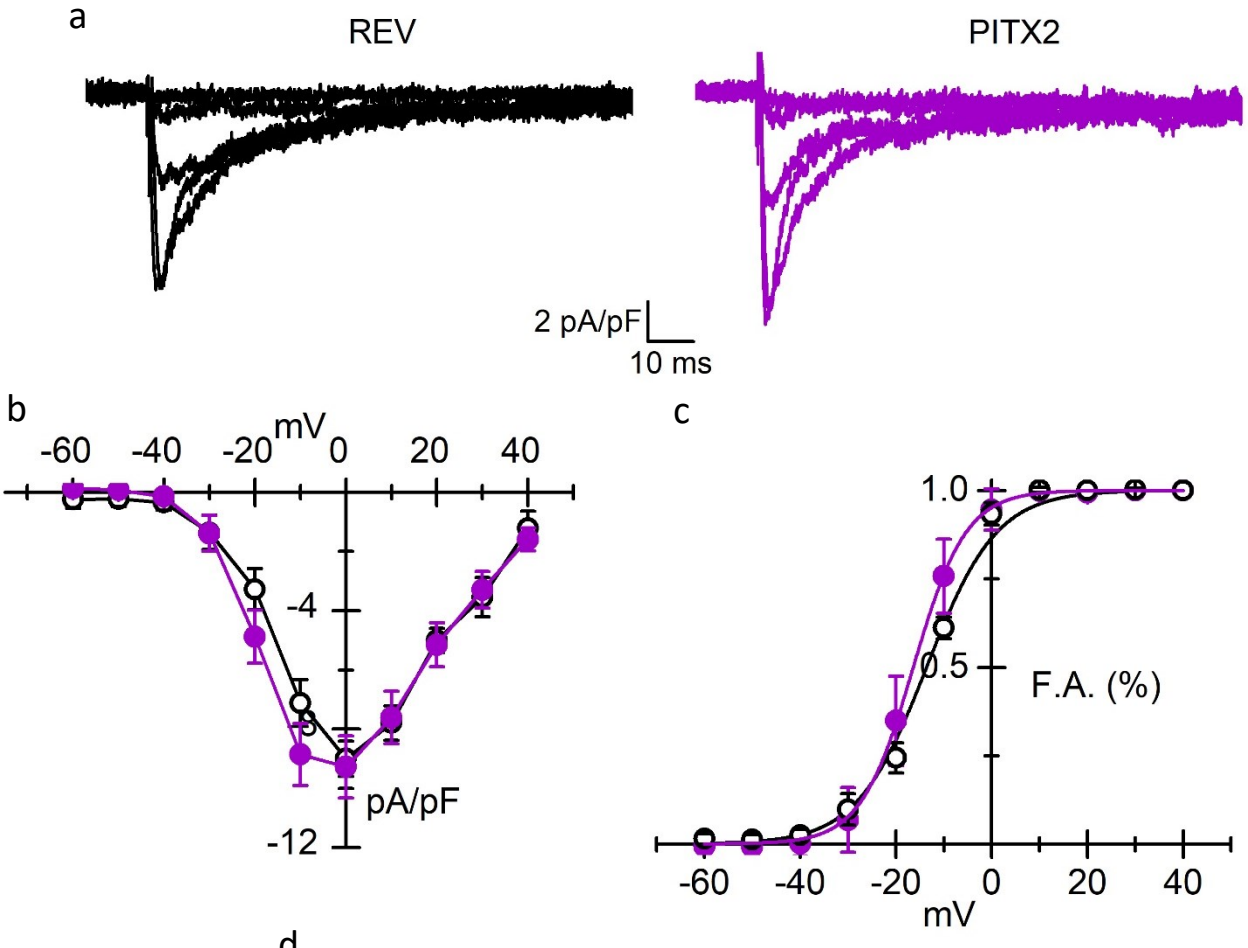

d

	V_{half} (mV)	ISF
PITX2	-16.40 ± 0.88	5.39 ± 0.50
REV	-13.49 ± 0.74	6.15 ± 0.80

Figure 24: representative traces of I_{CaL} recorded in REV (Black) and PITX2 (Pink)-haCMs (a); I-V relationship (b), Activation Curves (c), AC parameters (d).

Sodium current

Sodium current is the conductance that shapes the rapid phase 0 depolarization of the action potential, defining its steepness and amplitude. Preliminary data on this current in REV and PITX2-haCMs revealed a current density at -20 mV of -119.92 ± 17.96 pA/pF (n=10) and -165.08 ± 88.29 pA/pF (n=5) respectively (figure 25a and b). Because of the large variability in densities (especially in the PITX2 cells, more experiments are necessary to understand the effect of PITX2 mutation on this current, whose increase may easily explain the difference observed in the AP parameters. Activation curves reported in figure 25c did not change either (table 25d).

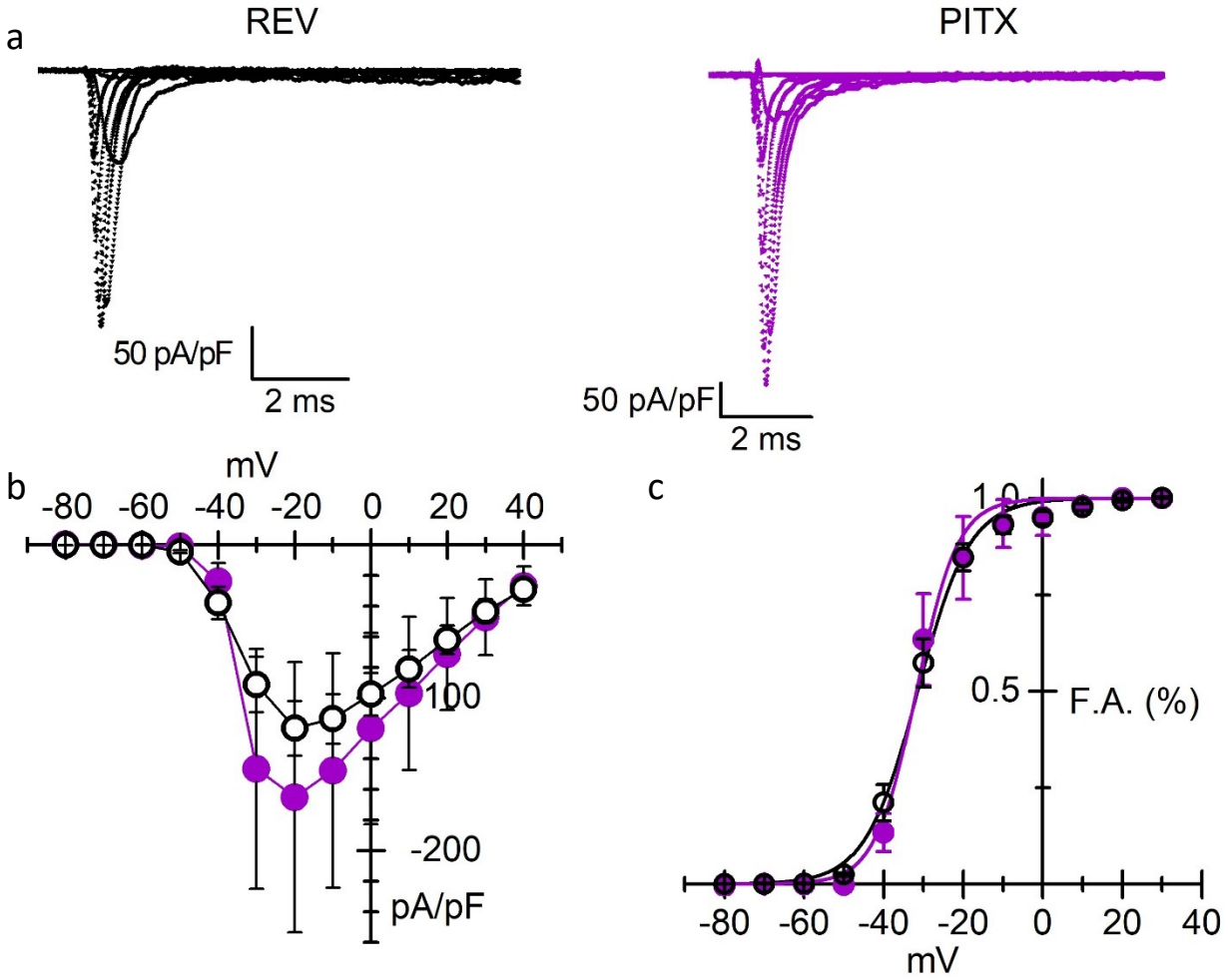

d

	V_{half} (mV)	ISF
PITX2	-30.07 ± 3.57	5.09 ± 1.52
REV	-31.88 ± 1.45	6.03 ± 0.64

Figure 25: representative traces of I_{Na} recorded in REV (Black) and PITX2 (Pink)-haCMs (a); I-V relationship (b), Activation Curves (c), AC parameters (d).

Metabolic characterization

Since the metabolic dysregulation in atrial cardiomyocytes seems to occur before and likely to induce the electrical ones[96], seahorse analysis has been performed on day 20 haCMs for evaluating oxidative phosphorylation and glycolysis in the two cell lines. In figure 26a OCR and ECAR are plotted overlapped: in the basal condition PITX2-haCMs had a higher oxygen consumption rate than REV-haCMs. Subsequent addition of Oligomycin (specific inhibitor of the ATPase) revealed that PITX2-haCMs have a higher decrease in the OCR compared to REV-haCMs, that is better appreciable in figure 26b. GlycoATP production, evaluated as combining ECAR buffer factors and mitochondrial-associated acidification evaluated in presence of Rotenone plus Antimycin A, was equal in haCMs derived from PITX2 and REV

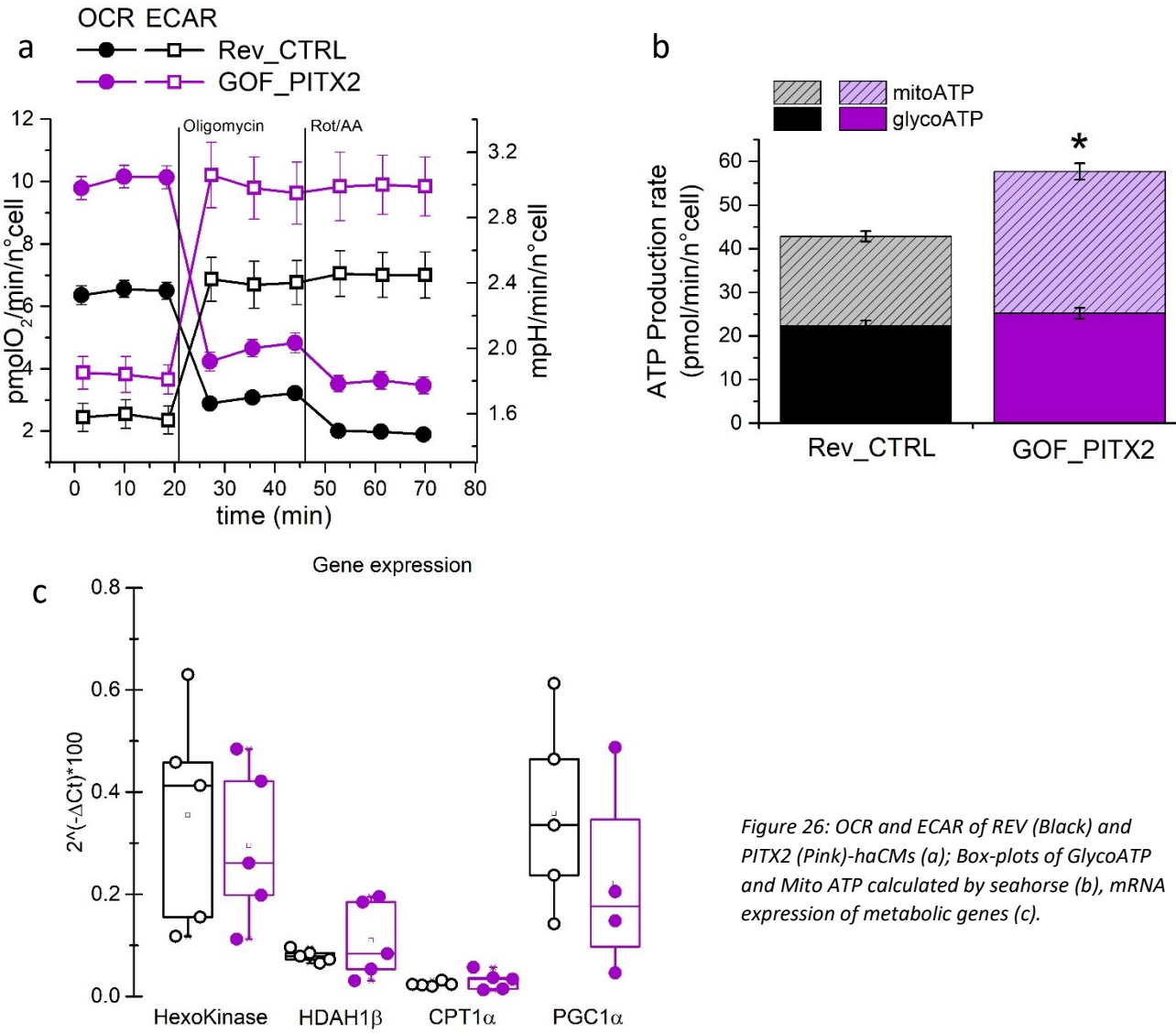

Figure 26: OCR and ECAR of REV (Black) and PITX2 (Pink)-haCMs (a); Box-plots of GlycoATP and Mito ATP calculated by seahorse (b), mRNA expression of metabolic genes (c).

lines (figure 26b). So, the higher metabolism in PITX2-haCMs was more likely due to a higher oxidative phosphorylation.

In figure 26c were plotted mRNA expression analysis of metabolic enzymes linked to glycolysis (Hexokinase) or fatty acid β-oxidation (CPT1α and HADH1β) or mitochondrial biogenesis (PGC1α), these data revealed no differences between haCMs derived from between lines.

DISCUSSION

AF is the most common arrhythmic disorder worldwide with an ever-increasing incidence. It is linked to comorbidities and age, but genetic background also seems to play a considerable role in its onset; indeed, having a relative with AF increases the chances of developing it[94]. Therefore, a better understanding of this "new" risk factor is needed to recognize and possibly prevent the onset of AF. This will also help unravel the molecular mechanisms underlying initiation of this arrhythmia, which has been difficult so far because working with cells that have experienced the atrial fibrillation, make it is difficult to distinguish between the electrical/morphological causes and the consequences due to the maladaptive remodelling.

GWAS studies identified various single nucleotides polymorphisms that are correlated with AF and therefore considered suitable candidates for further studies, including PITX2 gene whose genetic locus was liked to SNPs mostly associated with early onset AF[95,108]. The transcription factor PITX2 is essential during cardiac development, in the inhibition of ectopic growth of the pacemaker and in the correct formation of myocardium associated with pulmonary veins, all crucial areas in arrhythmias beginning[64,83,90] and it is found both down and upregulated in AF patients[98].

hIPSc lines with a GOF mutation in heterozygosis of PITX2 gene[54,55] represent a perfect model to unravel PITX2 role in AF onset and to investigate whether the mutation triggers the arrhythmia. hpCMs obtained with a standard differentiation provided an overview on the effect of PITX2 mutation in a cardiac/sinoatrial-like context. This GOF mutation did not alter the expression of PITX2 isoforms in hpCMs coherently with the data previously published[55]. Given the importance of this transcription factor during development and to exclude alterations in cardiac commitment, cTNT expression has been evaluated and found comparable among the two populations, as well as the expression of myosin heavy (MYH6, MYH7) and light (MYL7, MYL2) chains (data not shown). Interestingly, only the ratio between immature/atrial myosin heavy chain versus the ventricular isoform (MYH6/MYH7) was higher in PITX2-hpCMs than CTRLs-hpCMs; the relative higher amount of myosin atrial isoform may suggest that this GOF mutation induced a more immature/atrial phenotype. This can easily be referred to the developmental role of PITX, whose expression mark the boundaries of atria formation and therefore its GOF can stimulate the atrial isoforms expression.

Spontaneous APs were recorded from small clusters of pacemaker cardiomyocytes (hpCMs)[109] derived from PITX2 and three unrelated CTRLs. PITX2-hpCMs had a lower beating frequency than the CTRLs ones. This evidence is particularly important since, a bradycardic sinus node is an ideal substrate for unmasking AF[110].

Physiologically, a lower heart rate is associated with a longer AP duration and vice versa; PITX2-hpCMs, on the other hand, have a shorter duration of the late repolarization phases (APD50 and 90) compared to CTRLs-hpCMs. This can be associated either with a reduced L-type calcium current or an increased delayed rectifier potassium current, all conductances already demonstrated to be altered or directly modulated by PITX2[100]. In the literature, a shortened APD was associated with loss of PITX2 rather than GOF[111]; it is also true that

both loss- and gain-of-function induce similar electrical effect on L-type calcium current[100,102] or metabolic effect[104] therefore some consequences may be due to dysregulation of PITX2 levels rather than to a specific amount of the transcription factor. Another modified APs parameter was the amplitude, which was higher in PITX2-hpCMs than in CTRLs; APA was closely correlated with APs phase 0 and had already been found reduced in mice with a PITX2 deficiency [99], suggesting that a PITX2 GOF may have opposite effects.

PITX2-hpCMs electrical profile can easily relate to an ideal pathophysiological behaviour for AF onset, but since AF is, by definition, an atrial pathology, we decided to concentrate our focus on developing an atrial-like model for the analysis of the single currents. For this reason, we first generated a clone of hiPSc line in which the specific PITX2 mutation has been reverted and then we applied a commercial kit reported to increase the hIPSc-derived atrial cardiomyocytes yield from PITX2 and its isogenic control (REV) lines.

The appropriate atrial differentiation was successfully assessed with qPCR analysis of some atrial markers (NR2F2, PITX2C, KCN5A and Sarcolipin) and cTNT. Furthermore, the absence of differences in expression of these genes indicate that PITX2 mutation do not influence differentiation capacity into haCMs. Besides the molecular characterization, for our aim it was important to assess the presence of I_{Kur} in haCMs, being this conductance very specific for atrial cells. I_{Kur} showed no differences between PITX2 and REV-haCMs while it was significantly higher than that recorded from CTRL-hpCMs.

Even with “atrial” classification, single haCMs had spontaneously beating activity due to the 2D differentiation procedure which is known to produce hIPSc-derived CMs with a certain degree of immaturity[112]. Spontaneous APs analysis highlighted some differences with the APs previously recorded from hpCMs clusters. When the analysis of spontaneous APs was conducted in PITX2 and REV-haCMs, differences were evident compared to results obtained with hpCMs. First, PITX2 and REV-haCMs had comparable beating rate while

PITX2 hpCMs are bradycardic; second, APD (both at 50% and 90% of repolarization) is not altered by the mutation; third, PITX2-haCMs, like hpCMs had a higher APA and also a steeper upstroke velocity compared to REV-haCMs. These differences may be attributable to the different reasons: 1- cellular context: clusters beat slower than single CMs derived from the same line because of their electrical coupling with neighbouring cells, which in addition to hpCMs may contain other cell types, such as fibroblast, thus slowing down APs propagation. 2- it appears that PITX2 mutation somehow impairs the APs propagation by slowing it down, a condition not appreciable in single cells. 3- the PITX2 mutation may have different outcomes in sinoatrial-like (hpCMs) cells than in atrial-like cells because PITX2 is known to interfere with the sinoatrial genetic program[86]. This makes these data not mutually exclusive but informative on the impact of the PITX2 mutation in the various cardiac districts. A context-specific effect of the PITX2 GOF mutation can be hypothesized: where PITX2 is usually not expressed, as in a pacemaker environment, its GOF mutation induced bradycardia altering both depolarization ad repolarization phases, while in an atrial context its alteration concerns phase 0 of the action potential.

In the literature, L-type calcium current is one of the conductances found mostly altered by PITX2 absence or abundance[100,102] and thus one of the first studied in haCMs; preliminary data reported here did not show any differences either in density nor in kinetic properties of I_{CaL}. Even if the numbers of haCMs analysed must be increased, the small variability of the data already collected suggests that this mutation had no effect on this current.

A Loss-of-function mutation in HCN channels was linked to an early onset AF[2], as well as f-channel GOF[36] so it was interesting to evaluate I_f properties: V_{half} was negatively shifted in PITX2-haCMs compared to REV one, implying that this current contributed less during the slow diastolic depolarization phases.

Furthermore, data on APs in haCMs revealed a greater APA and a steeper upstroke velocity in PITX2 than in REV-haCMs, suggesting sodium current involvement. A direct link between PITX2 and the sodium current has not yet been discovered, although a mathematical model of Pitx2c-deficient CMs has calculated a reduction in the availability of Na channels as a consequence of a depolarized resting membrane potential[98]. Our GOF mutation, on the other hand, does not seem to alter the maximum diastolic potential (the more negative voltage reached in autorhythmic cells), ruling out a greater availability of non-inactivated sodium channels. The increased APA suggests instead a greater underlying sodium current. This was not corroborated by the preliminary data on I_{Na}, even though a large variability combined with a low number of analysed haCMs did not allow a precise evaluation of the Na current.

One of the less known roles of PITX2 is to indirectly regulate the cellular red-ox status during myogenesis and in the presence of lesion[105,113]. Moreover, the role of metabolism in the onset of AF is underestimated even though it seems that both PITX2 GOF and loss induced metabolic alterations that precede the pathology[104]. Considering this, it was interesting to find that PITX2-haCMs had a higher basal oxygen consumption rate compared to REV one, having a higher mitochondrial ATP production rate, and this was found 10 days prior to electrophysiological analysis. This is consistent with previous data obtained in zebrafish where overexpressed PITX2 was associated with enrichment in genes related to oxidative phosphorylation[104]. It would be interesting to investigate whether this enhanced oxidative phosphorylation is coupled with a powered antioxidant pathways or an increased ROS content.

In conclusion, PITX2 heterozygous point mutation (rs138163892) seems to alter the electrical activity in a context-dependent way, also enhancing the oxidative metabolism of

CMs. All these features have been linked to AF, indicating a plausible role of this specific mutation in the onset of the disease.

GENERAL CONCLUSION

The self-renewal and pluripotency properties of stem cells make them an *in vitro* model widely used to study physiological and pathological state of organs, for drugs screening, and can be considered as the future for personalized therapeutic procedures. Indeed, with the right stimuli, stem cells can differentiate into majority of cellular types and thus representing not only a potential unlimited source of samples for research but also potential candidate for transplantation into injured tissue.

As regards studies in the cardiac field, the protocols for the generation cardiomyocytes are constantly refined and evolving, therefore the use of CMs derived from stem cells is increasingly common and stimulated by the scientific community. They are mainly used for the study of functional[36,114], structural and metabolic[115] alterations at the base of pathologies involving the heart, but also are a useful tool for drugs screening and safety validation[116].

In this thesis, mESc-derived cardiomyocytes have been used to show that lack of STRN contributes to establishing a pro-arrhythmogenic substrate, modifying the electrical profile of mCMs; these effects are probably mediated, directly or not, by the interaction between STRN and microtubules. The mESc model was particularly important to achieve these results as it can be easily manipulated, it is cost-effective regarding cells maintenance and differentiation, and produce functional cardiomyocytes in 14 days. Since manual patch-clamp is a low throughput technique, the time-effective feature was a particularly important advantage in obtaining a good experimental number. Instead, the most important limitation was the non-human context of the STRN-KO effect analysis; this is something not completely required in such a study, as this is a completely KO and not a patient-specific mutation. Therefore, this work wants to be a functional characterization of the alterations caused by STRN loss proposing an underline mechanism which, even if it needs to be

further investigated, representing a useful reference study for future patient specific STRN mutation.

This patient-related condition is instead represented by the second part of the thesis, in which the functional characterization of PITX2 heterozygous GOF mutation was necessary to find out whether this mutation predisposed or caused atrial fibrillation onset, a circumstance suggested by the enhanced oxidative metabolism and functional alterations of cardiomyocytes. These results were obtained thanks to hiPSc-derived CMs, that fully addressed one of the major gaps in the field of cardiac research: obtain a suitable cell source for patient specific mutation. Moreover, the capability to obtain different hiPSc-CMs subtype (haCMs and hpCMs) allows us to hypothesize the mutation functional dysregulation occurs depending on the cardiac district analyzed, a speculation that needs to be further deepen. The major known limitation of this model, the CMs immaturity, is still present but this does not belittle the goodness of the data since it a comparative analysis where PITX2, isogenic control and published control cell lines[36] had the same degree of differentiation.

In conclusion, the data obtained, also considering what were the initial aims, make mESc and hiPSc derived cardiomyocytes a useful tool to investigate the molecular basis of functional alterations causing a pro-arrhythmic behavior due to of genetic alterations.

REFERENCES

1. Altomare, C. *et al.* Heteromeric HCN1–HCN4 channels: a comparison with native pacemaker channels from the rabbit sinoatrial node. *J. Physiol.* **549**, 347–359 (2003).

2. Macri, V. *et al.* A novel trafficking-defective HCN4 mutation is associated with early-onset atrial fibrillation. *Heart Rhythm* **11**, 1055–1062 (2014).

3. Barbuti Andrea *et al.* Localization of Pacemaker Channels in Lipid Rafts Regulates Channel Kinetics. *Circ. Res.* **94**, 1325–1331 (2004).

4. Moroni, A. *et al.* Kinetic and ionic properties of the human HCN2 pacemaker channel. *Pflüg. Arch.* **439**, 618–626 (2000).

5. Matsui, Y., Zsebo, K. & Hogan, B. L. Derivation of pluripotential embryonic stem cells from murine primordial germ cells in culture. *Cell* **70**, 841–847 (1992).

6. Miura, T., Mattson, M. P. & Rao, M. S. Cellular lifespan and senescence signaling in embryonic stem cells. *Aging Cell* **3**, 333–343 (2004).

7. Bryja, V., Bonilla, S. & Arenas, E. Derivation of mouse embryonic stem cells. *Nat. Protoc.* **1**, 2082–2087 (2006).

8. Maltsev, V. A., Rohwedel, J., Hescheler, J. & Wobus, A. M. Embryonic stem cells differentiate in vitro into cardiomyocytes representing sinusnodal, atrial and ventricular cell types. *Mech. Dev.* **44**, 41–50 (1993).

9. Takahashi, T. *et al.* Ascorbic Acid Enhances Differentiation of Embryonic Stem Cells Into Cardiac Myocytes. *Circulation* **107**, 1912–1916 (2003).

10. Gassanov, N., Er, F., Zagidullin, N. & Hoppe, U. C. Endothelin induces differentiation of ANP-EGFP expressing embryonic stem cells towards a pacemaker phenotype. *FASEB J.* **18**, 1710–1712 (2004).

11. Kolossov, E. *et al.* Identification and characterization of embryonic stem cell-derived pacemaker and atrial cardiomyocytes. *FASEB J.* **19**, 1–25 (2005).

12. White, S. M. & Claycomb, W. C. Embryonic stem cells form an organized, functional cardiac conduction system in vitro. *Am. J. Physiol. Heart Circ. Physiol.* **288**, H670-679 (2005).

13. Hidaka, K. *et al.* Chamber-specific differentiation of Nkx2.5-positive cardiac precursor cells from murine embryonic stem cells. *FASEB J. Off. Publ. Fed. Am. Soc. Exp. Biol.* **17**, 740–742 (2003).

14. Scavone Angela *et al.* Embryonic Stem Cell–Derived CD166+ Precursors Develop Into Fully Functional Sinoatrial-Like Cells. *Circ. Res.* **113**, 389–398 (2013).

15. Benzoni, P. *et al.* The funny current: Even funnier than 40 years ago. Uncanonical expression and roles of HCN/f channels all over the body. *Prog. Biophys. Mol. Biol.* (2021) doi:10.1016/j.pbiomolbio.2021.08.007.

16. Takahashi, K. & Yamanaka, S. Induction of Pluripotent Stem Cells from Mouse Embryonic and Adult Fibroblast Cultures by Defined Factors. *Cell* **126**, 663–676 (2006).

17. Takahashi, K. *et al.* Induction of pluripotent stem cells from adult human fibroblasts by defined factors. *Cell* **131**, 861–872 (2007).

18. Barbuti, A., Benzoni, P., Campostrini, G. & Dell'Era, P. Human derived cardiomyocytes: A decade of knowledge after the discovery of induced pluripotent stem cells. *Dev. Dyn.* **245**, 1145–1158 (2016).

19. Lewandowski, J. & Kurpisz, M. Techniques of Human Embryonic Stem Cell and Induced Pluripotent Stem Cell Derivation. *Arch. Immunol. Ther. Exp. (Warsz.)* **64**, 349–370 (2016).

20. Kamakura, T. *et al.* Ultrastructural Maturation of Human-Induced Pluripotent Stem Cell-Derived Cardiomyocytes in a Long-Term Culture. *Circ. J.* **77**, 1307–1314 (2013).

21. Marczenke, M. *et al.* Cardiac Subtype-Specific Modeling of Kv1.5 Ion Channel Deficiency Using Human Pluripotent Stem Cells. *Front. Physiol.* **8**, (2017).

22. Devalla, H. D. *et al.* Atrial-like cardiomyocytes from human pluripotent stem cells are a robust preclinical model for assessing atrial-selective pharmacology. *EMBO Mol. Med.* **7**, 394–410 (2015).

23. Zhang, Q. *et al.* Direct differentiation of atrial and ventricular myocytes from human embryonic stem cells by alternating retinoid signals. *Cell Res.* **21**, 579–587 (2011).

24. Lee, J. H., Protze, S. I., Laksman, Z., Backx, P. H. & Keller, G. M. Human Pluripotent Stem Cell-Derived Atrial and Ventricular Cardiomyocytes Develop from Distinct Mesoderm Populations. *Cell Stem Cell* **21**, 179-194.e4 (2017).

25. DiFrancesco, D., Ferroni, A., Mazzanti, M. & Tromba, C. Properties of the hyperpolarizing-activated current (if) in cells isolated from the rabbit sino-atrial node. *J. Physiol.* **377**, 61–88 (1986).

26. Mangoni, M. E. *et al.* Voltage-dependent calcium channels and cardiac pacemaker activity: From ionic currents to genes. *Prog. Biophys. Mol. Biol.* **90**, 38–63 (2006).

27. Maltsev, A. V., Yaniv, Y., Stern, M. D., Lakatta, E. G. & Maltsev, V. A. RyR-NCX-SERCA Local Cross-Talk Ensures Pacemaker Cell Function at Rest and During the Fight-or-Flight Reflex. *Circ. Res.* **113**, e94–e100 (2013).

28. Baruscotti, M., Barbuti, A. & Bucchi, A. The cardiac pacemaker current. *J. Mol. Cell. Cardiol.* **48**, 55–64 (2010).

29. Yasui, K. *et al.* If Current and Spontaneous Activity in Mouse Embryonic Ventricular Myocytes. *Circ. Res.* **88**, 536–542 (2001).

30. Michels, G. *et al.* Direct evidence for calcium conductance of hyperpolarization-activated cyclic nucleotide-gated channels and human native If at physiological calcium concentrations. *Cardiovasc. Res.* **78**, 466–475 (2008).

31. Verkerk, A. O. & Wilders, R. Pacemaker Activity of the Human Sinoatrial Node: An Update on the Effects of Mutations in HCN4 on the Hyperpolarization-Activated Current. *Int. J. Mol. Sci.* **16**, 3071–3094 (2015).

32. Milanesi, R., Baruscotti, M., Gnecchi-Ruscone, T. & DiFrancesco, D. Familial sinus bradycardia associated with a mutation in the cardiac pacemaker channel. *N. Engl. J. Med.* **354**, 151–157 (2006).

33. Baruscotti, M. *et al.* A gain-of-function mutation in the cardiac pacemaker HCN4 channel increasing cAMP sensitivity is associated with familial Inappropriate Sinus Tachycardia. *Eur. Heart J.* **38**, 280–288 (2017).

34. Milano, A. *et al.* HCN4 Mutations in Multiple Families With Bradycardia and Left Ventricular Noncompaction Cardiomyopathy. *J. Am. Coll. Cardiol.* **64**, 745–756 (2014).

35. Zhou, J. *et al.* A Novel HCN4 Mutation, G1097W, Is Associated With Atrioventricular Block. *Circ. J.* **78**, 938–942 (2014).

36. P, B. *et al.* Human iPSC modelling of a familial form of atrial fibrillation reveals a gain of function of If and ICaL in patient-derived cardiomyocytes. *Cardiovasc. Res.* **116**, 1147–1160 (2020).

37. Catterall, W. A., Goldin, A. L. & Waxman, S. G. International Union of Pharmacology. XLVII. Nomenclature and Structure-Function Relationships of Voltage-Gated Sodium Channels. *Pharmacol. Rev.* **57**, 397–409 (2005).

38. Savio Galimberti, E., Gollob, M. & Darbar, D. Voltage-Gated Sodium Channels: Biophysics, Pharmacology, and Related Channelopathies. *Front. Pharmacol.* **3**, 124 (2012).

39. Isom, L. L. Sodium channel beta subunits: anything but auxiliary. *Neurosci. Rev. J. Bringing Neurobiol. Neurol. Psychiatry* **7**, 42–54 (2001).

40. Dong, C., Wang, Y., Ma, A. & Wang, T. Life Cycle of the Cardiac Voltage-Gated Sodium Channel NaV1.5. *Front. Physiol.* **11**, 609733 (2020).

41. Song, W. & Shou, W. Cardiac Sodium Channel Nav1.5 Mutations and Cardiac Arrhythmia. *Pediatr. Cardiol.* **33**, 943–949 (2012).

42. Catterall, W. A., Lenaeus, M. J. & Gamal El-Din, T. M. Structure and Pharmacology of Voltage-Gated Sodium and Calcium Channels. *Annu. Rev. Pharmacol. Toxicol.* **60**, 133–154 (2020).

43. Mangoni, M. E. *et al.* Functional role of L-type Cav1.3 Ca2+ channels in cardiac pacemaker activity. *Proc. Natl. Acad. Sci.* **100**, 5543–5548 (2003).

44. Kodama, I. *et al.* Regional differences in the role of the Ca2+ and Na+ currents in pacemaker activity in the sinoatrial node. *Am. J. Physiol.-Heart Circ. Physiol.* **272**, H2793–H2806 (1997).

45. Zhang, Q., Chen, J., Qin, Y., Wang, J. & Zhou, L. Mutations in voltage-gated L-type calcium channel: implications in cardiac arrhythmia. *Channels* **12**, 201–218 (2018).

46. Curran, M. E. *et al.* A molecular basis for cardiac arrhythmia: HERG mutations cause long QT syndrome. *Cell* **80**, 795–803 (1995).

47. Abbott, G. W. *et al.* MiRP1 Forms IKr Potassium Channels with HERG and Is Associated with Cardiac Arrhythmia. *Cell* **97**, 175–187 (1999).

48. Brugada, R. *et al.* Sudden Death Associated With Short-QT Syndrome Linked to Mutations in HERG. *Circulation* **109**, 30–35 (2004).

49. Olson, T. M. *et al.* Kv1.5 channelopathy due to KCNA5 loss-of-function mutation causes human atrial fibrillation. *Hum. Mol. Genet.* **15**, 2185–2191 (2006).

50. Yang, Y. *et al.* Novel KCNA5 loss-of-function mutations responsible for atrial fibrillation. *J. Hum. Genet.* **54**, 277–283 (2009).

51. Barbuti, A. *et al.* Molecular composition and functional properties of f-channels in murine embryonic stem cell-derived pacemaker cells. *J. Mol. Cell. Cardiol.* **46**, 343–351 (2009).

52. Motlagh, D., Alden, K. J., Russell, B. & García, J. Sodium current modulation by a tubulin/GTP coupled process in rat neonatal cardiac myocytes. *J. Physiol.* **540**, 93–103 (2002).

53. Aasen, T. *et al.* Efficient and rapid generation of induced pluripotent stem cells from human keratinocytes. *Nat. Biotechnol.* **26**, 1276–1284 (2008).

54. Mora, C. *et al.* Generation of induced pluripotent stem cells (iPSC) from an atrial fibrillation patient carrying a PITX2 p.M200V mutation. *Stem Cell Res.* **24**, 8–11 (2017).

55. Mechakra, A. *et al.* A Novel PITX2c Gain-of-Function Mutation, p.Met207Val, in Patients With Familial Atrial Fibrillation. *Am. J. Cardiol.* **123**, 787–793 (2019).

56. Hwang, J. & Pallas, D. C. STRIPAK complexes: Structure, biological function, and involvement in human diseases. *Int. J. Biochem. Cell Biol.* **47**, 118–148 (2014).

57. Steinberg, S. F. & Brunton, L. L. Compartmentation of G Protein-Coupled Signaling Pathways in Cardiac Myocytes. *Annu. Rev. Pharmacol. Toxicol.* **41**, 751–773 (2001).

58. Nader, M. *et al.* Cardiac striatin interacts with caveolin-3 and calmodulin in a calcium sensitive manner and regulates cardiomyocyte spontaneous contraction rate. *Can. J. Physiol. Pharmacol.* **95**, 1306–1312 (2017).

59. Gaillard, S. *et al.* Targeting of Proteins of the Striatin Family to Dendritic Spines: Role of the Coiled-Coil Domain. *Traffic* **7**, 74–84 (2006).

60. Gordon, J. *et al.* Protein phosphatase 2a (PP2A) binds within the oligomerization domain of striatin and regulates the phosphorylation and activation of the mammalian Ste20-Like kinase Mst3. *BMC Biochem.* **12**, 54 (2011).

61. Smith, T. F. Diversity of WD-repeat proteins. *Subcell. Biochem.* **48**, 20–30 (2008).

62. A novel calmodulin-binding protein, belonging to the WD-repeat family, is localized in dendrites of a subset of CNS neurons. *J. Cell Biol.* **134**, 1051–1062 (1996).

63. Nader, M. The SLMAP/Striatin complex: An emerging regulator of normal and abnormal cardiac excitation-contraction coupling. *Eur. J. Pharmacol.* **858**, 172491 (2019).

64. Sotoodehnia, N. *et al.* Common variants in 22 loci are associated with QRS duration and cardiac ventricular conduction. *Nat. Genet.* **42**, 1068–1076 (2010).

65. Nader, M. *et al.* Tail-anchored membrane protein SLMAP is a novel regulator of cardiac function at the sarcoplasmic reticulum. *Am. J. Physiol.-Heart Circ. Physiol.* **302**, H1138–H1145 (2012).

66. Guzzo, R. M., Salih, M., Moore, E. D. & Tuana, B. S. Molecular properties of cardiac tail-anchored membrane protein SLMAP are consistent with structural role in arrangement of excitation-contraction coupling apparatus. *Am. J. Physiol.-Heart Circ. Physiol.* **288**, H1810–H1819 (2005).

67. Meurs, K. M. *et al.* Genome-wide association identifies a deletion in the 3' untranslated region of Striatin in a canine model of arrhythmogenic right ventricular cardiomyopathy. *Hum. Genet.* **128**, 315–324 (2010).

68. Meurs, K. M. *et al.* Association of Dilated Cardiomyopathy with the Striatin Mutation Genotype in Boxer Dogs. *J. Vet. Intern. Med.* **27**, 1437–1440 (2013).

69. Meurs, K. M. Arrhythmogenic Right Ventricular Cardiomyopathy in the Boxer Dog: An Update. *Vet. Clin. North Am. Small Anim. Pract.* **47**, 1103–1111 (2017).

70. Lahav-Ariel, L. *et al.* Striatin is a novel modulator of cell adhesion. *FASEB J.* **33**, 4729–4740 (2019).

71. Gardner, M. K., Zanic, M. & Howard, J. Microtubule catastrophe and rescue. *Curr. Opin. Cell Biol.* **25**, 14–22 (2013).

72. Amos, L. A. & Schlieper, D. Microtubules and Maps. in *Advances in Protein Chemistry* vol. 71 257–298 (Academic Press, 2005).

73. White, E. Mechanical modulation of cardiac microtubules. *Pflüg. Arch. - Eur. J. Physiol.* **462**, 177 (2011).

74. Sontag, J.-M., Nunbhakdi-Craig, V., White, C. L., Halpain, S. & Sontag, E. The Protein Phosphatase PP2A/Bα Binds to the Microtubule-associated Proteins Tau and MAP2 at a Motif Also Recognized by the Kinase Fyn. *J. Biol. Chem.* **287**, 14984–14993 (2012).

75. Kaźmierczak-Barańska, J., Pęczek, Ł., Przygodzka, P. & Cieślak, M. J. Downregulation of striatin leads to hyperphosphorylation of MAP2, induces depolymerization of microtubules and inhibits proliferation of HEK293T cells. *FEBS Lett.* **589**, 222–230 (2015).

76. Shih, P.-Y., Lee, S.-P., Chen, Y.-K. & Hsueh, Y.-P. Cortactin-binding protein 2 increases microtubule stability and regulates dendritic arborization. *J. Cell Sci.* **127**, 3521–3534 (2014).

77. Caporizzo, M. A., Chen, C. Y. & Prosser, B. L. Cardiac microtubules in health and heart disease. *Exp. Biol. Med.* **244**, 1255–1272 (2019).

78. Steele, D. F. & Fedida, D. Cytoskeletal roles in cardiac ion channel expression. *Biochim. Biophys. Acta BBA - Biomembr.* **1838**, 665–673 (2014).

79. Casini, S. *et al.* Tubulin polymerization modifies cardiac sodium channel expression and gating. *Cardiovasc. Res.* **85**, 691–700 (2010).

80. Maltsev, V. A. & Undrovinas, A. I. Cytoskeleton modulates coupling between availability and activation of cardiac sodium channel. *Am. J. Physiol.-Heart Circ. Physiol.* **273**, H1832–H1840 (1997).

81. Cox, C. J. *et al.* Differential regulation of gene expression by PITX2 isoforms. *J. Biol. Chem.* **277**, 25001–25010 (2002).

82. Campione, M. *et al.* The homeobox gene Pitx2: mediator of asymmetric left-right signaling in vertebrate heart and gut looping. *Dev. Camb. Engl.* **126**, 1225–1234 (1999).

83. Logan, M., Pagán-Westphal, S. M., Smith, D. M., Paganessi, L. & Tabin, C. J. The transcription factor Pitx2 mediates situs-specific morphogenesis in response to left-right asymmetric signals. *Cell* **94**, 307–317 (1998).

84. Yoshioka, H. *et al.* Pitx2, a bicoid-type homeobox gene, is involved in a lefty-signaling pathway in determination of left-right asymmetry. *Cell* **94**, 299–305 (1998).

85. Franco, D., Christoffels, V. M. & Campione, M. Homeobox transcription factor Pitx2: The rise of an asymmetry gene in cardiogenesis and arrhythmogenesis. *Trends Cardiovasc. Med.* **24**, 23–31 (2014).

86. Barbuti, A. & Robinson, R. B. Stem Cell–Derived Nodal-Like Cardiomyocytes as a Novel Pharmacologic Tool: Insights from Sinoatrial Node Development and Function. *Pharmacol. Rev.* **67**, 368–388 (2015).

87. Kitamura, K. *et al.* Mouse Pitx2 deficiency leads to anomalies of the ventral body wall, heart, extra- and periocular mesoderm and right pulmonary isomerism. *Dev. Camb. Engl.* **126**, 5749–5758 (1999).

88. Campione, M. *et al.* Pitx2 expression defines a left cardiac lineage of cells: evidence for atrial and ventricular molecular isomerism in the iv/iv mice. *Dev. Biol.* **231**, 252–264 (2001).

89. Liu, Q. *et al.* Disruption of mesoderm formation during cardiac differentiation due to developmental exposure to 13- cis -retinoic acid. *Sci. Rep.* **8**, 1–11 (2018).

90. Mommersteeg, M. T. M. *et al.* Molecular Pathway for the Localized Formation of the Sinoatrial Node. *Circ. Res.* **100**, 354–362 (2007).

91. Zoni-Berisso, M., Lercari, F., Carazza, T. & Domenicucci, S. Epidemiology of atrial fibrillation: European perspective. *Clin. Epidemiol.* **6**, 213–220 (2014).

92. Kirchhof, P. *et al.* 2016 ESC Guidelines for the management of atrial fibrillation developed in collaboration with EACTS. *Eur. Heart J.* **37**, 2893–2962 (2016).

93. Weng, L.-C. *et al.* Heritability of Atrial Fibrillation. *Circ. Cardiovasc. Genet.* **10**, e001838 (2017).

94. Mahida, S., Lubitz, S. A., Rienstra, M., Milan, D. J. & Ellinor, P. T. Monogenic atrial fibrillation as pathophysiological paradigms. *Cardiovasc. Res.* **89**, 692–700 (2011).

95. Gudbjartsson, D. F. *et al.* Variants conferring risk of atrial fibrillation on chromosome 4q25. *Nature* **448**, 353–357 (2007).

96. Ye, J. *et al.* A Functional Variant Associated with Atrial Fibrillation Regulates PITX2c Expression through TFAP2a. *Am. J. Hum. Genet.* **99**, 1281–1291 (2016).

97. Martin, R. I. R. *et al.* Genetic variants associated with risk of atrial fibrillation regulate expression of PITX2, CAV1, MYOZ1, C9orf3 and FANCC. *J. Mol. Cell. Cardiol.* **85**, 207–214 (2015).

98. Syeda, F. *et al.* PITX2 Modulates Atrial Membrane Potential and the Antiarrhythmic Effects of Sodium-Channel Blockers. *J. Am. Coll. Cardiol.* **68**, 1881–1894 (2016).

99. Chinchilla, A. *et al.* PITX2 insufficiency leads to atrial electrical and structural remodeling linked to arrhythmogenesis. *Circ. Cardiovasc. Genet.* **4**, 269–279 (2011).

100. Pérez-Hernández, M. *et al.* Pitx2c increases in atrial myocytes from chronic atrial fibrillation patients enhancing I_{Ks} and decreasing $I_{Ca,L}$. *Cardiovasc. Res.* **109**, 431–441 (2016).

101. Kirchhof, P. *et al.* PITX2c is expressed in the adult left atrium, and reducing Pitx2c expression promotes atrial fibrillation inducibility and complex changes in gene expression. *Circ. Cardiovasc. Genet.* **4**, 123–133 (2011).

102. Lozano-Velasco, E. *et al.* Pitx2 impairs calcium handling in a dose-dependent manner by modulating Wnt signalling. *Cardiovasc. Res.* **109**, 55–66 (2016).

103. Tao, Y. *et al.* Pitx2, an atrial fibrillation predisposition gene, directly regulates ion transport and intercalated disc genes. *Circ. Cardiovasc. Genet.* **7**, 23–32 (2014).

104. Collins, M. M. *et al.* Early sarcomere and metabolic defects in a zebrafish pitx2c cardiac arrhythmia model. *Proc. Natl. Acad. Sci.* **116**, 24115–24121 (2019).

105. Tao, G. *et al.* Pitx2 promotes heart repair by activating the antioxidant response after cardiac injury. *Nature* **534**, 119–123 (2016).

106. Alexios, S. A. *et al.* Redox State in Atrial Fibrillation Pathogenesis and Relevant Therapeutic Approaches. *Curr. Med. Chem.* **26**, 765–779 (2019).

107. Ghezelbash, S., Molina, C. E. & Dobrev, D. Altered Atrial Metabolism: An Underappreciated Contributor to the Initiation and Progression of Atrial Fibrillation. *J. Am. Heart Assoc.* **4**, e001808.

108. Ellinor, P. T. *et al.* Meta-analysis identifies six new susceptibility loci for atrial fibrillation. *Nat. Genet.* **44**, 670–675 (2012).

109. Giannetti, F. *et al.* A detailed characterization of the hyperpolarization-activated “funny” current (If) in human-induced pluripotent stem cell (iPSC)–derived cardiomyocytes with pacemaker activity. *Pflüg. Arch. - Eur. J. Physiol.* **473**, 1009–1021 (2021).

110. Nattel, S. & Dobrev, D. Electrophysiological and molecular mechanisms of paroxysmal atrial fibrillation. *Nat. Rev. Cardiol.* **13**, 575–590 (2016).

111. Bai, J. *et al.* In silico investigation of the mechanisms underlying atrial fibrillation due to impaired Pitx2. *PLOS Comput. Biol.* **16**, e1007678 (2020).

112. Campostrini, G., Windt, L. M., van Meer, B. J., Bellin, M. & Mummery, C. L. Cardiac Tissues From Stem Cells. *Circ. Res.* **128**, 775–801 (2021).

113. L’honoré, A. *et al.* Redox Regulation by Pitx2 and Pitx3 Is Critical for Fetal Myogenesis. *Dev. Cell* **29**, 392–405 (2014).

114. Benzoni, P. *et al.* Dual role of miR-1 in the development and function of sinoatrial cells. *J. Mol. Cell. Cardiol.* **157**, 104–112 (2021).

115. Da Dalt, L. *et al.* PCSK9 deficiency rewires heart metabolism and drives heart failure with preserved ejection fraction. *Eur. Heart J.* **42**, 3078–3090 (2021).

116. Sala, L. *et al.* Use of hiPSC-Derived Cardiomyocytes to Rule Out Proarrhythmic Effects of Drugs: The Case of Hydroxychloroquine in COVID-19. *Front. Physiol.* **12**, (2022).

ADDITIONAL PROJECTS

hiPSc-derived CMs, as mentioned above, represent a good cellular model for studying cardiac arrhythmias and cardiac pathologies in a human model, especially when there is a need to maintain a specific genetic background.

One of the projects I was involved in during my PhD, consisted in the full characterization of the electrical and molecular properties of the funny current expressed in hiPSc-derived pacemaker cardiomyocytes (hpCMs) at three differentiation timings. This work is particularly important since to date, the electrophysiological properties of human SAN myocytes are still greatly unknown. This work represents a useful comparative reference for future studies on the role of I_f (and the HCN channels underlying it) in human rhythm disturbances. This was my first published work as first author and it is found attached to this thesis.

The laboratory in which I have worked during my PhD is internationally renowned for the work on HCN channels conducting the pacemaker I_f current. The funny current has been particularly studied in the heart and neurons and has been extensively associated with functional and dysfunctional properties of excitable cells. In the last few years however, a good wealth of works demonstrating an active involvement of HCN/f-current in many cell functions in non-excitable cell/organs have been published. Together with my colleagues, I have co-authored a review that collects all this information regarding these “Uncanonical expression and roles of HCN/f channels all over the body”, which can be found below.

In collaboration with professor Norata’s laboratory, I co-authored a publication concerning how the Proprotein Convertase Subtilisin/Kexin Type 9 (PCSK9) deficiency affects heart metabolism and function. In this work, hIPSc-derived CMs were used to confirm the physiological role of PCSK9 in lipids uptake and mitochondrial function, helping to

demonstrate that an impaired cardiac metabolism leads to heart failure. The complete work is attached below.

As stated in the introduction, mESc can be differentiated in vitro into functional mature sinoatrial cells. Pacemaker mCMs were then used to assess the specific role of miR-1, the most abundant microRNA in the heart. In this work we have demonstrated that miR-1 play a dual role in cardiac pacemaker cells: it positively regulates the development of SAN precursors while at the same time modulates the beating rate of pacemaker cells through a specific inhibition of HCN4 channels translation. This work that I co-authored is listed below.

APPENDIX 1

Pflügers Archiv - European Journal of Physiology (2021) 473:1009–1021
https://doi.org/10.1007/s00424-021-02571-w

ION CHANNELS, RECEPTORS AND TRANSPORTERS

A detailed characterization of the hyperpolarization-activated "funny" current (I_f) in human-induced pluripotent stem cell (iPSC)–derived cardiomyocytes with pacemaker activity

Federica Giannetti[1] · Patrizia Benzoni[1] · Giulia Campostrini[1,2] · Raffaella Milanesi[1,3] · Annalisa Bucchi[1] · Mirko Baruscotti[1] · Patrizia Dell'Era[4] · Alessandra Rossini[5] · Andrea Barbuti[1]

Received: 22 October 2020 / Revised: 1 April 2021 / Accepted: 19 April 2021 / Published online: 2 May 2021

Abstract

Properties of the funny current (I_f) have been studied in several animal and cellular models, but so far little is known concerning its properties in human pacemaker cells. This work provides a detailed characterization of I_f in human-induced pluripotent stem cell (iPSC)–derived pacemaker cardiomyocytes (pCMs), at different time points. Patch-clamp analysis showed that I_f density did not change during differentiation; however, after day 30, it activates at more negative potential and with slower time constants. These changes are accompanied by a slowing in beating rate. I_f displayed the voltage-dependent block by caesium and reversed (E_{rev}) at − 22 mV, compatibly with the 3:1 K^+/Na^+ permeability ratio. Lowering $[Na^+]_o$ (30 mM) shifted the E_{rev} to − 39 mV without affecting conductance. Increasing $[K^+]_o$ (30 mM) shifted the E_{rev} to − 15 mV with a fourfold increase in conductance. pCMs express mainly *HCN4* and *HCN1* together with the accessory subunits CAV3, KCR1, MiRP1, and SAP97 that contribute to the context-dependence of I_f. Autonomic agonists modulated the diastolic depolarization, and thus rate, of pCMs. The adrenergic agonist isoproterenol induced rate acceleration and a positive shift of I_f voltage-dependence (EC_{50} 73.4 nM). The muscarinic agonists had opposite effects (Carbachol EC_{50}, 11,6 nM). Carbachol effect was however small but it could be increased by pre-stimulation with isoproterenol, indicating low cAMP levels in pCMs. In conclusion, we demonstrated that pCMs display an I_f with the physiological properties expected by pacemaker cells and may thus represent a suitable model for studying human I_f-related sinus arrhythmias.

Keywords Funny current · Human-induced pluripotent stem cells (hiPSC) · Sinus node · HCN channels · Pacemaker

Introduction

Rhythmicity of cardiac contractions derives from the spontaneous electrical oscillations of the sinoatrial node (SAN). In these cells, at the end of the repolarizing phase of the action potential, a slow diastolic depolarization (DD) drives the membrane potential to the threshold for firing the next action potential. Although the DD is due to a complex interplay of various ionic mechanisms, the pacemaker "funny" current (I_f) plays a pivotal role [18]. The I_f, described for the first time in 1979 in rabbit sinoatrial cardiomyocytes, owes its name to its unusual property of being activated upon hyperpolarization. f-channels are non-selective channels conducting a mixed Na^+ and K^+ current that display a dual voltage and ligand gating, being activated upon membrane hyperpolarization and direct binding of cAMP. In mammals, f-channels are the product of the HCN gene family consisting of 4 isoforms (HCN1-4). In the SAN of many species, HCN4 is the most abundant isoform followed by HCN1 and to a lesser extent HCN2 [8, 11, 13]. The importance of f-channels to cardiac rhythmicity is demonstrated by the fact that mutations in *HCN4* have been found in patients with several sinus arrhythmias, such as sinus bradycardia, inappropriate sinus tachycardia, sinus node disease but also with atrial fibrillation and ventricular non-compaction [17]. Moreover, alterations in either the physiological levels of HCN channel or in I_f current properties have been linked to other arrhythmias and cardiomyopathy [9, 35].

Federica Giannetti and Patrizia Benzoni contributed equally to this work.

This article is part of the special issue on Recent Progress with hPSCs for Drug Discovery in Pflügers Archiv—European Journal of Physiology

✉ Andrea Barbuti
andrea.barbuti@unimi.it

Extended author information available on the last page of the article

The majority of studies addressing the physiological and pathological role of I_f have been performed in rabbit and murine SAN cells [12, 16]. This choice derives from the difficulty of retrieving human SAN tissue. Indeed, while atrial and ventricular cardiomyocytes can be isolated from small biopsies during various types of surgeries, the SAN, due to its function and dimension is practically inaccessible. So far, only few studies analysed HCN channel expression in the human SAN [13, 28] and only one study described the properties of I_f in three cells isolated from a diseased human SAN [39].

The possibility to differentiate pluripotent stem cells into cardiomyocytes has opened a new opportunity to obtain SAN-like cells. Previous studies have demonstrated that SAN-like cells derived from mouse embryonic stem cells (mESC) show an I_f current with properties very similar to those of the native mouse SAN cells [5, 36]. Similarly, human induced pluripotent stem cells (hiPSC) have made easily available a source of human pacemaker cardiomyocytes, giving us the unique opportunity to analyse the properties of the human I_f current. Here we present a full functional characterization of the I_f current recorded from regularly and spontaneously beating cardiomyocytes, here dubbed pCMs (pacemaker cardiomyocytes), at different time points of differentiation.

Material and methods

Maintenance of hiPSCs lines and cardiac differentiation

All the hiPSC lines used were from healthy donors. We used previously characterized and published hiPSC lines [1, 9] derived both from females and male donors of different ages. Moreover, a new line has been generated from blood cells of a healthy male donor (age 52) following an informed consent, in agreement with the declaration of Helsinki and its use was approved by the ethical committee of the Università degli Studi di Milano (nr. 29/15). Human iPSC lines were maintained on Matrigel-coated plates in TeSR-E8 medium (Stem Cell Technologies). Cells were passaged using Tryple Express (Thermo Fisher Scientific) every 4 days and seeded at the density of 20,000 cells/cm^2. Cardiac differentiation was induced at least 30 passages after the generation of the lines and were used up to passage 140. Within this interval, we did not observe any significant variation in either the differentiation capacity or in cardiomyocytes yield. Cardiac differentiation was carried out on hiPSC monolayers using the PSC Cardiomyocyte Differentiation Kit (Thermo Fisher Scientific), following the manufacturer's instructions. Briefly, when iPSCs reached 70–80% of confluency, cardiomyocyte differentiation medium A was added; after 48 h, medium was replaced with cardiomyocyte differentiation medium B, and after other 48 h, medium was replaced with the cardiomyocyte maintenance medium (CMM) that was refreshed every 2 days. hiPSC-derived cardiomyocytes were maintained in culture for 15, 30, or 60 days.

Quantitative reverse transcriptase PCR (qRT-PCR) analysis

Total RNA was isolated using TRIzol (Thermo Fisher Scientific). GoScript™ Reverse Transcription System (Promega) was used to synthesize cDNA following the manufacturer's instructions. For each gene, qRT-PCR was performed on technical duplicates or triplicates from at least 4 independent experiments, using 10 ng of cDNA with the iQTMSYBR® Green Supermix (Bio-Rad) using the iCycler Bioer System (BIOER). Expression data were analysed using 2^(-ΔCT) method using β-actin (*ACTB*) as housekeeping gene. Gene expression levels were normalized to cardiac Troponin-T (*TNNT2*) levels to account for differences in cardiomyocytes yield among various differentiation experiments. Primers used are given below.

ACTB	F: CACTCTTCC AGCCTTCCTTC	R: AGTGATCTCCTT CTGCATCCT
TNNT2	F: AAGCCCAGG TCGTTCATGCCC	R: CTCCATGCGCTT CCGGTGGA
HCN1	F: TGAAGCTGA CAGATGGCT CTT	R: CTGGCAGTACGA CGTCCTTT
HCN2	F: CTGATCCGC TACATCCATCA	R: AGATTGCAGATC CTCATCACC
HCN3	F: TGGATCCTA CTTTGGGGAGA	R: ATGGTCCACGCT GAGTGAGT
HCN4	F: AACAGGAGA GGGTCAAGTCG	R: ATCAGGTTTCCC ACCATCAG
CAV3	F: CGAGGACAT AGTCAAGGT GGAT	R: AGAAGGAGA TGCAGGCGAAC
KCNE2 (MiRP1)	F: ACTGCATAG CAGGAGGGA AGC	R: TCAGCATCAACT TTGGCTTGG
ALG10 (KCR1)	F: CTGGCTTGT ACCTGGTGTCA	R: GGATACTTGAGG CAGCCTTGT
DLG1 (SAP97)	F: GGTCACGCC TCTCTTCAGAC	R: CACACACCTTGC CCTAGCC

Immunofluorescence (IF) staining and Western blot analysis

hiPSC-CMs were fixed in 4% paraformaldehyde and incubated in a blocking PBS solution with 0.3% Triton X-100 (Sigma-Aldrich) and 3% Donkey serum, for 45 min. Antibodies used are reported below. Nuclei were stained with

0.5 µg/ml DAPI. Western blot analyses were carried out loading 120 µg of protein extracts; proteins were separated by SDS-PAGE and transferred onto PVDF membranes. Chemiluminescence signals were acquired with the Chemidoc system (BioRAD) after membrane incubation with SuperSignal™ West Pico/Fempto PLUS Chemiluminescent Substrate (Thermo Fisher Scientific). Membranes were incubated with primary antibodies overnight at 4 °C and secondary antibodies for 1 h at RT under agitation. Mouse anti-cardiac Troponin (Abcam, clone 1C11, 1:1000), rat anti-HCN4 (Abcam, 1:2000), mouse anti-HCN1 (Termofisher, 1:1000), rabbit anti-CAV3 (Abcam, 1:500), appropriate secondary antibodies conjugated to HRP (Jackson ImmunoResearch, 1:10,000) for WB, and Alexa −488 and −594 coniugated (Jackson ImmunoResearch, 1:600) for IF were applied. Densitometric analyses of WB bands for HCNs isoforms were performed using Image J software.

Electrophysiological analysis

hiPSC-derived cardiomyocytes were isolated at day 15, 30, or 60 with tripsyn-EDTA (Sigma) and plated on fibronectin (Corning)-coated dish. Electrophysiological experiments were performed using either the ruptured or perforated patch-clamp configuration at 36 ± 1 °C on pCM. The extracellular Tyrode solution (pH 7.4) contained (mM): 137 NaCl, 5 KCl, 2 $CaCl_2$, 1 $MgCl_2$, 10 D-glucose, 10 Hepes–NaOH. Patch pipettes had a resistance of 4–7 MΩ and 10-12 MΩ, for voltage- and current-clamp recordings, respectively, when filled with intracellular-like solution (pH 7.1) containing (mM) the following: 120 KCl, 20 Na-HEPES, 10 MgATP, 0.1 EGTA-KOH, 2 $MgCl_2$.

The I_f current was recorded from isolated pCM adding $BaCl_2$ (1 mM) and $MnCl_2$ (2 mM) to the Tyrode solution (CTRL condition) to minimize interference from K^+ and Ca^{2+} currents. I_f was activated from a holding potential (hp) of −30 mV by applying 10-mV hyperpolarizing voltage steps from −35 to −125-mV long enough to reach steady-state activation, followed by a fully activating step at −125 mV. Steady-state current density was calculated as the ratio between current intensity and cell capacitance at all voltages. Activation curves were obtained from normalized tail currents and fitted to the Boltzmann equation:

$$y = 1/\left(1 + \exp\left(\left(V - V_{1/2}\right)/s\right)\right)$$

where $V_{1/2}$ is the half-activation voltage and s the inverse slope factor. Activation time constants (τ) were calculated by fitting traces to a single exponential curve in the range −75/–125 mV, after an initial delay.

Fully activated current density–voltage (I/V) relations from day 30 pCMs were determined as previously published [20]. Briefly, I_f was recorded from a hp of −35 mV by applying pairs of steps at −125 mV (all channels open) and +20 mV (all channels closed) each one followed by test steps in the range −120/ +20 mV (in 20 mV increments); fully activated current was determined as the arithmetical difference between initial current amplitude elicited by test steps at the same voltage. To block the I_f current, 2 mM CsCl was added to the control solution. The potassium-dependence was studied increasing the external K^+ concentration to 30 mM using the following external solution (in mM): 110 NaCl, 1.8 $CaCl_2$, 0.5 $MgCl_2$, 30 KCl, 1 BaCl, 2 $MnCl_2$, 5 HEPES NaOH (pH 7.4). Sodium-dependence was studied decreasing the external Na^+ concentration to 30 mM, using the following external solution (mM): 30 NaCl, 107 NMDG-Cl, 5 KCl, 2 $CaCl_2$, 1 $MgCl_2$, 10 D-glucose, 10 Hepes–NaOH (pH 7.4).

To dissect the effect of autonomic agonists on I_f and rate, isoproterenol (from 10 to 3000 nM) or carbachol (from 1 to 1000 nM) has been added to either Tyrode or control solution from concentrated stock solutions. The voltage shifts were calculated as previously reported [4] by applying hyperpolarizing pulses from − 30 mV (hp) to a voltage close to $V_{1/2}$ and compensating the differences in current amplitude caused by drugs perfusion by manually changing the amplifier holding command. Shifts were plotted against drug concentrations and fitted to the Hill equation:

$$y = Y\max^{x^n} \Big/ _{k^n + x^n}$$

where Ymax represents the maximal shift, k the EC_{50}, and n the Hill coefficient.

Statistics

Data were analysed with Clampfit 10 (Molecular Devices) and Origin Pro 9 (OriginLab). Normal distribution of data points was assessed using the Kolmogorov–Smirnov test; groups were compared with one-way ANOVA followed by pairwise comparison using Fisher's test. $P < 0.05$ defines statistical significance. Normally-distributed data are presented as Mean ± Standard Error of the Mean (SEM).

Results

Kinetic properties of I_f

Differentiation of hiPSC into cardiomyocytes is usually monitored by the appearance of spontaneously beating activity in the culture dishes, which strongly indicates the presence of a proportion of spontaneously contracting pacemaker cells. Following single cell isolation, we run patch clamp experiments only on cardiomyocytes showing regular pacemaker activity, here dubbed pCM (pacemaker cardiomyocytes). Figure 1a shows three representative action potentials (APs) recorded from single pCM at d15, 30, and 60, as indicated. AP parameters (Fig. 1 table) are in line with those previously reported for specifically selected nodal like cells [34]. Application of hyperpolarizing steps in the range −35/−125 mV to pCM elicited time- and voltage-dependent inward currents with electrophysiological properties compatible with I_f. Figure 1b shows representative traces recorded from pCMs at day 15 (triangle), day 30 (circle), and day 60 (square) of differentiation. Mean cell capacitance at the three time points was similar (20.3 ± 1.0 pF $n = 19$, 23.2 ± 1.9 pF $n = 21$, and 19.2 ± 2.1 pF $n = 13$ at days 15, 30, and 60, respectively). As shown by the steady-state *I-V* curves, current density did not vary significantly with time (Fig. 1c).

Analysis of the activation curves shows that at days 30 and 60, the voltage-dependence of I_f shifted slightly but significantly to more negative potentials than at day 15 (Fig. 1d). Finally, the analysis of activation time constant (τ) revealed that at day 15, the I_f current activated with significantly faster τ than at later differentiation days, in the range −75 to −115 mV (Fig. 1e).

hiPSC-CMs express HCN isoforms and accessory subunits

In order to evaluate the subunit composition of the I_f current, we first investigated the expression of the HCN isoforms of beating cultures at d15, 30, and 60.

From box plots in Fig. 2a, it is clear that HCN4 and HCN1 are the most abundant isoforms expressed at all time points, in accordance with literature data on SAN cells of various species and on stem cell-derived SAN-like cells. HCN1 mRNA was more expressed at day 30 than at both day 15 and day 60; HCN2 expression increased significantly at day 60; HCN3 expression was almost absent at day 15 but increased at later time points remaining however low. Transcript levels of HCN channels in human ventricular samples are shown for comparison. In agreement with literature data, HCN4 and HCN1 are not expressed in the human ventricle.

We also analysed the expression of several known auxiliary proteins of f-channels (Fig. 2b) such as caveolin-3 (CAV3), KCR-1, MiRP-1, and SAP97 that, interacting with HCN, finely modulate their functional properties [7, 32, 35]. All genes were expressed in hiPSC-CMs.

Panel c shows Western blot analysis at each differentiation time-point for HCN1, HCN4, and cTnT. HCN4 is the prevalent isoform expressed at the protein level, at all time-points. It is worth noting that the densitometry analysis revealed that the HCN1/HCN4 ratio is significantly higher at day 15 than at the other time points (d15, 2.07*; day 30, 0,30; d60, 0,07. $n = 3$, $P < 0.05$ by Anova), pointing to a higher contribution of the fast-activating HCN1 isoform at d15 than at later time points. These data agree with and support the kinetics data shown in Fig. 1d and e.

Figure 2d shows a representative immunofluorescence image of hiPSC-CMs co-stained with anti-HCN4 and -caveolin-3 antibodies. As previously demonstrated, the co-expression of these two proteins is characteristic of pacemaker/SAN cardiomyocytes of different species [4, 33, 36].

These differences are compatible with a certain degree of functional maturation likely due to a variation in the context-dependence and/or stoichiometry of HCN subunits between d15 and d30. For this reason, the following analysis were carried out only at day 30, a good compromise between time of differentiation and maturity.

Ionic nature of I_f

In Fig. 3a, representative current traces recorded applying the protocol described in the "Material and methods" section for obtaining the fully activated *I-V* relationship of I_f are shown. The reversal potential (E_{rev}) estimated from the *I-V* was around − 22 mV (Fig. 3c), a value compatible with the mixed sodium and potassium permeability typical of I_f. Addition of caesium (2 mM), a well-known blocker of the I_f current, to the extracellular solution almost completely suppressed the inward component of I_f, especially at the most negative potentials (Fig. 3b and c), while did not affect the outward current, in agreement with the previously-reported voltage-dependent block [15].

In panel 3d, the effects of varying the external concentrations of Na^+ and K^+ on the fully activated *I-V* relations are shown. Changing the external potassium concentration from 5 to 30 mM increased conductance density more than fourfold (from 58.6 ± 4.9 to 256.0 ± 40.6 pS/pF, $n = 30$ and $n = 14$ respectively) and induced a positive shift of the E_{rev} (to about − 15 mV; Fig. 3d, filled triangles). When the I_f was recorded in the low sodium (30 mM) external solution, conductance did not change significantly (46.9 ± 4.8 pS/pF,

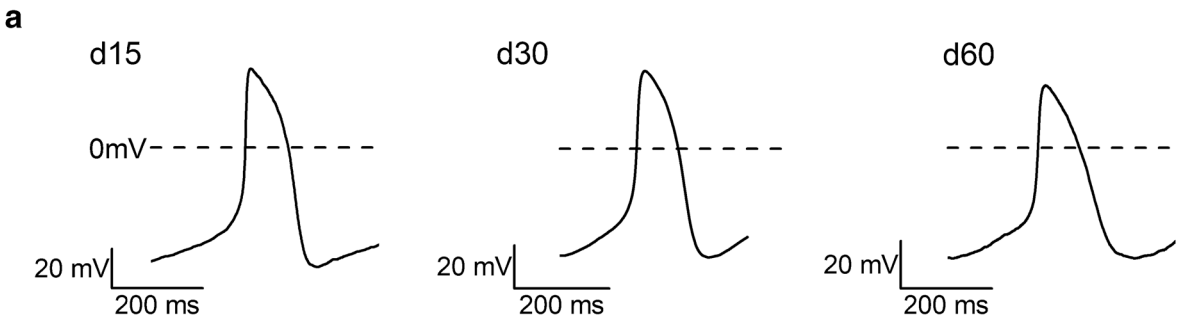

	N	Rate (Hz)	dV/dt max	MDP (mV)	APA (mV)	APD50 (ms)	APD90 (ms)	APD90c (ms)
d15	5	2.8 ± 0.1*	8.9 ± 0.5	-59.3 ± 4.7	94.2 ± 4.5	64.1 ± 4.6*	78.6 ± 5.5*	130.7 ± 10.4
d30	11	2.0 ± 0.7	12.0 ± 1.7	-53.6 ± 1.8	97.7 ± 2.5	120.2 ± 10.6	150.5 ± 12.7	194.9 ± 10.2
d60	4	1.8 ± 0.4	7.0 ± 2	-52.9 ± 3.9	80.2 ± 6.7	86.75 ± 5.8	129.2 ± 9.6	170.1± 24.1

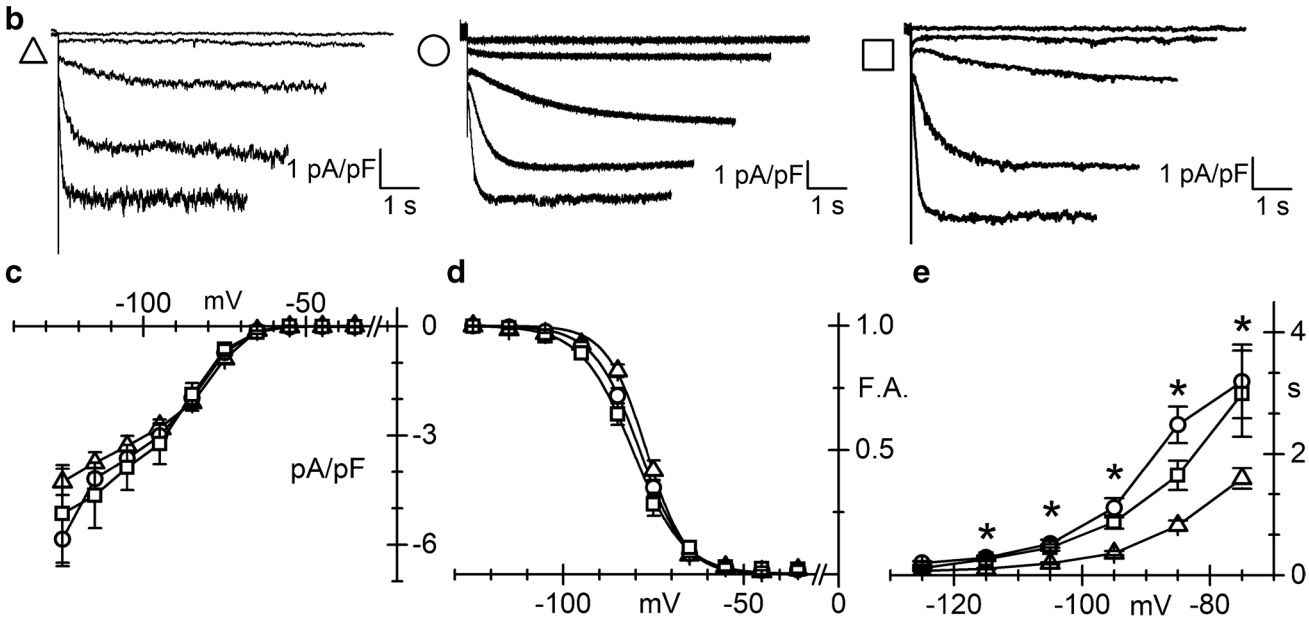

Fig. 1 Action potential properties and I_f density and kinetic in pCM. **a** (Top) Representative spontaneous action potentials recorded from d15, 30, and 60 pCMs, as indicated; (Bottom) Summary table of the AP parameters: APA, action potential amplitude; MDP, maximum disatolic potential; APD, action potential duration at 50% (APD50) or 90% (APD90) of repolarization; APD90c, rate corrected APD90. **b** Representative traces of the I_f current density recorded in the range −35/−115 mV (20 mV increment), at the three different differentiation stages (d15, triangles; d30, circles; d60, squares throughout the figure)**. c** Plot of mean I_f current density–voltage relations obtained at the different time points. Mean values at −115 mV were as follows: −3.75 ± 0.29 pA/pF (n = 19), −4.19 ± 0.45 pA/pF (n = 21), and −4.64 ± 0.90 pA/pF (n = 13). **d** Plot of the mean I_f activation curves; $V_{1/2}$ and inverse-slope factors were as follows: −76.5 ± 0.71* mV and 4.8 ± 0.36 (n = 19), −79.0 ± 0.8 mV and 5.6 ± 0.36 (n = 21), −81.2 ± 1.37 mV and 6.4 ± 0.47 (n = 13) at days 15, 30, and 60, respectively. Asterisk indicates P = 0.041 day 15 vs 30 and P = 0.0011 day 15 vs 60. **e** Plots of I_f activation time constant (τ) in the range −75 to −125 mV. Mean τ values at −75 mV were as follows: 1.6 ± 0.2 s* n = 19; 3.2 ± 0.61 s n = 21; 2.9 ± 0.71 s n = 13, at days 15, 30, and 60, respectively**.** Asterisk indicates P = 0.0423 day 15 vs 30 and P = 0.0454 day 15 vs and 60

n = 14) while the E_{rev} shifted to more negative voltages (around − 38 mV, Fig. 3d inset empty triangles). These effects are compatibles with previously reported data of I_f in rabbit SAN [20].

Modulation of I_f and spontaneous action potential rate by sympathetic and parasympathetic agonists

A well-studied modulatory mechanism of heart rate is based on a direct cAMP-dependent modulation of the funny current by autonomic neurotransmitters [19]. Here we assessed how I_f responded to different concentrations of both the

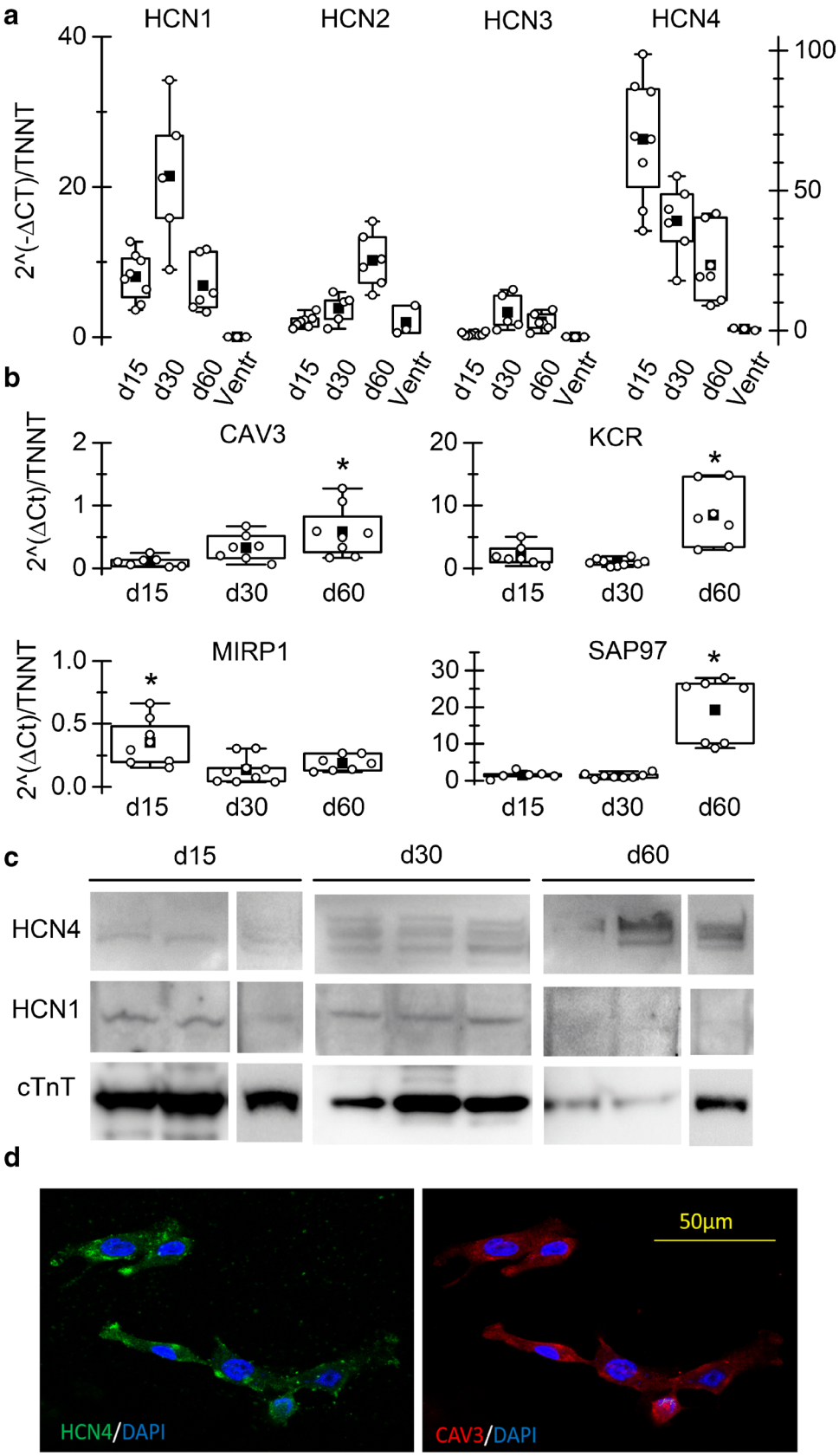

Fig. 2 hiPSC-CMs express HCN isoforms and auxiliary proteins. **a** Box-plot showing qRT-PCR analysis of HCN1-4 genes in iPSC-CMs at d15, 30, and 60, as indicated; Troponin T expression was used as reference gene in each sample to normalize for cardiomyocyte yield in different differentiations. **b** qRT-PCR analysis of genes known to be f-channels auxiliary subunits (caveolin-3-CAV3; Alpha-1,2-Glucosyltransferase-KCR1; Discs large homolog 1-SAP97; and Potassium channel βsubunit-MIRP1) in beating cultures at the various time points. **c** WB analysis of HCN4 and HCN1 in three hiPS-CM cultures at the various time points. cTnT expression was used for estimating content in cardiomyocytes. **d** Confocal microscopy image of hiPSC-CM showing co-expression of HCN4 (green) and caveolin-3 (red); nuclei were counterstained with DAPI (blue)

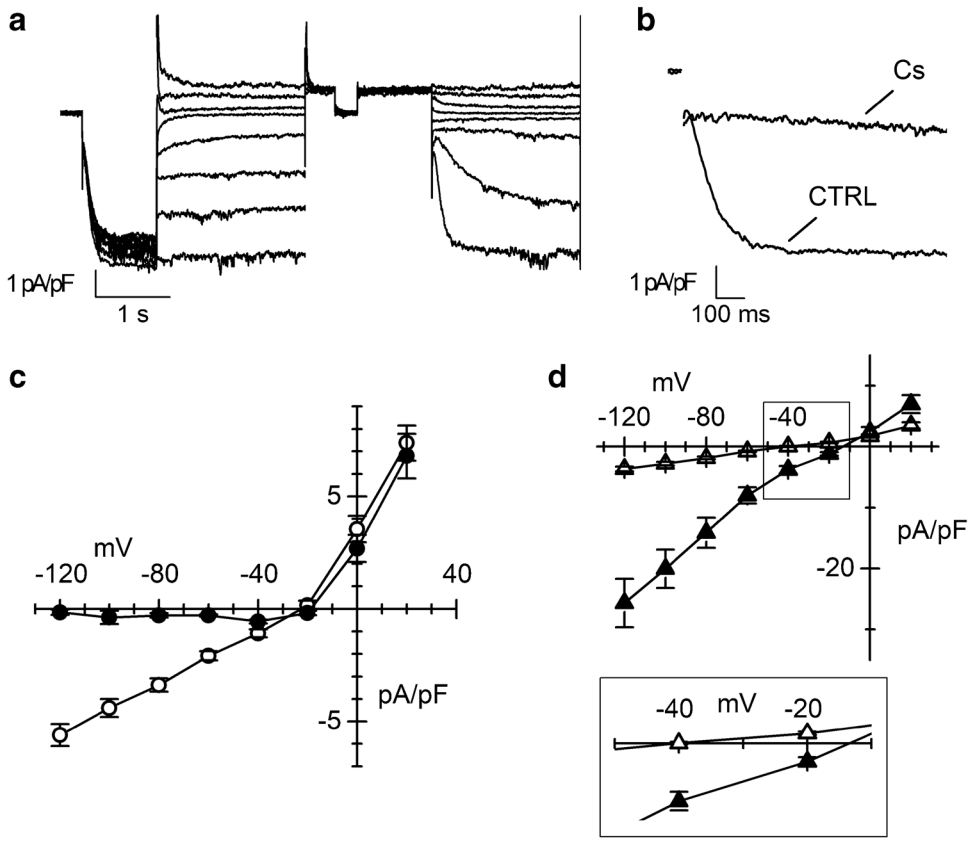

Fig. 3 Characterization of the ionic nature of I_f current. **a** Representative normalized I_f traces recorded at day 30 of differentiation elicited by the protocol used to obtain the fully activated *I-V*. **b** I_f traces recorded at −125 mV before (CTRL) and during the superfusion of 2 mM Caesium (Cs) at day 30 of differentiation. **c** Mean fully activated *I-V* relations obtained without (empty circles, $n=27$) or with 2 mM Cs (black circles, $n=20$). **d** Mean fully activated *I-V* relations in the presence of 30 mM external potassium (filled triangles, $n=13$) or 30 mM external sodium (empty triangles, $n=14$). The inset shows a blow up of the *x*-axis to appreciate changes in the E_{rev}

β-adrenergic agonist isoproterenol (Iso) and the muscarinic agonist carbachol (CCh).

In Fig. 4a and b, the time course (a) of the I_f amplitude, elicited by voltage steps in the range −80/−95 mV, before (Tyr), during (Iso) superfusion of 1 µM Iso, and after washout (WO) is shown together with representative traces, overlapped (b). As expected, isoproterenol reversibly increased I_f amplitude by shifting the activation curve to positive potentials. The shifts of the activation curve were calculated as described in the "Material and methods" section. The plot in Fig. 4c shows the dose–response curve of the shift, obtained with concentrations of Iso ranging between 10 and 3000 nM. Data points fitting with the Hill equation (see "Material and methods" section) gave a half-maximal effective concentration (EC_{50}) of 73.4 nM and a Hill number of 0.96.

In Fig. 4d, e, and f, the time course, current traces, and dose–response curve of the shift obtained perfusing the parasympathetic agonist CCh at different concentrations (1 to 1000 nM) are shown. Perfusion of 100 nM CCh induced a reduction of the current amplitude (CCh in Fig. 4d and e) corresponding to a leftward shift of the activation curve of about 3 mV. Fitting of the dose–response curve with the Hill equation resulted in an EC_{50} of 11.6 nM and a Hill number of 0.8.

Since responses to CCh were smaller than expected from literature data [21, 41], we re-evaluated the effect of 100 nM CCh after previous stimulation of I_f with 100 nM Iso (Iso and Iso + CCh in Fig. 4e). Data in Fig. 4g–i show that under this experimental conditions, 100 nM CCh caused a mean shift of 6.4 ± 0.81 mV ($n=5$), significantly higher than the 2.9 ± 0.34 mV shift caused by 100 nM CCh alone ($n=4$). These data indicate that pCMs have low basal level of cAMP.

We finally evaluated the effects of Iso (1 µM) and Ach (100 nM) on action potentials recorded from small aggregates of 30 day-old spontaneously beating pCMs. In Fig. 5a and b, representative time-courses of the beating rates before, during, and after Iso or Ach superfusion are plotted.

As expected, Iso accelerated, while ACh slowed the spontaneous beating rate. In panel 5c and 5d, stretches of action potential recordings in Tyrode (continuous line) and Iso or ACh (dashed line) are shown overlapped to highlight the changes in the slope of the diastolic depolarization (DD). Panels 5e and 5f show the dot plot of the % change in beating activity elicited by Iso (mean increase + 102.7 ± 16.0%, $n=13$) and ACh (mean decrease − 12.5 ± 1.7%, $n=7$). Coherently with the effect of the drugs on the I_f, the slope of the DD significantly increased from 0.014 ± 0.002 to 0.029 ± 0.004 V/s during Iso superfusion ($P=0.0023$; $n=13$), but only slightly decreased with the muscarinic agonist (0.011 ± 0.002 V/s; $P=0.4731$; $n=7$). Again, the small effect of ACh on the DD is compatible with low intracellular cAMP levels.

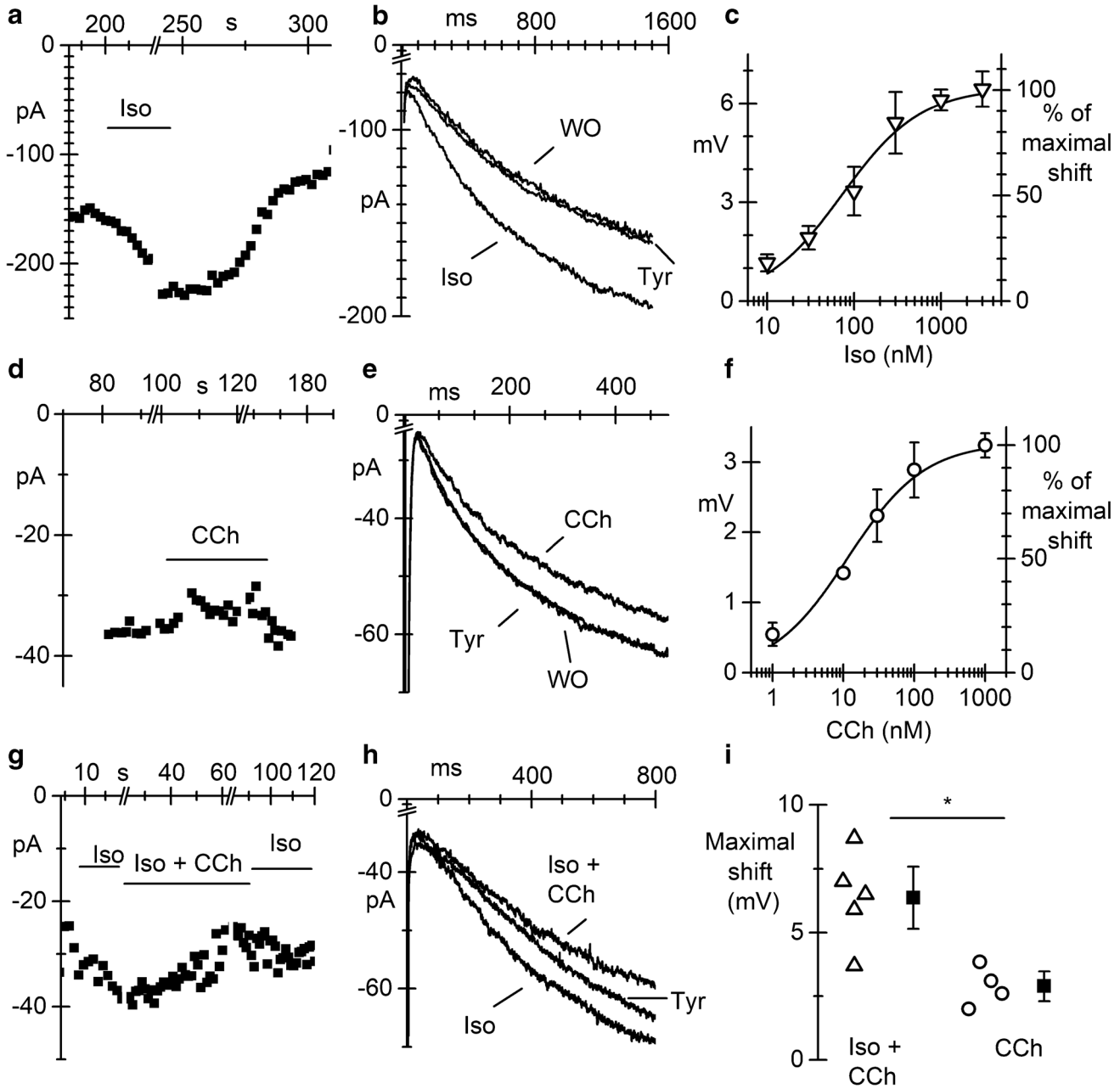

Fig. 4 I_f current in pacemaker pCMs is modulated by sympathetic and parasympathetic agonists. **a** Time course of I_f current elicited by voltage steps at − 80 mV at d30 during perfusion of 1 µM isoproterenol (Iso). **b** Overlapped I_f traces in Tyrode (Tyr), during iso perfusion and after wash-out (WO). **c** Dose–response curve for isoproterenol. **d** Time course of I_f current elicited by voltage steps at −95 mV at d30 during perfusion of 100 nM carbachol (Cch). **e** Representative I_f current traces recorded before (Tyr), during (CCh), and after carbachol wash-out (WO). **f** Plot of dose–response curve for CCh. Continuous lines in panels **c** and **f** represent the best fitting to the Hill equation. **g** Time course of I_f current elicited by voltage steps at − 95 mV at d30 during perfusion of 100 nM iso alone and Iso + Cch 100 nM. **h** Overlapped I_f traces in Tyrode (Tyr), during superfusion of Iso (Iso), and during Iso+CCh.. **i** Dot plot of the shifts of the I_f activation curve caused by 100 nM CCh with or without pre-stimulation with 100 nM Iso, as indicated. *$P = 0.0096$

Discussion

In the last years, hiPSC-derived cardiomyocytes have been extensively used to model heart pathophysiology, in particular genetic arrhythmias such as long QT syndrome, CPVT, Brugada syndrome, and atrial fibrillation [9, 27, 31, 38]. Being patient- and pathology-specific, hiPSC-derived cardiomyocytes are the perfect tools for studying in vitro both the pathological mechanisms and drug response [24]. Moreover, this model overcome the problem of the paucity of the human cardiac cell availability.

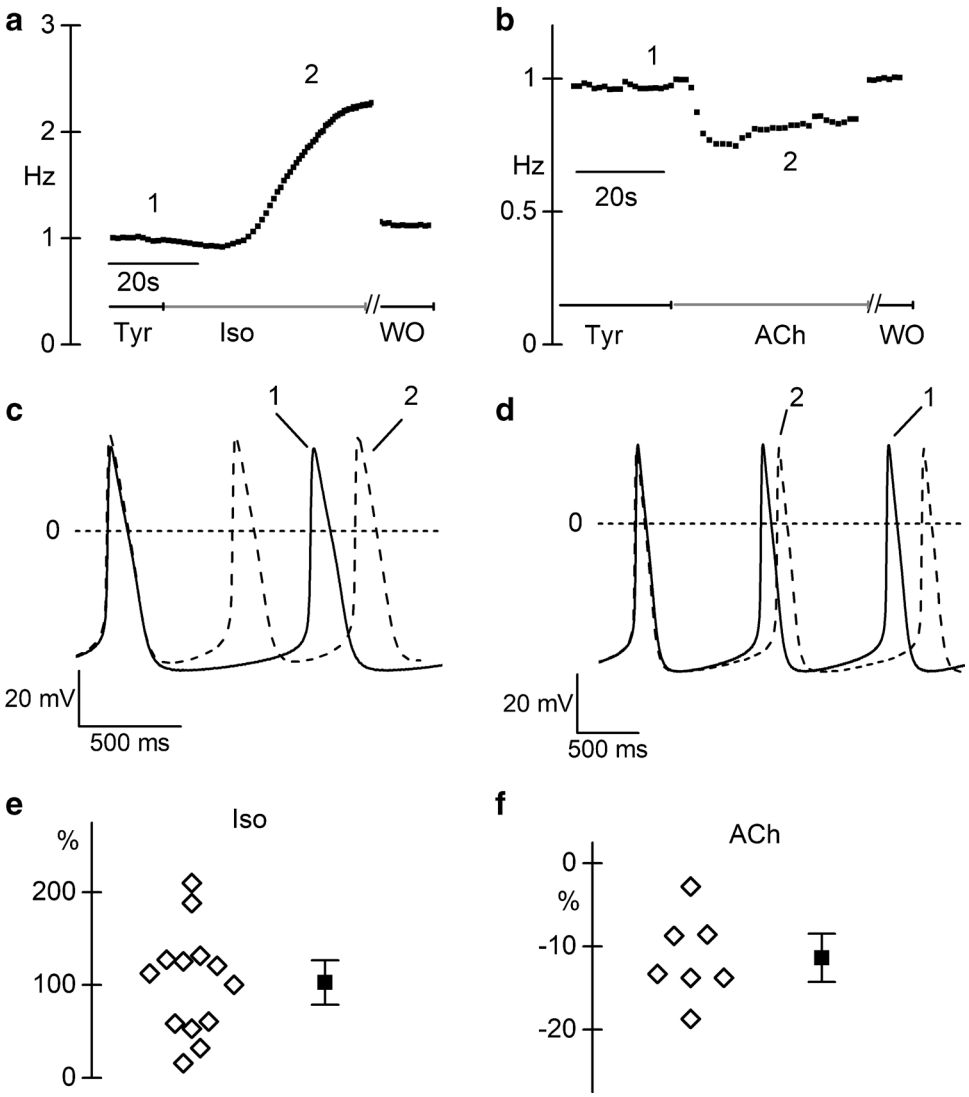

Fig. 5 Spontaneous rate of pCMs is modulated by sympathetic and parasympathetic agonists. **a** Representative time course of the action potential rate in clusters of pCMs at 30 days of differentiation before, during 1 μM isoproterenol perfusion, and after washout, as indicated. **b** Representative time course of the action potential rate before, during, and after washout of 100 nM acetylcholine (ACh) perfusion. **c**, **d** Representative action potential traces recorded before (solid line) and during (dashed line) isoproterenol (**c**) and Ach (**d**) stimulation; traces correspond to points 1 and 2 in of the respective time courses. **e**, **f** Dot plot of the percentage change in firing rate during 1 μM Iso (**e**) and 100 nM Ach (**f**). Mean ± SEM value is reported as filled square and whiskers

The main limitation of iPSC-derived cardiac cell as a model to study working cardiomyocytes consists in their immature electrical phenotype. A functional marker of this immaturity is the permanence of spontaneous pacemaker activity which is associated with the persistently high expression of the I_f current and the very low levels of I_{K1} [23]. Interestingly, however, these two features are the prototypical functional markers of sinoatrial cells. Thus, hiPSC-derived cardiomyocytes may represent a favourable model for studying human pacemaker activity of sinoatrial-like cells. For this reason, this paper characterized the I_f current restricting the electrophysiological recordings to only pCMs, that is those cells showing a regular spontaneous beating activity.

Under our experimental conditions, we observed that the I_f current density remained constant over time in culture. Our values are comparable with those previously reported in the literature both for hESC-CMs and iPSC-CMs [10, 30]; however, they are slightly smaller than those observed in diseased human SAN cells [39]. Of note, despite we did not employed any specific selection to enrich the culture in SAN-like myocytes, the mean I_f densities reported here for pCMs (−4.3, −5.8, −5.2 at −125 mV, at days 15, 30, and 60 respectively) are compatible with the I_f density reported by Protze et al. in selected sinoatrial-like cells (~4.5 pA/pF at −120 mV) and much higher than that reported for ventricular-like cells (~1.5 pA/pF at −120 mV) [34]. This evidence suggests that the choice of spontaneously beating cells is a convenient and reliable method to select *bona fide* sinoatrial-like cells, when culture purity is not an issue.

Between day 15 and day 30, we observed a slightly but significant leftward shift of the $V_{1/2}$ of the activation curves. A similar shift has been previously demonstrated in hESC due to

a specific HCN4-Caveolin-3 interaction [10], shift that can be reverted by caveolae disruption with Methyl-β-cyclodextrin or by disruption of the caveolin-binding motif of HCN4 [6]. The mean $V_{1/2}$ value reported in our study is within the physiological range for I_f to contribute to the DD, and close to the values reported for hESC-derived cardiomyocytes at similar maturation stages [10], and in mature rabbit SAN [3]. However, it differs by 20 mV from that reported for human SAN cells (around −97 mV). This difference, and in particular a negative $V_{1/2}$ may be due to methodological reasons (such as failure to reach current steady-state activation at depolarized voltages or from the presence of different extent of current run-down [20], and/or from the remodelling of the pathological human SAN cells analysed by Verkerk et al. [39].

The maturation of the properties of the funny current with time in pCMs is also indicated by changes in the τ of activation. pCMs at day 15 have significantly faster τ than at days 30 and 60. At these later stages, τ values are comparable with those found in the literature for rabbit SAN cells [3] and for human SAN cells [39]. Slower activation kinetics and more negative activation voltages (for the same current–density) would lead to a lower contribution of I_f during the slow diastolic depolarization and consequently a decreased rate. Accordingly, we found that spontaneous rate of pCMs significantly decreased from 1.27 ± 0.31 Hz at day 15 ($n = 20$) to 0.88 ± 0.47 Hz at day 30 ($n = 26$; $P = 0.0025$, data not shown).

Fully activated *I-V* relation of I_f shows a slight outward rectification and the expected reversal potential around −20 mV, compatible with the mixed Na^+/K^+ selectivity typical of both rabbit I_f [20] and heterologously expressed human HCN channels [29]. This is further confirmed by the dependence of I_f on the external Na^+ and K^+ concentrations. In agreement with data of DiFrancesco et al. in calf purkinje fibres [14] and in rabbit SAN cells[20], increasing $[K^+]_o$ induced a small positive shift of E_{rev} and a fourfold increase in conductance, while lowering $[Na^+]_o$ concentration resulted only in a more negative E_{rev}. Furthermore, 2 mM Cs in the external solution reduced the inward component of I_f without affecting the conductance at potentials more positive than the E_{rev} [20].

In the human heart, HCN channels are widely distributed and their isoform expression ratio changes according with the type, function, and maturation of the cardiomyocytes. The conduction system, and in particular the sinus node of many mammalian species, expresses mostly HCN4 and HCN1, while the working myocardium expresses predominantly the HCN2 isoform [7]. In the mouse, HCN4 is the first isoform expressed during cardiogenesis when the primary myocardium forms, and later in development, its expression remains restricted to the sinoatrial node and the conduction system [2]. Here we show that pCMs express HCN4 and HCN1 mRNA as the predominant isoforms. These data are also in agreement with data obtained from SAN-like cells obtained after selection/enrichment procedure [34, 37] and from human SAN cells [13, 28].

It is now well established that the properties of the native I_f do not depend exclusively on the specific HCN subunits but also on their interaction with several accessory subunits, which influence channel trafficking, subcellular localization, and fine tune conductance and kinetics [35]. The accessory subunits MiRP1 SAP97, KCR1, and caveolin3 are all expressed in pCMs.

Finally, we provided here, for the first time, the whole dose–response curves of human I_f to autonomic stimulation. Increasing doses of isoproterenol progressively shifted the activation curve to more positive voltages with a maximum shift recorded of around 6 mV at saturating doses, a shift similar to that previously reported for rabbit SAN cells [4]. Hill fitting revealed an EC_{50} value close to that previously reported in rabbit SAN [40]. The muscarinic agonist carbachol progressively shifted the activation curve to more negative voltages with an EC_{50} of 11.6 nM, equal to that obtained in rabbit SAN [21, 40]. However, maximal shift with CCh was only of ~ 3 mV compared to the more than 6 mV reported in rabbit SAN [42]. We believe that the reason for the small effect of CCh in our pCMs is the low level of cAMP; indeed, pre-stimulation of the adenylate cyclase with 100 nM isoproterenol increased the response to 100 nM CCh to 6.4 mV compared to the 2.9 mV without pre-stimulation. These data clearly rule out the lack of expression of either muscarinic receptors or associated G proteins and that instead pCMs functionally express important proteins necessary for autonomic modulation of the I_f current and spontaneous rate. The low level of cAMP may for example derive from the high activity of phosphodiesterases (PDEs). The role of PDEs and in particular PDE3 and PDE4 in hiPS-CM has been recently shown in various works in which their inhibition resulted in the increase of basal cAMP level [22, 25, 26]. We may speculate that the low level of cAMP and high PDE activity may also explain the significantly slower time constant of the isoproterenol-mediated rate acceleration (7.6 ± 1.0 s) than the time constant of the rate slowing due to muscarinic receptors activation (3.4 ± 0.8 s).

Finally, we evaluated how these rate-modulators affect the beating activity of pCMs clusters; as expected and in line with the low cAMP levels, 1 μM Iso doubled the rate, while 100 nM ACh decreased it only by 13%; the same concentration of ACh applied to rabbit SAN cells led to a 68% decrease in the action potential rate [21]. Interestingly, a linear regression analysis of basal rate vs agonist-induced rate change revealed that, while the isoproterenol-induced increase in rate results mildly but significantly correlated to basal rate (Pearson's r value = −0.56, $P < 0.05$), the Ach-induced decrease in rate is not correlated (Perason's r value = 0.35, $P = 0.43$). All these data suggest that in our model, the muscarinic pathway is present and functional but because of the low basal cAMP levels, the response is blunted.

In conclusion, this work provides the first complete description of the properties of I_f in human-induced pluripotent stem cell (iPSC)–derived pacemaker cardiomyocytes. The set of kinetics and modulatory parameters provided here may represent useful comparative elements for future studies of cardiac diseases in which alterations of the I_f current or of HCN channels may play an important role in the onset of the pathology, as recently demonstrated [9].

Funding Open access funding provided by Università degli Studi di Milano within the CRUI-CARE Agreement. This work was supported by the Fondazione Cariplo Grant numbers 2014–1090 to AB and 2014–0822 to PDE and MB; and by the Department of Innovation, Research and Universities of the Autonomous Province of Bolzano-South Tyrol (Italy) to AR.

Data availability All data supporting the findings of this study are available within the article and from the corresponding author on reasonable request.

Declarations

Ethical approval All the hiPSC lines used were from healthy donors. We used previously published hiPSC lines [1, 9] and a new line generated from blood cells of donors following an informed consent, in agreement with the declaration of Helsinki and their use was approved by the ethical committee of the Università degli Studi di Milano (nr. 29/15).

Consent for publication All authors have read and consented to the publication of the manuscript.

Competing interests The authors declare no competing interests.

References

1. Aasen T, Raya A, Barrero MJ, Garreta E, Consiglio A, Gonzalez F, Vassena R, Bilic J, Pekarik V, Tiscornia G, Edel M, Boue S, Izpisua Belmonte JC (2008) Efficient and rapid generation of induced pluripotent stem cells from human keratinocytes. Nat Biotechnol 26:1276–1284. https://doi.org/10.1038/nbt.1503
2. Barbuti A, Robinson RB (2015) Stem cell-derived nodal-like cardiomyocytes as a novel pharmacologic tool: insights from sinoatrial node development and function. Pharmacol Rev 67:368–388. https://doi.org/10.1124/pr.114.009597
3. Barbuti A, Gravante B, Riolfo M, Milanesi R, Terragni B, DiFrancesco D (2004) Localization of pacemaker channels in lipid rafts regulates channel kinetics. Circ Res 94:1325–1331
4. Barbuti A, Terragni B, Brioschi C, DiFrancesco D (2007) Localization of f-channels to caveolae mediates specific beta2-adrenergic receptor modulation of rate in sinoatrial myocytes. J Mol Cell Cardiol 42:71–78
5. Barbuti A, Crespi A, Capilupo D, Mazzocchi D, Baruscotti M, DiFrancesco D (2009) Molecular composition and functional properties of f-channels in murine embryonic stem cell-derived pacemaker cells. J Mol Cell Cardiol 46:343–351
6. Barbuti A, Scavone A, Mazzocchi N, Terragni B, Baruscotti M, Difrancesco D (2012) A caveolin-binding domain in the HCN4 channels mediates functional interaction with caveolin proteins. J Mol Cell Cardiol 53:187–195. https://doi.org/10.1016/j.yjmcc.2012.05.013
7. Baruscotti M, Barbuti A, Bucchi A (2010) The cardiac pacemaker current. J Mol Cell Cardiol 48:55–64. https://doi.org/10.1016/j.yjmcc.2009.06.019
8. Baruscotti M, Bucchi A, Viscomi C, Mandelli G, Consalez G, Gnecchi-Rusconi T, Montano N, Casali KR, Micheloni S, Barbuti A, DiFrancesco D (2011) Deep bradycardia and heart block caused by inducible cardiac-specific knockout of the pacemaker channel gene Hcn4. Proc Natl Acad Sci U S A 108:1705–1710
9. Benzoni P, Campostrini G, Landi S, Bertini V, Marchina E, Iascone M, Ahlberg G, Olesen MS, Crescini E, Mora C, Bisleri G, Muneretto C, Ronca R, Presta M, Poliani PL, Piovani G, Verardi R, Di Pasquale E, Consiglio A, Raya A, Torre E, Lodrini AM, Milanesi R, Rocchetti M, Baruscotti M, DiFrancesco D, Memo M, Barbuti A, Dell'Era P (2020) Human iPSC modelling of a familial form of atrial fibrillation reveals a gain of function of If and ICaL in patient-derived cardiomyocytes. Cardiovasc Res 116:1147–1160. https://doi.org/10.1093/cvr/cvz217
10. Bosman A, Sartiani L, Spinelli V, Del Lungo M, Stillitano F, Nosi D, Mugelli A, Cerbai E, Jaconi M (2013) Molecular and functional evidence of HCN4 and caveolin-3 interaction during cardiomyocyte differentiation from human embryonic stem cells. Stem Cells Dev 22:1717–1727. https://doi.org/10.1089/scd.2012.0247
11. Brioschi C, Micheloni S, Tellez JO, Pisoni G, Longhi R, Moroni P, Billeter R, Barbuti A, Dobrzynski H, Boyett MR, DiFrancesco D, Baruscotti M (2009) Distribution of the pacemaker HCN4 channel mRNA and protein in the rabbit sinoatrial node. J Mol Cell Cardiol 47:221–227
12. Bucchi A, Barbuti A, Difrancesco D, Baruscotti M (2012) Funny current and cardiac rhythm: insights from HCN knockout and transgenic mouse models. Front Physiol 3:240. https://doi.org/10.3389/fphys.2012.00240
13. Chandler NJ, Greener ID, Tellez JO, Inada S, Musa H, Molenaar P, DiFrancesco D, Baruscotti M, Longhi R, Anderson RH, Billeter R, Sharma V, Sigg DC, Boyett MR, Dobrzynski H (2009) Molecular architecture of the human sinus node: insights into the function of the cardiac pacemaker. Circulation 119:1562–1575
14. DiFrancesco D (1981) A study of the ionic nature of the pacemaker current in calf Purkinje fibres. J Physiol 314:377–393
15. DiFrancesco D (1982) Block and activation of the pace-maker channel in calf purkinje fibres: effects of potassium, caesium and rubidium. J Physiol 329:485–507
16. Difrancesco D (2013) Funny channel gene mutations associated with arrhythmias. J Physiol. https://doi.org/10.1113/jphysiol.2013.253765
17. DiFrancesco D (2015) HCN4, sinus bradycardia and atrial fibrillation. Arrhythmia Electrophysiol Rev 4:9–13. https://doi.org/10.15420/aer.2015.4.1.9

18. DiFrancesco D (2019) A brief history of pacemaking. Front Physiol 10:1599. https://doi.org/10.3389/fphys.2019.01599
19. DiFrancesco D, Tortora P (1991) Direct activation of cardiac pacemaker channels by intracellular cyclic AMP. Nature 351:145–147
20. DiFrancesco D, Ferroni A, Mazzanti M, Tromba C (1986) Properties of the hyperpolarizing-activated current (if) in cells isolated from the rabbit sino-atrial node. J Physiol 377:61–88
21. DiFrancesco D, Ducouret P, Robinson RB (1989) Muscarinic modulation of cardiac rate at low acetylcholine concentrations. Science 243:669–671
22. Giacomelli E, Meraviglia V, Campostrini G, Cochrane A, Cao X, van Helden RWJ, Krotenberg Garcia A, Mircea M, Kostidis S, Davis RP, van Meer BJ, Jost CR, Koster AJ, Mei H, Miguez DG, Mulder AA, Ledesma-Terron M, Pompilio G, Sala L, Salvatori DCF, Slieker RC, Sommariva E, de Vries AAF, Giera M, Semrau S, Tertoolen LGJ, Orlova VV, Bellin M, Mummery CL (2020) Human-iPSC-derived cardiac stromal cells enhance maturation in 3D cardiac microtissues and reveal non-cardiomyocyte contributions to heart disease. Cell Stem Cell 26(862–879):e811. https://doi.org/10.1016/j.stem.2020.05.004
23. Goversen B, van der Heyden MAG, van Veen TAB, de Boer TP (2018) The immature electrophysiological phenotype of iPSC-CMs still hampers in vitro drug screening: special focus on IK1. Pharmacol Ther 183:127–136. https://doi.org/10.1016/j.pharmthera.2017.10.001
24. Gunaseeli I, Doss MX, Antzelevitch C, Hescheler J, Sachinidis A (2010) Induced pluripotent stem cells as a model for accelerated patient- and disease-specific drug discovery. Curr Med Chem 17:759–766. https://doi.org/10.2174/092986710790514480
25. Hasan A, Mohammadi N, Nawaz A, Kodagoda T, Diakonov I, Harding SE, Gorelik J (2020) Age-dependent maturation of iPSC-CMs leads to the enhanced compartmentation of beta2AR-cAMP signalling. Cells 9. https://doi.org/10.3390/cells9102275
26. Iqbal Z, Ismaili D, Dolce B, Petersen J, Reichenspurner H, Hansen A, Kirchhof P, Eschenhagen T, Nikolaev VO, Molina CE, Christ T (2021) Regulation of basal and norepinephrine-induced cAMP and ICa in hiPSC-cardiomyocytes: effects of culture conditions and comparison to adult human atrial cardiomyocytes. Cell Signal 82:109970. https://doi.org/10.1016/j.cellsig.2021.109970
27. Jung CB, Moretti A, Mederos y Schnitzler M, Iop L, Storch U, Bellin M, Jung M, Dorn T, Ruppenthal S, Pfeiffer S, Goedel A, Dirschinger RJ, Seyfarth M, Lam JT, Sinnecker D, Gudermann T, Lipp P, Laugwitz KL (2012) Dantrolene rescues arrhythmogenic RYR2 defect in a patient-specific stem cell model of catecholaminergic polymorphic ventricular tachycardia. EMBO Mol Med 4:180–191. https://doi.org/10.1002/emmm.201100194
28. Li N, Csepe TA, Hansen BJ, Dobrzynski H, Higgins RS, Kilic A, Mohler PJ, Janssen PM, Rosen MR, Biesiadecki BJ, Fedorov VV (2015) Molecular mapping of sinoatrial node HCN channel expression in the human heart. Circ Arrhythm Electrophysiol 8:1219–1227. https://doi.org/10.1161/CIRCEP.115.003070
29. Ludwig A, Zong X, Stieber J, Hullin R, Hofmann F, Biel M (1999) Two pacemaker channels from human heart with profoundly different activation kinetics. EMBO J 18:2323–2329
30. Ma J, Guo L, Fiene SJ, Anson BD, Thomson JA, Kamp TJ, Kolaja KL, Swanson BJ, January CT (2011) High purity human-induced pluripotent stem cell-derived cardiomyocytes: electrophysiological properties of action potentials and ionic currents. Am J Physiol Heart Circ Physiol 301:H2006-2017. https://doi.org/10.1152/ajpheart.00694.2011
31. Moretti A, Bellin M, Welling A, Jung CB, Lam JT, Bott-Flugel L, Dorn T, Goedel A, Hohnke C, Hofmann F, Seyfarth M, Sinnecker D, Schomig A, Laugwitz KL (2010) Patient-specific induced pluripotent stem-cell models for long-QT syndrome. N Engl J Med 363:1397–1409
32. Peters CJ, Chow SS, Angoli D, Nazzari H, Cayabyab FS, Morshedian A, Accili EA (2009) In situ co-distribution and functional interactions of SAP97 with sinoatrial isoforms of HCN channels. J Mol Cell Cardiol 46:636–643
33. Petkova M, Atkinson AJ, Yanni J, Stuart L, Aminu AJ, Ivanova AD, Pustovit KB, Geragthy C, Feather A, Li N, Zhang Y, Oceandy D, Perde F, Molenaar P, D'Souza A, Fedorov VV, Dobrzynski H (2020) Identification of key small non-coding microRNAs controlling pacemaker mechanisms in the human sinus node. J Am Heart Assoc 9:e016590. https://doi.org/10.1161/JAHA.120.016590
34. Protze SI, Liu J, Nussinovitch U, Ohana L, Backx PH, Gepstein L, Keller GM (2017) Sinoatrial node cardiomyocytes derived from human pluripotent cells function as a biological pacemaker. Nat Biotechnol 35:56–68. https://doi.org/10.1038/nbt.3745
35. Sartiani L, Mannaioni G, Masi A, Novella Romanelli M, Cerbai E (2017) The hyperpolarization-activated cyclic nucleotide-gated channels: from biophysics to pharmacology of a unique family of ion channels. Pharmacol Rev 69:354–395. https://doi.org/10.1124/pr.117.014035
36. Scavone A, Capilupo D, Mazzocchi N, Crespi A, Zoia S, Campostrini G, Bucchi A, Milanesi R, Baruscotti M, Benedetti S, Antonini S, Messina G, DiFrancesco D, Barbuti A (2013) Embryonic stem cell-derived CD166+ precursors develop into fully functional sinoatrial-like cells. Circ Res 113:389–398. https://doi.org/10.1161/CIRCRESAHA.113.301283
37. Schweizer PA, Darche FF, Ullrich ND, Geschwill P, Greber B, Rivinius R, Seyler C, Muller-Decker K, Draguhn A, Utikal J, Koenen M, Katus HA, Thomas D (2017) Subtype-specific differentiation of cardiac pacemaker cell clusters from human induced pluripotent stem cells. Stem Cell Res Ther 8:229. https://doi.org/10.1186/s13287-017-0681-4
38. Selga E, Sendfeld F, Martinez-Moreno R, Medine CN, Tura-Ceide O, Wilmut SI, Perez GJ, Scornik FS, Brugada R, Mills NL (2018) Sodium channel current loss of function in induced pluripotent stem cell-derived cardiomyocytes from a Brugada syndrome patient. J Mol Cell Cardiol 114:10–19. https://doi.org/10.1016/j.yjmcc.2017.10.002
39. Verkerk AO, Wilders R, van Borren MM, Peters RJ, Broekhuis E, Lam K, Coronel R, de Bakker JM, Tan HL (2007) Pacemaker current (I(f)) in the human sinoatrial node. Eur Heart J 28:2472–2478
40. Zaza A, Robinson RB, DiFrancesco D (1996) Basal responses of the L-type Ca2+ and hyperpolarization-activated currents to autonomic agonists in the rabbit sino-atrial node. J Physiol 491(Pt 2):347–355
41. Zaza A, Rocchetti M, DiFrancesco D (1996) Modulation of the hyperpolarization-activated current (I(f)) by adenosine in rabbit sinoatrial myocytes. Circulation 94:734–741
42. Zhang H, Holden AV, Noble D, Boyett MR (2002) Analysis of the chronotropic effect of acetylcholine on sinoatrial node cells. J Cardiovasc Electrophysiol 13:465–474. https://doi.org/10.1046/j.1540-8167.2002.00465.x

Authors and Affiliations

Federica Giannetti[1] · Patrizia Benzoni[1] · Giulia Campostrini[1,2] · Raffaella Milanesi[1,3] · Annalisa Bucchi[1] · Mirko Baruscotti[1] · Patrizia Dell'Era[4] · Alessandra Rossini[5] · Andrea Barbuti[1]

1 The Cell Physiology MiLab, Department of Biosciences, Università degli Studi di Milano, Via Celoria 26, 20133 Milano, Italy

2 Present Address: Department of Anatomy and Embryology, Leiden University Medical Center, Einthovenweg 20, 2333ZC Leiden, The Netherlands

3 Present Address: Dipartimento di Medicina Veterinaria, Università degli Studi di Milano, Via dell'Università 6, 26900 Lodi, Italy

4 Cellular Fate Reprogramming Unit, Department of Molecular and Translational Medicine, University of Brescia, viale Europa 11, 25123 Brescia, Italy

5 Institute for Biomedicine, Eurac Research, Affiliated Institute of the University of Lübeck, Viale Druso 1, 39100 Bolzano, Italy

APPENDIX 2

Progress in Biophysics and Molecular Biology xxx (xxxx) xxx

Contents lists available at ScienceDirect

Progress in Biophysics and Molecular Biology

journal homepage: www.elsevier.com/locate/pbiomolbio

The funny current: Even funnier than 40 years ago. Uncanonical expression and roles of HCN/f channels all over the body

Patrizia Benzoni [a, 1], Giorgia Bertoli [a, 1], Federica Giannetti [a], Chiara Piantoni [a, c], Raffaella Milanesi [a, d], Matteo Pecchiari [b], Andrea Barbuti [a], Mirko Baruscotti [a], Annalisa Bucchi [a, *]

[a] The Cell Physiology MiLab, Department of Biosciences, Università degli Studi di Milano, Via G. Celoria 26, 20133, Milan, Italy
[b] Department of Pathophysiology and Transplantation, Università degli Studi di Milano, Via L. Mangiagalli 32, 20133, Milan, Italy
[c] Present Address: Institute of Neurophysiology, Hannover Medical School, Carl-Neuberg-Str.1, 30625, Hannover, Germany
[d] Present Address: Dipartimento di Medicina Veterinaria, Università degli Studi di Milano, Via Dell'Università 6, 26900, Lodi, Italy

ARTICLE INFO

Article history:
Received 4 March 2021
Received in revised form
25 June 2021
Accepted 9 August 2021
Available online xxx

Keywords:
Max 6) I_f current
I_h current
Hyperpolarization-activated current
HCN channels
Leukocytes
Smooth muscle

ABSTRACT

Discovered some 40 years ago, the I_f current has since been known as the "pacemaker" current due to its role in the initiation and modulation of the heartbeat and of neuronal excitability. But this is not all, the funny current keeps entertaining the researchers; indeed, several data discovering novel and uncanonical roles of f/HCN channel are quickly accumulating. In the present review, we provide an overview of the expression and cellular functions of HCN/f channels in a variety of systems/organs, and particularly in sour taste transduction, hormones secretion, activation of astrocytes and microglia, inhibition of osteoclastogenesis, renal ammonium excretion, and peristalsis in the gastrointestinal and urine systems. We also analyzed the role of HCN channels in sustaining cellular respiration in mitochondria and their participation to mitophagy under specific conditions. The relevance of HCN currents in undifferentiated cells, and specifically in the control of stem cell cycle and in bioelectrical signals driving left/right asymmetry during zygote development, is also considered. Finally, we present novel data concerning the expression of HCN mRNA in human leukocytes.

We can thus conclude that the emerging evidence presented in this review clearly points to an increasing interest and importance of the "funny" current that goes beyond its role in cardiac sinoatrial and neuronal excitability regulation.

1. Introduction

Pioneering studies carried out in the mid-1950s proposed that the deactivation of a time dependent potassium conductance, dubbed IK2, could represent the electrical event responsible for the spontaneous depolarization observed in Purkinje Fibers (Noble, 1960; Weidmann, 1951). In the mid-late 1970s this view was challenged by studies on rabbit sinoatrial node (SAN) preparations/cells that pointed the attention to an inward current activated upon hyperpolarization and, due to this unusual property, named the "funny" current or I_f (Brown et al., 1979; Maylie et al., 1979; Noma and Irisawa, 1976; Seyama, 1976; Weiss et al., 1978). The mysterious dualism between the two processes: IK2 decay and the activating inward I_f, was finally solved by Dario DiFrancesco in his seminal study of 1981 where he reinterpreted the IK2 current (DiFrancesco, 1981) demonstrating that this phantom IK2 decay was nothing else than the real I_f current. Taken together these studies set the stage for the undisputable evidence that the I_f current provides a fundamental contribution to cardiac pacemaker generation and modulation. For a more comprehensive historical review of the "birth" of I_f see Carmeliet (2019) (Carmeliet, 2019), and DiFrancesco (2020) (DiFrancesco, 2020). Since its discovery, several elegant studies have thoroughly analyzed the kinetics and ionic features of I_f demonstrating that they were appropriate to support a fundamental role in the generation of the diastolic depolarization and modulation of heart rate. Due to this functional role associated with the intrinsic automaticity of pacemaker cells the funny current has

* Corresponding author. Department of Biosciences, Università degli Studi di Milano, via Celoria 26, 20133 Milano, Italy.
E-mail address: annalisa.bucchi@unimi.it (A. Bucchi).
[1] These authors equally contributed to the study.

https://doi.org/10.1016/j.pbiomolbio.2021.08.007
0079-6107/

since been known also as the "pacemaker" current. Soon after its discovery in the heart, the search for a similar current in neurons began and, by the end of the '80s, an almost identical current was identified and dubbed I_h (Pape and McCormick, 1989). With the introduction of molecular biology techniques in the ion channel field, the molecular correlates of the native f-current were identified and four Hyperpolarization-activated Cyclic Nucleotide-gated genes (HCN1-4) were cloned (Robinson and Siegelbaum, 2003). This step further made it possible to map the expression pattern of HCN channels in many cells and tissues. After 40 years, the role of this tiny conductance, responsible for initiating and modulating the heartbeat and neuronal excitability, is expanding far beyond these canonical functions. Indeed, data have accumulated demonstrating novel uncanonical roles of f/HCN channels. In the present review, we provide a comprehensive overview of the expression pattern HCN channels and, when available, their cellular functions in taste buds, glia, pituitary gland, blood cells, bones, smooth muscles, gastrointestinal system and urinary system. Moreover, HCN channel expression/role in the zygote, in stem cells and in mitochondria are also reviewed. To maintain the same nomenclature throughout this review, we will always refer to native currents as I_f or f-current independently from the type of cells/tissue in which it was studied.

2. HCN channels in oocyte maturation and fertilization

Understanding the physiological mechanisms controlling maturation and fertilization of mammalian oocytes is a fascinating task for its potential application in the treatment of infertility, and fine-tuning of both membrane resistance (Rm) and membrane voltage (Vm) is a critical step in these processes. Multiple studies have indeed confirmed the presence in ovarian and sperm cells of several ion channels and described their role in controlling the electrical properties of these cells (Agoston et al., 2004; Kunz et al, 2002, 2006; McCulloh and Levitan, 1987; Platano et al., 2005). In particular, Yeh and colleagues (Yeh et al., 2008) have identified HCN1, HCN2 and HCN3 proteins in several types of ovary cells (oocytes, granulosa cells, theca cells, and corpora lutea, Table 1) with an expression pattern depending on the maturation state of the oocytes. HCN4 was instead identified only in oocytes and its expression level declined throughout the reproduction lifespan (Yeh et al., 2008). Interestingly, an indirect evidence supporting the functional role of HCN channels comes from the observation that the widely used chemotherapy drug cisplatin causes a dose-dependent decrease of HCN2 expression in antral follicle granulosa and thecal cells and of HCN4 in oocytes (Yeh et al., 2009). Although this effect is clearly not the only one associated with the ovarian damage induced by cisplatin, it strongly suggests the involvement of the HCN channels/I_f current in oocytes (patho) physiology, and provides an additional stimulus to identify the exact role of this current.

The presence of a HCN-like channel, named SpIH, has also been found in the tail of Sea urchin sperm (Gauss et al., 1998). Expression studies showed that the SpIH current shares many features with the mammalian I_f, but it also has the unique property of a rapid and incomplete inactivation. Curiously, the well-known direct HCN modulator cAMP removes the inactivation and increases the channel conductance without significantly affecting the voltage dependence of the activation. The authors speculate that the role of this channel might be to respond to the membrane hyperpolarization and cAMP increase induced by the interaction between the sperm and the Speract molecules released by sea urchin eggs, to control the flagellar beating and thus sperm movement towards the eggs (Gauss et al., 1998). It is however important to mention that so far, neither HCN nor HCN-like channels have been reported in human sperm.

3. HCN channels in left-right patterning during zygote development

It is well-known that bioelectrical signals provide, together with biochemical gradients, important cues in determining proper *in vivo* morphogenesis (Levin, 2014; Levin and Stevenson, 2012), and particularly the HCN4 currents represent one of these instructive signals for the *in vivo* left-right embryo patterning process. In *Xenopus laevis* embryos, HCN4 is expressed at a very early stage (2-cell stage) and its specific downregulation, through injection of a dominant negative (DN) HCN4 mRNA, into either one of the two blastomeres, resulted in cardiac mis-localization of the morphogenetic patterning genes *Xnr-1, Lefty, Pitx2, and BMP-4* (Pitcairn et al., 2017). In a different study, the same group extended the results beyond heart morphogenesis and demonstrated that HCN4 channels are widely expressed in *Xenopus* embryos up to embryonic stage 9. This evidence agrees well with the observation reported by Pai et al. (2017) that pharmacological inhibition of the f-current (with either ZD7288, 100 μM or ivabradine, 400 μM) at early embryo stages (stage 1−10) caused gut, heart, and gallbladder heterotaxia (*situs inversus*) in ~86% of tadpoles. Inhibition of HCN4 at more advanced stages (stages 10−40) instead did not cause any significant increase in heterotaxia compared to non-treated embryos (Pai et al., 2017).

Here, and in several other experiments described in this review, f-channel blockers (Bucchi et al., 2007) have been employed as a tool to identify the role of the f-current in the functional context of the cells/tissue under investigation. It is of capital importance to be aware that f-channel selectivity is valid within certain range of concentrations (Fig. 1) which may be profoundly influenced according to the type of experiment carried out (single cells or in multicellular/tissue).

4. HCN channels in cell proliferation and apoptosis: evidence from stem and cancer cells

Since its original discovery in the Sinus Node and in neurons, the role of the I_f current has been associated with the excitability of terminally differentiated cells. However, in more recent years, the presence of f/HCN channels has been also reported in Embryonic Stem Cells (ESC) that are unspecialized, pluripotent cells endowed with almost unlimited self-renewal capability but able to differentiate into the derivatives of all three germ layers, when exposed to appropriate stimuli. The recognition of these cells as a potentially unlimited source of new cardiomyocytes, both for basic research and for cell-based therapies, prompted the characterization of their electrical properties. The functional expression of f/HCN channels in undifferentiated ESC (Table 1) was addressed for the first time in 2005 by Wang et al. (2005). These authors reported that 30% of mouse mESCs exhibit a modest hyperpolarization-activated inward current, which was reversibly inhibited by the I_f blockers Caesium (Cs^+) and ZD7288. RT-PCR analysis carried out in mESC revealed the expression of the HCN2 and HCN3 isoforms, with a prevalence of HCN3; HCN1 and HCN4 signal were not detected **(**Table 1**)** (Wang et al., 2005). The kinetic features of the current, together with its lack of response to isoproterenol (1 μM) modulation, further supported a prevalent role of the cAMP insensitive HCN3 isoform. This conclusion was then confirmed by Lau et al. (2011) with protein expression studies. Different results were however obtained by Barbuti et al. (2009) who identified all four HCN transcripts in mESC but could not record any detectable current. Contradictory results were also found in relation to the HCN expression in human (h)ESC. While Wang and colleagues (Wang et al., 2005) failed to detect the presence of f/HCN transcripts and current in hESC, Sartiani et al. (2007) reported both the expression of HCN1, 2 and 4 channels

Table 1
Comprehensive overview of HCN channels expression and I_f current properties in the cellular and subcellular systems reported in this review. N.D. = not detectable; empty space = not assessed; *, by eye; §, recordings performed at external high potassium; dev = during development.

Subtype	HCN mRNA				HCN protein				amplitude-density	V half (mV)	Refs
	1	2	3	4	1	2	3	4			
Oocytes					x	x	x	x			(Yeh et al., 2008)
Rat											
Granulosa, and techal cells; corpora lutea					x	x	x				
Rat											
Embryonic stem cells	N.D/ x	x	x	N.D/ x		N.D	x		N.D/−2.2 ± 0.4 pA/pF @ −120 mV		(Lau et al., 2011; Wang et al., 2005; Barbuti et al., 2009)
Human	N.D/ x	N.D./ x	N.D.	N.D./ x	x	x		x	N.D./-3 pA/pF * @ −130 mV	−99.5 ± 1.4	(Wang et al., 2005; Sartiani et al., 2007)
Neuronal stem cells	N.D	x	x	N.D		x	x				(Johard et al., 2020)
Mouse											
Human		x	x								
Mitochondria					N.D.	N.D.	x	N.D.	−100 pA * @ −120 mV§		(León-Aparicio et al., 2019)
Human embryonic kidney (HEK)											
Rat renal cortex					N.D.	x	x	N.D.	−180 pA * @ −120 mV§		
Rat Cardiomyocytes					N.D.	x	x	x	−20 pA * @ −140 mV	−95 ± 7	Padilla-Flores et al., 2020
Pituitary Cells	x	x	x	x	N.D/ x	x	x	x			(Kretschmannova et al., 2012; Calejo et al., 2014)
Rat - mixed population											
Rat- lactotrophs									−1.5 ± 0.4 pA/pF @ −120 mV §	−94.1 ± 2.7	(Kretschmannova et al., 2012; Gonzalez-Iglesias et al., 2006)
Rat-gonadotrophs									−1.1 ± 0.1 pA/pF @ −120 mV §	−83.2 ± 3.3	Kretschmannova et al., 2012
Rat-somatotrophs									−1.7 ± 0.3 pA/pF @ −120 mV § −2.4 ± 0.4 pA @ −120 mV	−93.2 ± 3.4	(Kretschmannova et al., 2012; Simasko and Sankaranarayanan, 1997)
Rat-thyrotrophs									−2.8 ± 0.6 pA/pF @ −120 mV §		Kretschmannova et al., 2012
Pancreas	x	x	x	x							(El-Kholy et al., 2007)
Rat, mouse islets											
β-cells Mouse (MIN6)	x	x	x	x					−36.4 ± 6.1 pA/pF @ −130 mV§	−87.1 ± 1.7	
Rat β-cells					x	x	x	x	−37.4 ± 4.6 pA/pF @ −130 mV§ −50 pA * @ −140 mV	−84.3 ± 3.9	(El-Kholy et al., 2007; Zhang et al., 2009)
Human β-cells	x			x	x						Dorrell et al., 2016
Rat α- cells						x					Zhang et al., 2008
α- cells-Mouse (α-TC6)	x	x	x	x		x			−100/-300 * pA @ −140 mV§	−102 ± 1	
Taste Receptors	x	N.D.	N.D.	x	x			x	−70 pA* @ −140 mV	−105 ± 5	(Stevens et al., 2001)
Rat											
Astrocytes	x	x	x	x	x	N.D	N.D	N.D	−73.3 ± 29.6 pA @ −150 mV		(Honsa et al., 2014; Rusnakova et al., 2013)
Mouse Cortex											
Rat Cortex, Spinal cord									−900 pA * @ −140 mV	−98	Guatteo et al., 1996
Rat Hippocampal					N.D	N.D	N.D	x dev	−103.3 ± 32.7 pA @ −150 mV		(Honsa et al., 2014; Seo et al., 2015)
Microglia	x	x	x	x	x	x	x	N.D			(Vay et al., 2020)
Rat											
Osteoclast	x	N.D	N.D	x				x	−70 pA * @ −140 mV		Notomi et al., 2015
Mouse											
Uterine SMC									−6 pA/pF * @-130 mV	−84.3	(Okabe et al., 1999)
Rat circular											
Rat longitudinal									0/-1 pA/pF* @-120 mV		(Satoh, 1995; Okabe et al., 1999)
Corpus cavernous SMC							x	x			(Gur et al., 2019)
Human											
Lymphatic SMC	x	x	x	x	x	x	x	x			(Negrini et al., 2016)
Rat											
Sheep									−50 ± 12 pA @ −120 mV	−81 ± 1.8	McCloskey et al., 1999
Gastro-intestinal (ICCs)					N.D	x	x	x			(O'Donnell et al., 2015)
Human Colon											
Mouse Colon	N.D./ x	N.D./ x	x	N.D./ x				x			(Shahi et al., 2014; Lee et al., 2017)
Mouse Small intestine	N.D	N.D	N.D	N.D							Shahi et al., 2014
Mouse Jejunum	N.D.	x	x	x				x			Lee et al., 2017
Gastro-intestinal (Enteric neurons)					N.D	x	x	x			(O'Donnell et al., 2015)
Human Colon											
Mouse	x	x	x	x	x	x	N.D	N.D.			(Xiao et al., 2004; Yang et al., 2012)
Rat					x	x	N.D	N.D.			Xiao et al., 2004
Guinea pig					N.D.	x	N.D.	x	Myenteric: 305 ± 48.7 pA @ −100 mV	Myenteric: −85	(Galligan et al., 1990; Xiao et al., 2004)

(*continued on next page*)

Table 1 (*continued*)

Subtype	HCN mRNA				HCN protein				amplitude-density	V half (mV)	Refs
	1	2	3	4	1	2	3	4			
									Submucous: 172 ± 80 pA @-120 mV	Submucous: −95 ± 5.5	
Intestinal (SMC)									−50 pA *@ −120 mV	−91 *	Yanagida et al., 2000
Guinea pig -Circular											
Rabbit -Longitudinal									−100 pA * @ −100 mV	- 84	Benham et al., 1987
Kidney	x	x	x	x	x	x	x	x			(Calejo et al., 2014; López-González et al., 2020)
Rat whole-tissue											
Rat collecting duct cells	x	x	x	x		x			−500 pA * @ −140 mV	−102 ± 2	(Bolívar et al., 2008; Carrisoza-Gaytán et al., 2011; Uawithya et al., 2008)
Rat Proximal tubule					x		x				López-González et al., 2016
Rat thick ascending limb of Henle					N.D.		x				López-González et al., 2016
Ureteral putative pacemaker cells					x			x			He et al., 2018
Human											
Mouse							x				Hurtado et al., 2014
Bladder (ICCs)					x	x	x	x			Xue et al., 2012
Human											
Rat	x	x	x	x	x	x	x	x	−50 pA * @ −120 mV		(He et al. 2012, 2018; Dong et al., 2016; Deng et al., 2015; Lu et al., 2020)
Mouse					x			x			Wu et al., 2017
Bladder (Mucosae)	x	x	x	x	x	x	x	x			Kashyap et al., 2015
Human											
Rat	x	x	x	x	x	x	x	x			Kashyap et al., 2015
Bladder (detrusor SMC)	x	x	x	x	x	x	x	x			Kashyap et al., 2015
Human											
Rat	x	x	x	x	N.D./ x	N.D./ x	N.D./ x	N.D./ x	−200 pA * @ −140 mV	−74	(Green et al., 1996; Kashyap et al., 2015; He et al., 2012; Dong et al., 2016)
Mouse	x	x									Al-Naggar et al., 2019
Leukocytes	N.D.	x	x	N.D.							Fig. 3 this review
Human total Leukocytes											
Human Lymphocyte	N.D.	x	x	N.D.							
Human Granulocyte	N.D.	N.D.	x	N.D.							

and the corresponding I_f current in hESC (Table 1). Obviously, these studies paved the way to further investigations with the aim to unravel the role of this current in ESC. Studies in pluripotent mESCs, demonstrated the involvement of HCN3 channels in cell cycle progression; indeed, blocking the associated current with either ZD7288 (0.1–30 μM) or Cs^+ (1–10 mM) caused a dose-dependent decrease of cell proliferation (Lau et al., 2011). For example, 10 μM ZD7288, significantly increased their doubling time (from 28 to 37 h) by prolonging the S phase at the expenses of the G2/M phase (Fig. 2) (Omelyanenko et al., 2016). Prolongation of the S phase was caused by a slower rate of the DNA replication process, indicating a role of HCN channels in cell cycle progression, however the pharmacological block of I_f did not affect either the expression of pluripotency markers, or the capability of the mESC to differentiate into derivatives of the three germ layers (Lau et al., 2011; Omelyanenko et al., 2016).

Altogether the most relevant observations carried out in studies on cell cycle were: i) cells were more hyperpolarized during the S phase than during the G0/G1 phase (Lau et al., 2011; Ng et al., 2010) and ii) a sustained hyperpolarization of the membrane (corresponding to a block of the I_f current) induced mitotic arrest that could be reverted by membrane potential depolarization (Sundelacruz et al., 2009). Based on these experiments it is thus possible to speculate that membrane depolarization at the end of the S phase represents a necessary step for the transition to G2/M phase.

The presence of f/HCN channels has recently been reported also in mouse neuronal stem cells (mNSCs) (Table 1). In these cells HCN2 represents the dominant isoform and its expression increases during the progression of the cell cycle (Johard et al., 2020). Block of the HCN current halted the proliferation of mNSC and caused their accumulation in the G0/G1 phase (Fig. 2). In agreement with this observation, the arrest of cell cycle in G0 was characterized by alteration of markers of active proliferation (down-regulation)and of quiescence (up-regulation). Also, genes associated with differentiation processes were not upregulated, supporting the evidence that HCN block did not induce differentiation (Johard et al., 2020). It is worth noting that, despite these channels are significantly involved in cell cycle progression both in mESC and in mNSC, the isoforms involved are different.

Cell cycling is a central issue in cancer development and therefore the HCN contribution to this event may represent a novel potential pharmacological target. Johard et al. (2020) have recently shown that, in healthy NSC exposed to radiotherapy, the block of HCN channels (ZD7288, 10 μM) exerted a protective effect increasing their survival; however, when the same experimental protocol was applied to brain tumour cells (which also express HCN channels), radiotherapy fully maintained its ability to decrease cell survival. A clear understanding of the role of HCN channels in cancer cell proliferation is still lacking even if emerging evidence confirms their functional relevance. For example, Norberg and colleagues (Norberg et al., 2010) have shown that in a cellular model of a non-small-cell lung carcinoma (NSCLC), protein kinase C (PKC) inhibition, induced by the chemotherapy drugs staurosporine and PKC412, caused cell apoptosis due to a prolonged Ca^{2+} import mediated by HCN2 channels. Indeed, the effect of chemotherapy drugs was abolished when NSCLC cells were transfected with a siRNA specifically downregulating HCN2; similarly, transfection of HEK cells with HCN2 made these cells sensitive to staurosporine and PKC412. According to the authors, the drug-induced Ca^{2+} increase mediated by HCN2 channels represents the trigger for the mitochondrial release of apoptosis-inducing factor (AIF), followed by cell death. Although HCN channels mostly conduct Na^+ and K^+, HCN2 and HCN4 are also permeable to Ca^{2+} (Michels et al., 2008),

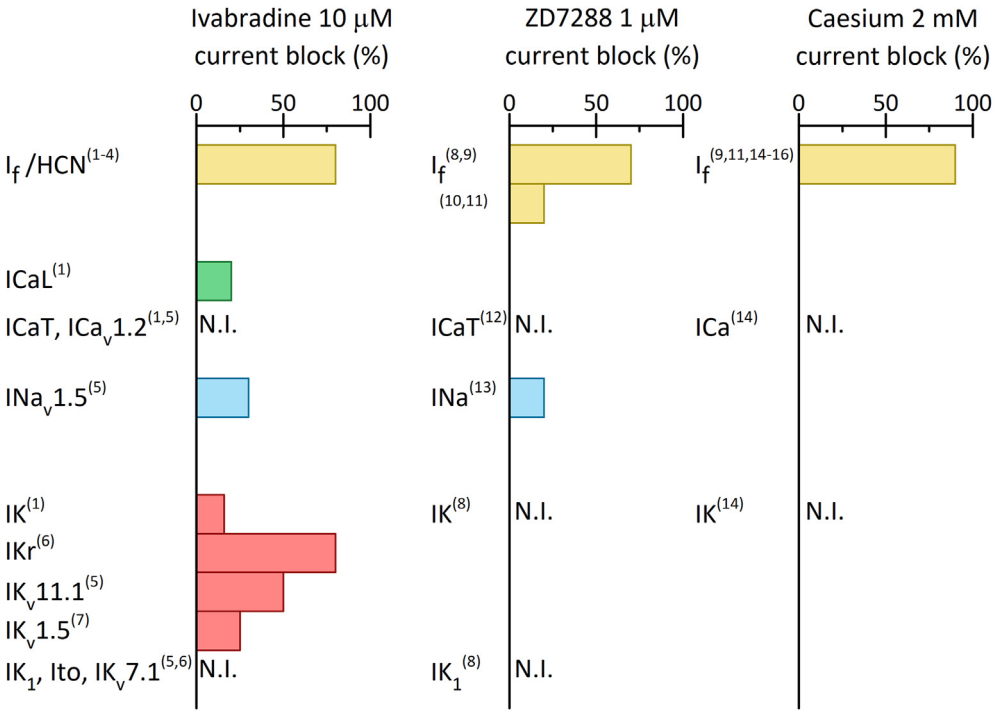

Fig. 1. Inhibitory effect of three "f-channels blockers" on the I_f and on a panel of additional currents. *Percentage current reduction induced in different types of cells by ivabradine (10 μM), ZD7288 (1 μM), and Cs^+ (2 mM). In some cases the % of block at the indicated doses was extrapolated by eye from the dose-response curve; for simplicity, when multiple data were available and quantitatively coherent we decided to show the "average" inhibition. N.I.:No inhibition: in this case the drug was tested but it did not elicit any effect. Data were collected from the literature as follows: 1,* (Bois et al., 1996)*; 2,* (Demontis et al., 2009)*; 3,* (Hsiao et al., 2019)*; 4,* (Stieber et al., 2006)*; 5,* (Haechl et al., 2019)*; 6,* (Koncz et al., 2011)*; 7,* (Delpón et al., 1996)*; 8,* (BoSmith et al., 1993)*; 9,* (Harris and Constanti, 1995)*; 10,* (Gasparini and DiFrancesco, 1997)*; 11,* (Satoh and Yamada, 2000)*; 12,* (Sánchez-Alonso et al., 2008)*; 13,* (Wu et al., 2012)*; 14,* (Denyer and Brown, 1990)*; 15,* (DiFrancesco, 1982)*; 16,* (Giannetti et al., 2021).

and Ca^{2+} permeability increases when HCN2 channels, that are normally phosphorylated by PKC at Threonine 549, become dephosphorylated (Norberg et al., 2010). This specific cell death mechanism, triggered by PKC inhibitors and mediated by HCN2, has also been found in primary cultures of rat cortical neurons (Norberg et al., 2010). Although unrelated to cancer, the Ca^{2+} influx through HCN channels followed by the AIF-mediated apoptosis has also been proposed as the mechanism behind the degeneration of Spiral Ganglion Neurons (SGNs) associated with the age-related hearing loss (Shen et al., 2018). Shen and colleagues demonstrated that HCN1 and HCN2 increased their expression in SGNs of old mice, and this increase correlated with the presence of AIF in the SNG nuclei. Further support to this mechanism comes from the observation that AIF-mediated degeneration of SNGs is increased by cAMP-induced activation of HCN channels by the adenylyl cyclase agonist forskolin (20 μM) (Shen et al., 2018). Lastly, it is worth mentioning that DNA-methylation analysis in colorectal cancer metastasis identified HCN4 as a biomarker for a poor prognosis (Ili et al., 2020).

5. HCN channels in cellular respiration and energy production

Mitochondria, the powerhouse of the cells, generate large amount of ATP through the cellular respiration process. In the matrix side of the inner mitochondria membrane (IMM), the presence of a negative potential ($\Delta\Psi m$, between −120 and −180 mV) is a necessary condition for the occurrence of oxidative phosphorylation since it provides a large driving force for mitochondria K^+ uptake which is necessary to counteract the flux generated by the K^+/H^+ antiporters. However, the evidence that under physiological conditions, most of the known mitochondrial K^+ channels are closed (Padilla-Flores et al., 2020) prompted to search for novel candidate for K^+ entry. Recently, two proteomic profiling studies of mitochondrial proteins identified several interacting partners of the HCN channels (León-Aparicio et al., 2019; Padilla-Flores et al., 2020); based on this evidence the authors proposed that HCN channels may provide a background K^+ influx into the IMM. The HCN isoforms expression in mitochondria depends on the specific cellular type: for example, HCN2, and HCN3 are expressed in the kidneys (León-Aparicio et al., 2019), while HCN2, HCN3, and HCN4 are present in cardiomyocytes, and HCN3 is the most abundant (Padilla-Flores et al., 2020) (Table 1).

Patch-clamp analysis carried out in both kidney mitochondria and cardiomyocyte mitoplasts, revealed a consistent ZD7288-sensitive hyperpolarization-activated current (Table 1). Interestingly, individual overexpression of single HCN isoforms in mitochondria of HEK293 cells shows that only HCN3 determines a current with kinetic properties similar to those recorded in the mitochondria of the renal cortex.

The expression level of HCN3 channels in kidney mitochondria increases during metabolic acidosis which is known to cause mitochondrial stress and selective autophagy driven by the depolarization of the IMM. Lopez-Gonzalez and collaborators (López-González et al., 2020) speculated that the increased expression of mitoHCN3 may be required to dissipate the membrane potential, thus initiating the mitochondrial autophagic process.

In cardiac mitoplast, instead, the kinetic properties of the I_f current were coherent with the functional expression of HCN2/HCN3/HCN4 hetero tetramers. Block of HCN channels by ZD7288 further hyperpolarized the $\Delta\Psi m$ and decreased the mitochondrial O_2 consumption (León-Aparicio et al., 2019; Padilla-Flores et al., 2020).

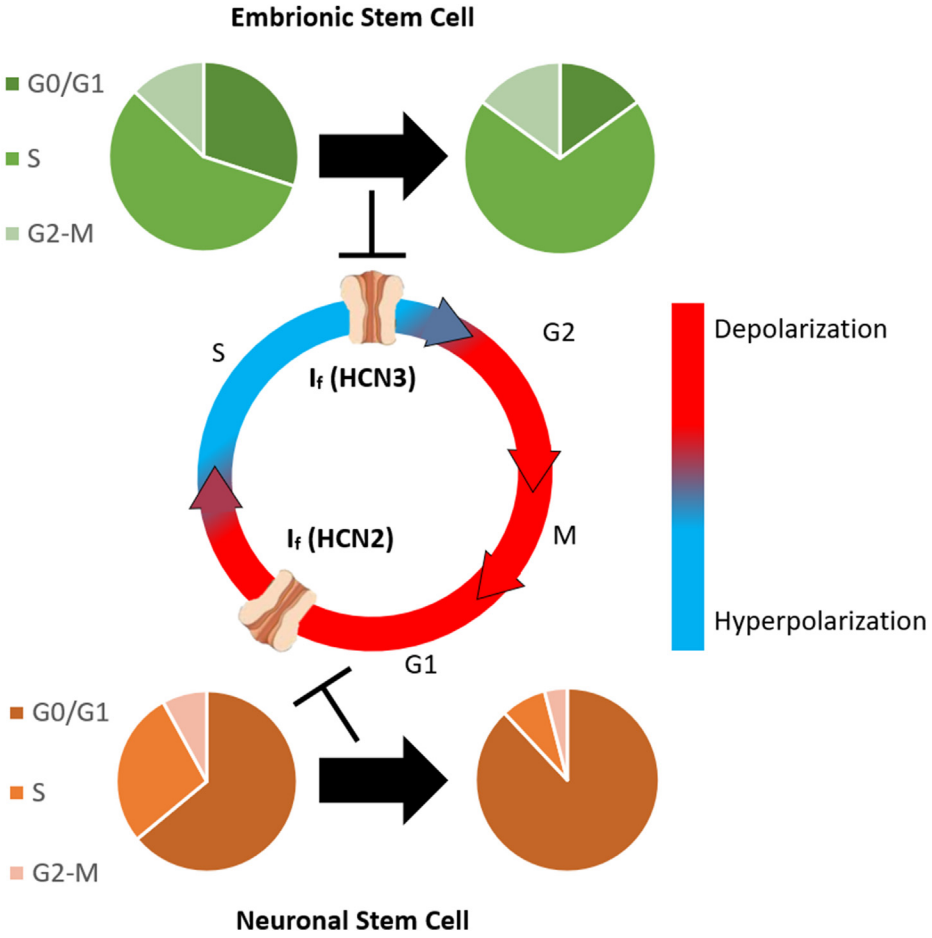

Fig. 2. Effect of *HCN channel block in the cell cycle progression of mouse Embryonic Stem Cells and Neuronal Stem Cells. Block of HCN3 and HCN2 channels expressed in mouse embryonic stem and neuronal stem cells, respectively, induces cell proliferation arrest with accumulation of cells in either the S phase (mESC) or in the G0/G1 phase (mNSC). Membrane voltage during normal cell cycle: blue corresponds to the hyperpolarized state and red to the depolarized state. See text for more details.*

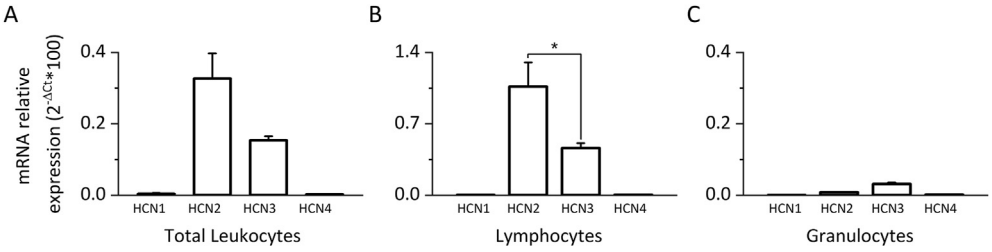

Fig. 3. HCNs mRNA profiling in human leukocytes. Relative HCN mRNA abundance assessed by means of qRT-PCR carried out in human total leukocytes (A) and in pure populations of human lymphocytes (B) and granulocytes (C) isolated from blood samples of 5 healthy subjects. Lymphocytes and granulocytes were isolated by flow cytometry. In all experiments, HCN mRNA expression was normalized to α-Tubuline (housekeeping gene) using the $2^{-\Delta Ct}$ method. Reproducible and reliable quantifications could be obtained only for HCN2 and HCN3 with the exception of HCN2 in granulocytes. *p < 0.05, Student-test.

In conclusion, according to these studies, HCN channels, and specifically HCN3, are part of the background conductances that maintain a proper K^+ influx into the IMM of mitochondria thus allowing the optimal $\Delta\Psi m$ for ATP synthesis favouring cellular respiration and ATP production.

6. HCN channels in endocrine cells

Secretory pathways are fundamental physiological processes allowing the transport of proteins and lipids from intracellular organelles to the plasma membrane where they can be released in the extracellular space. The membrane expression of HCN channels and their involvement in the regulation of exocytotic processes has been studied in different systems (Table 1); below an overview of these studies is provided.

6.1. Anterior pituitary cells

There are six types of endocrine anterior pituitary cells and they are named according to the primary hormones which are secreted:

gonadotrophs, corticotrophs, melanotrophs, thyrotrophs, somatotrophs, and lactotrophs. Each of these cell types has a typical action potential profile (tall and sharp single spikes or a variety of bursting activity) that are associated with different waves of intracellular Ca^{2+} oscillations ultimately resulting in specific pattern of hormones release (Fletcher et al., 2018). The mechanisms that control the complex electrical activity and the exocytosis of these cells are still not clear, however they require cell-type specific differential expression of ion channels. Several currents have been proposed as modulators of the spontaneous firing, and the I_f current may be one of them (Fletcher et al., 2018). All four HCN transcripts were detected in a heterogeneous population of rat anterior pituitary cells cultured for 24 h, and HCN2, HCN3 and HCN4 proteins were identified by Western blot (Kretschmannova et al., 2012) (Table 1). Patch-clamp studies recorded the I_f current in the majority of cultured thyrotrophs, gonadotrophs, and somatotrophs cells (Kretschmannova et al., 2012; Simasko and Sankaranarayanan, 1997), while experiments performed in freshly isolated and cultured rat lactotrophs cells indicated that I_f was present only in a fraction of cells (30–40%) (Gonzalez-Iglesias et al., 2006; Kretschmannova et al., 2012; Simasko and Sankaranarayanan, 1997) (Table 1). The effect of the I_f block on the spontaneous activity of pituitary cells was evaluated in several studies, but conflicting results were obtained and only some of them reported a reduction in the firing frequency (Chu et al., 2010; Kretschmannova et al., 2012; Simasko and Sankaranarayanan, 1997). This discrepancy clearly points out that further work is needed to improve our understanding of the I_f function in the spontaneously activity pituitary cells.

Another important functional pathway which may involve the contribution of the I_f current consists in the molecular events that couple the activation of G-protein coupled receptors (GPCR) to the secretory activity of pituitary cells (Kretschmannova et al., 2012). Indeed, agonists of GPCRs are physiological regulators of the electrical activity of these cells and it is known that G_s or G_i-dependent changes in cAMP and Gq/11-dependent depletion of PIP2 can regulate HCN channels (Baruscotti et al., 2005; Pian et al., 2007). Interestingly, Calejo and collaborators (Calejo et al., 2014) reported the expression of HCN2 channels both in the plasma membrane and in (or nearby) the membrane of secretory vesicles of rat lactotrophs cells. Functional studies aimed at investigating a possible involvement of HCN current in exocytosis were performed by increasing the HCN current density in rat lactotrophs cells (via HCN2 over-expression) and by inhibiting the current with ZD7288 (100 μM). These studies concluded that the exocytic activity is likely regulated by localized increases of Ca^{2+} levels caused by permeation through HCN2 channels.

6.2. Pancreatic cells

Pancreatic islet cells have a dynamic electrical activity which is pivotal for hormones secretion in response to metabolic changes; HCN channels have been found among the ion channels expressed on β- and α-cells membranes that may thus contribute to insulin and glucagon secretion (Dorrell et al., 2016; El-Kholy et al., 2007; Zhang et al., 2008, 2009) (Table 1). All HCN isoforms have been detected at the mRNA level in mouse and rat islets with HCN2 being the predominant subunit in the mouse, and HCN3 and HCN4 the main isoforms in the rat. Immunostaining experiments carried out in the rat model, showed that β-cells express all HCN isoforms; investigation in α-cells was limited to HCN2 and its presence was confirmed. In humans, the scenario is somewhat different since only HCN1 and HCN4 are present and differentially express depending on the β-cell subtypes (Dorrell et al., 2016). In rat β-cells and in clonal TC6 α-cells, a HCN-mediated inward current has been characterized and the canonical I_f properties have been reported (Table 1) (El-Kholy et al., 2007; Zhang et al., 2008). Even though the specific role played by the current in these cells is still unclear, a possible mechanism may involve the regulation of the membrane input resistance (Zhang et al., 2009). Dorrell and colleagues (Dorrell et al., 2016) reported that HCN current inhibition (with 30 mM ivabradine) had a dual effect on insulin secretion in human islets: during basal condition, ivabradine increased insulin secretion, while a reduction was observed during glucose-stimulation. However, when the effect of the HCN block was tested in isolated β-like cells generated from human pluripotent precursors, only the stimulation of basal secretion activity was observed (Dorrell et al., 2016). Data collected in rat islets showed somewhat different results; indeed HCN2 over-expression increased basal insulin secretion, while suppression of HCN current, through overexpression of the dominant negative HCN2-AYA channels, decreased glucose-stimulated insulin secretion only at low (2.5 mM) external K^+ concentrations (Zhang et al., 2009). Comparison between data obtained in human and rat islets indicate that either HCN channels may have species-specific effects or they may reflect different experimental conditions (e.g. over-expression, unspecific effects due to high ivabradine concentrations).

In mouse clonal TC6 α-cells, inhibition of HCN current with ZD7288 (100 μM) increased glucagon secretion, while stimulation of the HCN current by lamotrigine reduced glucagon release (Zhang et al., 2008). Similarly, HCN current inhibition by ZD7288 (100 μM) or cilobradine (5 μM) increased glucagon release from rat islets (Zhang et al., 2008).

Further investigations are required to properly identify the mechanisms linking HCN channels and exocytosis; however, possible roles may involve regulation of membrane input resistance, mixed Ca^{2+} and Na^+ influx, and/or cytoskeleton interaction between HCN channels and exocytotic machinery (Zhang et al, 2008, 2009).

7. HCN channels role in sour taste transduction

In vertebrates, the sour stimulus (i.e. protons) is detected by taste receptors by means of a transduction pathway that includes protein receptors and ion channels. The presence of the I_f current was first identified in rat in 2001 by Steven and collaborators (Stevens et al., 2001) who detected the expression of HCN1 and HCN4 proteins in a subset of taste receptors cells of the vallate papilla (Table 1). Three main elements indicate that HCN channels may play a role in sour taste transduction: *i*) the I_f current in these cells is increased by external sour stimuli, *ii*) lowering the extracellular pH induces a dose-dependent modulation of the activation curve of heterologously expressed HCN1 and HCN4 channels, *iii*) cells expressing HCN channels do not express the transduction elements involved in sweet and bitter taste detection (Stevens et al., 2001).

8. HCN channels in glial cells

The expression of HCN channels in neuronal cells of the Central Nervous System (CNS) has been extensively documented in a large number of studies, and several reviews provide detailed descriptions of their role (Biel et al., 2009; Santoro and Shah, 2020). Interestingly, the presence of these channels has also been reported in astrocytes and microglia.

Astrocytes are the prevalent glial cells in the brain, where they perform several regulatory functions (Kimelberg and Nedergaard, 2010). The first recording of an I_f-like current in cultured cortical and spinal cord astrocytes was accomplished in 1996 by Guatteo et al. (Table 1) (Guatteo et al., 1996), but only 17 years later

Rusnakova and colleagues (Rusnakova et al., 2013) detected the HCN mRNA in postnatal (P10 to P50) astrocytes. In 2015, Seo et al. (2015) analyzed the HCN isoform expression during hippocampal development and demonstrated the presence of HCN4-positive astrocytes in the *stratum lacunosum moleculare*. The evidence that HCN4 expression was lost at P21 was strongly suggestive of a stage-specific role in early astrogliogenesis. Interestingly, despite the fact that under physiological conditions adult glial cells express low or negligible I_f current, after focal cerebral ischemia, mRNA (HCN1, HCN2 and HCN3) and protein (HCN1 and HCN3) (Table 1) expression in astrocytes increased significantly both in rat hippocampus and mouse cortex (Honsa et al., 2014; Rusnakova et al., 2013). In isolated cortical astrocytes, 5 weeks after ischemia these changes in expression were accompanied by a depolarization of the resting potential, a decrease of membrane resistance (Rm), and the presence of a substantial ZD7288-sensitive I_f current. Similar effects were observed in hippocampal reactive astrocytes after global cerebral ischemia, even though in these cells the membrane resistance was not affected (Honsa et al., 2014). An increase of HCN1 and HCN2 immunoreactivity in GFAP + astrocytes was also recently reported in the hippocampus of gerbils 4 days after the induction of 5 min transient global cerebral ischemia (Park et al., 2019).

Microglia represents the tissue-resident macrophages in the CNS and mediate cell homeostasis and inflammatory processes. Microglia cells display a constant movement of their processes in order to detect insults and, based on different types of stimuli, they may induce either neurotoxicity or neuroprotection. Many ion channels and cell surface receptors shape these functions (Izquierdo et al., 2019). In a recent paper Vay and colleagues (Vay et al., 2020) provided the first evidence that isolated microglial cells express all HCN isoforms (Table 1), however, only HCN2 exhibited expression changes after pro- and anti-inflammatory stimuli. Curiously, HCN inhibition by ZD7288 (10–30 μM) resulted in an unexpected depolarization of the cell membrane potential and a sustained increase of intracellular Ca^{2+}. This evidence led to speculate that, as observed in some neurons, a sustained background HCN current may both reduce Rm and depolarize the cell thus influencing the gating state of other voltage-dependent channels (e.g K^+ and Ca^{2+} channels). The membrane hyperpolarization expected upon HCN blockade could therefore be masked by activation/inactivation of these channels, whose effect on membrane voltage may be amplified by the increased Rm caused by the block of HCN channels. In this study, the authors also showed that differential expression of HCN isoforms is differently regulated by pro- and anti-inflammatory polarization of microglia (Vay et al., 2020). HCN2 channels were significantly downregulated by a pro-inflammatory stimulus and strongly upregulated by an anti-inflammatory stimulus, HCN3 expression was reduced in both conditions, and HCN1 and HCN4 expression was not affected.

HCN block induced either by ZD7288 (10–30 μM) or by siRNA-mediated HCN2 silencing decreased the expression of the pro- and anti-inflammatory markers stimulated by treatments with lipopolysaccharides (LPS) and interleukin-4 (IL4), respectively. These data suggest that inhibition of HCN, primarily HCN2, hinders the correct activation of microglia, likely by a modification of intracellular Ca^{2+} signalling. The switch of microglial cells from a resting to an active state is also characterized by cell proliferation, however this process was limited by the inhibition of HCN channels by 30 μM ZD7288 (Vay et al., 2020).

9. HCN channels in osteoclasts

Bone resorption requires osteoclasts differentiation (osteoclastogenesis) and activation (Boyle et al., 2003). An interesting observation made by Notomi et al. (2015) in mouse osteoclast precursor-like cells (RAW 246.7 monocyte macrophage lineage osteoclast precursor cells) revealed that, in the presence of RANKL (Receptor Activator of Nuclear factor Kappa-B Ligand), membrane hyperpolarization accelerates their differentiation toward osteoclasts. The same group also reported the expression of HCN4 proteins both in RAW cells and in mouse bone marrow–derived osteoclasts; furthermore, the HCN-mediated current was recorded in osteoclasts derived from RAW 246.7 cells (RAW-OC) (Table 1).

Functional studies indicated that HCN channels activation inhibits the hyperpolarization-induced osteoclastogenesis process (Notomi et al., 2015). An additional role of HCN channels in the modulation of osteoclastogenesis was revealed analysing the prostaglandin E2 (PGE2) pathway. While PGE2 stimulates the differentiation of osteoclasts (Kobayashi et al., 2005), it also activates the production of cAMP, which increases the open probability of HCN channels. Interestingly, when the contribution of HCN to membrane potential of RAW cells is removed by siRNA-mediated HCN4 knockdown, PGE2-induced osteoclastogenesis is potentiated.

10. HCN channels in smooth muscles

10.1. Uterus

Myometrial smooth muscle displays an intrinsic pacemaker activity which drives uterine contractions, and several factors, including hormones, stretch, and paracrine molecules can modulate this activity. Uterine contractions occur both in the non-pregnant state (during the menstrual cycle) and during gestation, and according to different physiological or pathophysiological conditions they vary in frequency, duration, amplitude, and direction of propagation (Aguilar and Mitchell, 2010; Wray and Prendergast, 2019). To date, the mechanism behind the pacemaker activity of the uterus is still largely unknown, and neither an anatomical pacemaker region, nor the presence of widely distributed pacemaker cells, have been identified. However, based on the evidence that small isolated myometrial strips show spontaneous rhythmic contractions, it is likely that some myocytes are endowed with an intrinsic pacemaker activity (Wray and Prendergast, 2019; Young, 2018).

The involvement of the I_f current in myometrial automaticity was suggested in the 1990s when the current was measured in freshly isolated single longitudinal and circular smooth muscle cells isolated from pregnant rat uterus (Table 1) (Okabe et al., 1999; Satoh, 1995). The I_f density was larger in circular than in longitudinal myometrial cells and this finding well correlates with the evidence that spontaneous APs were frequently observed in circular but not in longitudinal myocytes. This observation led to the hypothesis that the slow activation of the I_f current at resting membrane potential might cause a slow depolarization, driving the membrane potential to the threshold for AP firing. In agreement with this conjecture, Okabe et al. (1999) observed a reduction in the spontaneous contraction rate of circular muscles following Cs-induced I_f block (IC_{50} of 0.15 mM). Additional data indicated that I_f inhibition by ZD7288 (100–200 μM) decreased the force amplitude of spontaneous and oxytocin-induced contractions of longitudinal uterine strips isolated from in-term pregnant rats (Alotaibi et al., 2017). Unexpectedly, in addition to decrease the force amplitude, ZD7288 also increased the frequency of contractions. The interpretation of these results is not straightforward since ZD7288 was used at high concentrations and therefore non-specific effect on other ion channels are likely contributing.

10.2. Corpus cavernous

The beneficial effects of ivabradine on erectile dysfunction (ED) observed in patients with heart failure and in ApoE knockout mice,

have been attributed to the drug-induced reduction of heart rate, endothelial oxidative stress, and penile fibrosis (Baumhäkel et al., 2010; Mert et al., 2018). Recently, Gur and colleagues (Gur et al., 2019) verified the hypothesis that HCN channels may also be functionally expressed in the smooth muscle of the corpus cavernous. Their study indeed identified the presence of HCN3 and HCN4 proteins in smooth muscle cells of the human penile corpus cavernous (Table 1) and showed that ivabradine (100 nM-1 mM) was able to induce a concentration-dependent relaxation of tissue strips of the human corpus cavernous previously contracted by phenylephrine. This effect was independent from the Nitric Oxide (NO)/soluble guanylyl cyclase pathway since it was maintained in the presence of both nonspecific nitric oxide synthase (NAME) and soluble guanylyl cyclase (ODQ) inhibitors. Gur and co-workers thus proposed that the direct inhibition of HCN channels in penile tissue may contribute to the beneficial effects of ivabradine on ED, and that HCN block may be a useful treatment for patients who have cardiovascular risk factors and ED (Gur et al., 2019). In addition, they also reported the evidence that ivabradine may affect other ion channels such as L-type Ca^{2+} and K^{+} channels.

10.3. Lymphatic vessels

Smooth muscle cells of the lymphatic ducts walls exhibit spontaneous contractions that are preceded by either a single or a complex pattern of APs (Kirkpatrick and McHale, 1977; Ward et al., 1991). A similar activity was more recently confirmed by Telinius and colleagues (Telinius et al., 2015) in isolated thoracic and mesenteric human lymphatic vessels. The main feature of these APs is the presence of a slow depolarization process that drives the cell membrane potential from the most negative value, reached at the end of the repolarization process, to the threshold for the next AP. The first suggestion that a hyperpolarization-activated inward current similar to I_f might be involved in these spontaneous electrical oscillations came from a study of Allen and McHale, 1988 on bovine lymphatic ducts. However, it was only in 1999 that McCloskey (McCloskey et al., 1999) fully described the I_f current in freshly isolated sheep mesenteric lymphatic smooth muscle cells (Table 1), and showed that blockade of this current by Cs^{+} (1 mM) or by ZD7288 (1 μM) decreased the frequency of spontaneous contractions in intact lymphatic vessels. Similar results were obtained in rat smooth muscle cells of peripheral diaphragmatic lymphatic vessels by Negrini and co-workers (Negrini et al., 2016) who demonstrated the expression of all HCN isoforms (Table 1) and the ability of HCN channels blockers (Cs^{+}, ivabradine, and ZD7288) to reversibly decrease the rate of contraction and to increase the end-diastolic diameter in a dose-dependent manner. The authors proposed that, during the diastolic phase, the inward current carried by HCN channels contributes to depolarize the cell up to the threshold for Ca^{2+} channels activation, which would in turn trigger the lymphatic muscle contraction (Negrini et al., 2016). However, the functional role of HCN channels is still not clear as proved by data indicating that intermediate concentrations of ZD7288 increased, rather than decreased, the frequency of contractions, a phenomenon observed also in other types of smooth muscles, such as the bladder detrusor (Green et al., 1996) and the portal vein smooth muscle (Greenwood and Prestwich, 2002).

11. HCN channels in the gastrointestinal system

The presence of HCN channels has been widely reported in all the cells associated with gastrointestinal (GI) mobility and in particular in the interstitial cells of Cajal (ICCs), in enteric neurons, and in smooth muscle cells (Table 1).

11.1. Interstitial cells of Cajal

Interstitial cells of Cajal (ICCs) are specialized mesenchymal pacemaker cells organized in networks that are electrically coupled to smooth muscle cells and are distributed in several parts of the gastrointestinal wall. ICCs are able to generate a basic slow electrical rhythm that modulate the phasic contractions of gastrointestinal smooth muscle cells. According to Sanders et al. (2014), the pacemaker mechanisms responsible for the automaticity of ICCs involve both the spontaneous release of Ca^{2+} from intracellular stores and the activity of membrane ion channels such as Ca^{2+}-activated Cl^{-} channels (Ano1) and T-type Ca^{2+} channels. However, in 2014 the presence of HCN1 and HCN3 transcripts was successfully reported in cultured murine c-kit and Ano1 positive colonic ICCs cells by Shahi and co-workers (Shahi et al., 2014), and in 2015 HCN2, HCN3, and HCN4 proteins were detected by immunofluorescence staining in human colonic ICCs (O'Donnell et al., 2015). When mouse colonic ICCs were maintained in culture for 2–3 days, they exhibited spontaneous APs that were reduced by I_f inhibitors (5 mM Cs^{+}, 10 μM ZD7288, 10 μM zatebradine and 10 μM genistein). Taken together these data raised the hypothesis that HCN channels may participate in the generation of the colonic ICCs pacemaker activity. Interestingly, the same authors demonstrated that the I_f current inhibitors had no effect on spontaneous activity of small intestinal ICCs and this is in agreement with the lack of HCN channels expression in cultured c-kit and Ano1-positive ICCs of the small intestine. These results indicate that different pacemaker mechanisms likely contribute to the activity of different areas of the GI tract (Shahi et al., 2014).

Transcriptome analysis of freshly isolated cells from the murine *tunica muscolaris* of the jejunum and colon (JICCs and CICCs, respectively) reported positive signals for HCN2, HCN3, and HCN4 in both cell types (Table 1). HCN4 was the most abundant isoform in JICCs and the least expressed in CICCs; the presence of HCN4 was also confirmed at the protein level (Lee et al., 2017). In addition to the full HCN4 transcript, JICCs also express truncated HCN4 variants (HCN4v2 and HCN4v3) both encoding for the same 795 aa-long truncated polypeptide lacking the entire N-terminal and the S1–S4 segments.

HCN channels have also been proposed to regulate the pacemaker activity of ICCs of murine gastric antrum cells (Si et al., 2012), and the association between gastrointestinal pathologies and impaired expression of HCN channels in ICCs, strengthens the role of these channels in regulating gastrointestinal motility (Guo et al., 2017; O'Donnell et al., 2015). Guo and co-workers (Guo et al., 2017) indeed showed that mice with malignant ascites developed gastrointestinal dysmotility associated with impaired peristaltic activity likely caused by an alteration of the ICCs morphology and by a decreased expression of HCN2 and Ca^{2+} transient in these cells.

11.2. Enteric neurons

The presence of the I_f current was first described in guinea pig myenteric AH neurons and in a small fraction of both S and AH neurons of the submucous plexus (Galligan et al., 1990; Messenger et al., 1994). Since then, the presence of HCN channels in murine, guinea-pig, zebrafish, and human neurons of the enteric nervous system (ENS) has been reported in several studies (Table 1) (Fujii et al., 2020; O'Donnell et al., 2015; Xiao et al., 2004; Yang et al., 2012). Xiao et al. demonstrated that the HCN1, HCN2, and HCN4 isoforms are differently expressed in different neurons of the myenteric and of the submucosal plexuses, and their relative abundance depends on the species investigated (Xiao et al., 2004). A more detailed characterization of the HCN2 positive neurons in the GI tract of mice was performed by Yang and co-workers (Yang

et al., 2012) who reported the protein expression mainly in cholinergic neurons of the myenteric plexus that possess processes positioned in close proximity to ICCs. Although these authors did not present functional data, they suggested that HCN2 channels activation would facilitate the release of acetylcholine from cholinergic neurons and activate the muscarinic M receptors of ICCs thus affecting the peristalsis. O'Donnel and co-workers (O'Donnell et al., 2015) carried out immunofluorescence staining experiments in the human colon and identified the presence of HCN2, HCN3 and HCN4 channels in both the myenteric and submucosal plexuses. Interestingly, the same authors analyzed colon samples of patients suffering from Hirschsprung's disease and Western blot experiments showed a decrease of the HCN3 protein signal, indicating a possible involvement of this isoform in the pathophysiology of this disease. Experiments performed in the zebrafish model also suggested the involvement of the HCN4 channel of the enteric neurons in regulating retrograde peristalsis (Fujii et al., 2020).

11.3. Gastrointestinal smooth muscle cells

The I_f current was identified in isolated longitudinal smooth muscle cells of rabbit Jejunum (Benham et al., 1987) and in circular smooth muscle cells of guinea pig ileal muscle (Yanagida et al., 2000) (Table 1). Obviously, the presence of the current suggests a possible involvement in the slow depolarization observed in response to hyperpolarizing current stimuli, possibly caused by various inhibitory neurotransmitters and hormones.

12. HCN channels in the urinary system

HCN channels have been identified in various parts of the urinary system (Table 1): kidneys (Bolívar et al., 2008; Calejo et al., 2014a; Carrisoza-Gaytán et al., 2011; López-González et al, 2016, 2020), uretere (Hashitani et al., 2017; He et al., 2018; Hurtado et al, 2010, 2014), and bladder (Al-Naggar et al., 2019; Deng et al., 2015; Dong et al., 2016; He et al., 2012; Kashyap et al, 2015, 2020; Lu et al., 2020; Mader et al., 2018; Wu et al., 2017; Xue et al., 2012).

12.1. Kidneys

In 2008 Bolivar et al. (Bolívar et al., 2008) carried out the first recording of a hyperpolarization-activated voltage- and time-dependent inward current in primary cultures of rat inner medullary collecting duct (IMCD) cells. This current, dubbed I_{vti}, displayed the typical features of the I_f current: mixed K^+ and Na^+ permeability, voltage dependence of kinetics parameters, and modulation by cAMP and by $[K^+]_o$, however, it exhibited an anomalous pharmacological profile since it was insensitive to Cs^+ and ZD7288 block, but blocked by Cadmium (Bolívar et al., 2008). Attempts to identify the molecular nature of the current resulted in the identification of HCN1, HCN2 and HCN4 mRNA expression, however the presence at the protein level was investigated and confirmed only for HCN2 (Table 1). Whether the peculiar pharmacological profile of this channel is due to an alternative splicing form of HCN mRNA or to post-translational modification is at present unknown and extremely puzzling. Several other groups confirmed the expression of HCN2 and also of HCN3 channels in rat kidneys, and further studies described these channels as important players in the regulation of the acid–base and K^+ balance (Calejo et al., 2014a; Carrisoza-Gaytán et al., 2011; López-González et al, 2016, 2020; Padilla-Flores et al., 2020; Uawithya et al., 2008). The HCN signals were immunodetected on the basolateral membrane of acid-secreting intercalated and principal cells of the connecting tubule and of the collecting duct both in the cortex and in the medulla. When heterologously expressed in oocytes, HCN2 channels displayed permeability to NH_4^+ with a strong dependence on the extracellular NH_4Cl concentration and were inhibited by ZD7288 (Carrisoza-Gaytán et al., 2011). Despite the authors identified the HCN2 expression both in the acid-secreting intercalated and in principal cells, a specific role of HCN2 channels in regulating NH_4^+ excretion was confirmed only in the former cell type, where ZD7288 (10 μM) reduced the slope of acidification of the tubular contents. Based on this evidence, the authors suggested that the selective expression of HCN2 channels in the basolateral membrane of acid-secreting intercalated cells may represent a physiological mechanism favouring NH_4^+ uptake in the collecting duct and thus its urinary excretion (Carrisoza-Gaytán et al., 2011). Concerning the role of HCN channels in principal cells, the authors speculate that the entrance of Na^+ through HCN2 and HCN3 channels could provide a stimulus for promoting K^+ uptake via the basolateral Na^+-K^+-ATPase and its excretion through voltage-gated K^+ channels on the apical membrane (Carrisoza-Gaytán et al., 2011; López-González et al., 2020).

The expression of full length and N-terminal truncated HCN1 and HCN3 proteins has been reported in the apical membranes of cortical and medullary proximal tubules of rat nephrons (Table 1), and HCN3 was the sole isoform immunodetected in the medullary Thick Ascending Limb of Henle (MTALH) (López-González et al., 2016). Interestingly, the expression of HCN3 channel forms has been reported to be regulated by K^+ diet (López-González et al., 2016). Since a thorough discussion of the physiological roles of HCN channels in the various regions of the nephron is beyond the aim of the present work, we refer the interested readers to the original studies (Carrisoza-Gaytán et al., 2011; López-González et al, 2016, 2020). To summarize the main points of these studies, we can conclude that there is now solid evidence indicating that in mammalian kidney, HCN channels, and particularly HCN2 and HCN3, play an important role in regulating Na^+, K^+ and NH_4^+ homeostasis.

12.2. Ureteral tract

The progression of urine from the renal pelvis to the bladder depends on the coordinated peristalsis originating in the pelvis-kidney junction (PKJ (Hurtado et al., 2014, 2010),). A rhythmic activity is indeed initiated in the PKJ by specialized pacemaker cells that are coupled via gap junction to the surrounding smooth muscle cells. In a series of studies aimed at understanding the mechanism underlying the rhythmic activity, Hurtado et al. (Hurtado et al, 2010, 2014) reported a high level of expression of HCN3 proteins in PKJ cells. Despite no direct recording of the HCN3 current was carried out, the researchers used the optical mapping technique to demonstrate that 30 μM of ZD7288 caused a severe desynchronization of the proximal-to distal contraction and at a higher dose (90 μM) it completely blocked both the electrical activity and contractility (Hurtado et al., 2010). Similar results were obtained in studies on human ureteral preparations (He et al., 2018) where treatment with ZD7288 (50 μM) inhibited the amplitude but not the frequency of spontaneous contractions of ureteral smooth muscle strips. According to the authors the spontaneous contracting activity likely originates in putative pacemaker cells, the so called interstitial-like cells of Cajal (ICCs), also identified in the bladder (see paragraph 12.3 below), which express both HCN1 and HCN4 channels together with c-kit, a specific marker of ICC. However, as recognized by the authors, due to the lack of solid electrophysiological evidence, no definite conclusion on f-current function in these cells can be drawn (He et al., 2018).

12.3. Bladder

In 1996 an I_f–like, Cs^+ and ZD7288 sensitive inward-rectifying current with mixed Na^+/K^+ permeability was described in rat detrusor smooth muscle cells (Table 1) (Green et al., 1996). Since this initial observation several additional studies addressed the involvement of the HCN channels in the regulation of bladder excitability and reported the presence of all HCN isoforms in the detrusor muscle, ICCs, and in the mucosal layer of the urinary bladder (Al-Naggar et al., 2019; Deng et al., 2015; Dong et al., 2016; Kashyap et al, 2015, 2020; Lu et al., 2020; Mader et al., 2018; Wu et al., 2017; He et al., 2012; Xue et al., 2012) (Table 1). While the expression of HCN channels in the various regions of the bladder is therefore an established evidence, a thorough understanding of their role is still missing. In their original work, Green and collaborators (Green et al., 1996) revealed that a sustained treatment with the I_f blocker ZD7288 induced a dose-dependent increase of both the amplitude and, surprisingly, the frequency of spontaneous phasic contractions of rat detrusor muscle strips. More recently, Kashyap and co-workers (Kashyap et al., 2015) demonstrated that application of Lamotrigine (10 nM-100 μM), an anticonvulsant known to increase the HCN-mediated current, displayed a relaxant effect on the detrusor muscle of the rat bladder and that this effect was blocked by application of ZD7288 (10 μM). The I_f blocker caused a dose dependent increase in force of contraction, which was more pronounced in mucosa-free bladder strips, than in intact bladder strips. Similar studies carried out on human bladder strips confirmed the observations from the animal models (Mader et al., 2018). Indeed, this group demonstrated that exposure to ZD7288 (50 μM) caused tonic contractions and increased both the amplitude and the spontaneous frequency of phasic contractions, and that the activation of HCN channels with Lamotrigine induced relaxation in both mouse and human bladder, reducing the effect of ZD7288.

Recently, Kashyap et al. (2020) provided an integrated explanation for the role of HCN channels in the bladder and proposed that the HCN channels found in the mucosa, in the cholinergic nerve terminals, and in the detrusor muscle are constitutively active. According to these authors, the HCN current exerts an inhibitory effect both on neurotransmitters release and on spontaneous contractions of detrusor smooth muscle and these effects are likely due to an HCN-mediated attenuation of N- and T-type voltage-gated Ca^{2+} channels activity (Kashyap et al., 2020).

In contrast with these data, other authors reported that application of both ZD7288 (10–50 μM) and ivabradine (30–90 μM) induced relaxation of rat bladder strips (Aydin et al., 2018; Deng et al., 2015). Interestingly, Deng and colleagues (Deng et al., 2015) showed that in a pathological model of detrusor muscle overactivity, all HCN isoforms were upregulated and higher doses of ZD7288 was necessary to cause relaxation.

HCN channels distribution and function have been also investigated in the bladder of a rat model of diabetic cystopathy (DCP), a disease characterized by increased urinary frequency and incontinence (Dong et al., 2016); in this study a decreased HCN/I_f expression was observed in ICCs. In agreement with this finding, DCP ICCs were less sensitive to cAMP modulation induced by forskolin (a permeable Adenylyl Cyclase agonist) and to ZD7288 treatment. Of note, this decrease in HCN expression has been associated with a DCP-dependent decrease in the number of caveolae (and of caveolin-3 levels) and knockdown of caveolin-3 in control ICCs elicited a phenotype similar to that of DCP since it decreased both the HCN protein expression and the I_f current (Dong et al., 2016). This finding is in agreement with previous works demonstrating that caveolin-3 interacts with and modulates HCN function, and impairment of such interaction decreases the expression of channels (Barbuti et al, 2007, 2012).

13. HCN channels in leukocytes

Several studies have elegantly shown that the I_f blocker ivabradine, a drug used in the clinic to reduce heart rate, also displays relevant effects on endothelial functions, oxidative stress, and lymphocytes migration (Bonadei et al., 2018; Dallapellegrina et al., 2020; Li et al., 2016; Walcher et al., 2010). For example, ivabradine treatment of transgenic ApoE-deficient mice resulted in a protective action against atherosclerosis progression by activating anti-inflammatory pathways (Aquila et al., 2018; Custodis et al., 2008). In another study carried out in a mouse model of cardiac inflammation, the authors reported that ivabradine prevented the progression from myocarditis to dilated cardiomyopathy, and this effect was associated with a reduction of the p38 MAPK pathways and a downregulation of several pro-inflammatory cytokines (Dallapellegrina et al., 2020; Gammone et al., 2020; Yue-Chun et al., 2016). To explain these findings it was originally proposed that the decrease of the vascular shear-stress associated with the drug-induced bradycardia could represent the causative link between ivabradine treatment and the reduced inflammatory state (Speranza et al., 2012).

Our group considered that additional mechanisms may also be involved; for example, the established evidence that many ion channels play relevant functional roles in the immune response of white blood cells (Feske et al., 2015) raised the possibility that these cells also express HCN channels. To explore the presence of HCN signal in leukocytes, we therefore performed a preliminary investigation to detect the presence of HCN mRNA signals in human leukocytes (see details in the methods at the end of this section). Quantitative RT-PCR experiments, carried out on total leukocytes isolated from blood samples of 5 unrelated adult individuals (25-50 year-old), are shown in panel A of Fig. 2. This experiment detected significant mRNA levels for the HCN2 and HCN3 isoforms, with a prevalence of HCN2. HCN1 and HCN4 displayed instead negligible expression levels (Table 1 and Fig. 3). To explore further this interesting evidence, we isolated individual populations of lymphocytes and granulocytes by flow cytometry. Quantitative RT-PCR experiments confirmed the presence of robust HCN2 and HCN3 signals in lymphocytes, while in granulocytes HCN3 was the only isoform that could be reproducibly identified. Although preliminary, these data demonstrate the presence of isoform-specific mRNA signals in selected immune cell populations, thus suggesting a possible functional role of the channels in these cells. Even though these studies did not address the presence of HCN proteins, they open the possibility that the immuno-modulation exerted by ivabradine may also depend on the inhibition of HCN channels eventually expressed in lymphocytes. Indeed, several types of ion channels have already been described in leukocytes where they play fundamental roles in controlling cell membrane potentials and Ca^{2+} influx leading to modulation of gene expression and inflammatory responses (Grune et al., 2021). In line with this evidence Pillozzi et al. (2016) reported that hHERG inhibition in acute leukemia lymphoid cells exerts an antileukemic effect. The presence a tight crosstalk between the heart and circulating leukocytes is a well-established concept that has been investigated also at the molecular level. For example, studies on G-protein-coupled receptors and connexins 40 and 43 have shown that the oscillation in the expression of these proteins associated with cardiac dysfunctions are mirrored by similar changes in peripheral leukocytes (Lazzerini et al., 2019; Schiattarella et al., 2015). Further expression and functional studies must carefully and convincingly address the biological role of HCN in leukocytes and eventually explore the existence of a correlation with HCN expression in cardiac cells.

Methods: Blood samples were treated to induce lysis of red blood cells, and then centrifuged for 5 min at 200×*g* to precipitate

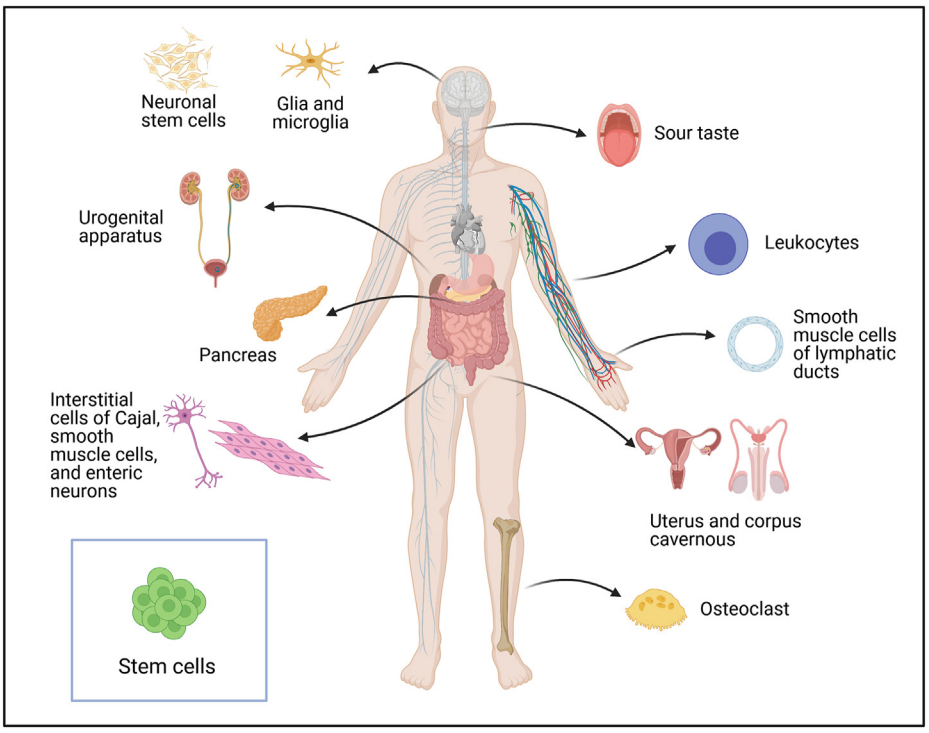

Fig. 4. *Cartoon of "uncanonical" expression pattern of HCN channels. The body districts where HCN channels display canonical functions (heart and central/peripheral nervous systems) are shown in gray, while colored insets are used to identify the sites of uncanonical functions described in this review. This scheme is based on data obtained both in human and/or animal models. "Created with BioRender.com".*

leukocytes. The cell pellet was then resuspended in appropriate buffer (Phosphate-Buffered Saline 1X (PBS) + FBS 10% + EDTA 5 mM) prior to isolating lymphocytes and granulocytes by flow cytometry analysis (FACSAria II BD Biosciences) on the basis of their cellular dimensions (forward scatter) and cytoplasmic complexity (side scatter). RNA was extracted both from single populations and from total leukocites and treated with DNASe (DNase I/RNase free, Thermo Scientific). A commercially available kit (Maxima First Strand cDNA Synthesis Kit, Thermo Scientific) was used to synthesize cDNA, and quantitative RT-PCRs were carried out with SYBR Green kit (Thermo Fisher Scientific). α-tubulin was used as the housekeeping gene to normalize the results of the genes of interest (HCN), according to the ΔCt method. Specific primers were designed using Primer-blast software. Statistical analysis (Student's T-test) was performed using OriginPro 2020. Experiments were approved by the Ethical Committee of the University of Milan.

14. Conclusions

The data presented in this review clearly illustrate that the presence of the I_f/HCN current is not limited to the heart and nervous system, but a variety of additional excitable and non-excitable cells also express these channels (Fig. 4). In some cases, the physiological functions of the I_f current are well-established, while in others they are still partly obscure due to contradictory or still unclear data. For example, many studies use I_f inhibitors to prove/disprove the role of HCN channels, but in several cases the concentrations used raise serious concern since at inappropriate (i.e. high) doses they lose their selectivity for the I_f current and may elicit unspecific effects on other ionic currents. However, the wide distribution of these channels in mammalian tissues convincingly indicates that their identification as "pacemaker" channels proposed at the beginning of their journey is just one aspect of their complex contribution to "electrical beauty" of many cell types.

Funding

This research did not receive any specific grant from funding agencies in the public, commercial, or not-for-profit sectors.

Conflict of interest

The authors declare that they have no competing financial interests or personal relationships that could be perceived to have influenced the work reported in this paper.

CRediT authorship contribution statement

Patrizia Benzoni: Writing – review & editing. **Giorgia Bertoli:** Writing – review & editing. **Federica Giannetti:** Writing – review & editing. **Chiara Piantoni:** Investigation. **Raffaella Milanesi:** Investigation. **Matteo Pecchiari:** Investigation. **Andrea Barbuti:** Conceptualization, Writing – review & editing. **Mirko Baruscotti:** Conceptualization, Writing – review & editing. **Annalisa Bucchi:** Conceptualization, Writing – review & editing.

Declaration of competing interest

None.

References

Agoston, A., Kunz, L., Krieger, A., Mayerhofer, A., 2004. Two types of calcium channels in human ovarian endocrine cells: involvement in steroidogenesis. J. Clin. Endocrinol. Metab. 89, 4503–4512. https://doi.org/10.1210/jc.2003-032219.

Aguilar, H.N., Mitchell, B.F., 2010. Physiological pathways and molecular mechanisms regulating uterine contractility. Hum. Reprod. Update 16, 725–744. https://doi.org/10.1093/humupd/dmq016.

Al-Naggar, I.M., Hardy, C.C., Taweh, O.G., Grabauskas, T., Mulkey, D.K., Kuchel, G.A., Smith, P.P., 2019. HCN as a mediator of urinary homeostasis: age-associated changes in expression and function in adrenergic detrusor relaxation.

Journals Gerontol. - Ser. A Biol. Sci. Med. Sci. 74, 325–329. https://doi.org/10.1093/gerona/gly137.
Allen, J.M., McHale, N.G., 1988. The effect of known K +-channel blockers on the electrical activity of bovine lymphatic smooth muscle. Pflugers Arch. Eur. J. Physiol. 411, 167–172.
Alotaibi, M., Kahlat, K., Nedjadi, T., Djouhri, L., 2017. Effects of ZD7288, a hyperpolarization-activated cyclic nucleotide-gated (HCN) channel blocker, on term-pregnant rat uterine contractility in vitro. Theriogenology 90, 141–146. https://doi.org/10.1016/j.theriogenology.2016.11.022.
Aquila, G., Morelli, M.B., Vieceli Dalla Sega, F., Fortini, F., Nigro, P., Caliceti, C., Ferracin, M., Negrini, M., Pannuti, A., Bonora, M., Pinton, P., Ferrari, R., Rizzo, P., 2018. Heart rate reduction with ivabradine in the early phase of atherosclerosis is protective in the endothelium of ApoE-deficient mice. J. Physiol. Pharmacol. 69, 35–52. https://doi.org/10.26402/jpp.2018.1.04.
Aydin, H.R., Turgut, H., Kurt, A., Sahan, R., Kalkan, O.F., Eren, H., Ayar, A., 2018. Ivabradine inhibits carbachol-induced contractions of isolated rat urinary bladder. Adv. Clin. Exp. Med. 27, 893–897. https://doi.org/10.17219/acem/71197.
Barbuti, A., Terragni, B., Brioschi, C., DiFrancesco, D., 2007. Localization of f-channels to caveolae mediates specific β2-adrenergic receptor modulation of rate in sinoatrial myocytes. J. Mol. Cell. Cardiol. 42, 71–78. https://doi.org/10.1016/j.yjmcc.2006.09.018.
Barbuti, A., Crespi, A., Capilupo, D., Mazzocchi, N., Baruscotti, M., DiFrancesco, D., 2009. Molecular composition and functional properties of f-channels in murine embryonic stem cell-derived pacemaker cells. J. Mol. Cell. Cardiol. 46, 343–351. https://doi.org/10.1016/j.yjmcc.2008.12.001.
Barbuti, A., Scavone, A., Mazzocchi, N., Terragni, B., Baruscotti, M., DiFrancesco, D., 2012. A caveolin-binding domain in the HCN4 channels mediates functional interaction with caveolin proteins. J. Mol. Cell. Cardiol. 53, 187–195. https://doi.org/10.1016/j.yjmcc.2012.05.013.
Baruscotti, M., Bucchi, A., DiFrancesco, D., 2005. Physiology and pharmacology of the cardiac pacemaker ("funny") current. Pharmacol. Ther. 107, 59–79. https://doi.org/10.1016/j.pharmthera.2005.01.005.
Baumhäkel, M., Custodis, F., Schlimmer, N., Laufs, U., Böhm, M., 2010. Heart rate reduction with ivabradine improves erectile dysfunction in parallel to decrease in atherosclerotic plaque load in ApoE-knockout mice. Atherosclerosis 212, 55–62. https://doi.org/10.1016/j.atherosclerosis.2010.03.002.
Benham, C.D., Bolton, T.B., Denbigh, J.S., Lang, R.J., 1987. Inward rectification in freshly isolated single smooth muscle cells of the rabbit jejunum. J. Physiol. 383, 461–476. https://doi.org/10.1113/jphysiol.1987.sp016421.
Biel, M., Wahl-Schott, C., Michalakis, S., Zong, X., 2009. Hyperpolarization-activated cation channels: from genes to function. Physiol. Rev. 89, 847–885. https://doi.org/10.1152/physrev.00029.2008.
Bois, P., Bescond, J., Renaudon, B., Lenfant, J., 1996. Mode of action of bradycardic agent, S 16257, on ionic currents of rabbit sinoatrial node cells. Br. J. Pharmacol. 118, 1051–1057. https://doi.org/10.1111/j.1476-5381.1996.tb15505.x.
Bolívar, J.J., Tapia, D., Arenas, G., Castañón-Arreola, M., Torres, H., Galarraga, E., 2008. A hyperpolarization-activated, cyclic nucleotide-gated, (I h-like) cationic current and HCN gene expression in renal inner medullary collecting duct cells. Am. J. Physiol. Cell Physiol. 294, 893–906. https://doi.org/10.1152/ajpcell.00616.2006.
Bonadei, I., Sciatti, E., Vizzardi, E., Fabbricatore, D., Pagnoni, M., Rossi, L., Carubelli, V., Lombardi, C.M., Metra, M., 2018. Effects of ivabradine on endothelial function, aortic properties and ventricular-arterial coupling in chronic systolic heart failure patients. Cardiovasc. Ther. 36, e12323. https://doi.org/10.1111/1755-5922.12323.
BoSmith, R.E., Briggs, I., Sturgess, N.C., 1993. Inhibitory actions of ZENECA ZD7288 on whole-cell hyperpolarization activated inward current (If) in Guinea-pig dissociated sinoatrial node cells. Br. J. Pharmacol. 110, 343–349.
Boyle, W.J., Simonet, W.S., Lacey, D.L., 2003. Osteoclast differentiation and activation. Nature 423, 337–342. https://doi.org/10.1038/nature01658.
Brown, H.F., DiFranceso, D., Noble, S.J., 1979. How does adrenaline accelerate the heart? Nature 280, 235–236. https://doi.org/10.1038/280235a0.
Bucchi, A., Barbuti, A., Baruscotti, M., DiFrancesco, D., 2007. Heart rate reduction via selective "funny" channel blockers. Curr. Opin. Pharmacol. https://doi.org/10.1016/j.coph.2006.09.005.
Calejo, Ana I., Jorgačevski, J., Rituper, B., Guček, A., Pereira, P.M., Santos, M.A.S., Potokar, M., Vardjan, N., Kreft, M., Gonçalves, P.P., Zorec, R., 2014. Hyperpolarization-activated cyclic nucleotide-gated channels and cAMP-dependent modulation of exocytosis in cultured rat lactotrophs. J. Neurosci. 34, 15638–15647. https://doi.org/10.1523/JNEUROSCI.5290-13.2014.
Calejo, Ana I., Reverendo, M., Silva, V.S., Pereira, P.M., Santos, M.A.S., Zorec, R., Gonçalves, P.P., 2014a. Differences in the expression pattern of HCN isoforms among mammalian tissues: sources and implications. Mol. Biol. Rep. 41, 297–307. https://doi.org/10.1007/s11033-013-2862-2.
Carmeliet, E., 2019. Pacemaking in cardiac tissue. From Ik2 to a coupled-clock system. Phys. Rep. https://doi.org/10.14814/phy2.13862.
Carrisoza-Gaytán, R., Rangel, C., Salvador, C., Saldaña-Meyer, R., Escalona, C., Satlin, L.M., Liu, W., Zavilowitz, B., Trujillo, J., Bobadilla, N.A., Escobar, L.I., 2011. The hyperpolarization-activated cyclic nucleotide-gated HCN2 channel transports ammonium in the distal nephron. Kidney Int. 80, 832–840. https://doi.org/10.1038/ki.2011.230.
Chu, Z., Takagi, H., Moenter, S.M., 2010. Hyperpolarization-activated currents in Gonadotropin-Releasing Hormone (GnRH) neurons contribute to intrinsic excitability and are regulated by gonadal steroid feedback. J. Neurosci. 30, 13373–13383. https://doi.org/10.1523/JNEUROSCI.1687-10.2010.
Custodis, F., Baumhäkel, M., Schlimmer, N., List, F., Gensch, C., Böhm, M., Laufs, U., 2008. Heart rate reduction by ivabradine reduces oxidative stress, improves endothelial function, and prevents atherosclerosis in apolipoprotein E-deficient mice. Circulation 117, 2377–2387. https://doi.org/10.1161/CIRCULATIONAHA.107.746537.
Dallapellegrina, L., Sciatti, E., Vizzardi, E., 2020. Ivabradine and endothelium: an update. Ther. Adv. Cardiovasc. Dis. 14. https://doi.org/10.1177/1753944720934937, 1753944720934937.
Delpón, E., Valenzuela, C., Pérez, O., Franqueza, L., Gay, P., Snyders, D.J., Tamargo, J., 1996. Mechanisms of block of a human cloned potassium channel by the enantiomers of a new bradycardic agent: S-16257-2 and S-16260-2. Br. J. Pharmacol. 117, 1293–1301. https://doi.org/10.1111/j.1476-5381.1996.tb16728.x.
Demontis, G.C., Gargini, C., Paoli, T.G., Cervetto, L., 2009. Selective Hcn1 channels inhibition by ivabradine in mouse rod photoreceptors. Invest. Ophthalmol. Vis. Sci. 50. https://doi.org/10.1167/iovs.08-2659, 1948–55.
Deng, T., Zhang, Q., Wang, Q., Zhong, X., Li, L., 2015. Changes in hyperpolarization-activated cyclic nucleotide-gated channel expression and activity in bladder interstitial cells of Cajal from rats with detrusor overactivity. Int. UrogynEcol. J. Pelvic Floor Dysfunct. 26, 1139–1145. https://doi.org/10.1007/s00192-015-2632-x.
Denyer, J.C., Brown, H.F., 1990. Pacemaking in rabbit isolated sino-atrial node cells during Cs+ block of the hyperpolarization-activated current if. J. Physiol. 429, 401–409. https://doi.org/10.1113/jphysiol.1990.sp018264.
DiFrancesco, D., 1981. A new interpretation of the pace-maker current in calf Purkinje fibres. J. Physiol. 314, 359–376. https://doi.org/10.1113/jphysiol.1981.sp013713.
DiFrancesco, D., 1982. Block and activation of the pace-maker channel in calf purkinje fibres: effects of potassium, caesium and rubidium. J. Physiol. 329, 485–507. https://doi.org/10.1113/jphysiol.1982.sp014315.
DiFrancesco, D., 2020. A brief history of pacemaking. Front. Physiol.
Dong, X., Song, Q., Zhu, J., Zhao, J., Liu, Q., Zhang, T., Long, Z., Li, J., Wu, C., Wang, Q., Hu, X., Damaser, M., Li, L., 2016. Interaction of Caveolin-3 and HCN is involved in the pathogenesis of diabetic cystopathy. Sci. Rep. 6, 1–14. https://doi.org/10.1038/srep24844.
Dorrell, C., Schug, J., Canaday, P.S., Russ, H.A., Tarlow, B.D., Grompe, M.T., Horton, T., Hebrok, M., Streeter, P.R., Kaestner, K.H., Grompe, M., 2016. Human islets contain four distinct subtypes of β cells. Nat. Commun. 7, 1–9. https://doi.org/10.1038/ncomms11756.
El-Kholy, W., MacDonald, P.E., Fox, J.M., Bhattacharjee, A., Xue, T., Gao, X., Zhang, Y., Stieber, J., Li, R.A., Tsushima, R.G., Wheeler, M.B., 2007. Hyperpolarization-activated cyclic nucleotide-gated channels in pancreatic β-cell. Mol. Endocrinol. 21, 753–764. https://doi.org/10.1210/me.2006-0258.
Feske, S., Wulff, H., Skolnik, E.Y., 2015. Ion channels in innate and adaptive immunity. Annu. Rev. Immunol. 33, 291–353. https://doi.org/10.1146/annurev-immunol-032414-112212.
Fletcher, P.A., Sherman, A., Stojilkovic, S.S., 2018. Common and diverse elements of ion channels and receptors underlying electrical activity in endocrine pituitary cells. Mol. Cell. Endocrinol. 463, 23–36. https://doi.org/10.1016/j.mce.2017.06.022.
Fujii, K., Nakajo, K., Egashira, Y., Yamamoto, Y., Kitada, K., Taniguchi, K., Kawai, M., Tomiyama, H., Kawakami, K., Uchiyama, K., Ono, F., 2020. Gastrointestinal neurons expressing HCN4 regulate retrograde peristalsis. Cell Rep. 30, 2879–2888. https://doi.org/10.1016/j.celrep.2020.02.024 e3.
Galligan, J.J., Tatsumi, H., Shen, K.Z., Surprenant, A., North, R.A., 1990. Cation current activated by hyperpolarization (IH) in Guinea pig enteric neurons. Am. J. Physiol. Liver Physiol. 259, G966–G972. https://doi.org/10.1152/ajpgi.1990.259.6.G966.
Gammone, M.A., Riccioni, G., Massari, F., D'Orazio, N., 2020. Beneficial effect of ivabradine against cardiovascular diseases. Front. Biosci. 12, 161–172.
Gasparini, S., DiFrancesco, D., 1997. Action of the hyperpolarization-activated current (Ih) blocker ZD 7288 in hippocampal CA1 neurons. Pflügers Archiv 435, 99–106. https://doi.org/10.1007/s004240050488.
Gauss, R., Seifert, R., Kaupp, U.B., 1998. Molecular identification of a hyperpolarization-activated channel in sea urchin sperm. Nature 393, 583–587. https://doi.org/10.1038/31248.
Giannetti, F., Benzoni, P., Campostrini, G., Milanesi, R., Bucchi, A., Baruscotti, M., Dell'Era, P., Rossini, A., Barbuti, A., 2021. A detailed characterization of the hyperpolarization-activated "funny" current (If) in human-induced pluripotent stem cell (iPSC)-derived cardiomyocytes with pacemaker activity. Pflügers Archiv. https://doi.org/10.1007/s00424-021-02571-w.
Gonzalez-Iglesias, A.E., Kretschmannova, K., Tomic, M., Stojilkovic, S.S., 2006. ZD7288 inhibits exocytosis in an HCN-independent manner and downstream of voltage-gated calcium influx in pituitary lactotrophs. Biochem. Biophys. Res. Commun. 346, 845–850. https://doi.org/10.1016/j.bbrc.2006.05.194.
Green, M.E., Edwards, G., Kirkup, A.J., Miller, M., Weston, A.H., 1996. Pharmacological characterization of the inwardly-rectifying current in the smooth muscle cells of the rat bladder. Br. J. Pharmacol. 119, 1509.
Greenwood, I.A., Prestwich, S.A., 2002. Characteristics of hyperpolarization-activated cation currents in portal vein smooth muscle cells. Am. J. Physiol. Physiol. 282, C744–C753.
Grune, J., Yamazoe, M., Nahrendorf, M., 2021. Electroimmunology and cardiac arrhythmia. Nat. Rev. Cardiol. https://doi.org/10.1038/s41569-021-00520-9.
Guatteo, E., Stanness, K.A., Janigro, D., 1996. Hyperpolarization-activated ion currents in cultured rat cortical and spinal cord astrocytes. Glia 16, 196–209. https://doi.org/10.1002/(SICI)1098-1136(199603)16:3<196::AID-

GLIA2>3.0.CO;2-0.
Guo, T., Li, Jiade, Li, Jing, Kong, D., Bi, C., He, Z., Tang, D., Jin, X., 2017. Association between hyperpolarization-activated channel in interstitial cells of cajal and gastrointestinal dysmotility induced by malignant ascites. Oncol. Lett. 13, 1601–1608. https://doi.org/10.3892/ol.2017.5652.
Gur, S., Alzweri, L., Yilmaz-Oral, D., Kaya-Sezginer, E., Abdel-Mageed, A.B., Sikka, S.C., Hellstrom, W.J.G., 2019. Ivabradine, the hyperpolarization-activated cyclic nucleotide-gated channel blocker, elicits relaxation of the human corpus cavernosum: a potential option for erectile dysfunction treatment. Aging Male 1–10. https://doi.org/10.1080/13685538.2019.1678125, 0.
Haechl, N., Ebner, J., Hilber, K., Todt, H., Koenig, X., 2019. Pharmacological profile of the bradycardic agent ivabradine on human cardiac ion channels. Cell. Physiol. Biochem. 53, 36–48. https://doi.org/10.33594/000000119.
Harris, N.C., Constanti, A., 1995. Mechanism of block by ZD 7288 of the hyperpolarization-activated inward rectifying current in Guinea pig substantia nigra neurons in vitro. J. Neurophysiol. 74, 2366–2378. https://doi.org/10.1152/jn.1995.74.6.2366.
Hashitani, H., Nguyen, M.J., Noda, H., Mitsui, R., Higashi, R., Ohta, K., Nakamura, K.I., Lang, R.J., 2017. Interstitial cell modulation of pyeloureteric peristalsis in the mouse renal pelvis examined using FIBSEM tomography and calcium indicators. Pflugers Arch. Eur. J. Physiol. 469, 797–813. https://doi.org/10.1007/s00424-016-1930-6.
He, P., Deng, J., Zhong, X., Zhou, Z., Song, B., Li, L., 2012. Identification of a hyperpolarization-activated cyclic nucleotide-gated channel and its subtypes in the urinary bladder of the rat. Urology 79, 1411. https://doi.org/10.1016/j.urology.2012.01.037 e7-1411.e13.
He, F., Yang, Z., Dong, X., Fang, Z., Liu, Q., Hu, X., Yi, S., Li, L., 2018. The role of HCN channels in peristaltic dysfunction in human ureteral tuberculosis. Int. Urol. Nephrol. 50, 639–645. https://doi.org/10.1007/s11255-018-1816-y.
Honsa, P., Pivonkova, H., Harantova, L., Butenko, O., Kriska, J., Dzamba, D., Rusnakova, V., Valihrach, L., Kubista, M., Anderova, M., 2014. Increased expression of hyperpolarization-activated cyclic nucleotide-gated (HCN) channels in reactive astrocytes following ischemia. Glia 62, 2004–2021. https://doi.org/10.1002/glia.22721.
Hsiao, H.-T., Liu, Y.-C., Liu, P.-Y., Wu, S.-N., 2019. Concerted suppression of Ih and activation of Ik(M) by ivabradine, an HCN-channel inhibitor, in pituitary cells and hippocampal neurons. Brain Res. Bull. 149, 11–20. https://doi.org/10.1016/j.brainresbull.2019.03.016.
Hurtado, R., Bub, G., Herzlinger, D., 2010. The pelvis–kidney junction contains HCN3, a hyperpolarization-activated cation channel that triggers ureter peristalsis. Kidney Int. 77, 500–508. https://doi.org/10.1038/ki.2009.483.
Hurtado, R., Bub, G., Herzlinger, D., 2014. A molecular signature of tissues with pacemaker activity in the heart and upper urinary tract involves coexpressed hyperpolarization-activated cation and T-type Ca2+ channels. Faseb. J. 28, 730–739. https://doi.org/10.1096/fj.13-237289.
Ili, C., Buchegger, K., Demond, H., Castillo-Fernandez, J., Kelsey, G., Zanella, L., Abanto, M., Riquelme, I., López, J., Viscarra, T., García, P., Bellolio, E., Saavedra, D., Brebi, P., 2020. Landscape of genome-wide dna methylation of colorectal cancer metastasis. Cancers 12, 1–20. https://doi.org/10.3390/cancers12092710.
Izquierdo, P., Attwell, D., Madry, C., 2019. Ion channels and receptors as determinants of microglial function. Trends Neurosci. 42, 278–292. https://doi.org/10.1016/j.tins.2018.12.007.
Johard, H., Omelyanenko, A., Fei, G., Zilberter, M., Dave, Z., Abu-Youssef, R., Schmidt, L., Harisankar, A., Vincent, C.T., Walfridsson, J., Nelander, S., Harkany, T., Blomgren, K., Andäng, M., 2020. HCN channel activity balances quiescence and proliferation in neural stem cells and is a selective target for neuroprotection during cancer treatment. Mol. Canc. Res. 18, 1522–1533. https://doi.org/10.1158/1541-7786.mcr-20-0292.
Kashyap, M., Yoshimura, N., Smith, P.P., Chancellor, M., Tyagi, P., 2015. Characterization of the role of HCN channels in β3-adrenoceptor mediated rat bladder relaxation. Bladder 2, 15. https://doi.org/10.14440/bladder.2015.44.
Kashyap, M., Singh, N., Yoshimura, N., Chermansky, C., Tyagi, P., 2020. Constitutively active HCN channels constrain detrusor excitability and modulate evoked contractions of human bladder 8, 163–176.
Kimelberg, H.K., Nedergaard, M., 2010. Functions of astrocytes and their potential as therapeutic targets. Neurotherapeutics 7, 338–353. https://doi.org/10.1016/j.nurt.2010.07.006.
Kirkpatrick, C.T., McHale, N.G., 1977. Electrical and mechanical activity of isolated lymphatic vessels [proceedings]. J. Physiol. 272, 33P–34P.
Kobayashi, Y., Mizoguchi, T., Take, I., Kurihara, S., Udagawa, N., Takahashi, N., 2005. Prostaglandin E2 enhances osteoclastic differentiation of precursor cells through protein kinase A-dependent phosphorylation of TAK1*. J. Biol. Chem. 280, 11395–11403. https://doi.org/10.1074/jbc.M411189200.
Koncz, I., Szél, T., Bitay, M., Cerbai, E., Jaeger, K., Fülöp, F., Jost, N., Virág, L., Orvos, P., Tálosi, L., Kristóf, A., Baczkó, I., Papp, J.G., Varró, A., 2011. Electrophysiological effects of ivabradine in dog and human cardiac preparations: potential antiarrhythmic actions. Eur. J. Pharmacol. 668, 419–426. https://doi.org/10.1016/j.ejphar.2011.07.025.
Kretschmannova, K., Kucka, M., Gonzalez-Iglesias, A.E., Stojilkovic, S.S., 2012. The expression and role of hyperpolarization-activated and cyclic nucleotide-gated channels in endocrine anterior pituitary cells. Mol. Endocrinol. 26, 153–164. https://doi.org/10.1210/me.2011-1207.
Kunz, L., Thalhammer, A., Berg, F.D., Berg, U., Duffy, D.M., Stouffer, R.L., Dissen, G.A., Ojeda, S.R., Mayerhofer, A., 2002. Ca2+-Activated, large conductance K+ channel in the ovary: identification, characterization, and functional involvement in steroidogenesis. J. Clin. Endocrinol. Metab. 87, 5566–5574. https://doi.org/10.1210/jc.2002-020841.
Kunz, L., Rämsch, R., Krieger, A., Young, K.A., Dissen, G.A., Stouffer, R.L., Ojeda, S.R., Mayerhofer, A., 2006. Voltage-dependent K+ channel acts as sex steroid sensor in endocrine cells of the human ovary. J. Cell. Physiol. 206, 167–174. https://doi.org/10.1002/jcp.20453.
Lau, Y.-T., Wong, C.-K., Luo, J., Leung, L.-H., Tsang, P.-F., Bian, Z.-X., Tsang, S.-Y., 2011. Effects of hyperpolarization-activated cyclic nucleotide-gated (HCN) channel blockers on the proliferation and cell cycle progression of embryonic stem cells. Pflügers Arch. - Eur. J. Physiol. 461, 191–202. https://doi.org/10.1007/s00424-010-0899-9.
Lazzerini, P.E., Laghi-Pasini, F., Acampa, M., Srivastava, U., Bertolozzi, I., Giabbani, B., Finizola, F., Vanni, F., Dokollari, A., Natale, M., Cevenini, G., Selvi, E., Migliacci, N., Maccherini, M., Boutjdir, M., Capecchi, P.L., 2019. Systemic inflammation rapidly induces reversible atrial electrical remodeling: the role of interleukin-6–mediated changes in connexin expression. J. Am. Heart Assoc. 8. https://doi.org/10.1161/JAHA.118.011006.
Lee, M.Y., Ha, S.E., Park, C., Park, P.J., Fuchs, R., Wei, L., Jorgensen, B.G., Redelman, D., Ward, S.M., Sanders, K.M., Ro, S., 2017. Transcriptome of interstitial cells of Cajal reveals unique and selective gene signatures. PloS One 1–25. https://doi.org/10.1371/journal.pone.0176031.
León-Aparicio, D., Salvador, C., Aparicio-Trejo, O.E., Briones-Herrera, A., Pedraza-Chaverri, J., Vaca, L., Sampieri, A., Padilla-Flores, T., López-González, Z., León-Contreras, J.C., Hernández-Pando, R., Escobar, L.I., 2019. Novel potassium channels in kidney mitochondria: the hyperpolarization-activated and cyclic nucleotide-gated HCN channels. Int. J. Mol. Sci. 20, 1–18. https://doi.org/10.3390/ijms20204995.
Levin, M., 2014. Endogenous bioelectrical networks store non-genetic patterning information during development and regeneration. J. Physiol. 592, 2295–2305. https://doi.org/10.1113/jphysiol.2014.271940.
Levin, M., Stevenson, C.G., 2012. Regulation of cell behavior and tissue patterning by bioelectrical signals: challenges and opportunities for biomedical engineering. Annu. Rev. Biomed. Eng. 14, 295–323. https://doi.org/10.1146/annurev-bioeng-071811-150114.
Li, B., Zhang, J., Wang, Z., Chen, S., 2016. Ivabradine prevents low shear stress induced endothelial inflammation and oxidative stress via mTOR/eNOS pathway. PloS One 11, e0149694.
López-González, Z., Ayala-Aguilera, C., Martinez-Morales, F., Galicia-Cruz, O., Salvador-Hernández, C., Pedraza-Chaverri, J., Medeiros, M., Hernández, A.M., Escobar, L.I., 2016. Immunolocalization of hyperpolarization-activated cationic HCN1 and HCN3 channels in the rat nephron: regulation of HCN3 by potassium diets. Histochem. Cell Biol. 145, 25–40. https://doi.org/10.1007/s00418-015-1375-6.
López-González, Z., Padilla-Flores, T., León-Aparicio, D., Gutiérrez-Vásquez, E., Salvador, C., León-Contreras, J.C., Hernández-Pando, R., Escobar, L.I., 2020. Metabolic acidosis and hyperkalemia differentially regulate cation HCN3 channel in the rat nephron. J. Mol. Histol. 51, 701–716. https://doi.org/10.1007/s10735-020-09916-2.
Lu, J.Y., Ying, X.W., Chen, X.L., Tu, W.Z., Li, S.S., Jiang, S.H., 2020. Effects of electroacupuncture at different acupoints on the histomorphology of neurogenic bladder and the expression of hyperpolarization-activated cyclic nucleotide-gated channels in interstitial cells of cajal in a rat model of suprasacral spinal cord i. Ann. Palliat. Med. 9, 3830–3838. https://doi.org/10.21037/apm-20-1827.
Mader, F., Müller, S., Krause, L., Springer, A., Kernig, K., Protzel, C., Porath, K., Rackow, S., Wittstock, T., Frank, M., Hakenberg, O.W., Köhling, R., Kirschstein, T., 2018. Hyperpolarization-activated cyclic nucleotide-gated non-selective (HCN) ion channels regulate human and murine urinary bladder contractility. Front. Physiol. 9, 753. https://doi.org/10.3389/fphys.2018.00753.
Maylie, J., Weiss, J., Morad, M., 1979. Pacemaker Currents and Extracellular K+ Activity in Rabbit Sa Node 25, Undefined-Undefined.
McCloskey, K.D., Toland, H.M., Hollywood, M.A., Thornbury, K.D., McHale, N.G., 1999. Hyperpolarisation-activated inward current in isolated sheep mesenteric lymphatic smooth muscle. J. Physiol. 521, 201–211. https://doi.org/10.1111/j.1469-7793.1999.00201.x.
McCulloh, D.H., Levitan, H., 1987. Rabbit oocyte maturation: changes of membrane resistance, capacitance, and the frequency of spontaneous transient depolarizations. Dev. Biol. 120, 162–169. https://doi.org/10.1016/0012-1606(87)90114-X.
Mert, K.U., Dural, M., Mert, G.Ö., Iskenderov, K., Özen, A., 2018. Effects of heart rate reduction with ivabradine on the international ındex of erectile function (IIEF-5) in patients with heart failure. Aging Male 21, 93–98. https://doi.org/10.1080/13685538.2017.1369943.
Messenger, J.P., Bornstein, J.C., Furness, J.B., 1994. Electrophysiological and morphological classification of myenteric neurons in the proximal colon of the Guinea-pig. Neuroscience 60, 227–244. https://doi.org/10.1016/0306-4522(94)90217-8.
Michels, G., Brandt, M.C., Zagidullin, N., Khan, I.F., Larbig, R., Van Aaken, S., Wippermann, J., Hoppe, U.C., 2008. Direct evidence for calcium conductance of hyperpolarization-activated cyclic nucleotide-gated channels and human native if at physiological calcium concentrations. Cardiovasc. Res. 78, 466–475. https://doi.org/10.1093/cvr/cvn032.
Negrini, D., Marcozzi, C., Solari, E., Bossi, E., Cinquetti, R., Reguzzoni, M., Moriondo, A., 2016. Hyperpolarization-activated cyclic nucleotide-gated channels in peripheral diaphragmatic lymphatics. Am. J. Physiol. Heart Circ. Physiol. 311. https://doi.org/10.1152/ajpheart.00193.2016. H892–H903.

Ng, S.-Y., Chin, C.-H., Lau, Y.-T., Luo, J., Wong, C.-K., Bian, Z.-X., Tsang, S.-Y., 2010. Role of voltage-gated potassium channels in the fate determination of embryonic stem cells. J. Cell. Physiol. 224, 165–177. https://doi.org/10.1002/jcp.22113.

Noble, D., 1960. Cardiac action and pacemaker potentials based on the Hodgkin-Huxley equations. Nature 188, 495–497. https://doi.org/10.1038/188495b0.

Noma, A., Irisawa, H., 1976. Membrane currents in the rabbit sinoatrial node cell as studied by the double microelectrode method. Pflügers Arch. Eur. J. Physiol. 364, 45–52. https://doi.org/10.1007/BF01062910.

Norberg, E., Karlsson, M., Korenovska, O., Szydlowski, S., Silberberg, G., Uhlén, P., Orrenius, S., Zhivotovsky, B., 2010. Critical role for hyperpolarization-activated cyclic nucleotide-gated channel 2 in the AIF-mediated apoptosis. EMBO J. 29, 3869–3878. https://doi.org/10.1038/emboj.2010.253.

Notomi, T., Kuno, M., Hiyama, A., Ohura, K., Noda, M., Skerry, T.M., 2015. Zinc-induced effects on osteoclastogenesis involves activation of hyperpolarization-activated cyclic nucleotide modulated channels via changes in membrane potential. J. Bone Miner. Res. 30, 1618–1626. https://doi.org/10.1002/jbmr.2507.

Okabe, K., Kajiya, H., Okamoto, F., Soeda, H., Inoue, Y., Kawarabayashi, T., 1999. Physiological significance of hyperpolarization-activated inward currents (I(h)) in smooth muscle cells from the circular layers of pregnant rat myometrium. Pflugers Arch. Eur. J. Physiol. 439, 76–85. https://doi.org/10.1007/s004240051130.

Omelyanenko, A., Sekyrova, P., Andäng, M., 2016. ZD7288, a blocker of the HCN channel family, increases doubling time of mouse embryonic stem cells and modulates differentiation outcomes in a context-dependent manner. SpringerPlus 5, 1–10. https://doi.org/10.1186/s40064-016-1678-7.

O'Donnell, A.M., Coyle, D., Puri, P., 2015. Decreased expression of hyperpolarisation-activated cyclic nucleotide-gated channel 3 in Hirschsprung's disease. World J. Gastroenterol. 21, 5635–5640. https://doi.org/10.3748/wjg.v21.i18.5635.

Padilla-Flores, T., López-González, Z., Vaca, L., Aparicio-Trejo, O.E., Briones-Herrera, A., Riveros-Rosas, H., Pedraza-Chaverri, J., León-Aparicio, D., Salvador, C., Sampieri, A., Escobar, L.I., 2020. “Funny” channels in cardiac mitochondria modulate membrane potential and oxygen consumption. Biochem. Biophys. Res. Commun. 524, 1030–1036. https://doi.org/10.1016/j.bbrc.2020.02.033.

Pai, V.P., Willocq, V., Pitcairn, E.J., Lemire, J.M., Paré, J.-F., Shi, N.-Q., McLaughlin, K.A., Levin, M., 2017. HCN4 ion channel function is required for early events that regulate anatomical left-right patterning in a nodal and lefty asymmetric gene expression-independent manner. Biol. Open 6, 1445. https://doi.org/10.1242/bio.025957. LP – 1457.

Pape, H.-C., McCormick, D.A., 1989. Noradrenaline and serotonin selectively modulate thalamic burst firing by enhancing a hyperpolarization-activated cation current. Nature 340, 715–718. https://doi.org/10.1038/340715a0.

Park, J.H., Kim, D.W., Lee, T.K., Park, C.W., Park, Y.E., Ahn, J.H., Lee, H.A., Won, M.H., Lee, C.H., 2019. Improved HCN channels in pyramidal neurons and their new expression levels in pericytes and astrocytes in the gerbil hippocampal CA1 subfield following transient ischemia. Int. J. Mol. Med. 44, 1801–1810. https://doi.org/10.3892/ijmm.2019.4353.

Pian, P., Bucchi, A., DeCostanzo, A., Robinson, R.B., Siegelbaum, S.A., 2007. Modulation of cyclic nucleotide-regulated HCN channels by PIP2 and receptors coupled to phospholipase C. Pflugers Arch. Eur. J. Physiol. https://doi.org/10.1007/s00424-007-0295-2.

Pillozzi, S., Masselli, M., Gasparoli, L., D'Amico, M., Polletta, L., Veltroni, M., Favre, C., Basso, G., Becchetti, A., Arcangeli, A., 2016. Macrolide antibiotics exert anti-leukemic effects by modulating the autophagic flux through inhibition of hERG1 potassium channels. Blood Canc. J. 6. https://doi.org/10.1038/bcj.2016.32 e423–e423.

Pitcairn, E., Harris, H., Epiney, J., Pai, V.P., Lemire, J.M., Ye, B., Shi, N.-Q., Levin, M., McLaughlin, K.A., 2017. Coordinating heart morphogenesis: a novel role for hyperpolarization-activated cyclic nucleotide-gated (HCN) channels during cardiogenesis in Xenopus laevis. Commun. Integr. Biol. 10. https://doi.org/10.1080/19420889.2017.1309488 e1309488–e1309488.

Platano, D., Magli, M.C., Ferraretti, A.P., Gianaroli, L., Aicardi, G., 2005. L- and T-type voltage-gated Ca2+ channels in human granulosa cells: functional characterization and cholinergic regulation. J. Clin. Endocrinol. Metab. 90, 2192–2197. https://doi.org/10.1210/jc.2004-1819.

Robinson, R.B., Siegelbaum, S.A., 2003. Hyperpolarization-activated cation currents: from molecules to physiological function. Annu. Rev. Physiol. 65, 453–480. https://doi.org/10.1146/annurev.physiol.65.092101.142734.

Rusnakova, V., Honsa, P., Dzamba, D., Ståhlberg, A., Kubista, M., Anderova, M., 2013. Heterogeneity of astrocytes: from development to injury - single cell gene expression. PloS One 8. https://doi.org/10.1371/journal.pone.0069734.

Sánchez-Alonso, J.L., Halliwell, J.V., Colino, A., 2008. ZD 7288 inhibits T-type calcium current in rat hippocampal pyramidal cells. Neurosci. Lett. 439, 275–280. https://doi.org/10.1016/j.neulet.2008.05.016.

Sanders, K.M., Ward, S.M., Koh, S.D., 2014. Interstitial cells: regulators of smooth muscle function. Physiol. Rev. 94, 859–907. https://doi.org/10.1152/physrev.00037.2013.

Santoro, B., Shah, M.M., 2020. Hyperpolarization-activated cyclic nucleotide-gated channels as drug targets for neurological disorders. Annu. Rev. Pharmacol. Toxicol. 60, 109–131. https://doi.org/10.1146/annurev-pharmtox-010919-023356.

Sartiani, L., Bettioli, E., Stillitano, F., Mugelli, A., Cerbai, E., Jaconi, M.E., 2007. Developmental changes in cardiomyocytes differentiated from human embryonic stem cells: a molecular and electrophysiological approach. Stem Cell. 25, 1136–1144. https://doi.org/10.1634/stemcells.2006-0466.

Satoh, H., 1995. Identification of a hyperpolarization-activated inward current in uterine smooth muscle cells during pregnancy. Gen. Pharmacol. 26, 1335–1338. https://doi.org/10.1016/0306-3623(95)00006-M.

Satoh, T.-O., Yamada, M., 2000. A bradycardiac agent ZD7288 blocks the hyperpolarization-activated current (Ih) in retinal rod photoreceptors. Neuropharmacology 39, 1284–1291. https://doi.org/10.1016/S0028-3908(99)00207-5.

Schiattarella, G.G., Magliulo, F., Cattaneo, F., Gargiulo, G., Sannino, A., Franzone, A., Oliveti, M., Perrino, C., Trimarco, B., Esposito, G., 2015. Novel molecular approaches in heart failure: seven trans-membrane receptors signaling in the heart and circulating blood leukocytes. Front. Cardiovasc. Med. 2. https://doi.org/10.3389/fcvm.2015.00013.

Seo, H., Seol, M.J., Lee, K., 2015. Differential expression of hyperpolarization-activated cyclic nucleotide-gated channel subunits during hippocampal development in the mouse. Mol. Brain 8, 1–14. https://doi.org/10.1186/s13041-015-0103-4.

Seyama, I., 1976. Characteristics of the rectifying properties of the sino-atrial node cell of the rabbit. J. Phy~iol.

Shahi, P.K., Choi, S., Zuo, D.C., Kim, M.Y., Park, C.G., Kim, Y.D., Lee, J., Park, K.J., So, I., Jun, J.Y., 2014. The possible roles of hyperpolarization-activated cyclic nucleotide channels in regulating pacemaker activity in colonic interstitial cells of Cajal. J. Gastroenterol. 49, 1001–1010. https://doi.org/10.1007/s00535-013-0849-3.

Shen, H., Liu, W., Geng, Q., Li, H., Lu, M., Liang, P., Zhang, B., Yamoah, E.N., Lv, P., 2018. Age-dependent up-regulation of HCN channels in spiral ganglion neurons coincide with hearing loss in mice. Front. Aging Neurosci. 10, 1–11. https://doi.org/10.3389/fnagi.2018.00353.

Si, X., Huang, L., Gong, Y., Lu, J., Lin, L., 2012. Role of calcium in activation of hyperpolarization-activated cyclic nucleotide-gated channels caused by cholecystokinin octapeptide in interstitial cells of cajal. Digestion 85, 266–275. https://doi.org/10.1159/000337077.

Simasko, S.M., Sankaranarayanan, S., 1997. Characterization of a hyperpolarization-activated cation current in rat pituitary cells. Am. J. Physiol. Metab. 272, E405–E414. https://doi.org/10.1152/ajpendo.1997.272.3.E405.

Speranza, L., Franceschelli, S., Riccioni, G., 2012. The biological effects of ivabradine in cardiovascular disease. Molecules 17, 4924–4935. https://doi.org/10.3390/molecules17054924.

Stevens, D.R., Seifert, R., Bufe, B., Müller, F., Kremmer, E., Gauss, R., Meyerhof, W., Kaupp, U.B., Lindemann, B., 2001. Hyperpolarization-activated channels HCN1 and HCN4 mediate responses to sour stimuli. Nature 413, 631–635. https://doi.org/10.1038/35098087.

Stieber, J., Wieland, K., Stöckl, G., Ludwig, A., Hofmann, F., 2006. Bradycardic and proarrhythmic properties of sinus node inhibitors. Mol. Pharmacol. 69, 1328–1337. https://doi.org/10.1124/mol.105.020701.

Sundelacruz, S., Levin, M., Kaplan, D.L., 2009. Role of membrane potential in the regulation of cell proliferation and differentiation. Stem Cell Rev. Reports 5, 231–246. https://doi.org/10.1007/s12015-009-9080-2.

Telinius, N., Majgaard, J., Kim, S., Katballe, N., Pahle, E., Nielsen, J., Hjortdal, V., Aalkjaer, C., Boedtkjer, D.B., 2015. Voltage-gated sodium channels contribute to action potentials and spontaneous contractility in isolated human lymphatic vessels. J. Physiol. 593, 3109–3122. https://doi.org/10.1113/JP270166.

Uawithya, P., Pisitkun, T., Ruttenberg, B.E., Knepper, M.A., 2008. Transcriptional profiling of native inner medullary collecting duct cells from rat kidney. Physiol. Genom. 32, 229–253. https://doi.org/10.1152/physiolgenomics.00201.2007.

Vay, S.U., Flitsch, L.J., Rabenstein, M., Monière, H., Jakovcevski, I., Andjus, P., Bijelic, D., Blaschke, S., Walter, H.L., Fink, G.R., Schroeter, M., Rueger, M.A., 2020. The impact of hyperpolarization-activated cyclic nucleotide-gated (HCN) and voltage-gated potassium KCNQ/Kv7 channels on primary microglia function. J. Neuroinflammation 17, 1–17. https://doi.org/10.1186/s12974-020-01779-4.

Walcher, T., Bernhardt, P., Vasic, D., Bach, H., Durst, R., Rottbauer, W., Walcher, D., 2010. Ivabradine reduces chemokine-induced CD4-positive lymphocyte migration. Mediat. Inflamm. 751313. https://doi.org/10.1155/2010/751313, 2010.

Wang, K., Xue, T., Tsang, S.-Y., Van Huizen, R., Wong, C.W., Lai, K.W., Ye, Z., Cheng, L., Au, K.W., Zhang, J., Li, G.-R., Lau, C.-P., Tse, H.-F., Li, R.A., 2005. Electrophysiological properties of pluripotent human and mouse embryonic stem cells. Stem Cell. 23, 1526–1534. https://doi.org/10.1634/stemcells.2004-0299.

Ward, S.M., Sanders, K.M., Thornbury, K.D., McHale, N.G., 1991. Spontaneous electrical-activity in isolated bovine lymphatics recorded by intracellular microelectrodes. In: JOURNAL OF PHYSIOLOGY-LONDON. CAMBRIDGE UNIV PRESS 40 WEST 20TH STREET, NEW YORK, NY, 10011-4211, P168–P168.

Weidmann, S., 1951. Effect of current flow on the membrane potential of cardiac muscle. J. Physiol. 115, 227–236. https://doi.org/10.1113/jphysiol.1951.sp004667.

Weiss, J., Maylie, J., Morad, M., 1978. Pacemaker currents and paracellular K+ accumulation in rabbit sinoatrial node. In: Frontiers of Biological Energetics. Elsevier, pp. 1417–1426. https://doi.org/10.1016/b978-0-12-225402-4.50079-6.

Wray, S., Prendergast, C., 2019. The myometrium: from excitation to contractions and labour. Advances in Experimental Medicine and Biology. https://doi.org/10.1007/978-981-13-5895-1_10.

Wu, X., Liao, L., Liu, X., Luo, F., Yang, T., Li, C., 2012. Is ZD7288 a selective blocker of hyperpolarization-activated cyclic nucleotide-gated channel currents? Channels 6, 438–442. https://doi.org/10.4161/chan.22209.

Wu, C., Dong, X., Liu, Q., Zhu, J., Zhang, T., Wang, Q., Hu, X., Yang, Z., Li, L., 2017. EP3 activation facilitates bladder excitability via HCN channels on ICCs. Biochem. Biophys. Res. Commun. 485, 535–541. https://doi.org/10.1016/j.bbrc.2017.01.131.

Xiao, J., Nguyen, T.V., Ngui, K., Strijbos, P.J.L.M., Selmer, I.S., Neylon, C.B., Furness, J.B.,

2004. Molecular and functional analysis of hyperpolarisation-activated nucleotide-gated (HCN) channels in the enteric nervous system. Neuroscience 129, 603–614. https://doi.org/10.1016/j.neuroscience.2004.08.027.

Xue, L., Li, Y., Han, X., Yao, L., Yuan, J., Qin, W., Liu, F., Wang, H., 2012. Investigation of hyperpolarization-activated cyclic nucleotide-gated channels in interstitial cells of Cajal of human bladder. Urology 80, 224. https://doi.org/10.1016/j.urology.2012.04.005 e13-224.e18.

Yanagida, H., Inoue, R., Tanaka, M., Ito, Y., 2000. Temperature-sensitive gating of cation current in Guinea pig ileal smooth muscle activated by hyperpolarization. Am. J. Physiol. Cell Physiol. 278, 40–48. https://doi.org/10.1152/ajpcell.2000.278.1.c40.

Yang, S., Xiong, C.jie, Sun, H.mei, Li, X., shuang, Zhang, quan, G., Wu, B., Zhou, D. shan, 2012. The distribution of HCN2-positive cells in the gastrointestinal tract of mice. J. Anat. 221, 303–310. https://doi.org/10.1111/j.1469-7580.2012.01546.x.

Yeh, J., Kim, B.S., Gaines, L., Peresie, J., Page, C., Arroyo, A., 2008. The expression of hyperpolarization activated cyclic nucleotide gated (HCN) channels in the rat ovary are dependent on the type of cell and the reproductive age of the animal: a laboratory investigation. Reprod. Biol. Endocrinol. 6, 2–9. https://doi.org/10.1186/1477-7827-6-35.

Yeh, J., Kim, B.S., Peresie, J., Page, C., 2009. Declines in levels of Hyperpolarization-activated Cation (HCN) channels in the rat ovary after cisplatin exposure. Reprod. Sci. 16, 986–994. https://doi.org/10.1177/1933719109339217.

Young, R.C., 2018. The uterine pacemaker of labor. Best Pract. Res. Clin. Obstet. Gynaecol. 52, 68–87. https://doi.org/10.1016/j.bpobgyn.2018.04.002.

Yue-Chun, L., Guang-Yi, C., Li-Sha, G., Chao, X., Xinqiao, T., Cong, L., Xiao-Ya, D., Xiangjun, Y., 2016. The protective effects of ivabradine in preventing progression from viral myocarditis to dilated cardiomyopathy. Front. Pharmacol. 7, 408. https://doi.org/10.3389/fphar.2016.00408.

Zhang, Y., Zhang, N., Gyulkhandanyan, A.V., Xu, E., Gaisano, H.Y., Wheeler, M.B., Wang, Q., 2008. Presence of functional hyperpolarisation-activated cyclic nucleotide-gated channels in clonal alpha cell lines and rat islet alpha cells. Diabetologia 51, 2290–2298. https://doi.org/10.1007/s00125-008-1166-x.

Zhang, Y., Liu, Y., Qu, J., Hardy, A., Zhang, N., Diao, J., Strijbos, P.J., Tsushima, R., Robinson, R.B., Gaisano, H.Y., Wang, Q., Wheeler, M.B., 2009. Functional characterization of hyperpolarization-activated cyclic nucleotide-gated channels in rat pancreatic β cells. J. Endocrinol. 203, 45–53. https://doi.org/10.1677/JOE-09-0068.

APPENDIX 3

ESC European Society of Cardiology

European Heart Journal (2021) **42**, 3078–3090
doi:10.1093/eurheartj/ehab431

TRANSLATIONAL RESEARCH
Heart failure and cardiomyopathies

PCSK9 deficiency rewires heart metabolism and drives heart failure with preserved ejection fraction

Lorenzo Da Dalt [1], Laura Castiglioni[2], Andrea Baragetti [1,6], Matteo Audano [1], Monika Svecla [1], Fabrizia Bonacina [1], Silvia Pedretti [1], Patrizia Uboldi[1], Patrizia Benzoni [3], Federica Giannetti [3], Andrea Barbuti [3], Fabio Pellegatta [4], Serena Indino [5], Elena Donetti [5], Luigi Sironi [2], Nico Mitro [1], Alberico Luigi Catapano [1,6]*, and Giuseppe Danilo Norata [1,4]*

[1]Department of Pharmacological and Biomolecular Sciences, Università degli Studi di Milano, Via balzaretti, 9, 20133 Milan, Italy; [2]Department of Pharmaceutical Sciences, Università degli Studi di Milano, Via Mangiagalli, 25, 20133 Milan, Italy; [3]Department of Biosciences, Università degli Studi di Milano, Via Celoria, 26, 20133 Milan, Italy; [4]Centro SISA per lo studio dell'Aterosclerosi, Ospedale Bassini, Via Massimo Gorki, 50, 20092 Cinisello Balsamo, Italy; [5]Department of Biomedical Science for Health, Università degli Studi di Milano, Via Mangiagalli, 31, 20133 Milan, Italy; and [6]IRCCS Multimedica Hospital, Via Milanese, 300, 20099 Sesto San Giovanni, Italy

Received 20 December 2020; revised 28 March 2021; editorial decision 15 June 2021; accepted 24 June 2021; online publish-ahead-of-print 12 July 2021

See page 3091 for the editorial comment on this article (doi:10.1093/eurheartj/ehab480)

Aims PCSK9 is secreted into the circulation, mainly by the liver, and interacts with low-density lipoprotein receptor (LDLR) homologous and non-homologous receptors, including CD36, thus favouring their intracellular degradation. As PCSK9 deficiency increases the expression of lipids and lipoprotein receptors, thus contributing to cellular lipid accumulation, we investigated whether this could affect heart metabolism and function.

Methods and results Wild-type (WT), *Pcsk9* KO, *Liver* conditional *Pcsk9* KO and *Pcsk9*/*Ldlr* double KO male mice were fed for 20 weeks with a standard fat diet and then exercise resistance, muscle strength, and heart characteristics were evaluated. *Pcsk9* KO presented reduced running resistance coupled to echocardiographic abnormalities suggestive of heart failure with preserved ejection fraction (HFpEF). Heart mitochondrial activity, following maximal coupled and uncoupled respiration, was reduced in *Pcsk*9 KO mice compared to WT mice and was coupled to major changes in cardiac metabolism together with increased expression of LDLR and CD36 and with lipid accumulation. A similar phenotype was observed in *Pcsk9*/*Ldlr* DKO, thus excluding a contribution for LDLR to cardiac impairment observed in *Pcsk9* KO mice. Heart function profiling of the liver selective *Pcsk9* KO model further excluded the involvement of circulating PCSK9 in the development of HFpEF, pointing to a possible role locally produced PCSK9. Concordantly, carriers of the R46L loss-of-function variant for PCSK9 presented increased left ventricular mass but similar ejection fraction compared to matched control subjects.

Conclusion PCSK9 deficiency impacts cardiac lipid metabolism in an LDLR independent manner and contributes to the development of HFpEF.

* Corresponding authors. Tel: +39 02 50318302 401, Fax: +39 02 50318386, Email: alberico.catapano@unimi.it (A.L.C.); Tel: +39 0250318313, Fax: +39 0250318386, Email: danilo.norata@unimi.it (G.D.N.)

Graphical Abstract

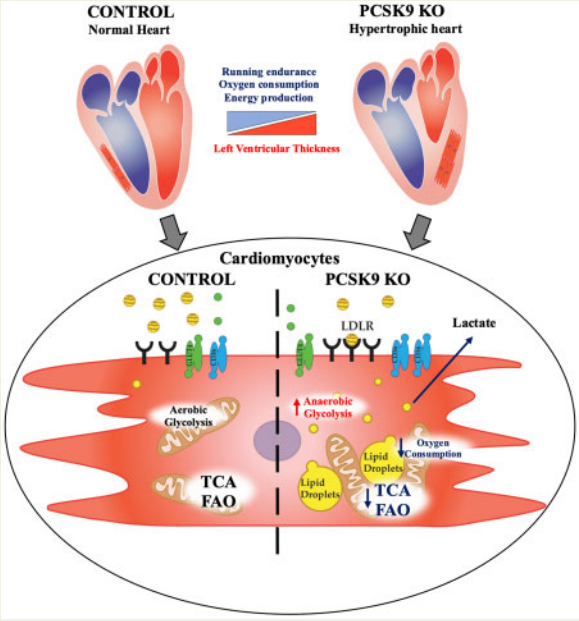

Impact of Pcsk9 deficiency on cardiac function and mitochondrial metabolism. Pcsk9 deficiency is associated with increased heart left ventricular thickness and reduced running performance independently of skeletal muscle alterations. Electron microscopy analysis showed increased cardiac accumulation of lipid droplets associated with a reduced density of mitochondrial cristae; this proffunctionally translated into impaired oxidative phosphorylation and mitochondrial metabolism in PCSK9 KO hearts.

Keywords PCSK9 • Heart • Cholesterol • LDLR • HFpEF

Translational perspective

PCSK9 inhibitors target circulating PCSK9, increase hepatic LDL receptor expression, and reduce LDL-cholesterol levels and ischaemic heart disease. On the contrary, genetic PCSK9 deficiency results in increased risk of developing diabetes or ectopic fat accumulation. Here, we extend this line of evidence showing that systemic PCSK9 deficiency results in heart failure with preserved ejection fraction, a finding independent of the modulation of LDL receptor and of circulating PCSK9. This observation supports the safety profile emerged so far with therapies targeting PCSK9, which are directed towards liver-derived circulating PCSK9.

Introduction

The heart largely uses aerobic metabolism for its energetic needs with the majority of adenosine triphosphate (ATP) being produced following fatty acid (FA) oxidation.[1]

Unlike the liver, the heart is not able to synthesize high amounts of FAs and, therefore, FA demand is primarily supported by the uptake from the circulation, where FAs are transported either as free FAs bound to albumin or as triglycerides in lipoproteins.[2] FAs are then dissociated from albumin or released from lipoproteins through the activity of lipoprotein lipase (LPL), and delivered to cardiomyocytes through FA transport proteins or FA translocases such as CD36. Lipoproteins deliver FAs, and cholesterol to cardiomyocytes by interacting with specific receptors on cell surface including the very low-density lipoprotein receptor (VLDLR).[3,4]

Cardiac lipid demand is a finely tuned process that balances lipid uptake and mitochondrial beta-oxidation to support cardiac metabolism with the need to prevent excessive lipid accumulation which on the contrary induces cardiomyocyte dysfunction.[5] In patients with heart failure, cardiomyocytes switch to glycolysis as preferred pathway for ATP generation, thus promoting cellular triacylglycerol (TAG) accumulation.[6] Lactate, ketone bodies, or amino acids[7] are used as source of energy alternative to FAs[7] in subjects with metabolic syndrome and diabetes.[8] At the molecular level, on one hand TAG accumulation and FA overload promote mitochondrial dysfunction and oxidative phosphorylation uncoupling in cardiomyocytes while

on the other hand contribute to the production of lipotoxic species including diacylglycerol, long-chain acyl-CoA, acylcarnitines and lysophospholipids, which contribute to heart failure.[5]

Several experimental observations have provided a connection between lipid accumulation and cardiac dysfunction. Mice lacking adipose triglyceride lipase present a marked cardiac accumulation of TAG paralleled by heart failure and premature death.[9] Similarly, the overexpression of both peroxisome proliferator-activated receptor alpha (PPARα) and gamma (PPARγ) increases FA oxidation but causes an imbalance in cardiac lipid metabolism as a consequence of FA uptake exceeding oxidation, thus leading to lipid accumulation.[10] On the same line, mice expressing glycosylphosphatidylinositol (GPI)-anchored human LPL (αMHC-LpL^{GPI}) selectively in cardiomyocytes have increased cardiac uptake and accumulation of lipids that are derived from circulating lipoproteins including triglycerides, FAs, and cholesterol.[11]

All together these data are consistent with the concept that promoting the activity of pathways involved in lipid uptake might contribute to cardiac lipid overload and toxicity and suggest that factors increasing lipoprotein receptor expression in the heart might result in cardiac dysfunction as was shown also for hypoxia inducing VLDLR-mediated cardiac lipotoxicity.[12]

Proprotein convertase subtilisin/kexin type 9 (PCSK9), a 692-amino acid glycoprotein, is known to control low-density lipoprotein receptor (LDLR) recycling.[13,14] In addition to LDLR, PCSK9 targets LDLR homologous and non-homologous receptors, including VLDLR,[15] ApoER2 (LRP8),[16] LRP1,[17] and CD36,[18] and, disrupts their recycling by inhibiting the dissociation from the lipoprotein in the endosome–lysosome compartment, thus promoting their degradation. As such, increased PCSK9 levels result in reduced recycling of these receptors, a finding extensively described in the liver. PCSK9, however, exerts extra-hepatic effects[19]; its deficiency is associated with impaired pancreatic beta-cell function[20] and increased risk of developing diabetes in humans.[20–22] Of note *Pcsk9* KO mice present increased body weight and visceral adipose tissue deposition, a finding confirmed in carriers of a PCSK9 loss-of-function variant.[23] The observation that these subjects also present increased epicardial adipose tissue,[23] coupled to the key role of PCSK9 in controlling key receptors involved in cardiac lipoprotein uptake provides the rationale for investigating whether PCSK9 deficiency impacts cardiac lipid metabolism and function. To this end, we tested the impact of PCSK9 deficiency on heart metabolism and function in an experimental setting where insulin response is preserved. *Pcsk9* KO mice were indeed fed standard fat diet for 20 weeks and we observed that PCSK9 deficiency affected lipid metabolism and energy production in the heart that lead to the thickening of the left ventricular wall and the development of heart failure with preserved ejection fraction (HFpEF). To further investigate the impact of this observation in the clinical setting, cardiac function was investigated in subjects carrying a loss-of-function polymorphism of PCSK9.

Methods

A detailed description of mice, echocardiographic analysis, exhaustion test, forelimb grip test, oxygen consumption rate, metabolomics, proteomics, western blot analysis, analysis of cholesterol accumulation in cardiac tissue, plasma dosages, bioinformatics, and statistical analysis is presented in the Supplementary material online.

Our study complies with the Declaration of Helsinki, the local ethics committee approved the research protocol, and informed consent was obtained from all subjects (or their legally authorized representative).

Results

Pcsk9 deficiency is associated with heart failure with preserved ejection fraction

To investigate whether the impact of PCSK9 on systemic and cellular lipid and lipoprotein metabolism might affect cardiac function, we evaluated heart morphology in *Pcsk9* KO and wild-type (WT) male mice fed for 20 weeks with standard fat diet. Electrocardiographic analysis (*Figure 1A*) of the heart of *Pcsk9* KO mice showed an increased thickness of the left ventricular posterior wall (LVPW) during both systole and diastole as compared to WT mice (*Figure 1B and C*) despite no difference in total body weight between the two groups (Supplementary material online, *Figure S1A*). This was coupled with an increased relative wall thickness (*Figure 1D*) in spite of similar left ventricular mass normalized on body weight ratio (*Figure 1E*) and ejection fraction (*Figure 1F*) in *Pcsk9* KO compared to WT mice, thus suggesting a concentric remodelling of the heart. To evaluate whether this profile associates with impaired cardiac functionality, exercise intolerance and running resistance in fatigue test were performed in WT and *Pcsk9* KO mice. The latter experienced a significant reduction of the running distance and the running time observed in the exhaustion test compared to WT mice (*Figure 1G and H*).

Of note, this phenotype was not the consequence of a reduced skeletal muscle performance as similar results were observed in the forelimb grip test (*Figure 1I*) coupled with no differences in oxygen consumption rate in soleus muscle between *Pcsk9* KO and WT mice (Supplementary material online, *Figure S1B*). These data indicate that *Pcsk9* KO mice present a profile suggestive of HFpEF.

Cardiac mitochondrial metabolism is altered in Pcsk9-deficient mice

Given the key role of PCSK9 in cellular lipid biology, we next evaluated the impact of PCSK9 deficiency on cardiac lipid metabolism and its relevance for heart energetic demand. Freshly isolated hearts from *Pcsk9* KO mice exhibited a significant reduction in oxygen consumption rate compared to control mice under maximal coupled and uncoupled respiration (*Figure 2A*). This finding, coupled with the reduced activity of the complex II of the electron transport chain (ETC) observed in *Pcsk9* KO mice (Supplementary material online, *Figure S2A and B*), prompted us to test whether ATP production was affected. ATP levels (*Figure 2B*) and ATP energy charge (*Figure 2C*) were reduced in the heart of *Pcsk9* KO mice compared to WT littermates together with other cofactors involved in energy production (Supplementary material online, *Figure S2D–K*). Moreover, a detailed proteomic analysis of cardiac tissue showed that the expression of several mitochondrial proteins was affected in *Pcsk9* KO heart compared to WT (Supplementary material online, *Figure S2A*), including those of key structural components of ETC complexes (*Figure 2D*). This finding was further confirmed by western blot analysis of

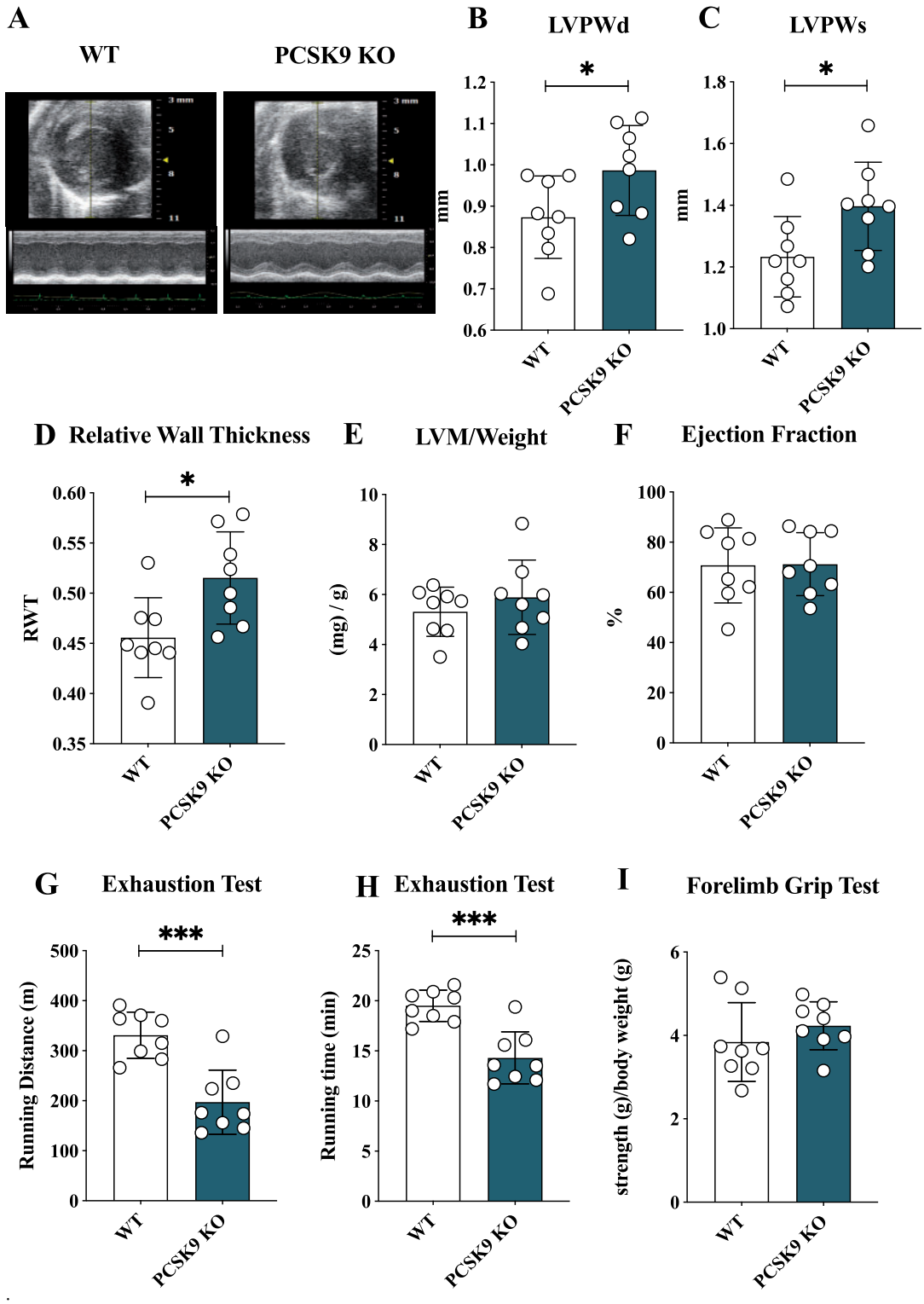

Figure 1 Pcsk9 deficiency is associated with heart failure with preserved ejection fraction. (*A*) Representative image of echocardiographic analysis for wild-type and Pcsk9 KO mice. (*B, C*) Left ventricular posterior wall thickness during systole ($P = 0.049$) and diastole ($P = 0.03$). (D–F) relative wall thickness (RWT) ($P = 0.02$), the left ventricular mass/weight ($P = 0.37$) and ejection fraction (%) ($P = 0.95$) are shown. (G, H) Running endurance following exhaustion test for wild-type and Pcsk9 KO mice is presented as running distance ($P = 0.0003$) and running time ($P = 0.0003$). (*I*) Results from the forelimb grip test are presented ($P = 0.33$). Data are shown as mean ± SD; $n = 8$ mice per group. Non-parametric *t*-test was used to compare each group. *$P < 0.05$ and ***<0.001.

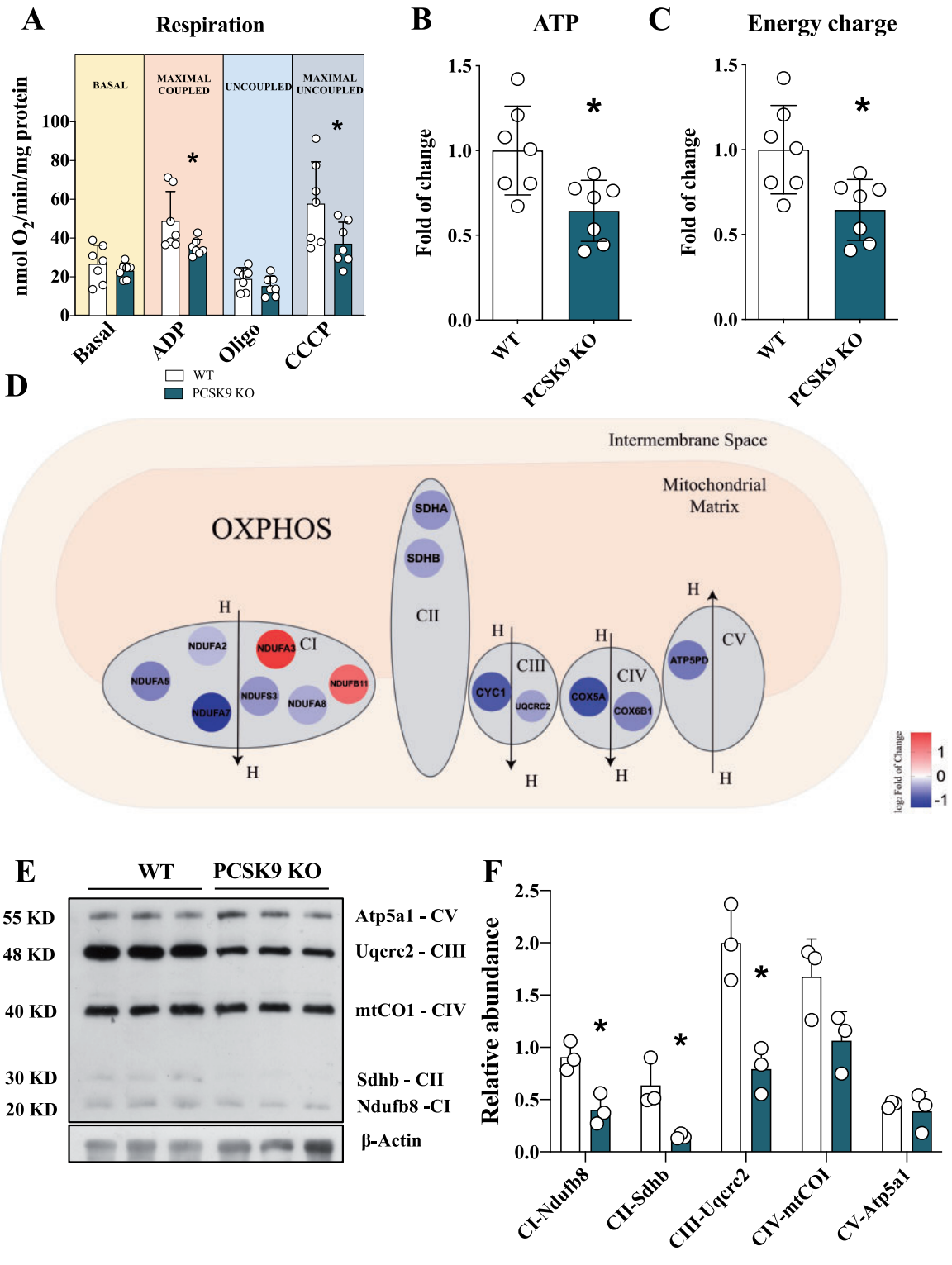

Figure 2 Pcsk9 deficiency is associated with mitochondrial dysfunction. (*A*) The oxygen consumption rate was investigated in the heart of *Pcsk9* KO mice and oxygen consumption was measured at basal, maximal coupled, uncoupled and maximal uncoupled conditions (Basal, $P = 0.39$; ADP, $P = 0.04$; Oligo, $P = 0.24$; CCCP, $P = 0.04$). Data are shown as mean ± SD; $n = 7$ mice per group. (*B* and *C*) Adenosine triphosphate ($P = 0.01$) quantification and energy charge ($P = 0.01$) of the heart. Data are shown as fold of change ± SD; $n = 7$ mice per group. (*D*) Relevant proteins of ETC are displayed. (*E*) Representative image of western blot of ETC complexes on heart lysate is showed. (*F*) Proteins quantification is normalized to beta-actin expression (CI, $P = 0.01$; CII, $P = 0.02$; CIII, $P = 0.008$; CIV, $P = 0.08$, CV, $P = 0.59$). Data are shown as mean ± SD; $n = 3$ mice per group. Non-parametric *t*-test was used to compare each group (*$P < 0.05$).

proteins representative of each mitochondrial complex, including NADH ubiquinone oxidoreductase subunit B8 (Ndufb8—Complex I), succinate dehydrogenase complex subunit B (Sdhb—Complex II), and ubiquinol-cytochrome C reductase core protein 2 (Uqcrc2—Complex III) that were significantly reduced in the heart of *Pcsk9* KO mice (*Figure 2E and F*) compared to WT littermates. This finding together with the reduction of complex II activity (Supplementary material online, *Figure S2B*) supports the possibility that FADH2 could undergo a less efficient entry of into the ETC, a process that could impact FA catabolism. In parallel with these findings, also mitochondrial DNA copy number was reduced (Supplementary material online, *Figure S2C*), suggesting that mitochondrial function and content are affected in the heart of *Pcsk9* KO mice.

We next asked whether this translates into altered cardiac metabolism. The combied analysis of metabolomic, proteomic, and lipidomic profiles in the heart of *Pcsk9* KO and of WT mice (*Figure 3A* and Supplementary material online, *Figure S3*) revealed that impaired mitochondrial activity results from: (i) impaired FA oxidation as supported by the increase of acyl-carnitines carrying medium-chain FA (C8 and C10) coupled to the reduction of β-oxidation enzymes, such as sterol carrier protein 2 (SCP2), enoyl-CoA hydratase, and short chain 1 (ECHS1) (*Figure 3A* and Supplementary material online, *Figure S3C and D*), and (ii) decreased tricarboxylic acid (TCA) cycle flux (*Figure 3A* and Supplementary material online, *Figure S3A and E*) as indicated by the reduced levels of TCA intermediates and enzymes catalyzing key enzymatic reactions. The reduced levels of glucose-6P (*Figure 3A* and Supplementary material online, *Figure S3B and F*) and the increased levels of lactate dehydrogenase coupled with increased lactate plasma levels (*Figure 3A*) further confirmed a switch to anaerobic metabolism, which, however, is not sufficient to support heart energy demand and indeed a net reduction in energy charge is observed in the heart of *Pcsk9* KO mice compared to WT (*Figure 2C*). Concordantly, functional pathway analysis of cardiac proteome showed increased cardiac dysfunction related to the inability of sustaining cellular energy demand (*Figure 3B*) and the electron microscopy analysis of mitochondria from both WT and *Pcsk9* KO hearts showed less dense and organized mitochondrial cristae in cardiomyocytes from *Pcsk9* KO heart compared to WT (*Figure 3C*).

PCSK9 deficiency results in increased LDLR and CD36 expression in the heart coupled with lipid accumulation

To get further insights into the molecular mechanisms underlying the dysfunctional cardiac phenotype, we investigated the expression of key PCSK9 targets in the heart. Both the expressions of LDLR and CD36 were increased in *Pcsk9* KO mice compared to WT littermates (*Figure 4A and B*). Of note, transmission electron microscopy analysis of the hearts showed longitudinally oriented myofibrils and regular intercalated discs in both WT and *Pcsk9* KO mice (*Figure 4C and D*). *Pcsk9* KO hearts, however, presented abundant lipid droplets tightly associated with mitochondria (*Figure 4D*), a characteristic barely appreciated in WT mice (*Figure 4C*). This observation further supports the presence of lipid accumulation in the heart of *Pcsk9* KO mice. The quantitative analysis of ultrathin sections showed that *Pcsk9* KO mice presented a statistically significant increase in the number of lipid droplets (*Figure 4E* and Supplementary material online, *Figure S4A*) as well as of lipid droplets diameter (*Figure 4F*). Moreover, increased total cholesterol (*Figure 4G*) and arachidonic acid levels (Supplementary material online, *Figure S4B*) but similar total triglyceride content (*Figure 4H*) were observed in the heart of *Pcsk9* KO mice compared to WT littermates. As expected, plasma cholesterol and triglyceride levels were lower in *Pcsk9* KO mice compared to WT[20] (Supplementary material online, *Figure S3G and H*).

The observation of increased lipid droplets number and cholesterol content, coupled with increased LDLR receptor expression in the heart of *Pcsk9* KO mice, points to a possible role of LDLR in promoting the increased cardiac lipid accumulation. To test this hypothesis, we characterized heart function, morphology, and metabolism in mice lacking both PCSK9 and LDLR (DKO).

DKO mice presented a significant reduction compared to *Ldlr* KO mice in the distance and the time of running observed in the exhaustion test (*Figure 5A and B*); this effect was not dependent on differences in skeletal muscle strength, as the results from the forelimb grip test were similar (*Figure 5C*). Notably heart left ventricular mass/weight and heart LVPW thickness in systole were significantly lower in *Ldlr* KO mice compared to WT (left ventricular mass/weight: WT 5.31 ± 0.98 vs. *Ldlr* KO 4.10 ± 0.91, $P = 0.04$) (LVPW: WT 1.23 ± 0.13 vs. *Ldlr* KO 1.10 ± 0.08, $P = 0.04$) (Supplementary material online, *Table S1*), a finding that fits with their reduced performance on running endurance compared to WT (running distance: WT 331.1 ± 46.20 vs. *Ldlr* KO 245.3 ± 40.93 m, $P = 0.049$) (Supplementary material online, *Figure S5A–C*). On the other hand, the echocardiographic profile of DKO was very similar to that observed in *Pcsk9* KO mice (*Figures 1B and 5C*), suggesting that the impact of PCSK9 on heart function does not depend on the modulation of LDLR expression and on changes in plasma cholesterol levels (Supplementary material online, *Figure S5D and E*). Indeed, echocardiographic analysis showed that DKO mice presented a significant left ventricular thickening during systole (*Figure 5D*) without alterations in ejection fraction (*Figure 5E*) compared to *Ldlr* KO mice. In addition, metabolic analysis showed that ATP levels and energy charge were still significantly reduced in DKO mice as compared to *Ldlr* KO mice (*Figure 5F and G*). This profile is consistent with a reduced flux of TCA cycle coupled with mitochondrial dysfunction (*Figure 5H*) in the heart, and with increased plasma levels of lactate (*Figure 5I* and Supplementary material online, *Figure S5F*). These data strongly support the concept that the increased cardiac LDLR expression induced by PCSK9 deficiency is not involved in the phenotype observed. To get further insights into the connection between PCSK9 and cardiomyocytes physiology, we performed a series of studies in cardiomyocytes differentiated from human pluripotent stem cells (iPSC-CMs). The acquisition of cardiomyocyte phenotype was documented by the increase, up to 300 folds, of troponin T expression (Supplementary material online, *Figure S6A*). VLDL supplementation leads to a significant increase in the expression of LDLR, CD36, LPL, glucose transporter type 4 (GLUT4), and FA synthase mRNA expression in iPSC-CMs compared to cells grown in control medium (Supplementary material online, *Figure S6B*). Moreover, VLDL treatment resulted in decreased mitochondrial mass (Supplementary material online, *Figure S6C*) and increased accumulation of neutral lipids (Supplementary material online, *Figure S6D*). These effects were reverted when cardiomyocytes were pre-treated with PCSK9 (Supplementary material online, *Figure S6E and F*) confirming a role for PCSK9 in regulating

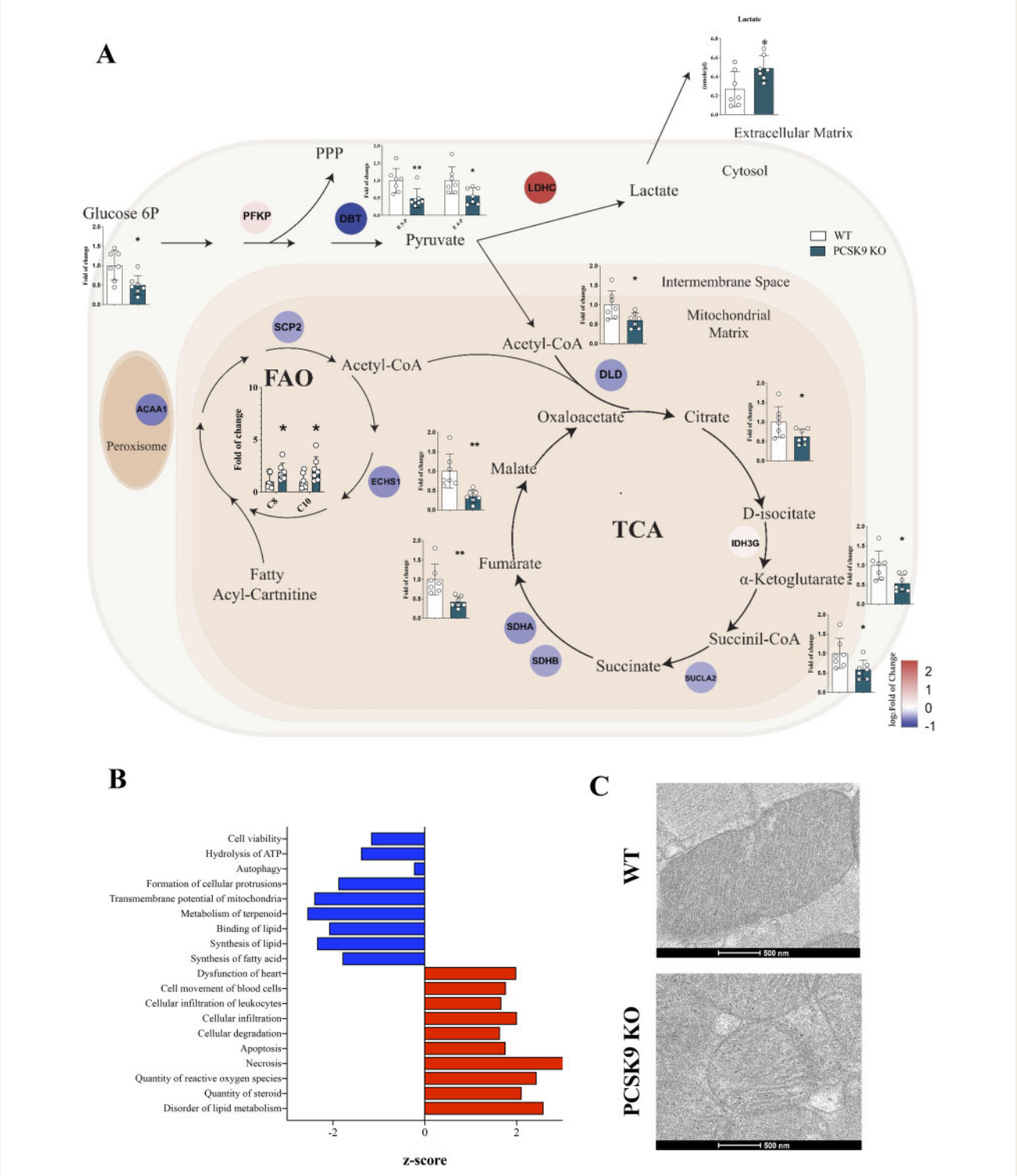

Figure 3 Metabolic profile of failing Pcsk9 KO heart. (*A*) Results from combined metabolomic, proteomic and lipidomic profile in the heart of *Pcsk9* KO mice compared to wild-type mice are shown. Metabolites that are significantly modulated (belonging to glycolysis, pentose phosphate pathway, Krebs cycle, or carnitines for beta-oxidation) (G6-P, $P = 0.012$; R5-P, $P = 0.01$; E4-P, $P = 0.02$; acetyl-CoA, $P = 0.02$; citrate, $P = 0.04$; α-ketoglutarate, $P = 0.01$; succinyl-CoA, $P = 0.03$; fumarate, $P = 0.003$; malate, $P = 0.003$; C8, $P = 0.048$; C10, $P = 0.048$) are shown in bar graph as fold of change ± SD; $n = 7$ mice per group. Proteins that were significantly modulated following proteomics analysis are shown as coloured dots. Plasma levels of lactate are shown ($P = 0.02$). Data are shown as mean ± SD; $n = 7$ per group. (B) Functional pathway analysis of proteomics data is presented. Hierarchical clustering is based on Pearson's correlation and heatmap showing relative protein expression values (z-score-transformed LFQ protein intensities) of n=65 proteins corresponding to ETC mitochondrial complexes in GO analysis (FDR < 0.05). Non-parametric t-test was used to compare each group. (*C*) Representative photomicrographs of myocardium mitochondria by transmission electron microscopy are shown. (*$P < 0.05$ and **<0.01)

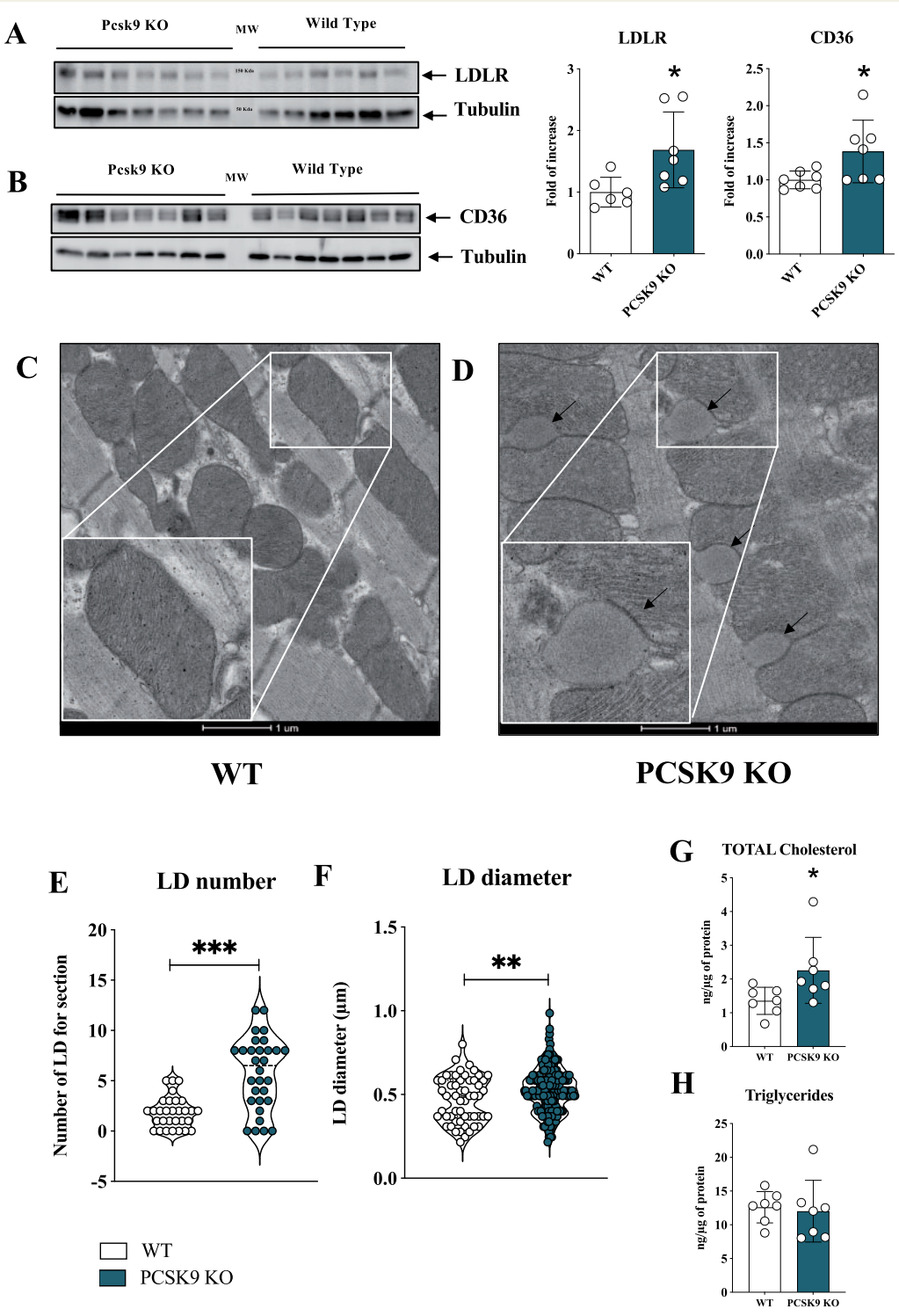

Figure 4 PCSK9 deficiency results in increased lipids and lipoprotein receptor expression coupled with cholesterol accumulation and the increase of lipid droplets in the heart. (*A*) Representative image and quantification of immunoblotting analysis for LDLR in cardiac tissue from *Pcsk9* KO and wild-type mice ($P = 0.03$). Data are shown as mean ± SD; $n = 6$ mice for the wild-type group and $n = 7$ mice for the *Pcsk9* KO group. (*B*) Representative image and quantification of immunoblotting analysis for CD36 in cardiac tissue from *Pcsk9* KO and wild-type mice ($P = 0.04$). Data are shown as mean ± SD; $n = 7$ mice for group. (*C* and *D*) Representative photomicrographs of myocardium by transmission electron microscopy in wild-type and *Pcsk9* KO mice are shown. Black arrows indicate lipid droplets. The inset panels show a magnification of wild-type mice (*C*) and of *Pcsk9* KO mice (*D*). Bars 1 µm. (*E* and *F*) Lipid droplets number ($P < 0.0001$) and diameter ($P = 0.008$) obtained from transmission electron microscopy analysis are shown as violin plot. (*G*) Intracardiac total cholesterol ($P = 0.04$) and (*E*) triglycerides levels ($P = 0.77$) are shown. Data are presented as mean ± SD; $n = 7$ mice for group. Non-parametric *t*-test was used to compare each group (*$P < 0.05$, **$P < 0.01$ and ***<0.001).

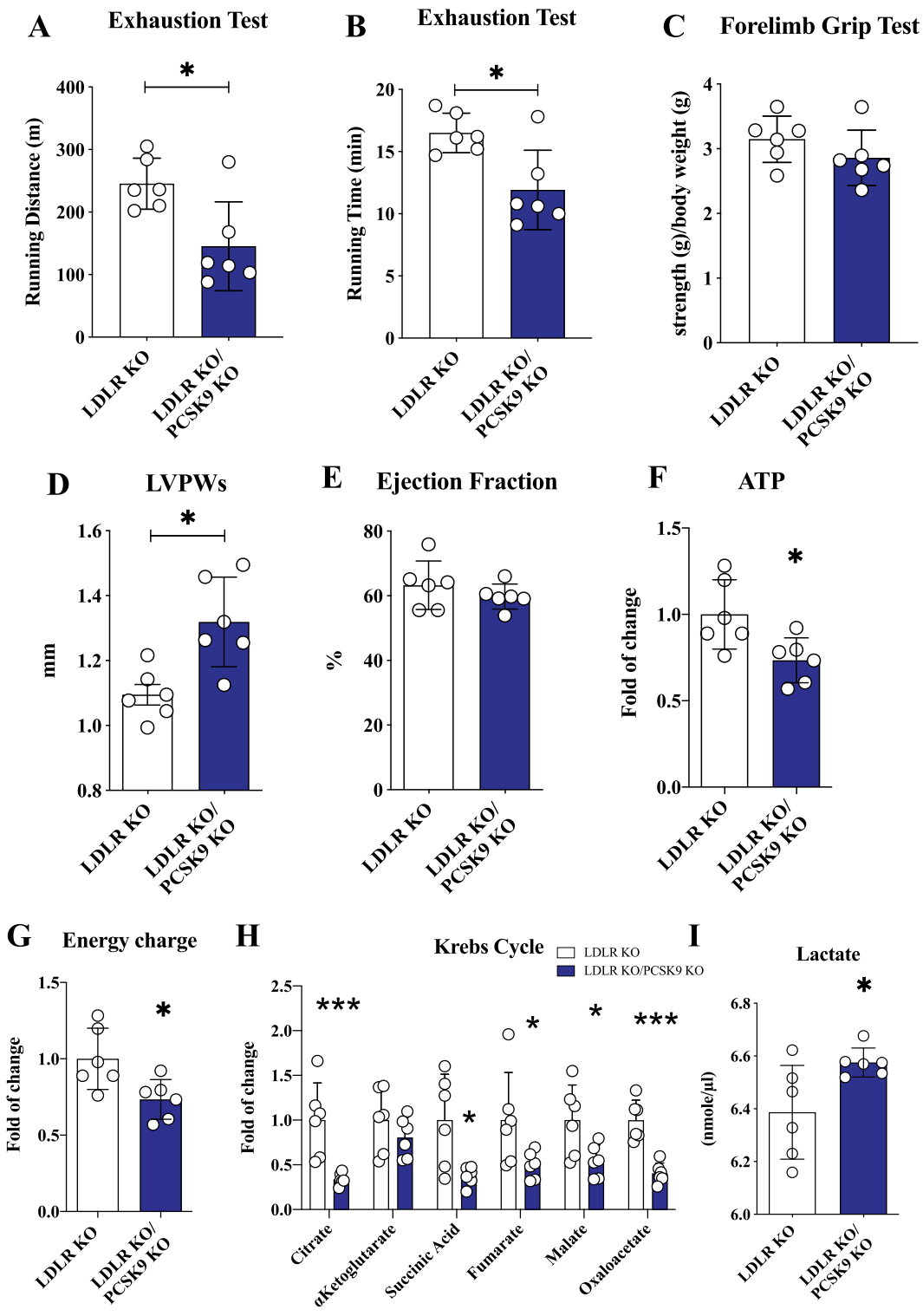

Figure 5 PCSK9 effect on cardiac function is not dependent on the LDLR. (*A* and *B*) Running endurance on exhaustion test of Ldlr KO and Pcsk9/Ldlr DKO mice is displayed as running distance ($P = 0.01$) and running time ($P = 0.01$). (*C*) Results from the forelimb grip test are displayed ($P = 0.23$). (*D* and *E*) Left ventricular posterior wall thickness during systole ($P = 0.01$) and ejection fraction ($P = 0.33$) are shown. (*F* and *G*) Adenosine triphosphate quantification ($P = 0.02$) and energy charge ($P = 0.02$) of the heart. Data are presented as mean ± SD. (*H*) Metabolites of the Krebs cycle are shown (citrate, $P = 0.003$; α-ketoglutarate, $P = 0.29$; succinyl-CoA, $P = 0.02$; fumarate, $P = 0.05$; malate, $P = 0.03$; oxaloacetate, $P = 0.0002$) as fold of change ± SD. (*I*) Plasma levels of lactate ($P = 0.03$) are shown as mean ± SD. $n = 6$ mice per group. Non-parametric *t*-test was used to compare each group (*$P < 0.05$ and ***<0.001).

lipids uptake and mitochondrial function in cardiomyocytes. In line with these findings, primary cardiomyocytes isolated from *Pcsk9* KO treated with VLDL showed reduced mitochondrial mass compared to WT and the same was true for primary cardiomyocytes isolated *Pcsk9*/*Ldlr* DKO (Supplementary material online, *Figure S6G*), thus further excluding a role for the LDLR in the phenotype observed.

Circulating PCSK9 does not impact heart metabolism

In both human and mice, circulating PCSK9 is largely contributed by the liver. Therefore, to separate the effect of circulating vs. locally produced PCSK9 on heart function, we profiled cardiac function and heart morphology in mice lacking PCSK9 production selectively in the liver (*AlbCre*+/*Pcsk9*$^{LoxP/LoxP}$ mice) and therefore deficient for PCSK9 only in the circulation.[20] The running distance and the running time observed in the exhaustion test were similar in *AlbCre*+/*Pcsk9*$^{LoxP/LoxP}$ mice compared to their *AlbCre*−/*Pcsk9*$^{LoxP/LoxP}$ counterpart (*Figure 6A and B*) as was muscular performance (*Figure 6C*). Accordingly, no differences emerged for left ventricular thickness during systole (*Figure 6D*), for ejection fraction (*Figure 6E*) as well as for several cardiac parameters (Supplementary material online, *Figure S7A–E*). Also, ATP production (*Figure 6F*), ATP energy charge (*Figure 6G*), Krebs cycle metabolites (*Figure 6H*), and glycolysis intermediates (Supplementary material online, *Figure S7F*) were not different in the heart of these mice. Circulating lactate levels (*Figure 6J*) and triglycerides (Supplementary material online, *Figure S7G*) were not affected in *AlbCre*+/*Pcsk9*$^{LoxP/LoxP}$ mice compared to their *AlbCre*−/*Pcsk9*$^{LoxP/LoxP}$ counterpart while cholesterol was significantly reduced in liver selective KO (Supplementary material online, *Figure S7H*). These data excluded a role for the deficiency of liver-produced (i.e. circulating) PCSK9 in the phenotype observed, rather pointing to locally produced PCSK9 deficiency as a driver of heart dysfunction.

Genetic PCSK9 loss of function is associated with altered cardiac phenotype in humans

To further translate our findings in humans, we evaluated the impact of a PCSK9 loss-of-function variant (R46L) on echocardiographic-based markers of cardiac functionality in a cohort of 2606 subjects from the general population (PLIC study). A pilot analysis of cardiac profile in 12 heterozygous R46L carriers (Supplementary material online, *Table S2*) showed that these subjects displayed significant increase in left ventricular mass index (*Figure 7A*) but similar ejection fraction (*Figure 7B*) compared to age- and sex-matched WT subjects. Interestingly, leg and arm skeletal muscle mass were comparable between heterozygous subjects and WT carriers (*Figure 7C*).

Discussion

In this work, we demonstrate that PCSK9 plays a key role in controlling heart metabolism and function. When PCSK9 is absent, the expression of key receptors involved in lipid and lipoprotein uptake is increased and results in heart cholesterol accumulation, impaired beta-oxidation and mitochondrial activity, thus affecting cardiac metabolism and function (*Graphical abstract*).

Unlike the liver, the heart cannot synthesize large amounts of FAs and therefore lipid demand is primarily fulfilled with the uptake from the circulation, which however needs to be properly controlled to limit an excessive uptake which may result in lipid accumulation and cellular lipotoxicity. Under these circumstances, cardiomyocytes switch their metabolism towards anaerobic glycolysis, which however does not fully compensate the elevated energetic demand. Physiologically, this shift triggers a series of morphological adaptations in the heart including increased left ventricular wall thickness to maintain ejection fraction. This profile is typical of HFpEF where cardiomyocytes switch their metabolism from FA oxidation into mitochondria, to glycolysis and ketone body utilization[24] as described in patients with hypertension[25] and obesity,[26] as well as with diabetes.[27]

Here we show that a similar profile is observed in PCSK9-deficient conditions in experimental models. A detailed profiling of cardiac metabolic signature revealed that oxygen consumption rate and ATP levels are reduced as a consequence of impaired mitochondrial function as suggested also by the changes in ETC protein complexes and activity. Previous observations highlighted that heart lipid accumulation drives lipotoxicity and contributes to heart metabolic switch; thus, the observation that PCSK9 deficiency results in increased cholesterol accumulation in the heart coupled with metabolic shift towards anaerobic glycolysis supports the hypothesis that PCSK9 plays a physiologically role in maintaining a proper balance of factors involved in lipid uptake by cardiomyocytes.

The obvious candidates for this activity are lipoprotein receptors, which, although expressed at a lower extent in the heart compared to other tissues, such as the liver, still play a critical role in controlling heart lipoprotein uptake and lipid metabolism.[28] The observation that the expression of both LDLR and CD36 two PCSK9 targets, is increased in the heart of *Pcsk9* KO mice could represent a matter of concern for patients treated with PCSK9 inhibitors, as the increase in LDLR recycling is responsible for increased lipoproteins uptake in liver and plasma cholesterol lowering, but might also influence heart lipid accumulation. To further elucidate this aspect, cardiac profile and running endurance were investigated in *Pcsk9*/*Ldlr* DKO mice and in *Ldlr* KO mice. Of note *Pcsk9*/*Ldlr* DKO mice still present heart dysfunction and the metabolic sequalae observed in *Pcsk9* KO mice, while *Ldlr* KO had a significantly lower left ventricular mass/weight and heart LVPW thickness in systole compared to WT, thus excluding a role for PCSK9/LDLR axis in the cardiac phenotype observed. Moreover, this finding suggests that eventually LDLR-mediated lipoprotein uptake, at least in the heart, does not result in lipid accumulation and cardiac metabolism impairment. Could pharmacological inhibition of PCSK9 result in increased cardiac lipid uptake and heart dysfunction? Data from large interventional trials with PCSK9 inhibitors did not report an increased incidence of heart failure.[29]

Current therapies targeting PCSK9 include monoclonal antibodies which act by sequestering circulating PCSK9,[30] and a gene silencing approach, which acts by selectively silencing PCSK9 mRNA expression in the liver.[31] Given that the liver contributes to circulating PCSK9 levels, both approaches reduce circulating PCSK9 but do not affect local PCSK9 production, except for the liver. To explore whether a complete lack of circulating PCSK9 could impact heart metabolism, cardiac function was evaluated in an experimental model lacking PCSK9 expression selectively in the liver, thus presenting

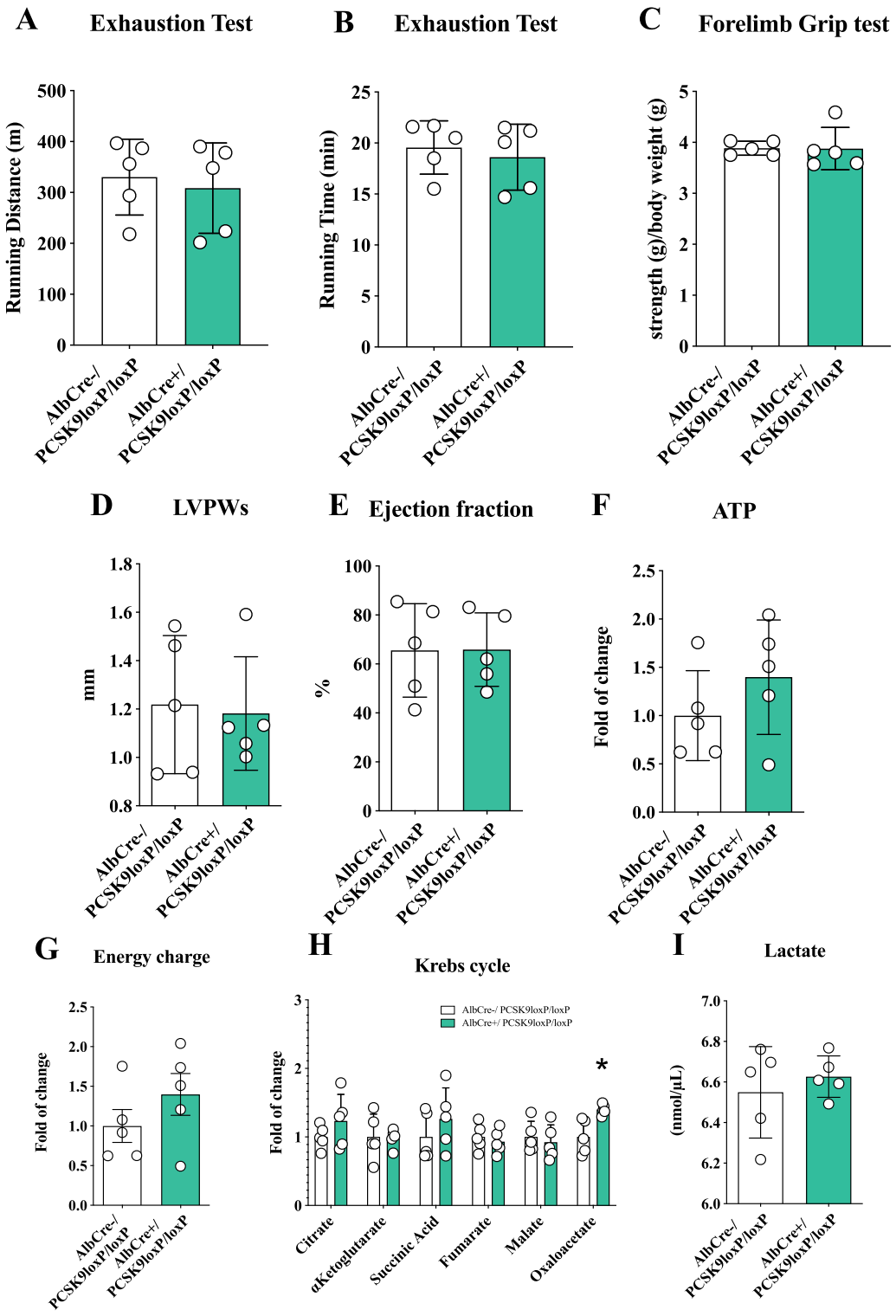

Figure 6 Circulating PCSK9 does not impact cardiac metabolism and heart structure. (*A* and *B*) Running endurance on exhaustion test of *AlbCre−/Pcsk9*$^{LoxP/LoxP}$ and *AlbCre+/Pcsk9*$^{LoxP/LoxP}$ mice is displayed as running distance ($P = 0.68$) and running time ($P = 0.63$). (*C*) Results from the forelimb grip test are displayed ($P = 0.98$). (*D* and *E*) Left ventricular posterior wall thickness during systole ($P = 0.83$) and ejection fraction ($P = 0.98$) are shown. (*F* and *G*) Adenosine triphosphate quantification ($P = 0.27$) and energy charge ($P = 0.627$) of the heart are presented. (*H*) Metabolites of the Krebs cycle (citrate, $P = 0.26$; α-ketoglutarate, $P = 0.91$; succinyl-CoA, $P = 0.33$; fumarate, $P = 0.57$; malate, $P = 0.63$; oxaloacetate, $P = 0.009$) are shown as fold of change ± SD. (*I*) Plasma levels of lactate ($P = 0.50$) are shown. Data are shown as mean ± SD; $n = 5$ mice per group. Non-parametric *t*-test was used to compare each group (*$P < 0.05$).

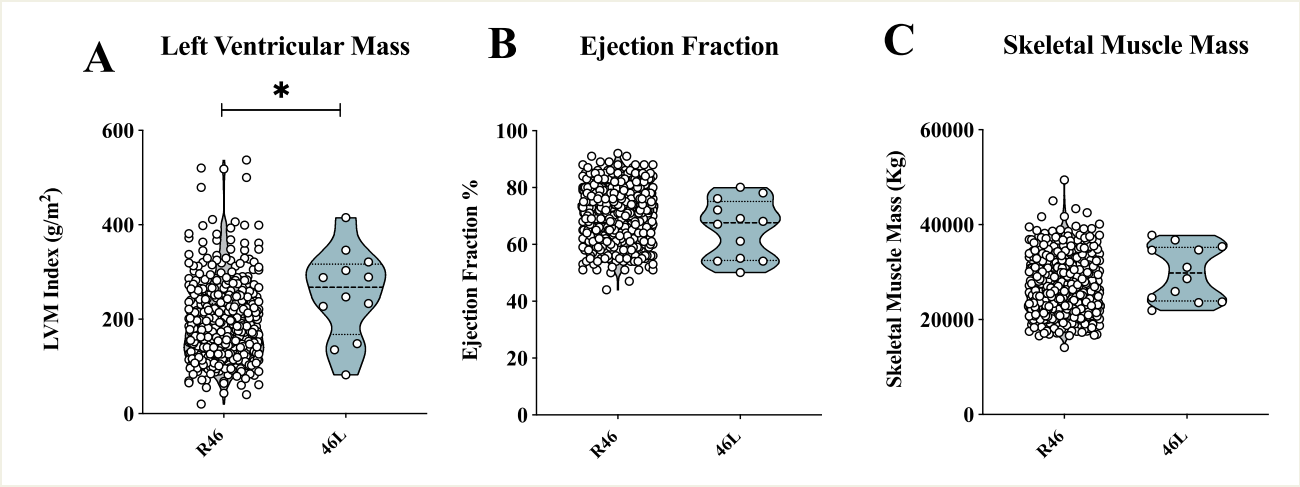

Figure 7 PCSK9 46L LOF individuals present heart failure with preserved ejection fraction. (*A* and *B*) Left ventricular mass index (g/m^2) ($P = 0.01$) and ejection fraction ($P = 0.10$) of PCSK9 R46 and 46L carriers are shown. (*C*) Leg and arm skeletal muscle mass (quantified by Dual X-Rays Absorbimetry, following Hansen's formula) ($P = 0.26$) is shown (R46, $n = 516$; 46L, $n = 12$). Non-parametric *t*-test was used to compare each group. (*$P < 0.05$).

undetectable circulating PCSK9 levels but unaltered expression in other tissues[20]; a phenotype which mimics that observed following PCSK9 inhibitors therapy. In this experimental model, exercise performance, heart morphology, metabolic signature, and oxygen consumption were similar to those of WT mice. This observation is seminal to exclude any possible impact of circulating PCSK9 deficiency on heart metabolism and is in line with the data on cardiac function observed in clinical trials with anti-PCSK9 therapies.

Which cells are then providing PCSK9 that is critical for the maintaineance of cardiomyocyte homeostasis and lipid balance?

Under basal conditions, PCSK9 is expressed at very low levels in the heart (Supplementary material online, *Figure S7I*) but is induced in vivo under ischaemic conditions[32] and in vitro following incubation with oxidized LDL.[33] It has been hypothesized that PCSK9 induction immediately after ischemia/reperfusion injury might protect the heart in the acute phase by stimulating autophagic process and the removals of damaged mitochondria,[32] an effect that could became deleterious over time as might lead to increased cell deterioration and cardiomyocyte death. It is also possible that PCSK9 produced locally by epicardial adipose tissue[34] contributes to this pathophysiological change, a finding supported by the observation that the R46L variant is associated with increased epicardial fat accumulation in humans,[23] independently of obesity or diabetes. However, we did not find any correlation between epicardial fat thickness and left ventricular mass (data not shown), supporting the hypothesis of an effect of PCSK9 on epicardial adipose tissue inflammation largely related to heart failure with reduced ejection fraction.[35] Future studies in larger cohorts should address whether PCSK9 loss-of-function variants are associated with an altered cardiac phenotype independently of the lower cardiovascular risk provided by the long-life reduction in LDL-cholesterol levels observed under these circumstances. We have to acknowledge that we profiled heart function in full *Pcsk9* KO mice and in liver selective PCSK9 KO models. While our findings excluded a role for circulating PCSK9 on the phenotype observed, a final confirmation for a selective role for PCSK9 in the heart should be determined in heart selective KO models. Similarly, the characterization of *Pcsk9/CD36* DKO will be of help to investigate whether PCSK9 production following cardiac stress might represent a feedback mechanism contributing to maintain a proper balance between heart lipid uptake and lipid accumulation, thus limiting potential side effects of heart lipotoxicity.

Supplementary material

Supplementary material is available at *European Heart Journal* online.

Acknowledgments

Part of this work was carried out at NOLIMITS, an advanced imaging facility established by the Università degli Studi di Milano. We would thank Dr Vincenzo Conte and Dr Elena Vezzoli (Electron Microscopy Laboratory, Department of Biomedical Sciences for Health) for their technical help in electron microscopy work. Proteomics part of this work was performed at Unitech OMICs platform of the Università degli Studi di Milano. For their help in processing MS samples, we would like to thank Dr Fiorenza Faré, Dr Giulia Garrone, and Prof. Giangiacomo Beretta. The Genotype–Tissue Expression (GTEx) portal was used to evaluate PCSK9 expression in RNA-seq level within multiple tissues (http://www.gtexportal.org/home/gene/PCSK9).

Funding

The work of the authors is supported by Fondazione Cariplo 2016-0852 (G.D.N.) and 2019-1560 (F.B.); Telethon Foundation (GGP19146) (G.D.N.); WI218287 Cardiovascular Grant, PCSK9 Competitive Grant Program (PCSK9006) (G.D.N.); European Foundation for the Study of Diabetes (EFSD)/Lilly European Diabetes Research Programme (G.D.N.);

Progetti di Rilevante Interesse Nazionale PRIN 2017 K55HLC (G.D.N.) and PRIN 2017 H5F943 (A.L.C.); "Cibo, Microbiota, Salute", "Vini di Batasiolo S.p.A", "Accademia di Medicina di Torino" AL_RIC19ABARA_01, The Peanut Institute Foundation "Research Award 2021" (A.B.); and "Post-Doctoral Fellowship 2020" by "Fondazione Umberto Veronesi" 2020-3318 (A.B.), 2021-4442 (F.B.). Department of excellence of Pharmacological and Biomolecular Sciences, Universita degli Studi di Milano (L.D.D.).

Conflict of interest: The authors have received research funding and/or honoraria for advisory boards, consultancy or speaker bureau from Aegerion (A.L.C.), Alnylam (G.D.N.), Amgen (A.L.C., G.D.N) AstraZeneca (A.L.C.), Eli Lilly (A.L.C.), Kowa (A.L.C.), Mediolanum (A.L.C.), Menarini (A.L.C.), Merck or MSD (A.L.C.), Novartis (G.D.N.), Pfizer (A.L.C., G.D.N.), Recordati (A.L.C.), Sanofi (A.L.C., G.D.N.), and Regeneron (A.L.C.). All other authors declared no conflict of interest.

References

1. Stanley WC, Recchia FA, Lopaschuk GD. Myocardial substrate metabolism in the normal and failing heart. *Physiol Rev* 2005;**85**:1093–1129.
2. Pulinilkunnil T, Rodrigues B. Cardiac lipoprotein lipase: metabolic basis for diabetic heart disease. *Cardiovasc Res* 2006;**69**:329–340.
3. van der Vusse GJ, van Bilsen M, Glatz JF. Cardiac fatty acid uptake and transport in health and disease. *Cardiovasc Res* 2000;**45**:279–293.
4. Bharadwaj KG, Hiyama Y, Hu Y, Huggins LA, Ramakrishnan R, Abumrad NA, Shulman GI, Blaner WS, Goldberg IJ. Chylomicron- and VLDL-derived lipids enter the heart through different pathways: in vivo evidence for receptor- and non-receptor-mediated fatty acid uptake. *J Biol Chem* 2010;**285**:37976–37986.
5. Goldberg IJ, Trent CM, Schulze PC. Lipid metabolism and toxicity in the heart. *Cell Metab* 2012;**15**:805–812.
6. Sharma S, Adrogue JV, Golfman L, Uray I, Lemm J, Youker K, Noon GP, Frazier OH, Taegtmeyer H. Intramyocardial lipid accumulation in the failing human heart resembles the lipotoxic rat heart. *FASEB J* 2004;**18**:1692–1700.
7. Tuunanen H, Ukkonen H, Knuuti J. Myocardial fatty acid metabolism and cardiac performance in heart failure. *Curr Cardiol Rep* 2008;**10**:142–148.
8. Dei Cas A, Khan SS, Butler J, Mentz RJ, Bonow RO, Avogaro A, Tschoepe D, Doehner W, Greene SJ, Senni M, Gheorghiade M, Fonarow GC. Impact of diabetes on epidemiology, treatment, and outcomes of patients with heart failure. *JACC Heart Fail* 2015;**3**:136–145.
9. Haemmerle G, Moustafa T, Woelkart G, Büttner S, Schmidt A, van de Weijer T, Hesselink M, Jaeger D, Kienesberger PC, Zierler K, Schreiber R, Eichmann T, Kolb D, Kotzbeck P, Schweiger M, Kumari M, Eder S, Schoiswohl G, Wongsiriroj N, Pollak NM, Radner FP, Preiss-Landl K, Kolbe T, Rülicke T, Pieske B, Trauner M, Lass A, Zimmermann R, Hoefler G, Cinti S, Kershaw EE, Schrauwen P, Madeo F, Mayer B, Zechner R. ATGL-mediated fat catabolism regulates cardiac mitochondrial function via PPAR-α and PGC-1. *Nat Med* 2011;**17**:1076–1085.
10. Son NH, Yu S, Tuinei J, Arai K, Hamai H, Homma S, Shulman GI, Abel ED, Goldberg IJ. PPARγ-induced cardiolipotoxicity in mice is ameliorated by PPARα deficiency despite increases in fatty acid oxidation. *J Clin Invest* 2010;**120**:3443–3454.
11. Yagyu H, Chen G, Yokoyama M, Hirata K, Augustus A, Kako Y, Seo T, Hu Y, Lutz EP, Merkel M, Bensadoun A, Homma S, Goldberg IJ. Lipoprotein lipase (LpL) on the surface of cardiomyocytes increases lipid uptake and produces a cardiomyopathy. *J Clin Invest* 2003;**111**:419–426.
12. Perman JC, Boström P, Lindbom M, Lidberg U, StÅhlman M, Hägg D, Lindskog H, Scharin Täng M, Omerovic E, Mattsson Hultén L, Jeppsson A, Petursson P, Herlitz J, Olivecrona G, Strickland DK, Ekroos K, Olofsson SO, Borén J. The VLDL receptor promotes lipotoxicity and increases mortality in mice following an acute myocardial infarction. *J Clin Invest* 2011;**121**:2625–2640.
13. Norata GD, Tavori H, Pirillo A, Fazio S, Catapano AL. Biology of proprotein convertase subtilisin kexin 9: beyond low-density lipoprotein cholesterol lowering. *Cardiovasc Res* 2016;**112**:429–442.
14. Seidah NG, Awan Z, Chrétien M, Mbikay M. PCSK9: a key modulator of cardiovascular health. *Circ Res* 2014;**114**:1022–1036.
15. Takahashi S, Sakai J, Fujino T, Hattori H, Zenimaru Y, Suzuki J, Miyamori I, Yamamoto TT. The very low-density lipoprotein (VLDL) receptor: characterization and functions as a peripheral lipoprotein receptor. *J Atheroscler Thromb* 2004;**11**:200–208.
16. Poirier S, Mayer G, Benjannet S, Bergeron E, Marcinkiewicz J, Nassoury N, Mayer H, Nimpf J, Prat A, Seidah NG. The proprotein convertase PCSK9 induces the degradation of low density lipoprotein receptor (LDLR) and its closest family members VLDLR and ApoER2. *J Biol Chem* 2008;**283**:2363–2372.
17. Canuel M, Sun X, Asselin MC, Paramithiotis E, Prat A, Seidah NG. Proprotein convertase subtilisin/kexin type 9 (PCSK9) can mediate degradation of the low density lipoprotein receptor-related protein 1 (LRP-1). *PLoS One* 2013;**8**:e64145.
18. Demers A, Samami S, Lauzier B, Des Rosiers C, Ngo Sock ET, Ong H, Mayer G. PCSK9 induces CD36 degradation and affects long-chain fatty acid uptake and triglyceride metabolism in adipocytes and in mouse liver. *Arterioscler Thromb Vasc Biol* 2015;**35**:2517–2525.
19. Perego C, Da Dalt L, Pirillo A, Galli A, Catapano AL, Norata GD. Cholesterol metabolism, pancreatic β-cell function and diabetes. *Biochim Biophys Acta Mol Basis Dis* 2019;**1865**:2149–2156.
20. Da Dalt L, Ruscica M, Bonacina F, Balzarotti G, Dhyani A, Di Cairano E, Baragetti A, Arnaboldi L, De Metrio S, Pellegatta F, Grigore L, Botta M, Macchi C, Uboldi P, Perego C, Catapano AL, Norata GD. PCSK9 deficiency reduces insulin secretion and promotes glucose intolerance: the role of the low-density lipoprotein receptor. *Eur Heart J* 2019;**40**:357–368.
21. Lotta LA, Sharp SJ, Burgess S, Perry JRB, Stewart ID, Willems SM, Luan J, Ardanaz E, Arriola L, Balkau B, Boeing H, Deloukas P, Forouhi NG, Franks PW, Grioni S, Kaaks R, Key TJ, Navarro C, Nilsson PM, Overvad K, Palli D, Panico S, Quirós J-R, Riboli E, Rolandsson O, Sacerdote C, Salamanca-Fernandez E, Slimani N, Spijkerman AMW, Tjonneland A, Tumino R, van der A DL, van der Schouw YT, McCarthy MI, Barroso I, O'Rahilly S, Savage DB, Sattar N, Langenberg C, Scott RA, Wareham NJ. Association between low-density lipoprotein cholesterol-lowering genetic variants and risk of type 2 diabetes: a meta-analysis. *JAMA* 2016; **316**:1383–1391.
22. Ference BA, Robinson JG, Brook RD, Catapano AL, Chapman MJ, Neff DR, Voros S, Giugliano RP, Davey Smith G, Fazio S, Sabatine MS. Variation in PCSK9 and HMGCR and risk of cardiovascular disease and diabetes. *N Engl J Med* 2016;**375**:2144–2153.
23. Baragetti A, Balzarotti G, Grigore L, Pellegatta F, Guerrini U, Pisano G, Fracanzani AL, Fargion S, Norata GD, Catapano AL. PCSK9 deficiency results in increased ectopic fat accumulation in experimental models and in humans. *Eur J Prev Cardiol* 2017;**24**:1870–1877.
24. Doenst T, Nguyen TD, Abel ED. Cardiac metabolism in heart failure: implications beyond ATP production. *Circ Res* 2013;**113**:709–724.
25. Rodeheffer RJ. Hypertension and heart failure: the ALLHAT imperative. *Circulation* 2011;**124**:1803–1805.
26. Alpert MA, Lavie CJ, Agrawal H, Aggarwal KB, Kumar SA. Obesity and heart failure: epidemiology, pathophysiology, clinical manifestations, and management. *Transl Res* 2014;**164**:345–356.
27. Kenny HC, Abel ED. Heart failure in type 2 diabetes mellitUs. *Circ Res* 2019;**124**:121–141.
28. Schulze PC, Drosatos K, Goldberg IJ. Lipid use and misuse by the heart. *Circ Res* 2016;**118**:1736–1751.
29. Santos RD, Stein EA, Hovingh GK, Blom DJ, Soran H, Watts GF, López JAG, Bray S, Kurtz CE, Hamer AW, Raal FJ. Long-term evolocumab in patients with familial hypercholesterolemia. *J Am Coll Cardiol* 2020; **75**:565–574.
30. Catapano AL, Pirillo A, Norata GD. New pharmacological approaches to target PCSK9. *Curr Atheroscler Rep* 2020; **22**:24.
31. Seidah NG, Prat A, Pirillo A, Catapano AL, Norata GD. Novel strategies to target proprotein convertase subtilisin kexin 9: beyond monoclonal antibodies. *Cardiovasc Res* 2019;**115**:510–518.
32. Ding Z, Wang X, Liu S, Shahanawaz J, Theus S, Fan Y, Deng X, Zhou S, Mehta JL. PCSK9 expression in the ischaemic heart and its relationship to infarct size, cardiac function, and development of autophagy. *Cardiovasc Res* 2018;**114**:1738–1751.
33. Wolf A, Kutsche HS, Schreckenberg R, Weber M, Li L, Rohrbach S, Schulz R, Schlüter KD. Autocrine effects of PCSK9 on cardiomyocytes. *Basic Res Cardiol* 2020; **115**:1093–1129.
34. Dozio E, Ruscica M, Vianello E, Macchi C, Sitzia C, Schmitz G, Tacchini L, Corsi Romanelli MM. PCSK9 expression in epicardial adipose tissue: molecular association with local tissue inflammation. *Mediators Inflamm* 2020;**2020**:1348913.
35. Packer M. Epicardial adipose tissue may mediate deleterious effects of obesity and inflammation on the myocardium. *J. Am. Coll. Cardiol* 2018; **71**:2360–2372.

APPENDIX 4

Journal of Molecular and Cellular Cardiology 157 (2021) 104–112

Contents lists available at ScienceDirect

Journal of Molecular and Cellular Cardiology

journal homepage: www.elsevier.com/locate/yjmcc

Dual role of miR-1 in the development and function of sinoatrial cells

P. Benzoni, L. Nava [1], F. Giannetti, G. Guerini, A. Gualdoni, C. Bazzini, R. Milanesi [2], A. Bucchi, M. Baruscotti, A. Barbuti [*]

The Cell Physiology MiLAb; Department of Biosciences, Università degli Studi di Milano, Milan, Italy

ARTICLE INFO

Keywords:
microRNA
miR-1
Sinus node
Embryonic stem cells
I_f current
HCN4

ABSTRACT

miR-1, the most abundant miRNA in the heart, modulates expression of several transcription factors and ion channels. Conditions affecting the heart rate, such as endurance training and cardiac diseases, show a concomitant miR-1 up- or down-regulation. Here, we investigated the role of miR-1 overexpression in the development and function of sinoatrial (SAN) cells using murine embryonic stem cells (mESC).

We generated mESCs either overexpressing miR-1 and EGFP (miR1OE) or EGFP only (EM). SAN-like cells were selected from differentiating mESC using the CD166 marker. Gene expression and electrophysiological analysis were carried out on both early mES-derived cardiac progenitors and SAN-like cells and on beating neonatal rat ventricular cardiomyocytes (NRVC) over-expressing miR-1.

miR1OE cells increased significantly the proportion of $CD166^+$ SAN precursors compared to EM cells (23% *vs* 12%) and the levels of the transcription factors TBX5 and TBX18, both involved in SAN development. miR1OE SAN-like cells were bradycardic (1,3 *vs* 2 Hz) compared to EM cells. In agreement with data on native SAN cells, EM SAN-like cardiomyocytes show two populations of cells expressing either slow- or fast-activating I_f currents; miR1OE SAN-like cells instead have only fast-activating I_f with a significantly reduced conductance. Western Blot and immunofluorescence analysis showed a reduced HCN4 signal in miR-1OE *vs* EM CD166+ precursors. Together these data point out to a specific down-regulation of the slow-activating HCN4 subunit by miR-1. Importantly, the rate and I_f alterations were independent of the developmental effects of miR-1, being similar in NRVC transiently overexpressing miR-1.

In conclusion, we demonstrated a dual role of miR-1, during development it controls the proper development of sinoatrial-precursor, while in mature SAN-like cells it modulates the HCN4 pacemaker channel translation and thus the beating rate.

1. Introduction

Heart development is a complex process that requires a precise temporal and spatial control of expression levels of many genes. This regulation involves microRNAs for modulating protein expression. Among the many miRNAs expressed during heart development, miR-1 is the most abundant in human and mouse heart [1]. miR-1 starts to be expressed in the mouse around E8.5 of development and its expression strongly increases after birth [2]. miR-1 derives from two transcripts (miR-1-1 and miR-1-2) with identical sequences, whose expression was reported both during cardiogenesis, in a chamber specific manner [3], and during mouse embryonic stem cell (mESC) differentiation, promoting mesoderm and cardiac formation [2]. Deletion of either miR-1-1 or miR-1-2 results in an analogue phenotype in mice: incompletely penetrant lethality, cardiomyocytes proliferative defects, and electrophysiological abnormalities; while the double knock-out is lethal before *E11.5* [4]. On the other hand, over-expression of miR-1 during heart development results in defective ventricular myocytes proliferation and causes hypoplasia of the cardiac ventricular conduction system [5,6]. So far, nothing is known regarding the specific effect of miR-1 on the development of sinoatrial (SAN) cardiomyocytes.

In the adult heart, miR-1 epigenetically modulates the expression of ion channels, connexins and regulatory proteins [7]. This regulation has an important role in the cardiac remodeling due to both pathological conditions, such as arrhythmic diseases (e.g. atrial fibrillation) [8], and physiological conditions, such as cardiac hypertrophy and bradycardia

* Corresponding author: Department of Biosciences, The Cell Physiology MiLAb, Università degli Studi di Milano, via Celoria 26, Milano 20133, Italy.
E-mail address: andrea.barbuti@unimi.it (A. Barbuti).
[1] Current address: Neuromodulation of Cortical and Subcortical Circuits Laboratory, Istituto Italiano di Tecnologia, Genova, Italy.
[2] Current address: Dipartimento di Medicina Veterinaria, Università degli Studi di Milano, Via dell'Università 6, 26900 Lodi, Italy.

https://doi.org/10.1016/j.yjmcc.2021.05.001
Received 7 September 2020; Received in revised form 27 April 2021; Accepted 3 May 2021
Available online 6 May 2021

following endurance training [9–11].

Here, we applied our previously published model of SAN-like cells derived from mESC [12], to specifically investigate and dissect the role of miR-1 in the development and function of the cardiac pacemaker.

2. Material and methods

2.1. mESC engineering and maintenance

Mouse ESCs (D3 line, ATCC-CRL11632) were grown and differentiated as embryoid bodies (EBs) as previously described [13].

To obtain mESC overexpressing miR-1 (miR1OE), downregulating miR-1 (ANTI-miR1) and the empty control line (EM), 2×10^6 cells were electroporated with 10 μg of linearized pEZX-MR04 plasmid or pEZX-AM02 plasmid (GeneCopoeia™) or empty vector (CmiR0001-MR04-GeneCopoeia™) using the A024 program of the Nucleofactor® II (Amaxa Byosystems) and the mESC Nucleofector kit (Lonza). Cells were then kept in stringent selection with 1 μg/mL puromycin for 2 weeks. The effect of puromycin selection was checked on non-electroporated mESC, which all died after 24–48 h in puromycin. After selection, single mESC colonies transfected with siRNA silencing miR-1 were manually picked using mCherry to clone only cells where the plasmid was properly integrated, while single mESC colonies transfected with miR-1 were sorted using the FACSAriaII flow-cytometer (BD Biosciences) by eGFP expression. This eGFP-based sorting procedure was repeated every 60–90 days on both EM and miR1OE mESC.

2.2. San-like CD166+ cell isolation and maintenance

EBs were detached from the plate at d8 of differentiation and dissociated to single cells for CD166-staining, as previously described [12]. Briefly, cells were incubated with the PE-conjugated rat anti-mouse CD166 antibody (eBioscience) or the corresponding isotype (PE-rat IgG) for 30 min at 4 °C under constant shaking. At the end of the incubation cells were washed and resuspended in PBS with the addition of 10% FBS, 1 mM $CaCl_2$ and 5 mmol/L EDTA. $CD166^+$cells were analyzed and sorted by FACSAriaII. $CD166^+$ cells were put to re-aggregate by gravity for 24 h in low-adhesion culture dishes in differentiating medium and subsequently plated at high density (5×10^4 cells/mm^2) to allow the formation of a compact layer, which was kept in culture for one week in differentiating medium supplemented with 2,5 μM ARA-C (Sigma-Aldrich). Molecular and electrophysiological analyses have been performed on the layers or on single cells following dissociation.

2.3. Proliferation analysis

EBs were collected from the plate at d6 of differentiation and dissociated to single cells using TryplE (Thermo-Fisher). Single cells suspension was fixed in cold ethanol at 70% for 1 h at −20 °C. Cells were incubated with the APC-conjugated anti-mouse Ki-67 antibody (Biolegend) or the corresponding isotype (APC-rat IgG) for 30 min at room temperature under constant shaking. At the end of the incubation cells were washed and resuspended in PBS with the addition of 10% FBS, 1 mM $CaCl_2$ and 5 mmol/L EDTA. Ki-67+ cells were analyzed by FACSAriaII.

2.4. Molecular analysis

Total mRNA was isolated using TRIzol (Thermo Fisher). Maxima First Strand cDNA synthesis kit (Thermo Fisher) was used to synthesize cDNA, while miRNAs were selected using miScript II RT Kit (Quiagen) following the manufacturer's instructions.

qRT-PCRs were performed in technical duplicate or triplicate using 10 ng cDNA with Maxima SYBR Green qPCR Master Mix (Thermo Fisher), or 2.5 ng miRNAs with miScript SYBR Green PCR Kit (Quiagen) in iCycler Bioer System (BIOER). Expression data were analyzed using 2^(-ΔCT) method relative to expression level of GAPDH as housekeeping gene or miR-16 as miRNA reference. Primers used are given below. qRT-PCR analysis was performed on differentiating cultures of at least 4 independent experiments.

OCT4 F:CTCCTTCTGCAGGGCTT R:GTTGGAGAAGGTGGAAAC

REX1 F:GGGCACTGATCCGCAAAC R:CAGCAGCTCCTGCACAC AGA

BRACHYURY-T F:GAAGAGCCTGCAGTACCGAG R:ACATCCTCC TGCCGTTCTTG

NODAL F:TACATCCAGAGCGTGCTGAAAC R:ACCCACACTCCTC CACAATC

GATA-4 F:GGAAGACACCCCAATCTCG R:CATGGCCCCACAATT GAC

NKX2.5 F:TTAGGAGAAGGGCGATGACT R:AGGTCCGAGACACC AGGCTA

SHOX2 F:GAAAGGACAAGGGCGTCA R:AACGTAGGTGCTTTAA GGATGC

TBX3 F:AGGAGCGTGTCTGTCAGGTT R: GCCATTACCTCCCCAA TTTT

TBX5 F:GGATGTCCTGGATGCAAAGT R:GGTTGGAGGTGACTTT GTGC

TBX18 F:TGATGGCCTCCAGAATGC R:CCGAGACTCTGGGAGG AAC

ISL1 F: CATCGAGTGTTTCCGCTGTGTAG R: GTGGTCTTCTCC GGCTGCTTGTGG

HCN1 F:CTCAGTCTCTTGCGGTTATTACG R:TGGCGAGGTCATA GGTCAT

HCN2 F:CCGCTGTTTGCCAATGC R:AGGCTGGAAGACCTCAAAT TTG

HCN4 F:GTCGGGTGTCAGGCGGGA R:GTGGGGGCCACCTGC TAT

CACNA1D F: GTTGTAAGTGCGGTAGAAAGCA R: CTGGTGCCTC TTGCATAGTTT

GJA1 F: GAACACGGCAAGGTGAAGAT R: GAGCGAGAGACACC AAGGAC

KCND2 F: TGGGCTACTGAGCAACCAG R: TGGATCCAGATTT GCTTATGAA

GAPDH F:TGTAGACCATGTAGTTGAGGTCA R:AGGTCGGTGTG AACGGATTTG

mmu -miR-1a-1-3p TGGAATGTAAAGAAGTATGTAT

mmu-miR-16-5P TAGCAGCACGTAAATTATTGGCG

2.5. Immunofluorescence and western blot analysis

MiR1OE and EM $CD166^+$ cells sorted by FACSAriaII at d8 of differentiation were solubilized in RIPA buffer. Western blot analyses were carried out loading 30 μg of whole cell protein extracts, separated by SDS-PAGE and transferred onto PVDF membranes. Antibodies used were anti-HCN1, anti HCN4 and anti-TNNT (1:1000; all from Thermo Fisher), and appropriate secondary antibodies HRP (Jackson ImmunoResearch, 1:10000). For chemiluminescent acquisition Chemidoc system (Bio-RAD) was used after membranes incubation with SuperSignal™ West Pico PLUS Chemiluminescent Substrate (Thermo Fisher).

SAN-like monolayers at d14 were fixed in paraformaldehyde (4%). Blocking and staining procedure was performed in PBS with 0.3% Triton X-100 (Sigma-Aldrich) and 3% Donkey serum, using the anti-HCN4 antibody (1:200, Alomone Labs). Nuclei were stained with 0,5 μg/mL DAPI. A Video Confocal Microscope (ViCo, Nikon) was used to acquire images. Corrected total cell fluorescence (CTCF) was analyzed by ImageJ software as Integrated density (area of ROI X mean fluorescence of background). Four different ROI and background readings were analyzed for each image and data averaged.

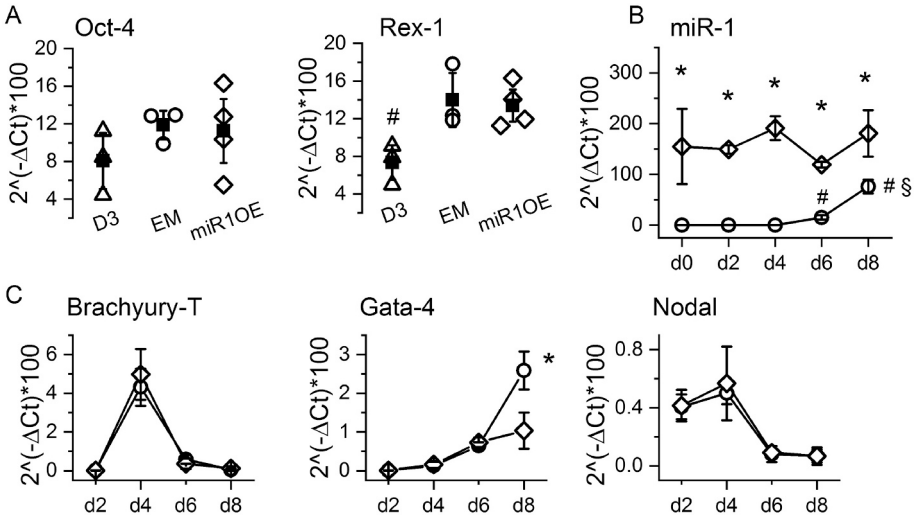

Fig. 1. miR-1 overexpression in mES neither alters pluripotency nor differentiation capacity.
(A) qRT-PCR analysis of the pluripotency genes Oct-4 and Rex-1 in the mES parental line D3 (triangles) and in the engineered mES lines EM (circles) and miR1OE (diamonds). Mean ± SEM values are reported overlapped as filled squares. GAPDH has been used as reference gene. (B) qRT-PCR analysis of miR-1 expression in the engineered miR1OE (diamonds) and EM (circles) mESC lines, from d0 to d8 of differentiation; miR-16 has been used as housekeeping miRNA. (C) qRT-PCR analysis of three early germ layer markers in mES lines EM (circles) and miR1OE (diamonds), from d0 to d8 of differentiation. Brachyury-T for early mesoderm, GATA-4 for early endoderm and Nodal for early ectoderm. GAPDH has been used as reference gene. *Indicates $p < 0.05$ by Student's *t*-test; #Indicates $p < 0.05$ by One-Way Anova vs d0,2,4; §$p < 0.05$ vs day6.

2.6. Neonatal rat ventricular cardiomyocytes (NRVC) transfection

All animal procedures were in accordance with the Italian and UE laws (D. Lgs n° 2014/26, 2010/63/UE) and approved by the committee of the Università degli Studi di Milano and by the Italian Minister of Health (protocol number 1197/2015).

NRVC were isolated from 3 days-old rat pups (Sprague Dawley, Envigo S.R.L.) as previously described [14]. Cardiomyocytes plated on 35 mm dishes were transiently transfected with the same pEZX-MR04 and empty plasmid CmiR0001-MR04, one day after isolation by Lipofectamine 2000 (Life Technologies) following manufacturer's instruction.

2.7. Electrophysiological analysis

Patch-clamp experiments in the whole-cell configuration were carried out on isolated SAN-like cells at day14 seeded on fibronectin (5 μg/cm^2) and on eGFP-NRVCs 30–36 h after transfection. Cells were superfused with Tyrode solution containing (mmol/L): 140 NaCl, 5.4 KCl, 1.8 $CaCl_2$, 1 $MgCl_2$, 10 D-glucose, 5 Hepes-NaOH; pH 7.4. Patch-clamp pipettes had a resistance of 5–7 MΩ when filled with the intracellular-like solution containing (mmol/L): 130 KCl, 10 NaCl, 1 EGTA-KOH, 0.5 $MgCl_2$, 2 ATP (Na-salt), 5 creatine phosphate, 0.1 GTP, 5 Hepes-KOH; pH 7.2. Tyrode was supplemented with 1 mM $BaCl_2$ and 2 mM $MnCl_2$ in order to dissect the funny current (I_f). I_f was activated from a holding potential (hp) of −30 mV applying 10 mV hyperpolarizing voltage steps to the range −35/−125 mV long enough to reach steady-state activation, followed by a fully activating step at −125 mV. Current density was obtained by normalizing current intensity to the cell capacitance. Activation curves were obtained from normalized tail currents at −125 mV and fitted to the Boltzmann equation to obtain the potential at which half of the channels are open ($V_{1/2}$) and the inverse slope factor s. The time constant of activation (τ) have been obtained by fitting the first part of the current traces to a mono-exponential function. Action potentials were recorded in the current-clamp mode from either SAN-like layers or from small spontaneously beating clusters of transfected NRVC (3–5 cells); AP parameters were analyzed as previously reported [15]. In SAN-like cells, conductance was obtained from the linear fit of the I-V data points where current was ohmic; for NRVC conductance was calculated as I/(E-Erev) with E −125 mV and Erev −15 mV. Response of I_f to adrenergic stimulation was evaluated as the shift in the $V_{1/2}$ after superfusing cells with 1 μM isoproterenol dissolved in the extracellular solution. All measures were performed at 36 ± 1 °C.

2.8. Statistical analysis

Statistical analysis was carried out using Origin Pro 9. Groups were compared using One-way ANOVA followed by pairwise comparison using Fisher's test. Student's *t*-test was used to compare two independent populations. For data not normally distributed, we performed a Kolmogorov's Test to compare the population distribution. $P < 0.05$ defines statistical significance. Data are presented as mean ± SEM or median. N indicates the number of experiments, n indicates the number of cells analyzed.

3. Results

3.1. Engineered mESC lines maintain pluripotency and cardiac differentiation potential.

In order to study the effects of miR-1 overexpression on pacemaker cells, we decided to generate stable lines of mESC (D3) expressing miR-1 and EGFP (miR1OE) under the control of a strong constitutive promoter (CMV) or the corresponding empty vector (EM) expressing EGFP only. Plasmids integration was favored by stringent puromycin selection (1 μg/mL) for two weeks. After this, we further selected EGFP-positive cells using a cells sorter (Supplementary Fig. S1).

We first evaluated whether the overexpression of miR-1 and/or EGFP could alter the pluripotency of the engineered cell lines. In Fig. 1A, we reported the expression levels of the pluripotency genes Oct4 and Rex1. Pluripotency markers were equally expressed in miR1OE and EM lines and both lines displayed a significant similar up-regulation of Rex1 compared to the parental D3 line.

We then checked the differentiation potential of these lines through embryoid bodies (EBs) formation. During differentiation from d0 to d8, we analyzed the expression of miR-1 and of Brachyury-T, Gata-4 and Nodal genes, markers of early mesoderm, endoderm and ectoderm, respectively [16]. Fig. 1B, shows the time-course of miR-1 expression in the EBs generated from both engineered lines. As expected, miR-1 is almost not expressed at early days (d0 to d4) in EM EBs and its level increases significantly between d6 and d8. miR-1 levels are constantly high in miR1OE EBs, as expected following overexpression induced by the CMV promoter. Nevertheless, miR1OE line differentiate properly and indeed the early markers of mesoderm, endoderm and ectoderm showed similar time-courses with the exception of GATA4 at d8, whose level was significantly lower in miR1OE than in EM, according to a possible role of miR-1 in the inhibition of endoderm [2].

In order to evaluate the cardiac differentiation potential of the engineered mESC lines, we monitored the percentage of EBs showing

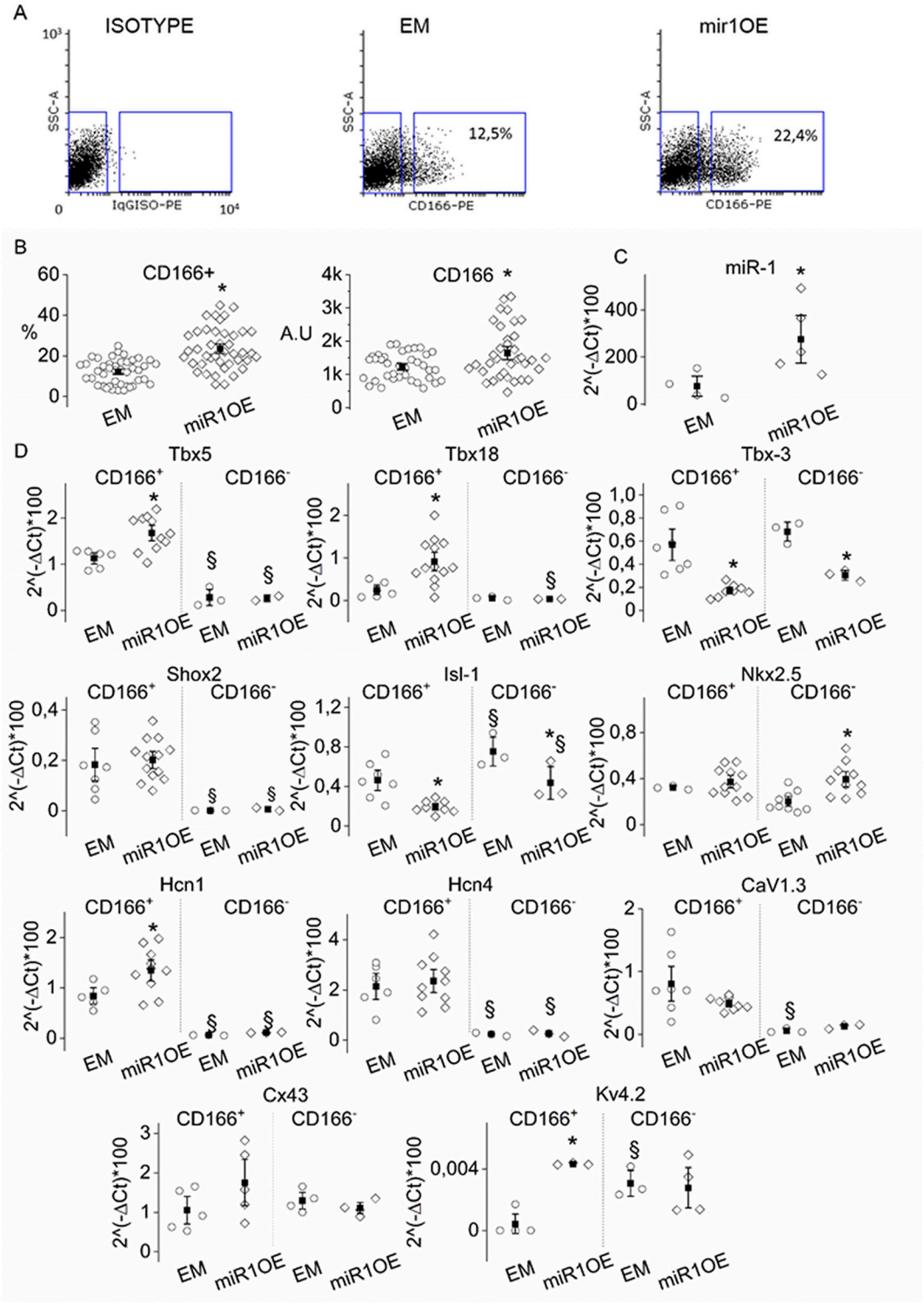

Fig. 2. The miR1OE line generates more CD166$^+$ SAN-like precursors and express higher levels of SAN markers.
(A) Representative dot plots showing the percentage of CD166$^+$ cells at d8 of differentiation in the engineered lines miR1OE and EM; left panel shows the isotype control. (B) left panel: dot plot of the percentage of CD166$^+$ cells at d8 in the engineered miR1OE (diamonds) and EM lines(circles); right panel: plot of the mean fluorescence intensity of CD166 staining in miR1OE (diamonds) and EM (circles) lines. Mean ± SEM values of % and mean fluorescence intensity, reported as filled squares, were: EM CD166$^+$ 12.2 ± 0.9% and 1230.8 ± 65.9 (N = 43); miR-1-OE CD166$^+$ 23.5 ± 1.6% and 1643.4 ± 132 (N = 42). (C) qRT-PCR expression levels of miR-1 in sorted CD166$^+$ cells at d8. (D) qRT-PCR analysis of transcription factors (Tbx3, Tbx5, Tbx18, Shox2, Isl1, Nx2.5), calcium channel Cav1.3 and HCN channel isoforms, connexin 43 and potassium channel Kv4.2 in miR1OE and EM CD166 positive and negative populations at d8. Mean values are reported as filled squares. miR-16 and GAPDH have been used as endogenous reference. *Indicates $p < 0.05$ by Student's *t*-test between miR1OE and EM, while §Indicates $p < 0.05$ by Student's *t*-test between positive and negative populations.

spontaneous contractions. EBs of both lines started to show beating foci around d6–7 and the proportion of beating EBs at d8, was equal: 85.2 ± 5.4% (EM, n = 334, N = 8), 87.6 ± 3.2% (miR1OE, n = 298, N = 8).

In parallel, we generated a mESC line constitutively expressing a siRNA specifically silencing miR-1 and the mCherry reporter (ANTI-miR1). The ANTI-miR1 line expressed the pluripotency markers Oct-4 and Rex-1 at levels comparable with EM and miR1OE lines (supplementary Fig. S2). ANTI-miR1 EBs at d8 showed absence of miR-1 expression (supplementary Fig. S2) and did not display any spontaneous beating, in agreement with the important role of miR-1 in cardiac differentiation/development.

3.2. *miR-1 overexpression increases CD166$^+$ pacemaker precursors and pacemaker transcription factors.*

To specifically isolate and study SAN development, we selected at d8 cells positive for CD166, a marker known to recognize specifically SAN precursors between d6 and d10 of EBs differentiation [12]. FACS analysis revealed a significantly higher percentage of CD166$^+$ cells in the miR1OE line than in the EM line (Fig. 2A and B left panel). Moreover, the miR1OE CD166$^+$ population had a higher mean fluorescence intensity than the EM CD166$^+$ population (Fig. 2B, right panel), indicating an increased expression of CD166 molecules on the plasma membrane. To evaluate a possible effect of miR-1 on cell proliferation EM and mir1OE cells were stained for Ki67 when miR-1 start to be expressed in EM line (d6); flow cytometry data demonstrated that the two cell lines have a similar proliferative potential (EM: 86.3 ± 1.7%, N = 5; miR-1 OE: 83.2 ± 2.0%, N = 5; Supplementary Fig. S3).

We then characterized sorted CD166$^+$ cells for the expression of miR-1 and of several transcription factors involved either in pacemaker development (Tbx5, Tbx18, Tbx3, Shox2, Isl-1) and function (HCN1, HCN4, Cav1.3) or in working myocardium development (Nkx2.5)and function (Cx43, Kv4.2). MiR1OE CD166$^+$ cells, besides showing a significantly higher levels of miR-1 (Fig. 2C), overexpressed also Tbx5 and Tbx18, while Shox2 did not change compared to EM CD166$^+$ cells (Fig. 2D) No differences in CD166$^-$ cells were observed. Tbx3 and Isl-1, both of which participate to SAN development, resulted significantly decreased both in CD166+ and CD166$^-$ miROE cells, pointing to a direct regulation of these factors by miR-1. Nkx2.5 expression did not vary in CD166$^+$ SAN precursor but was instead increased in miR1OE CD166$^-$ cells, confirming a previously reported role of miR-1 in the early phases of working cardiomyocytes development [2].

We also evaluated the expression levels of HCN1, HCN4 and CaV1.3, functional markers of sinus node and of Cx43 and KV4.2 ventricular genes expressed at low levels in SAN cells. [17]. We found HCN1 upregulated in miR1OE CD166$^+$ cells while HCN4, known to interact with miR-1, and Cav1.3 were not modulated. As expected, these three genes were similarly expressed at low levels in CD166$^-$ miR1OE and EM cells (Fig. 2D). We specifically evaluated HCN1 and HCN4 expression also at the protein level; the WB analysis shown in supplementary Fig. S3 clearly demonstrates a significant downregulation only of HCN4 in miR1OE CD166$^+$ cells at d8. Cx43 was not altered neither in CD166$^+$ nor in CD166$^-$ miR1OE cells. KV4.2 was upregulated at d8 but not at d14 (Supplementary Fig. S4C) in miR1OE CD166$^+$, in agreement with previous data [12].

These results support the idea that miR-1 is not only involved in the mesoderm and cardiac differentiation but plays a specific role in sinus node formation.

3.3. *miR1OE SAN-like cells are bradycardic and show altered I_f current.*

CD166$^+$ cells were maintained in culture as monolayers, until d14, for allowing proper maturation into fully competent sinoatrial-like (SAN-like) cells [12]. At this time point, miR-1 was still significantly overexpressed in miR1OE cells (Supplementary Fig. S4A). The functional effect of miR-1 was then assessed on SAN-like cells by patch-clamp analysis. miR1OE SAN-like aggregates had a slower spontaneous rate than EM aggregates (Fig. 3A). The slower rate of miR1OE cells derived from a significantly slower diastolic depolarization (DD) without any change in either take-off potential (TOP) or any other action potential parameter (MDP, APA, APD) (Fig. 3B).

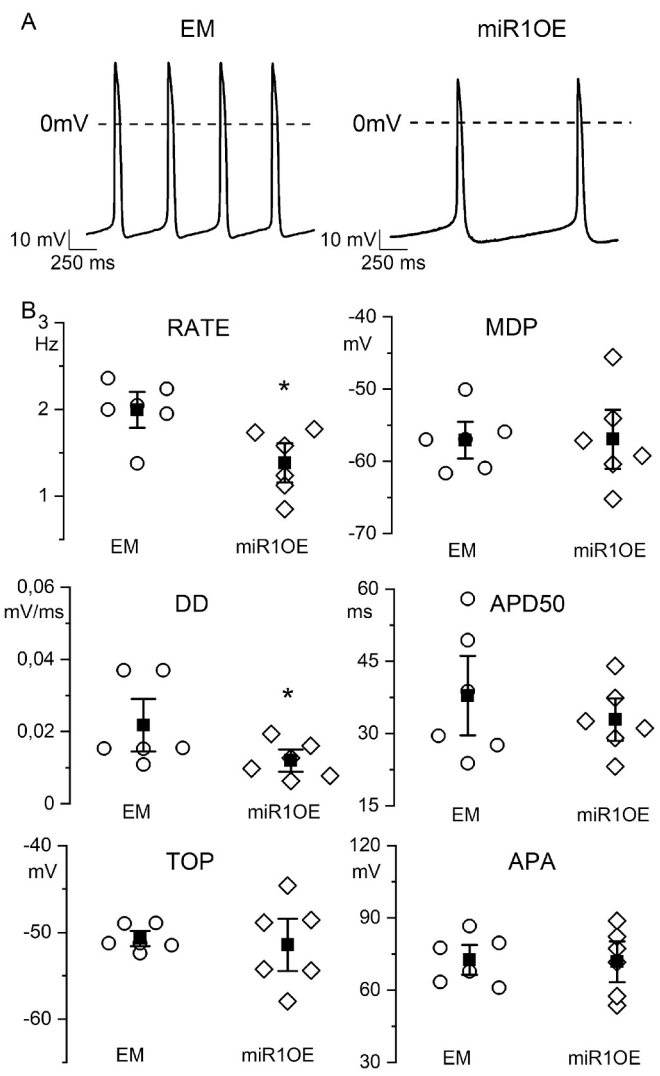

Fig. 3. miR1OE SAN-like cells at d14 shows decreased spontaneous firing rate. (A) Representative spontaneous action potential traces recorded from EM and miR1OE CD166$^+$ clusters, as indicated. (B) Scatter plots of the firing rate, diastolic depolarization (DD) slope, take-off potential (TOP), maximum diastolic potential (MDP), action potential duration at 50% or repolarization (APD50), and action potential amplitude (APA) of miR1OE (diamonds; n = 6, N = 6) and EM SAN-like cells (circles; n = 6, N = 6) at d14. Mean ± SEM values are reported as filled squares. Rate: 1.99 ± 0.14 Hz EM; 1.38 ± 0.15* Hz miR1OE; DD 0.021 ± 0.004 mV/ms EM; 0.012 ± 0.001* mV/ms miR1OE; TOP -51.1 ± 0.5 mV EM; −52.1 ± 1.5 mV miR1OE; APA 72.6 ± 4.1 mV EM, 71.8 ± 5.6 mV miR1OE; APD50: 37.8 ± 5.5 ms EM, 32.9 ± 2.9 ms miR1OE; MDP: −57.1 ± 1.7 mV EM, −56.9 ± 2.7 mV miR1OE. *Indicates $p < 0.05$ by Student's *t*-test.

As previously shown in mouse SAN cells [18] and in mES cell-derived pacemaker cells [13], we found two distinct populations of EM SAN-like cells: one with a fast activating I_f current (time constant $\tau < 1.5$ s at −75 mV) and one with a slow activating I_f ($\tau > 1.5$ s at −75 mV). Left and center panels of Fig. 4A show representative traces while Fig. 4BB depicts the τ plot of fast (empty symbols) and slow (filled symbols) I_f currents. This distinction may derive from the relative contributions of the fast HCN1 and slow HCN4 isoform to I_f, as previously reported [19].

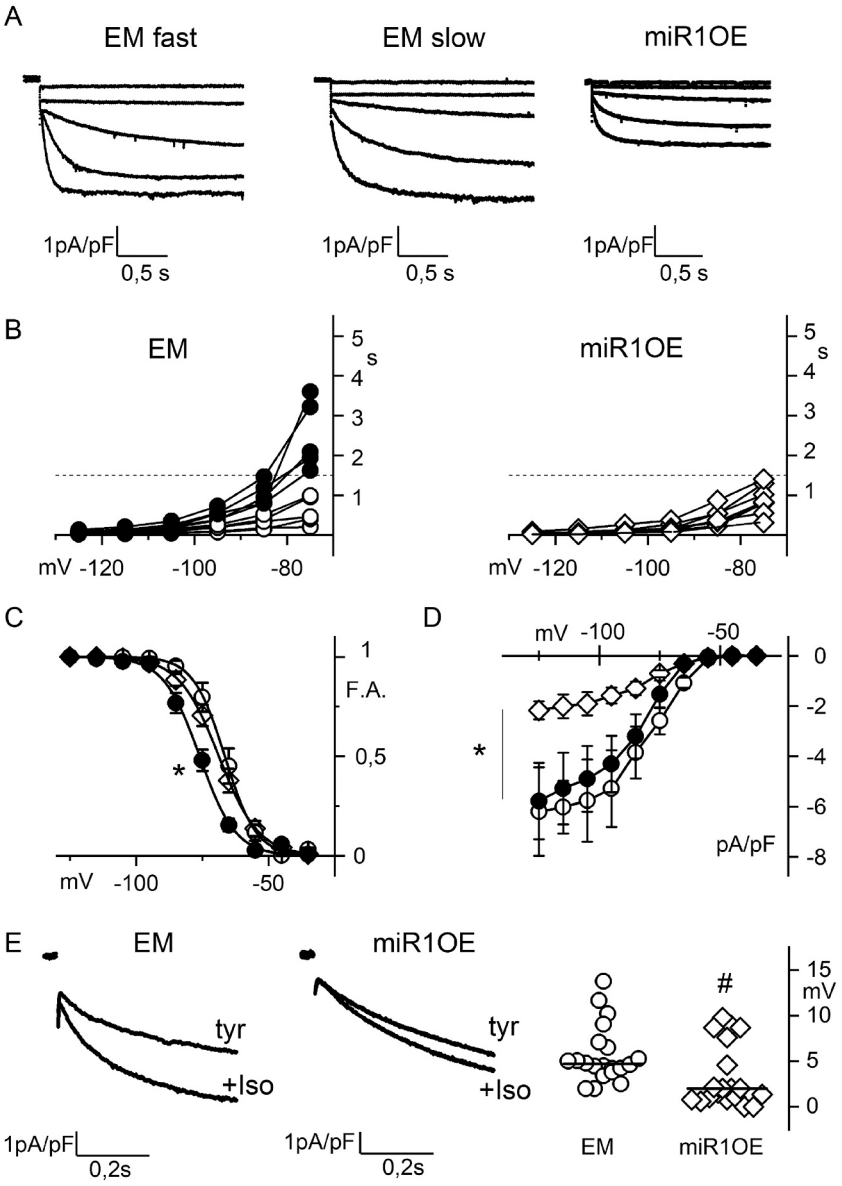

Fig. 4. miR1OE SAN-like cells at d14 display reduced I_f conductance and faster activation kinetics.
(A) Representative traces of I_f current recorded at −35, −55, −75, 95 and −115 mV in EM with fast and slow activation kinetics and in miR1OE SAN-like cells at d14, as indicated. (B) Plots of the activation time constant (τ) of I_f current recorded in EM (circle, left) and in miR1OE (diamonds, right) SAN-like cells. Time constants were arbitrary subdivided into slow (τ > 1.5 s at −75 mV, filled symbol) and fast (τ < 1.5 s at −75 mV, empty symbols). τ mean values were: 2.5 ± 0.3 s EM (n = 6, N = 4) for slow τ; 0.56 ± 0.13 s EM (n = 6, N = 3) and 0.82 ± 0.1 s miR1OE (n = 11, N = 6) for fast τ. (C) Mean activation curves of fast- and slow-activating I_f current in miR1OE and EM SAN-like cells. (Symbols as in B). $V_{1/2}$ and slope values were: −76.2 ± 1.4* mV and 6.5 ± 0.4* mV in EM slow (n = 6, N = 4), −66.7 ± 2.2 mV and 5.2 ± 0.2 mV EM fast (n = 6, N = 3), −68.8 ± 1.7 mV and 6.8 ± 0.7 mV in miR1OE (n = 11, N = 6). (D) Plot of mean I_f current density-voltage relation obtained from miR1OE (diamonds) and EM SAN-like cells (circles). Mean conductance value were: 52.5 ± 13.8 pS/pF (n = 6, N = 4) and 56.4 ± 15.0 pS/pF (n = 6, N = 3) for slow and fast EM, respectively, and 20.2 ± 4.3* pS/pF for fast miR1OE (n = 11, N = 6). (E) left panels: Representative traces of I_f current recorded before (Tyr) and during superfusion of 1 μM isoproterenol (+Iso) at -85 mV in EM and at -75 mV in miR1OE SAN-like cells at d14, as indicated. Right panel: dot plot of the shifts of the I_f activation curve caused by isoproterenol stimulation in EM and miR1OE SAN-like cells. Median is reported as solid line. Median values were:1.75# (n = 20, N = 2) in miR1OE and 4.71 (n = 20, N = 4) in EM SAN-like cells. *Indicates $p < 0.05$ by One-way Anova; #Indicates $p < 0.05$ by Kolmogorov test.

A larger contribution of the positive-activating HCN1 subunit to fast I_f emerged also from the analysis of the mean activation curves; indeed, I_f with fast τ activated at more positive voltages than I_f with slow τ (circles in Fig. 4C). Interestingly, miR1OE SAN-like cells displayed only the fast activating I_f (Fig. 4A and B right panel) which activated at potentials compatible with the fast I_f of EM cells (diamonds in Fig. 4C). Moreover, in accordance with the slower rate, I_f current density was significantly reduced in miR1OE than in EM SAN-like cells (Fig. 4D). No difference in cell capacitance was observed (miR1OE = 32.8 ± 4.7 pF, n = 11, N = 6; EM = 33.9 ± 3.5 pF, n = 12, N = 7).

Since HCN4 is much more responsive to cAMP than HCN1 [20], a specific downregulation of HCN4 is expected to decrease the ability of an adrenergic stimulus to shift I_f activation curve. We challenged EM and miR1OE SAN-like cells with 1 μM isoproterenol and analyzed the shift in I_f $V_{1/2}$. As shown in the representative traces and in the dot plot in Fig. 4E, isoproterenol induced a significantly smaller shift of I_f activation curve in miR1OE cells, a result compatible with a lower contribution of HCN4 to the native current. In Fig. 5A, representative confocal images of SAN-like aggregates at d14, stained with anti-HCN4 antibodies (red) are reported. In agreement with electrophysiological data and with WB analysis at d8, corrected total cell fluorescence analysis highlighted a significantly lower expression of HCN4 in miR1OE than in EM aggregates. Despite this difference, no change in the mRNA levels of HCN channels was observed at d14 (Supplementary Fig. S4C).

The presence of only the fast-activating I_f and the decrease of I_f density, together with the down-regulation of HCN4 staining, demonstrate a specific role of miR-1 in the translational repression of the HCN4 isoform.

3.4. *Neonatal rat ventricular cardiomyocytes transfected with miR-1show reduced beating rate and I_f current density.*

To prove that the functional alterations on the beating rate and the I_f current in SAN-like cells were not caused by the developmental effect of miR-1 on SAN precursors, we transiently transfected, with the same plasmids used to generate engineered mES lines, neonatal rat ventricular cardiomyocytes (NRVC) and carried out electrophysiological experiments on EGFP positive NRVC after 48 h. We chose NRVC because they are spontaneously active and express an I_f current carried mainly by HCN4 and HCN2 [21,22]. The spontaneous beating rate of EM NRVCs showed a large variability, with rates ranging from 0.52 to 4.74 Hz. NRVC overexpressing miR-1 instead displayed a lower variability and

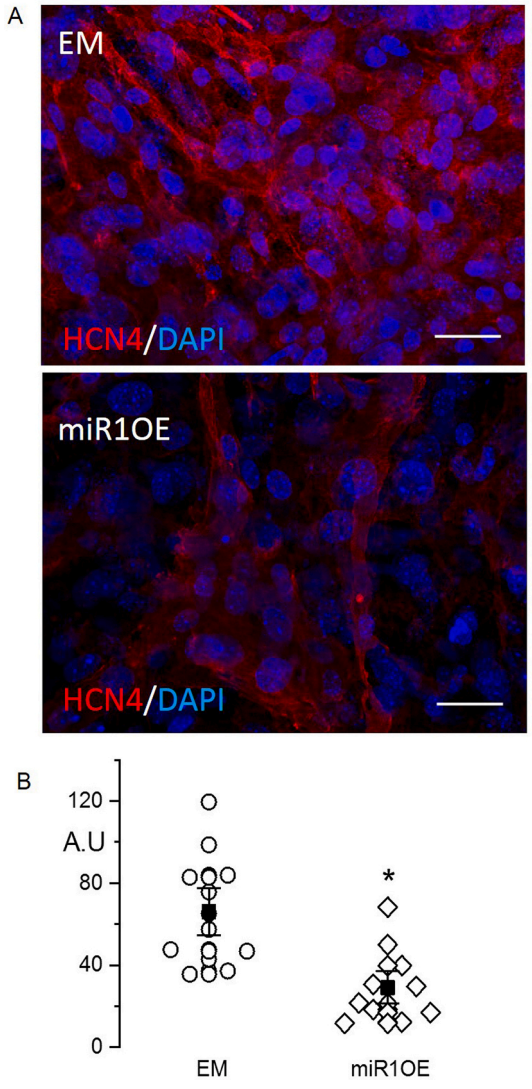

Fig. 5. miR-1 overexpression decreases HCN4 staining in SAN-like cells. (A) Representative images of EM and miR1OE SAN-like cells stained with anti-HCN4 antibodies. Nuclei were counterstained with DAPI. Scale bar: 20 μm. (B) Scatter plot of the corrected total cell fluorescence (CTCF) of HCN4 staining analyzed on EM and miR1OE SAN-like cells. Mean ± SEM values, reported as filled squares, were: 66102.2 ± 7637 in EM (n = 12, N = 2); 29,124.5 ± 5273* in miR1OE (n = 11, N = 2). *Indicates $p < 0.05$ by Student's *t*-test.

significantly lower rates ($p < 0.05$ by Kolmogorov's test, Fig. 6A).

As in SAN-like cells, we found that miR1-NRVC showed a significantly smaller I_f current than EM-NRVC, as highlighted by the mean conductance analysis (Fig. 6B left); no change in the activation curves was found (Fig. 6B right).

In conclusion, we have demonstrated that miR-1 exerts a dual epigenetic modulation on SAN-like cells: during the development, regulating the quote of sinus node precursors and in the mature SAN, modulating the I_f current and consequently the beating rate.

4. Discussion.

MicroRNAs are now recognized as important epigenetic modulators of cardiac pathophysiology. Among the thousands of miRNAs discovered so far, miR-1 is the most abundant in the heart and alterations in its level contribute to heart remodeling both during embryonic development and under specific physiological and pathological conditions [7].

Previous *in vivo* developmental studies analyzed the effect of miR-1 overexpression under the control of the β-myosin heavy chain promoter and revealed a decrease in the proliferation of ventricular myocytes, through the inhibition of Hand2 [5]. Overexpression of miR-1 under the control of α-myosin heavy chain promoter caused hypoplasia of the cardiac ventricular conduction system [6], and atrioventricular block in rodents [23], which appeared to dependent upon repression of the potassium channel Kir2.1 and the gap junction protein connexin 43 [8]. Besides these pieces of evidence, a direct role of miR-1 on sinus node development has not been reported yet.

Here we generated a mESC line constitutively overexpressing miR-1 and the relative control line and used a previously published method for isolating a pure population of $CD166^+$ SAN precursors from differentiating mESC, which mature in culture into fully functional SAN-like cells [12].

Importantly, the overexpression of miR-1, whose expression is normally negligible in undifferentiated mESC, did not impair either pluripotency or differentiation potency and indeed all three germ layers can be promptly generated upon EB formation. The only difference found was an inhibition of the early endoderm marker GATA-4 at d8, in agreement with previously reported data [2]. On the contrary, we demonstrated that, upon differentiation, miR-1 not only generated a percentage of CD166+ SAN-like cells twice that of control mES, but the level of CD166 was also higher. Interestingly, the data showing that, at d8, miR-1 expression in EM EBs is around half that in miR1OE EBs, together with the evidence that ANTI-miR1 EBs do not display any spontaneous beating, point out to a dose-dependent effect of miR-1. Moreover, the evidence that the early cardiac marker Brachyury have an identical time course of expression in EM and miR1OE lines rules out the possibility that the increased proportion of SAN precursors derives from a miR-1-dependent acceleration of development.

It is known that SAN progenitors develop around E8.5 from the sinus horns cells that express Tbx5 and Tbx18 while are negative for Nkx2.5, an inhibitor of the pacemaker gene program [17,24]. Interestingly, at d8, miR1OE $CD166^+$ cells showed significantly higher expression levels of both Tbx5 and Tbx18 while at the same time Nkx2.5 expression remained low. It is noteworthy that Nkx2.5 resulted instead upregulated in the miR81OE CD166-negative population compared to EM CD166-negative cells, in accordance with the role of miR-1 in the early development of $Nkx2.5^+$ cardiac chamber precursors [2].

Tbx3 plays an important role in the maintenance of SAN identity, by downregulating atrial gene program, rather than in promoting directly SAN development as evidenced by the fact that the HCN4+ SAN primordia develop also in the absence of Tbx3 [25]. The decrease of Tbx3 expression in miR1OE cells is not surprising; indeed, it was seen to be downregulated together with HCN4 in trained animals [11] and moreover bioinformatics data identify Tbx3 as a target of miR-1 (miRDB.org). The decrease in Isl-1 expression is less clear; however, at early phases (E8), SAN progenitors develop from Isl-1 negative cells that only later start to express Isl-1 [17].

Beyond its role in cardiac development, miR-1 is modulated by various pathological and physiological stimuli (*e.g.* hypertrophy, atrial fibrillation and endurance training) causing, among other effects, alteration in the normal heart rhythm. In both animal models and humans, for example, intense aerobic training causes mild ventricular hypertrophy and bradycardia. These latter physiological changes are accompanied by a decrease of miR-1 in the ventricle [26] and an increase in the SAN [11]. In these scenarios, changes in miR-1 have been associated with alteration in the pacemaker HCN channels, but no direct effects have been demonstrated. It is interesting to report that in mouse SAN the expression level of miR-1 is lower compared to that in ventricles (Supplementary Fig. S4B) and thus miR-1 levels result inversely proportional to I_f current density in these regions of the hearts. On this regard, Luo and colleagues demonstrated that down regulation of miR-1/miR-133 contributes to re-expression of pacemaker channel genes HCN2 and HCN4 in hypertrophic hearts [27]. miR-1 was found downregulated also in atria and ventricles affected by cardiac arrhythmias

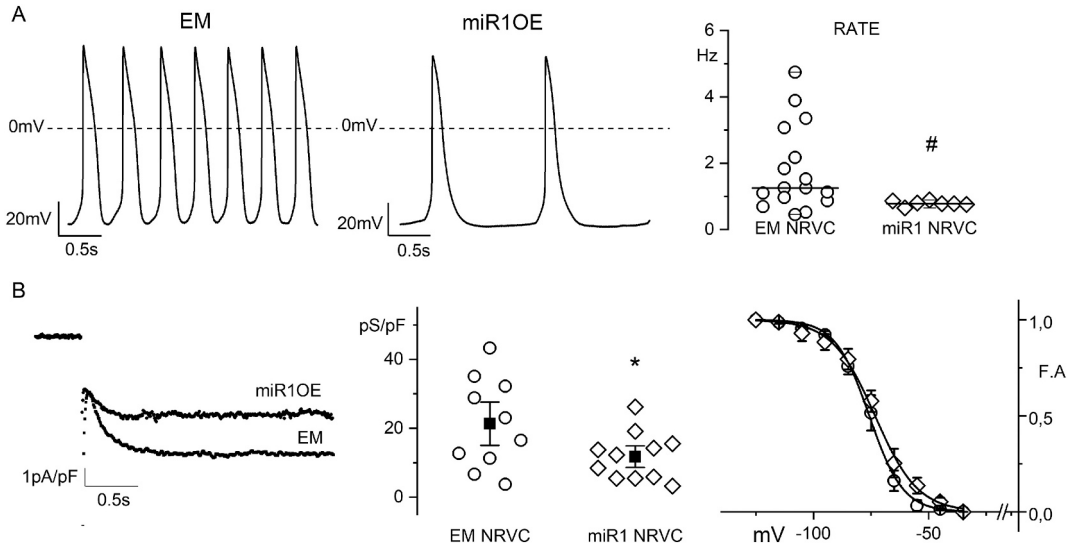

Fig. 6. NRVCs over expressing miR-1 show both decreased spontaneous firing rate and I_f conductance.
(A) Representative spontaneous action potential traces recorded from EM and miR1OE NRVCs, as indicated. Right panel, scatter plot of action potential rate of spontaneously beating NRVCs transfected with the empty (circles; n = 16, N = 5) or miR-1 vectors (diamonds; n = 7, N = 5). Median is shown as a solid line. Parameters values were: median rate 1.25 Hz EM; 0.78 Hz miR1OE. (B) Left, representative current traces recorded at −125 mV, from transfected NRVC as indicated; center, dots plot of mean I_f current conductance in EM (circles) and miR1OE (diamonds) NRVC. Mean conductance values (filled squares) were: 21.3 ± 4.2 pS/pF EM-NRVC (n = 10, N = 5); 11.8 ± 2.1 pS/pF miR1OE-NRVC (n = 11, N = 5). Right, mean activation curves of I_f current from miR1OE and EM-NRVC (symbols as in top panel). Mean $V_{1/2}$ and inverse slope factor values were: −76 ± 2.1 mV and 5.2 ± 0.7 mV EM (n = 11, N = 5), −74 ± 2.5 mV and 8.6 ± 1.1 mV miR1OE (n = 7, N = 5). *Indicates $p < 0.05$ by Student's *t*-test; #Indicates $p < 0.05$ by Kolmogorov's test.

such as atrial fibrillation or ventricular tachyarrhythmia, while the expression of several ion channels, among which HCN2, HCN4 was found upregulated [8,28,29]. On the contrary, up-regulation of miR-1 level in SAN can affect heart automaticity; D'Souza and coworkers demonstrated that in sinus node of trained animal models (mice and rats), which displayed intrinsic bradycardia and a decreased I_f current, miR-1 was upregulated [11]. Nevertheless, whether the decreased I_f was a direct consequence of miR-1 dysregulation was not assessed.

In the present work we provided a direct evidence that miR-1 upregulation causes a decrease in SAN-like cells rate due to I_f modulation. The lack of differences in qRT-PCR data together WB and immunofluorescence data showing a specific downregulation of HCN4 protein demonstrate that miR-1 modulate HCN4 by inhibiting mRNA translation rather than mRNA stability. This decrease translates into a significant decrease in the firing rate and in the I_f current density both in miR1OE SAN-like cells and in NRVC transiently overexpressing miR-1. This last evidence ruled out the possibility that the differences observed were the consequence of an inappropriate SAN development under constantly high levels of miR-1, but it was rather a direct epigenetic modulation of the pacemaker I_f current. Our data showing that in EM cells miR-1 expression rise from d4 to d8 and then falls again at d14 is in agreement with the previously shown raise in rate of SAN-like cells during prolonged culture, which recapitulate the physiological increase in heart rate observed during mouse embryonic and postnatal development [12].

It is known that miRNA may act either by degrading the target mRNA or by preventing its translation [30]. Because bioinformatic data (*e.g.* miRTareBase) show that HCN4 and HCN2, but not HCN1, displays a miR-1 consensus sequence, we evaluated the expression of HCN1, 2 and 4 isoforms in control and miR1OE $CD166^+$ cells. HCN1 was slightly but significantly upregulated at early stage of differentiation (d8) a difference that disappeared at d14, when functional analysis was carried out. In agreement with previous data and with its role in the working myocardium [12], HCN2 expression was negligible in SAN-like cells, independently of the miR-1 levels. HCN4 transcript, the main isoform of the sinoatrial I_f current [12], was unaltered by miR-1 over-expression both at d8 and d14. These data indicate that miR-1 act as an inhibitor of translation and are in accordance with a previous report showing that HCN4 and HCN2 mRNA levels were unchanged following antagomiR-1 treatment while protein levels of both isoforms were upregulated in the border zone of rat with myocardial infarction [31]. To evaluate an isoform specific functional effect of miR-1, we analyzed the kinetic properties (activation time constants (τ) and $V_{1/2}$) of the I_f current, which strictly depend on HCN isoforms expressed on the plasma membrane. HCN1 channels expressed in HEK cells show indeed faster τ (~0.5 s at −75 mV) and a 6.5 mV positive shift of $V_{1/2}$ than HCN4 channels (τ > 6 s at −75 mV) [19]. In native mouse SAN, and in mES-derived pacemaker cells [13,18], two populations of cells can be identified that express either a fast or slow-activating I_f; which likely derive from a different ratio of HCN4/HCN1 expression. While EM SAN-like cells display, as expected, both fast and slow-activating I_f, the latter activating at more hyperpolarized potentials, we have found here that miR1OE SAN-like cells show only the fast-activating and depolarized I_f. Moreover, we found that miR1OE cells show a decreased responsiveness to isoproterenol than EM cells. Although it is conceivable that the reduction of HCN4 may indirectly impact on the assembly of naïve hetero-tetrameric channels, our results are compatible with miR1OE f-channels having a more prevalent contribution of the fast activating, cAMP-insensitive HCN1 subunit; this is also supported by WB analysis that shows a decreased HCN4 but an unaltered HCN1 expression. A similar change in I_f time constants, but not in the $V_{1/2}$, has been previously reported in SAN cardiomyocytes in which the expression of HCN4 was genetically knocked out in adult mice [32]. Our electrophysiological data, together with immunofluorescence analysis of HCN4 expression in SAN-like aggregates (Fig. 5) clearly demonstrate that miR-1 over-expression specifically and significantly decreases the levels of the slowly activating HCN4 isoform.

It is interesting to report that when $CD166^-$ cells are re-aggregated and plated similarly to $CD166^+$ cells, EM $CD166^-$ cells showed small sparce spontaneously contracting regions, while miR1OE $CD166^-$ cells showed extended spontaneously contracting regions. However, the rate of contraction was similar (EM: 0.6 ± 0.2 Hz; miR1OE: 0.8 ± 0.1 Hz) and significantly lower than that of the $CD166^+$ counterparts (see Fig. 3). The larger beating area of miR1OE $CD166^-$ cells agree with the previously shown role of miR-1 in general cardiac mesoderm commitment

[2].

These findings consolidate the role of miR-1 as a fine modulator of cardiac automaticity. We have previously shown that the beating rate of mES-derived SAN-like cells increases with time in culture from d8 to d25 [12] and here we show by qPCR that in control EM line the levels of endogenous miR-1 decrease between d8 (75.9 ± 28.5) and d14 (26.5 ± 4.9) (see Figs. 2C and S4A). In line with the epigenetic role of miR-1 in controlling cardiomyocytes automaticity, it is noteworthy to mention that neonatal ventricular cardiomyocytes, which spontaneously beat and express HCN2 and HCN4 isoforms [21,22], become quiescent at later stage of maturation due to a reduction in the I_f current [33]. Here we show that indeed mouse heart ventricles express higher levels of miR-1 than SAN and atria (see Supplementary Fig. S4B). It is however important to underline that overexpression of miR-1 in SAN-like cells does not induce a switch in cell fate from SAN to ventricle as confirmed by the fact that ventricular genes (HCN2, CX43 and Kv4.2) are not modulated in $CD116^+$ cells(supplementary Fig. S4C).

The present study unravels for the first time a double role of miR-1 in sinus node; at early stage of cardiac development, increasing levels of miR-1 ensure the proper development of the cardiac mesoderm, in general, and of sinoatrial precursors, in particular. At later stages, once the mature SAN is formed, miR-1 plays a direct role in the functional expression of the HCN4 isoform that contribute to the I_f current and thus to the modulation of heart rate. This epigenetic modulation may be of particular importance for those conditions, such as atrial fibrillation and sick sinus syndrome in which miR-1 levels are modulated, leading to a pathological dysregulation of ion channels and cell excitability [34].

Funding.

This research did not receive any specific grant from funding agencies in the public, commercial, or not-for-profit sectors.

Declaration of Competing Interest.

None.

Acknowledgements

We thank Dr. Mark R. Boyett for kindly providing the pEZX-MR04 plasmid.

Appendix A. Supplementary data.

Supplementary data to this article can be found online at https://doi.org/10.1016/j.yjmcc.2021.05.001.

References

[1] Y. Liang, D. Ridzon, L. Wong, C. Chen, Characterization of microRNA expression profiles in normal human tissues, BMC Genomics 8 (2007) 166.
[2] K.N. Ivey, A. Muth, J. Arnold, F.W. King, R.F. Yeh, J.E. Fish, et al., MicroRNA regulation of cell lineages in mouse and human embryonic stem cells, Cell Stem Cell 2 (2008) 219–229.
[3] Y. Zhao, E. Samal, D. Srivastava, Serum response factor regulates a muscle-specific microRNA that targets Hand2 during cardiogenesis, Nature 436 (2005) 214–220.
[4] K. Wystub, J. Besser, A. Bachmann, T. Boettger, T. Braun, miR-1/133a clusters cooperatively specify the cardiomyogenic lineage by adjustment of myocardin levels during embryonic heart development, PLoS Genet. 9 (2013), e1003793.
[5] T.E. Callis, D.Z. Wang, Taking microRNAs to heart, Trends Mol. Med. 14 (2008) 254–260.
[6] E. Samal, M. Evangelista, G. Galang, D. Srivastava, Y. Zhao, V. Vedantham, Premature microRNA-1 expression causes hypoplasia of the cardiac ventricular conduction system, Front. Physiol. 10 (2019) 235.
[7] D.A. Chistiakov, A.N. Orekhov, Y.V. Bobryshev, Cardiac-specific miRNA in cardiogenesis, heart function, and cardiac pathology (with focus on myocardial infarction), J. Mol. Cell. Cardiol. 94 (2016) 107–121.
[8] G. Santulli, G. Iaccarino, N. De Luca, B. Trimarco, G. Condorelli, Atrial fibrillation and microRNAs, Front. Physiol. 5 (2014) 15.
[9] L. Elia, R. Contu, M. Quintavalle, F. Varrone, C. Chimenti, M.A. Russo, et al., Reciprocal regulation of microRNA-1 and insulin-like growth factor-1 signal transduction cascade in cardiac and skeletal muscle in physiological and pathological conditions, Circulation 120 (2009) 2377–2385.
[10] S. Gielen, G. Schuler, V. Adams, Cardiovascular effects of exercise training: molecular mechanisms, Circulation 122 (2010) 1221–1238.
[11] A. D'Souza, A. Bucchi, A.B. Johnsen, S.J. Logantha, O. Monfredi, J. Yanni, et al., Exercise training reduces resting heart rate via downregulation of the funny channel HCN4, Nat. Commun. 5 (2014) 3775.
[12] A. Scavone, D. Capilupo, N. Mazzocchi, A. Crespi, S. Zoia, G. Campostrini, et al., Embryonic stem cell-derived CD166+ precursors develop into fully functional sinoatrial-like cells, Circ. Res. 113 (2013) 389–398.
[13] A. Barbuti, A. Crespi, D. Capilupo, D. Mazzocchi, M. Baruscotti, D. Di Francesco, Molecular composition and functional properties of f-channels in murine embryonic stem cell-derived pacemaker cells, J. Mol. Cell. Cardiol. 46 (3) (2009) 343–351.
[14] D. Avitabile, A. Crespi, C. Brioschi, V. Parente, G. Toietta, P. Devanna, et al., Human cord blood CD34+ progenitor cells acquire functional cardiac properties through a cell fusion process, Am. J. Physiol. Heart Circ. Physiol. 300 (2011) H1875–H1884.
[15] A. Bucchi, M. Baruscotti, R.B. Robinson, D. DiFrancesco, Modulation of rate by autonomic agonists in SAN cells involves changes in diastolic depolarization and the pacemaker current, J. Mol. Cell. Cardiol. 43 (2007) 39–48.
[16] A. Leahy, J.W. Xiong, F. Kuhnert, H. Stuhlmann, Use of developmental marker genes to define temporal and spatial patterns of differentiation during embryoid body formation, J. Exp. Zool. 284 (1999) 67–81.
[17] A. Barbuti, R.B. Robinson, Stem cell-derived nodal-like cardiomyocytes as a novel pharmacologic tool: insights from sinoatrial node development and function, Pharmacol. Rev. 67 (2015) 368–388.
[18] M.E. Mangoni, J. Nargeot, Properties of the hyperpolarization-activated current (I (f)) in isolated mouse sino-atrial cells, Cardiovasc. Res. 52 (2001) 51–64.
[19] C. Altomare, B. Terragni, C. Brioschi, R. Milanesi, C. Pagliuca, C. Viscomi, et al., Heteromeric HCN1-HCN4 channels: a comparison with native pacemaker channels from the rabbit sinoatrial node, J. Physiol. 549 (2003) 347–359.
[20] C. Viscomi, C. Altomare, A. Bucchi, E. Camatini, M. Baruscotti, A. Moroni, et al., C terminus-mediated control of voltage and cAMP gating of hyperpolarization-activated cyclic nucleotide-gated channels, J. Biol. Chem. 276 (2001) 29930–29934.
[21] W. Shi, R. Wymore, H. Yu, J. Wu, R.T. Wymore, Z. Pan, et al., Distribution and prevalence of hyperpolarization-activated cation channel (HCN) mRNA expression in cardiac tissues, Circ. Res. 85 (1999) e1–e6.
[22] T. Muto, N. Ueda, T. Opthof, T. Ohkusa, K. Nagata, S. Suzuki, et al., Aldosterone modulates I(f) current through gene expression in cultured neonatal rat ventricular myocytes, Am. J. Physiol. Heart Circ. Physiol. 293 (2007) H2710–H2718.
[23] Y. Zhang, L. Sun, Y. Zhang, H. Liang, X. Li, R. Cai, et al., Overexpression of microRNA-1 causes atrioventricular block in rodents, Int. J. Biol. Sci. 9 (2013) 455–462.
[24] J.H. van Weerd, V.M. Christoffels, The formation and function of the cardiac conduction system, Development 143 (2016) 197–210.
[25] W.M. Hoogaars, A. Engel, J.F. Brons, A.O. Verkerk, F.J. de Lange, L.Y. Wong, et al., Tbx3 controls the sinoatrial node gene program and imposes pacemaker function on the atria, Genes Dev. 21 (2007) 1098–1112.
[26] T. Fernandes, V.G. Barauna, C.E. Negrao, M.I. Phillips, E.M. Oliveira, Aerobic exercise training promotes physiological cardiac remodeling involving a set of microRNAs, Am. J. Physiol. Heart Circ. Physiol. 309 (2015) H543–H552.
[27] X. Luo, H. Lin, Z. Pan, J. Xiao, Y. Zhang, Y. Lu, et al., Down-regulation of miR-1/miR-133 contributes to re-expression of pacemaker channel genes HCN2 and HCN4 in hypertrophic heart, J. Biol. Chem. 283 (2008) 20045–20052.
[28] Z. Girmatsion, P. Biliczki, A. Bonauer, G. Wimmer-Greinecker, M. Scherer, A. Moritz, et al., Changes in microRNA-1 expression and IK1 up-regulation in human atrial fibrillation, Heart Rhythm 6 (2009) 1802–1809.
[29] A. Curcio, D. Torella, C. Iaconetti, E. Pasceri, J. Sabatino, S. Sorrentino, et al., MicroRNA-1 downregulation increases connexin 43 displacement and induces ventricular tachyarrhythmias in rodent hypertrophic hearts, PLoS One 8 (2013), e70158.
[30] B. Yang, Y. Lu, Z. Wang, Control of cardiac excitability by microRNAs, Cardiovasc. Res. 79 (2008) 571–580.
[31] H.D. Yu, S. Xia, C.Q. Zha, S.B. Deng, J.L. Du, Q. She, Spironolactone regulates HCN protein expression through micro-RNA-1 in rats with myocardial infarction, J. Cardiovasc. Pharmacol. 65 (2015) 587–592.
[32] S. Herrmann, J. Stieber, G. Stockl, F. Hofmann, A. Ludwig, HCN4 provides a 'depolarization reserve' and is not required for heart rate acceleration in mice, EMBO J. 26 (2007) 4423–4432.
[33] K. Yasui, W. Liu, T. Opthof, K. Kada, J.K. Lee, K. Kamiya, et al., I(f) current and spontaneous activity in mouse embryonic ventricular myocytes, Circ. Res. 88 (2001) 536–542.
[34] O. Monfredi, M.R. Boyett, Sick sinus syndrome and atrial fibrillation in older persons - a view from the sinoatrial nodal myocyte, J. Mol. Cell. Cardiol. 83 (2015) 88–100.